SENP1 IN ISLET COMPENSATION AND FAILURE DURING HIGH FAT FEEDING

by

Haopeng Lin

A thesis submitted in partial fulfillment of the requirements for the degree of

Doctor of Philosophy

Department of Pharmacology
University of Alberta

ABSTRACT

Pancreatic β-cells are paramount for optimizing insulin secretion to metabolic need. The progression from non-diabetes to type 2 diabetes (T2D) is accompanied by β-cell compensation and decompensation. While β-cell decompensation is a hallmark of overt diabetes, β-cell compensation promotes insulin output, either through functional or mass increases, to maintain normoglycemia. The sentrin-specific SUMO protease-1 (SENP1) reverses a post translational modification (PTM) called SUMOylation, and this is required for physiological β-cell function. In contrast, SENP1 exerts a negative effect on β-cell survival under oxidative stress. This dual and opposite effect on function and survival has not been reconciled in the context of metabolic stress, where both β-cell functional and mass compensation are essential to maintain glucose homeostasis.

The present thesis shows that in short-term HFD exposure, an early stage of compensation where functional compensation is predominant, adaptive glucose-stimulated insulin secretion is accounted for by upregulation of cytosolic reducing signaling via SENP1, redox regulation of which is fine-tuned by a coordinated interaction between Zn^{2+} and cysteines 603 and 535 of the SENP1 catalytic domain. Loss of β-cell SENP1 impairs intraperitoneal glucose tolerance. Furthermore, under long-term high fat diet (HFD) exposure with decompensated glucose-stimulated insulin secretion and pronounced islet mass expansion, islet and β-cell SENP1 is required for maintaining oral glucose tolerance by ensuring robust incretin-stimulated insulin secretion at a point downstream of incretin receptors. Importantly, loss of SENP1 does not have any harmful effect on β-cell mass compensation.

These findings elucidate the molecular basis of SENP1 redox sensing and provide insights into the mechanisms how β-cell adopts different strategies for functional compensation at different

stages of compensation, establishing an indispensable role of SENP1 for β-cell functional compensation to maintain normoglycemia. Targeting SENP1 might emerge as a therapeutic intervention to rescue the β-cell functional decompensation commonly seen in T2D. (296 words).

PREFACE

This thesis is an original work by Haopeng (Frank) Lin. Research work received research ethics approval from the University of Alberta Animal Ethics Board, protocols AUP00000291 and AUP00000405, and the Human Ethics Board, protocols Pro00013094 and Pro00001754. All families of organ donors provided written informed consent to the use of pancreatic tissue in research.

Chapter 2 and 3 is to be submitted as Haopeng Lin, Kunimasa Suzuki, Nancy Smith, Xi Li, Lisa Nalbach, Sonia Fuentes, Aliya F Spigelman, Xiaoqing Dai, Austin Bautista, Mourad Ferdaoussi, Saloni Aggarwal, Andrew R Pepper, Emmanuel Ampofo, Leticia P Roma, Wen-hong Li, Patrick E MacDonald. Redox Sensing by the SUMO-Protease SENP1 Is Required for Adaptive Insulin Secretion upon Short-Term Metabolic Stress. In chapter 2, H. Lin was responsible for most of the data collection, data analysis, and manuscript composition. K. Suzuki, N. Smith, X. Li, L. Nalbach, S. Fuentes, A.F. Spigelman, X. Dai, A. Bautista, M. Ferdaoussi, S. Aggarwal, E. Ampofo, L.P. Roma, W. Li contributed to data collection and analysis as outlined in the figure legends. In chapter 3, H. Lin and K. Suzuki were responsible for data collection, analysis. P.E.MacDonald was the lead supervisory author and was involved with concept formation and editing of the manuscript.

Chapter 4 has been published as: Haopeng Lin, Nancy Smith, Aliya F Spigelman, Kunimasa Suzuki, Mourad Ferdaoussi, Tamadher A. Alghamdi, Sophie L Lewandowski, Yaxing Jin, Austin Bautista, Ying Wayne Wang, Jocelyn E. Manning Fox, Matthew J Merrins, Jean Buteau, Patrick E MacDonald. β-Cell Knockout of SENP1 Reduces Responses to Incretins and Worsens Oral Glucose Tolerance in High-Fat Diet-Fed Mice. *Diabetes 70.11 (2021): 2626-2638.* I was responsible for most of the data collection, data analysis, and manuscript composition. N. Smith, A.F. Spigelman, K. Suzuki, M. Ferdaoussi, T.A. Alghamdi, S.L. Lewandowski, Y. Jin, A. Bautista, Y.W. Wang and J.E. Manning Fox contributed to data collection as outlined in the figure legends. P.E.MacDonald was the lead supervisory author and was involved with concept formation and editing of the manuscript.

ACKNOWLEDGEMENTS

Patrick E MacDonald *– Pat, besides your scientific competence and guidance, what I value the most from you is your humbleness, considerateness, respectfulness as well as a bit of 'humor'. Your characteristics really make me feel inclusive and enjoy working in the lab. You totally change my stereotype against white people and teach me being a good person should come first before being a good scientist.*

Dr. William F Colmers and Dr. Thomas Simmen - *Thanks for having you as my committee members. You always motivate me to think out of the box and give me the sincerest advice.*

Kunimasa Suzuki - *Kuni, your work ethic and scientific insight really impress me. This thesis would not be possible without your significant contribution in the molecular biology. You are always the first one to step up and help, either experimentally or mentally.*

Nancy and Aliya *– Thanks for always supporting my research by providing lots of help on animal work and hormone secretion.*

Xiaoqing *– Thanks for helping me a lot not only on my scientific journey but also on driving me to TNT for grocery.*

Richard and Austin *– Thanks for your companionship. I will remember our time playing frisbee, squash, badminton, basketball, bouldering, swimming and talking about politics. Last but not least, I will not forget 'tumble the donut'.*

Past and present Macdonald members *– This would be a boring journey without all of you along the way.*

Dad and Mom - *Thanks for your relentless support for 30 years. It is both of you that help me become who I am. I feel so sorry for being so far away from both of you since I went to university. Dad, if you can hear me, I want to say I am so proud of you. You always think about me before yourself. I really wish you would be here and witness my graduation. I hope I make you proud. This is dedicated to you. Rest in peace.*

Wife *– I know this is tough for you to spend only one month every year with your husband. I promise I will spend the rest of my life with you in the future.*

Brother and sister-in-law *– Thanks for taking good care of Dad and Mom so I can fully focus on my study. I know it is not easy especially you just have twins.*

Li Ka Shing Foundation *– The scholarship changes my life. Thanks.*

TABLE OF CONTENTS

LIST OF TABLES

LIST OF FIGURES

GLOSSARY

°C	degree Celsius
µg	microgram
µL	microliter
µM	micromolar
µmol	micromole
AA	amino acid
ADP	adenosine diphosphate
ANOVA	analysis of variance
ATP	adenosine triphosphate
AUC	area under the curve
BMI	body mass index
Ca^{2+}	calcium ion
cAMP	cyclic Adenosine Monophosphate
CD	chow diet
CoA	coenzyme A
Cs	Cesium
Cys	cysteine
cyto	cytosol
DI	disposition index
DiR	1,1-dioctadecyl-3,3,3,3-tetramethylindotricarbocyanine iodide
EDTA	ethylene diamine tetraacetic acid
EGTA	ethylene glycol tetraacetic acid
ER	endoplasmic reticulum
Ex4	exendin4
FBS	fetal bovine serum
fF	femtofarad
FFA	free fatty acid
g	gram
GDH	glutamate dehydrogenase
GIP	glucose-dependent insulinotropic peptide
GLP-1	glucagon-like peptide-1
GLUT2	glucose transporter-2
GLUT4	glucose transporter-4
GOT1	glutamate-oxaloacetate transaminase-1
GPX	glutathione peroxidase
GRX1	glutaredoxin-1

GSH	glutathione
GSIS	glucose stimulated insulin secretion
GSR	glutathione reductase
GSSG	oxidized glutathione
h	hour
HbA1c	glycated hemoglobin
HbA1C	Hemoglobin A1c
HEPES	4-(2-hydroxyethyl)-1-piperazineethanesulfonic acid
HFD	high fat diet
HGP	hepatic glucose production
IC50	half-maximal inhibitory concentration
INSR	insulin receptor
IPGTT	intraperitoneal glucose tolerance test
KATP	ATP-sensitive potassium channel
KCl	potassium chloride
Kd	dissociation constant
Ki	inhibitory constant
KO	knock-out
KRB	Krebs-Ringer bicarbonate buffer
L	litre
M	molar
MAG	monoacylglycerol
mg	milligram
min	minute
mL	milliliter
mM	millimolar
mmol	millimole
mol	mole
mRNA	messenger ribonucleic acid
ms	millisecond
MT	metallothionine
Munc	mammalian uncoordinated protein
mV	millivolts
NaCl	sodium chloride
NADH	nicotinamide adenine dinucleotide
NADPH	nicotinamide adenine dinucleotide phosphate
NaHCO3	sodium bicarbonate
ng	nanogram
nM	nanomolar

nmol	nanomole
NNT	nicotinamide nucleotide transhydrogenase
NOX4	NADPH oxidase-4
OGTT	oral glucose tolerance test
Orp1	H_2O_2 sensing peroxidase
OxPhos	oxidative phosphorylation
pA	picoAmpere
PBS	phosphate buffered saline
pC	picocoulomb
PCR	polymerase chain reaction
PEP	phosphoenolpyruvate
PEPCK	phosphoenolpyruvate carboxykinase
pF	picofarad
PKA	protein kinase A
PKD1	protein kinase D1
pM	picomolar
PRDX	peroxiredoxin
PTM	posttranslational modification
roGFP	reduction-oxidation sensitive green fluorescent protein
RRP	readily releasable pool
RT-PCR	reverse-transcription-PCR
S-AMP	adenylosuccinate
SDS PAGE	SDS (or sodium dodecyl sulfate) polyacrylamide gel electrophoresis
SEM	standard error of the mean
SENP	sentrin/SUMO-specific proteases
SUMO	small ubiquitin-like modifier
Streptozotocin	STZ
Syt7	synaptotagmin-7
T1D	type 1 diabetes
T2D	type 2 diabetes
TCA	tricarboxylic acid cycle
TEA	tetraethyl ammonium
WT	wild type
Zn^{2+}	zinc ion

Chapter 1. Introduction

1.1 Pathogenesis of T2D

1.1.1 Introduction of T2D

Diabetes Mellitus refers to a chronic metabolic disorder characterized by abnormally elevated blood glucose resulting from insufficient production of, or poor response to, insulin. It is probably one of the oldest known metabolic diseases, first reported 3000 years ago, and continues to pose a threatening challenge to public health and economic growth as a global pandemic until now[1]. According to the World Health Organization, in 2021 around 422 million people are afflicted with diabetes. A whopping 825 billion dollars per year is spent on diabetes treatment globally[2]. In the wake of the COVID-19 pandemic, COVID-19 patients with diabetes have poorer glycemic control with higher risks of morbidity and mortality, possibly due to a direct effect of SARS-CoV-2 on β-cell function and survival[3]. Therefore, better disease prevention, treatment and cure are needed to control diabetes and minimize the negative impact.

The journey to discover the pathogenesis of diabetes wasn't a pleasure cruise. Despite the islet of Langerhans in the pancreas being discovered by Paul Langerhans in 1869[4] it wasn't until 1889 that Joseph von Mering and Oskar Minkowski established the role of the pancreas in the pathogenesis of diabetes by noticing the rapid development of diabetes in depancreatized dogs[5]. Later, the pancreatic islets were considered to be responsible for an important inner secretion by Laguesse[6], and the searching for the culprit for diabetes was finally narrowed down to the dysfunctional pancreatic islets by MacCallum[7]. In 1921, Banting, MacLeod, Best and Collip made a great step towards the therapy for diabetes by successfully discovering and extracting glucose-lowering insulin from pancreas[8]. From that point on, insulin therapy thrived and saved millions of

lives! Later in 1936, Harold Himsworth found that insulin therapy failed in some cases and discovered the "insulin-sensitive" and "insulin-insensitive" diabetes, commonly termed "type 1" and "type 2" diabetes today[9]. As the major source of insulin, pancreatic islets are essential to regulate insulin secretion dynamically and control glycemic level. The development of pancreatic islet biology has pushed forward the understanding of mechanisms underlying diabetes. However, the precise mechanism by which islet dysfunction occurs continues to be perplexing.

Basically, there are two major types of diabetes, i.e., type 1 diabetes (T1D) and type 2 diabetes (T2D). T1D is an autoimmune disease, the pathogenesis of which is caused by gradual destruction of pancreatic β-cells by immune cells. While T1D incidence accounts for 5-10% of global cases, T2D cases up to 90%, and represent the most common form of diabetes and a health crisis around the world[10]. The pathogenesis of T2D is distinct from that of T1D. T2D is mainly characterized by abnormalities in insulin secretion and insulin resistance. It is a multifactorial disease, which is not only associated with genetic predisposition, but also environmental factors such as diet, exercise, etc. Uncertainty about the pathogenesis of T2D persist, largely as to which metabolic abnormality initiates the development of T2D and how much contributes to it[11,12].

1.1.2 Insulin compensation for insulin resistance

T2D is a disease of insufficient insulin secretion and insulin resistance. In an early stage of prediabetes, compensatory insulin secretion ensues to maintain glucose homeostasis through upregulated insulin secretion and/or downregulated insulin clearance.

1.1.2.A Insulin compensation by β-cells

β-cell compensation describes a process where β-cell can increase insulin secretion by upregulating β-cell function or β-cell mass. It is important to maintain glucose homeostasis in

response to metabolic stress. β-cells experience five stages of changes in the progression to T2D. In stage 1, normal glucose tolerance (NGT) is maintained by enhanced glucose-stimulated insulin secretion (GSIS) via β-cell functional and mass compensation. In stage 2, fasting glucose is still normal but first phase GSIS is impaired, i.e., functional decompensation, leading to impaired glucose tolerance (IGT). Stages 1 and 2 are at the stage of prediabetes. In stage 3, the β-cell mass is not sufficient to compensate for insulin resistance and results in impaired fasting glucose. This stage is a decompensation stage and marks the occurrence of T2D, characterized by the failure of β-cells to compensate for insulin resistance and impaired fasting glucose[13,14]. Further deterioration of β-cell function and mass pushes progression from stage 3 to stage 4, where minimal insulin levels can barely prevent the ketosis which is commonly seen in stage 5 or T1D[15]. Further criteria for diagnosis of prediabetes and diabetes are in **Table 1**.

β-cells are capable of adapting to different situations, such as fasting or overnutrition states[16]. In the early stage of prediabetes, β-cells can ramp up insulin secretion to overcome insulin resistance and maintain glucose tolerance. Notably, insulin-resistant individuals do not develop T2D, due to the maintained compensatory increase of insulin secretion[17,18]. In individuals with normal glucose tolerance and β-cell function, insulin secretion and insulin resistance follow a hyperbolic relationship with a constant (insulin secretion × insulin sensitivity) called the "disposition index" (DI)[19,20]. Insulin-resistant individuals with successful insulin compensation can still maintain a constant DI, denoting an adaptive β-cell function in the face of metabolic demand. A reduced DI implies failure of the β-cell to compensate for insulin resistance in subjects susceptible to developing T2D[21]. For example, a longitudinal study in native American Pima Indians showed that those T2D progressors (those who develop T2D) gradually showed impaired glucose tolerance with lower DI value, indicative of a failure of insulin compensation for insulin

resistance[22]. Therefore, β-cell function and its ability to adapt to increasing metabolic stress is of importance to prevent T2D.

Table 1. Criteria for prediabetes and diabetes diagnosis.

Test	Prediabetes	Diabetes
FPG (mmol/L)	6.1–6.9	≥7.0
2hPG in a 75g OGTT (mmol/L)	7.8–11.0	≥11.1
HbA1C (%)	6.0–6.4	≥6.5
Random PG	—	≥11.1

FPG: fasting plasma glucose; 2hPG: 2-hour plasma glucose; OGTT, oral glucose tolerance; test; HbA1c: glycated hemoglobin; PG: plasma glucose. Adapted from Diabetes Canada Clinical Practice Guidelines[23].

1.1.2.B Insulin compensation by reduced insulin clearance

Hyperinsulinemia is not only determined by secretion from β-cell, but also from insulin clearance. As the primary site of insulin clearance, liver degrades at least 50% of insulin after the first pass, and a total of 80% of insulin is removed during whole insulin clearance[24]. Mechanistically, insulin binds to the insulin receptor (INSR) and mediates insulin endocytosis and degradation[25]. In a longitudinal study of compensation for fat-induced insulin resistance, reduced insulin clearance provides another route for compensation, contributing at least 50% of hyperinsulinemia level and sparing β-cells from overwork[26]. However, reduced insulin clearance is also identified as a critical factor in hepatic insulin resistance and hyperinsulinemia in obese and T2D subjects[27–29].

1.1.3 Dysregulated glucose disappearance in T2D

Glucose, an indispensable energetic fuel for most tissues, is tightly regulated by multiple organs. After carbohydrate food digestion and glucose absorption in the intestine, circulating plasma glucose levels increase and enter different tissues via glucose uptake. However, in T2D excessive plasma glucose cannot be sufficiently lowered and absorbed by peripheral tissues, such as skeletal muscle, adipose tissue and liver. The possible underlying mechanism for impaired glucose uptake in T2D includes dysregulation of insulin-dependent (insulin resistance) and insulin-independent (impaired glucose effectiveness) glucose uptake.

1.1.3.A Insulin-dependent glucose-disappearance and insulin-resistance

Insulin produced by the pancreatic β-cell is the only blood glucose-lowering hormone[30]. In response to increasing levels of circulating glucose, β-cells secrete insulin into the circulating blood flow. Circulating insulin can bind to the INSR on different tissues to induce glucose-uptake

and suppression of glucose production, resulting in a decrease of plasma glucose level. However, when peripheral tissues, such as skeletal muscle, adipose tissue and liver, are unresponsive to insulin and hyperinsulinemia is required to achieve the glucose-lowering effect, this is considered insulin resistance[31]. Impaired INSR signaling significantly contributes to insulin resistance and progression to T2D[31].

1.1.3.B Insulin-independent glucose-disposal and glucose effectiveness

Other than the insulin-dependent glucose-disposal pathway, blood glucose disposal can also occur in an insulin-independent way, i.e., glucose effectiveness. Glucose effectiveness depicts a process of glucose-induced glucose uptake and suppression of glucose production independent of insulin concentrations[32]. This process has been long established as a major determinant of intravenous glucose tolerance in healthy human subjects[33]. It contributes up to 71% of glucose disposal compared to insulin-dependent glucose disposal in intravenous glucose tolerance[34]. Mechanistically, acute postprandial glucose elevation promotes glucose-induced glucose uptake into peripheral tissues in a concentration-dependent fashion[35]. In addition, acute hyperglycemia could enhance glycogen stores and hence suppresses hepatic glucose release[36]. Furthermore, hyperglycemia decreases endogenous glucose production by inhibiting the generation of free fatty acid in the plasma, which is a substrate for gluconeogenesis[37]. Finally, additional glucose transporter-4 (GLUT4) can be induced on the cell surface of skeletal muscle by acute glucose, independent of insulin concentrations, thus increasing glucose disposal[38]. In T2D where insulin resistance develops, glucose effectiveness is largely abnormal and results in fasting and postprandial hyperglycemia[39,40].

1.1.4 Controversy regarding the role of β-cell compensation in hyperinsulinemia and insulin resistance for T2D pathogenesis.

Regulation of insulin secretion and action in glucose homeostasis is a delicate feedback loop process. Insulin resistance causes insulin compensation and hyperinsulinemia and vice versa. The effect of hyperinsulinemia and insulin resistance are bidirectional and it remains largely unknown whether hyperinsulinemia or insulin resistance is the primary cause to elicit T2D[11,12].

In the hypothesis defining hyperinsulinemia as the primary factor underlying T2D, β-cell compensation is assumed to hyper-secrete insulin in the presence of excessive nutrients, leading to hyperinsulinemia and insulin resistance[12,41]. In this case, hyperinsulinemia seems to be the culprit for T2D development. However, β-cell compensation is important for maintaining glucose homeostasis, and hyperinsulinemia can also be observed in people with T2D and impaired β-cell function[42]. This impaired β-cell function includes sustained insulin secretion at basal glucose and impaired first-phase insulin secretion[42,43]. The discrepancy about the role of hyperinsulinemia in T2D might lie at the failure of distinguishing basal hyperinsulinemia from glucose-stimulated insulin hypersecretion[11]. While the increased basal hyperinsulinemia could be due to hypersecretion of insulin from β-cells at low glucose caused by gluco- and lipo- toxicity[44], insulin hypersecretion at high glucose might denote 'β-cell compensation'. Furthermore, fasting insulin levels, instead of fed-state insulin, plays a major role in hyperinsulinemia and T2D[43]. Increased basal insulin secretion and decreased glucose-stimulated insulin secretion (GSIS) correlates with the conversion from normal glucose tolerance to T2D[45]. Therefore, increased basal insulin secretion and impaired first-phase insulin functional compensation might underlie the increased hyperglycemia, leading to sustained insulin release. Nonetheless, both dysregulated hyperinsulinemia and insulin resistance are potential contributors to T2D.

1.2 Islet biology

1.2.1 Stimulus-secretion coupling

The pancreatic β-cell is the major site of insulin production. As an endogenous 'glucometer', pancreatic β-cells monitor and regulate glucose levels by switching on/off insulin secretion. Glucose-activated insulin secretion is achieved by the coordinated activity of a 'triggering pathway' and multiple 'amplifying pathways'[46]. The classical model for triggering insulin secretion involves glucose transport into β-cell, glucose-induced elevation of ATP-to-ADP ratio, closure of ATP-sensitive potassium (K_{ATP}) channel to evoke action potential and opening of voltage-gated Ca^{2+} channels. The increase of cytosolic Ca^{2+} activates Ca^{2+}-sensitive exocytotic proteins to facilitate insulin granule exocytosis[47,48]. This pathway is often called the 'K_{ATP} channel-dependent pathway'.

Once a secretory response is triggered, its magnitude is determined by amplifying pathways that operate independently of K_{ATP} channels and cytosolic Ca^{2+} (often termed 'K_{ATP} channel-independent' pathways). After clamping K_{ATP} channels open with diazoxide and depolarizing islets with high extracellular KCl, glucose can still increases insulin secretion without changing Ca^{2+}, i.e., increasing Ca^{2+} efficacy[49]. A series of glucose metabolites facilitate the recruitment and fusion of insulin granules[50]. In a biphasic insulin secretion, while the triggering pathway provides a Ca^{2+} signal, amplifying pathways enhance secretory response to that elevation of Ca^{2+} and account for at least 50% both of the first and second phases of glucose-induced insulin secretion[51,52]. In addition, the glucose dependency of the triggering and amplifying pathways differ. While a threshold of 7 mM glucose is required to open Ca^{2+} channels and activate the triggering pathway, amplifying pathway is operative even below 7 mM glucose as revealed at a

clamped Ca^{2+} level by KCl and K_{ATP} channel opener diazoxide **(Figure 1)**[46]. It should be noted that operation of the amplifying pathway at low glucose levels (below 7 mM) does not involve a further change in Ca^{2+} concentration, but does require the presence of Ca^{2+} to manifest the low glucose effect[46]. Insulin amplifying pathways are mediated by a series of metabolites and secondary stimuli, which are further discussed below[50].

Figure 1. Glucose dependency of amplifying and triggering amplifying pathway.

Triggering pathway and amplifying pathway are operative in control islets. In the presence of KCl and diazoxide, the triggering Ca^{2+} signal is clamped, and insulin secretion profile of amplifying pathway is revealed. Adapted from Henquin JC[46].

Figure 1.

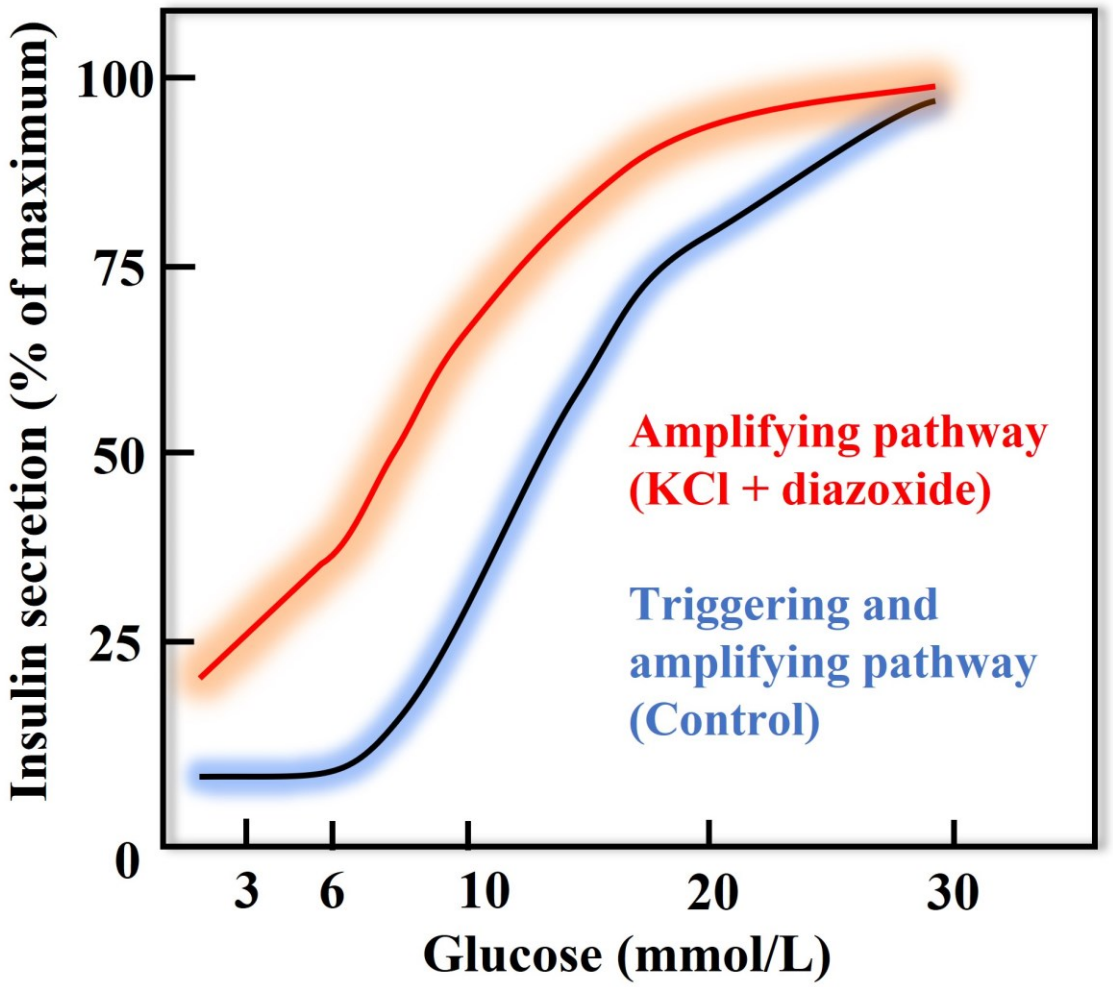
Insulin secretion (% of maximum)
100
75
50
25
0
3
6
10
20
30
Glucose (mmol/L)
Amplifying pathway
(KCl + diazoxide)
Triggering and
amplifying pathway
(Control)

1.2.1.A Metabolic control of the triggering pathway

The ATP-sensitive K_{ATP} channel is a major contributor to the triggering pathway, linking the ATP to a larger increase of Ca^{2+}. ATP derived from oxidative phosphorylation (OxPhos) is central to K_{ATP} channel closure, while MgADP stimulates K_{ATP} channel opening. Recent findings suggests that ATP derived from phosphoenolpyruvate (PEP) cycle, other than oxidative phosphorylation, can also contribute to the inactivation of K_{ATP} channel. ATP generated from PEP cycle switched on the triggering pathway, which is maintained by OxPhos-derived ATP[53,54]. In addition, glucose-induced H_2O_2 is reported to regulate K_{ATP} activity, participating in the initiation of triggering pathway[55]. Other metabolites, such as phosphatidylinositol bisphosphate (PIP_2) and long-chain acyl CoAs can also regulate K_{ATP} channels[56]. However, it still needs to be further investigation whether these are involved in glucose-stimulated insulin secretion in β-cells under physiological condition.

1.2.1.B Metabolic control of the amplifying pathway

Glucose metabolism generates essential metabolites and involves multiple pathways required for amplifying insulin secretion. Most importantly, pyruvate flux into the tricarboxylic acid (TCA) cycle through pyruvate carboxylase is predominant in generating metabolic factors driving the amplifying pathway[57]. A reductive (counter-clockwise) TCA cycle flux generates isocitrate or citrate from α-ketoglutarate through isocitrate dehydrogenase-2 (IDH2) in the mitochondria. Exported isocitrate or citrate can be reversed back to α-ketoglutarate, which transfers back to mitochondria to sustain this pyruvate-isocitrate cycle. This cycle results in the cytosolic generation of the metabolic coupling factor NADPH, required for amplifying insulin secretion[58,59]. Importantly, the pyruvate-isocitrate cycle is of more significance among other anaplerotic pathways to use citrate and isocitrate for the generation of NADPH, activation of

sentrin-specific protease-1 (SENP1) protein, and GSIS[57]. SENP1 is an important signal for insulin amplification. Further details about the insulin-amplifying effect of NADPH and SENP1 will be discussed in the section on redox-control of insulin secretion.

In addition to pyruvate-isocitrate cycle, glucose metabolism activates pentose phosphate pathway and generates NADPH, which potentially amplify insulin secretion. Alternatively, a GSIS product of pentose phosphate and purine pathway, adenylosuccinate (S-AMP), can also directly facilitate insulin amplification. Although the exact downstream mechanism remains uncertain, S-AMP requires SENP1, the same downstream target of pyruvate-isocitrate cycle, to amplify insulin secretion[60].

Glucose metabolism can generate mitochondrial GTP (mtGTP) to amplify insulin secretion. mtGTP is generated from TCA cycle and coupled to PEP cycle (mtGTP-PEP cycle), which activates pyruvate kinase to amplify insulin secretion[53,54]. The mechanism for pyruvate kinase in amplifying pathway involves the generation of pyruvate, anaplerotic fluxes into the TCA cycle and generation of NAD(P)H[53].

Amino acid signaling is important to amplify insulin secretion. Glutamate has long been established an important metabolic coupling factor in amplifying pathway[61,62]. In mitochondria, glutamate can be converted to 2-oxoglutarate by a mitochondrial enzyme glutamate dehydrogenase (GDH), providing sufficient substrate to maintain reductive TCA-dependent pyruvate-isocitrate cycle and export NADPH from mitochondria to cytosol for insulin exocytosis[58,63]. GDH activator, such as leucine, can allosterically activate GDH and enhance insulin secretion[64]. In cytosol, glutamate is derived mainly from α-ketoglutarate by glutamate-oxaloacetate transaminase 1 (GOT1) in glucose-stimulated malate-aspartate shuttle. Glutamate is

transported to insulin granules by incretin-induced cAMP/PKA signaling and enhance cAMP-dependent insulin secretion[65].

Lipid signaling is an important arm for amplification of insulin secretion[50]. It mainly operates through intracellular lipid signaling and free fatty acid (FFA) receptor signaling[66]. In intracellular signaling, glucose stimulates glycerol-3-phosphate and inhibits fatty acid oxidation, generating monoacylglycerol (MAG) via the glycerolipid/free fatty acid (GL/FFA) cycle. MAG shows high binding affinity for the exocytotic protein Munc13-1 and primes insulin granule for release[50,67]. In FFA receptor signaling, glucose generates FFA from GL/FFA cycle and 20-hydroxyeicosatetraenoic acid (20-HETE), which exit the cell and act in an autocrine manner to activate the FFA receptor[66,68]. FFA receptor signaling involves the participation of G protein-coupled receptor-40, PKD1, F-actin depolymerization and potentiation of second-phase insulin secretion.

cAMP is an important insulin amplifier induced by glucose. Glucose metabolism increases ATP and activate adenylyl cyclase isoform ADCY5, enhancing cAMP level[69,70]. Additionally, glucose-induced cAMP level requires constitutive activation of glucagon-like peptide-1 receptors[71]. The amplifying effect by cAMP involves key enzymes activation in glucose metabolism[72] and modulating insulin granule mobilization and priming[73,74].

1.2.2 Redox control of exocytosis

1.2.2.A Redox in mitochondria

Redox signals, such as NADPH, in mitochondria have significant effects on GSIS[50,75,76]. Glucose carbon mainly fluxes into TCA cycle in mitochondria, which generates reducing equivalent NADPH and might contribute to cytosolic NADPH level and glutathione signaling for

insulin amplification[50,77]. Nicotinamide nucleotide transhydrogenase (NNT) is a main enzyme for mitochondrial NADPH production, and inhibition of NNT causes a decline of GSIS[78,79]. Interestingly, the mitochondrial NADPH redox sensor iNAP3 indicates decreases in mitochondrial NADPH levels, while cytosolic increases in NADPH is indicated by iNAP1 and Apollo-NADP+[80,81]. In fact, the larger portion of NADPH is exported from mitochondria to the cytosol, mediated by the IDH2-dependent pyruvate-isocitrate shuttle through a reductive (counter-clockwise) TCA cycle[58]. The reductive cycle would lead to less production of mitochondrial NADH for oxidative phosphorylation and result in less mitochondrial H_2O_2 generation[80]. Therefore, redox reduction of mitochondrial GSH could be a combined effect of mitochondrial NADPH from NNT and decreased H_2O_2 as a result of reductive TCA cycle[82,83]. Overall, glucose metabolism favors export of mitochondrial NADPH to the cytosol at the expense of matrix NADH/NAD+ ratio and H_2O_2. Lack of H_2O_2 leads to GSH reduction in the mitochondria[80,83].

1.2.2.B Redox in the cytosol

NADPH is widely accepted as a dominant reducing equivalent and metabolic coupling factor for GSIS. An increase of NADPH in the cytosol is regulated by the pyruvate-isocitrate cycle, which involves the export of citrate/isocitrate to cytosol through mitochondrial citrate/isocitrate carrier (CIC). Catalysis of citrate/isocitrate to α-ketoglutarate by IDH1 generates the NADPH. Other pyruvate cycles, such as pyruvate-malate and pyruvate-citrate seems to be less impactful for cytosolic NADPH production and GSIS[57]. One of the downstream targets for NADPH is glutathione reductase (GSR). As a strong reducing equivalent, cytosolic NADPH reduces GSR to generate reduced glutathione (GSH) with the reducing power from GSH being relayed to glutaredoxin-1 (GRX1). SENP1 is then reduced and activated by GRX1, presumably leading to deSUMOylation of exocytotic machinery and enhanced insulin granule fusion. This isocitrate-to-

SENP1 signaling is one of the most important amplifying pathways controlling insulin secretory magnitude[59,84,85]. A recent study suggested that IDH1-generated NADPH might be redundant for the redox reduction of GSR and GSH reduction in GSIS[86]. In fact, other NADPH-producing pathway, such as pentose phosphate pathway could contribute to cytosolic NADPH production[87]. Although S-AMP derived from pentose phosphate pathway is postulated to contribute to insulin secretion via SENP1, NADPH might also explain the partial positive effect of pentose phosphate pathway on GSIS[60,88].

Another target for cytosolic NADPH to modulate GSIS is NADPH Oxidase-4 (NOX4). Upon increased cytosolic NADPH, NOX4 generates H_2O_2 thought to be required for the closure of K_{ATP} channel in the triggering pathway[55,89]. Contrary to this, cytosolic H_2O_2 is prone to being reduced during GSIS[90]. In addition, H_2O_2 impairs SENP1-dependent exocytosis[91,92]. The possibility for such a mysterious discrepancy might be due to the spatial and temporal control of redox signal. In fact, the NADPH/GSR/GSH/GRX/SENP1 redox relay constitutes a K_{ATP}-independent amplifying pathway for GSIS, while NADPH/NOX4/H_2O_2 mainly affects K_{ATP}-dependent triggering pathway[55,84]. SENP1 KO mouse islets exhibit impaired insulin amplification without significant effects on Ca^{2+} entry or K_{ATP} channel[84,93,94]. Instead, H_2O_2 derived from NADPH/NOX4/H_2O_2 pathway mainly mediates K_{ATP} channel inhibition to affect insulin secretion[55]. Moreover, the stimulatory effect of H_2O_2 on insulin secretion is mainly observed under low glucose, suggesting NADPH/NOX4/H_2O_2 is a critical triggering pathway component[89,95]. Perhaps, the NADPH signal can transition its targets temporally and spatially between NADPH/GSR/GSH/GRX/SENP1 and NADPH/NOX4/H_2O_2 to control triggering and amplifying of insulin secretion. A summary of these signaling pathways is illustrated **(Figure 2).**

The thioredoxin system is another important NADPH-dependent antioxidant system regulating redox state. However, thioredoxin (TXN) impairs insulin exocytosis in the presence of NADPH, indicating that TXN does not transduce reducing power to SENP1 but competes against GRX1 for reducing equivalents[59]. Interestingly, thioredoxin can reduce peroxiredoxin (PRDX), which is preferentially reactive with H_2O_2 and detoxifies it to H_2O under oxidative stress condition[96,97].

Catalase and glutathione peroxidase (GPX) are H_2O_2-degrading antioxidant and important in islet β-cell protection from oxidative stress[98–100]. However, overexpression of catalase does not interfere with GSIS, suggesting that it might be dispensable in SENP1 or H_2O_2 redox signaling[101]. Surprisingly, overexpression of a cytosol localized GPX1 in mice significantly enhances GSIS and even causes hyperinsulinemia[102,103]. In line with this, GSIS is impaired in GPX1 knockout islets[104]. Obviously, this is not due to its inactivating effect on H_2O_2 derived from NADPH/NOX4 signaling, because H_2O_2 in this pathway is an insulin secretagogue[105]. Although the exact mechanism for the positive effect of GPX1 is still missing, GPX1 might remove H_2O_2 and spare more reducing power for activation of NADPH/GSR/GSH/GRX/SENP1 signaling. Alternatively, despite GPX1 preferring H_2O_2 as a substrate, it is tempting to ask whether GPX1 directly modifies SENP1 cysteines and constitutes a GSH/GPX1/SENP1 redox relay, complementary to GSH/GRX/SENP1.

Figure 2. Glucose-Stimulated Cytosolic Redox Signaling for Insulin Secretion.

Glucose stimulates the generation of NADPH from pyruvate-isocitrate cycle and pentose phosphate pathway. On the one hand, NADPH promotes reduction of GSR, GSH and GRX1 to activate SENP1, which deSUMOylates exocytotic proteins to enhance insulin granule fusion. GPX1 might affect this redox signaling either through direct SENP1 activation or by removing H_2O_2 to prevent SENP1 inactivation. One the other hand, the pentose phosphate pathway generates NADPH for NOX4 to produce H_2O_2, which inhibits K_{ATP} channels and activates an intracellular Ca^{2+} response. S-AMP from the pentose phosphate pathway amplifies insulin secretion, dependent on the presence of SENP1. NADPH generated from the pyruvate-isocitrate cycle and pentose phosphate pathway might be interchangeably used for redox signaling. The mechanism remains unknown as to how GSH and H_2O_2 coordinate to ensure a robust GSIS. The dashed line and question mark indicate untested hypothesis or unknown mechanisms.

Figure 2.

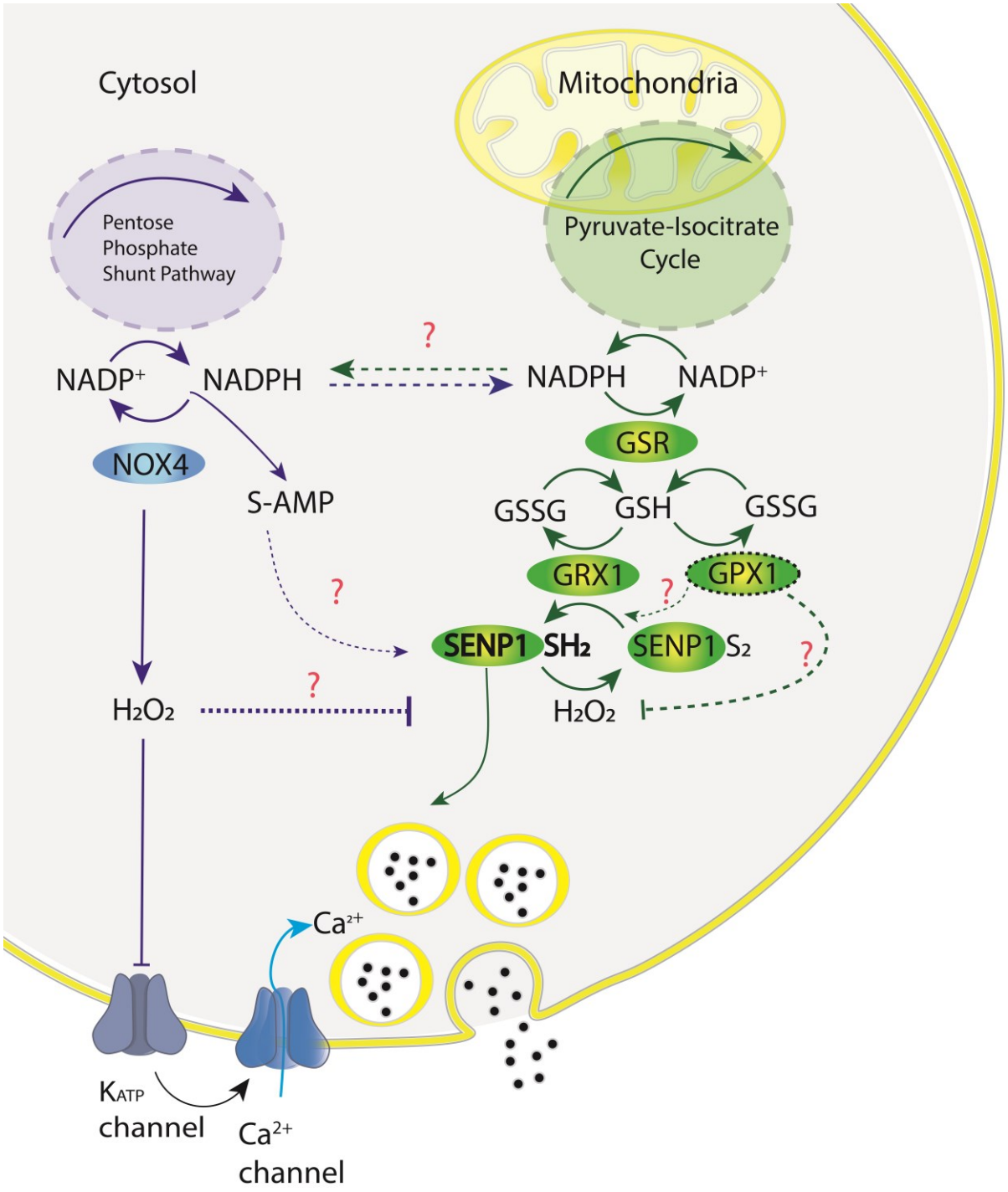
Cytosol
Mitochondria
Pentose
Phosphate
Shunt Pathway
Pyruvate-Isocitrate
Cycle
?
NADP+
NADPH
NADPH
NADP+
GSR
NOX4
S-AMP
GSSG
GSH
GSSG
GRX1
GPX1
?
?
SENP1 SH2
SENP1 S2
?
?
H2O2
H2O2
Ca2+
KATP
channel
Ca2+
channel

1.2.2.C Redox in other organelles

Endoplasmic reticulum (ER) is a cellular organelle that mediates insulin biosynthesis and enhances glucose-stimulated Ca^{2+} release[106], making Ca^{2+} channels or proteins potential targets for redox regulation. It has been shown that ryanodine receptors (RyRs) located on ER can mediate Ca^{2+}-induced Ca^{2+} release and GSIS via ROS regulation[107]. Nonetheless, limited studies have been done in pancreatic β-cells regarding how glucose-stimulated changes in ER redox state regulates insulin secretion. Instead, most studies focus on the role of ER redox on ER stress[108].

Similarly, studies on how peroxisomes regulate GSIS are rare. Interestingly, it has been documented that H_2O_2-removing anti-oxidant gene expression in peroxisomes is very low, possibly underlying the high susceptibility to oxidative stress in pancreatic β-cells[109,110].

1.2.2.D Redox and Zn^{2+}.

Autocrine Zn^{2+} signaling, following its co-release with insulin, has an inhibitory effect on GSIS, partially through modulating K_{ATP}/Ca^{2+} channels[111–114]. Although Zn^{2+} itself is redox-inert, the intracellular fluctuation of free Zn^{2+} can be tightly regulated by redox-sensitive Zn^{2+} carrier enzymes, one of which is metallothionein-1 (MT1)[115,116]. It has been shown that Zn^{2+} binds to cysteines in MT1 to form a Zn^{2+}/thiolate redox switch, which couples cellular redox to Zn^{2+} signaling[117,118]. MT1 has a high binding affinity for Zn^{2+} and low redox potential, rendering it easily oxidized to release Zn^{2+}[119]. Oxidized glutathione (GSSG) has been suggested to participate in Zn^{2+} transfer from MT1 to apo form (i.e., metal-free MT1, also called as thionein). On the other hand, GSH can inhibit Zn^{2+} release from MT1 or even mediate Zn^{2+} transfer from Zn^{2+} enzymes to thionein (the apo form of MT) [115,120]. MT1 is reported to negatively affect insulin secretion[121].

It remains to be studied if a redox change affects insulin secretion via Zn^{2+} transfer between MT1 and an unidentified target.

1.3 β-cell compensation in nutrient-induced metabolic stress

1.3.1 β-cell functional compensation

In the face of nutrient-induced metabolic stress, pancreatic β-cells can maintain glucose homeostasis by upregulating insulin output[44]. This adaptive ability is called β-cell compensation. Although it remains highly debated whether insulin hypersecretion resulting from β-cell compensation is a cause or consequence of insulin resistance, most evidence supports an early β-cell dysfunction, either due to a genetic defect or environmental stressor, as being the primary culprit for early pathogenesis of T2D[12,45]. Failure of β-cell compensation results in a relative insufficiency of insulin secretion, leading to T2D[19]. Increases in β-cell mass and insulin secretory function are two major forms of β-cell adaptive process to meet insulin demand. However, increases in β-cell insulin output appear to outweigh β-cell mass compensation in the maintenance of normoglycemia during the early prediabetes stage[122] **(Figure 3)**. Loss of the first phase of insulin secretion, rather than the reduced β-cell mass, is mainly associated with early T2D[123,124].

In a single cell sequencing study, while β-cells exhibit remarkable heterogeneity, the clusters containing the majority of β cells shows an increase of gene expression related to insulin secretion in a 7-day high fat diet intervention[125], emphasizing the importance of single β-cell functional compensation. Intracellular β-cell functional compensation can be achieved by enhancing performance at multiple stages in the stimulus-secretion coupling cascade, spanning from initial membrane depolarization, Ca^{2+} rise, sustained production of metabolites to secretory capacity[126]. All these steps are critical components constituting the triggering (K_{ATP} channel dependent) and amplifying (K_{ATP} channel independent) pathways. Functional compensation can be achieved by increasing glucose sensitivity of both triggering and amplifying pathways[127].

Figure 3. Contribution of β-cell functional and mass compensation to T2D pathogenesis.

This figure is adapted from Chen et al, 2017, Molecular Metabolism[128]. Under metabolic stress, such as HFD, β-cells compensate by increasing β-cell function early in prediabetes and enhancing proliferation later. However, persistent stress and workload can result in β-cell exhaustion and decompensation, thus leading to irreversible hyperglycemia and T2D.

Figure 3.

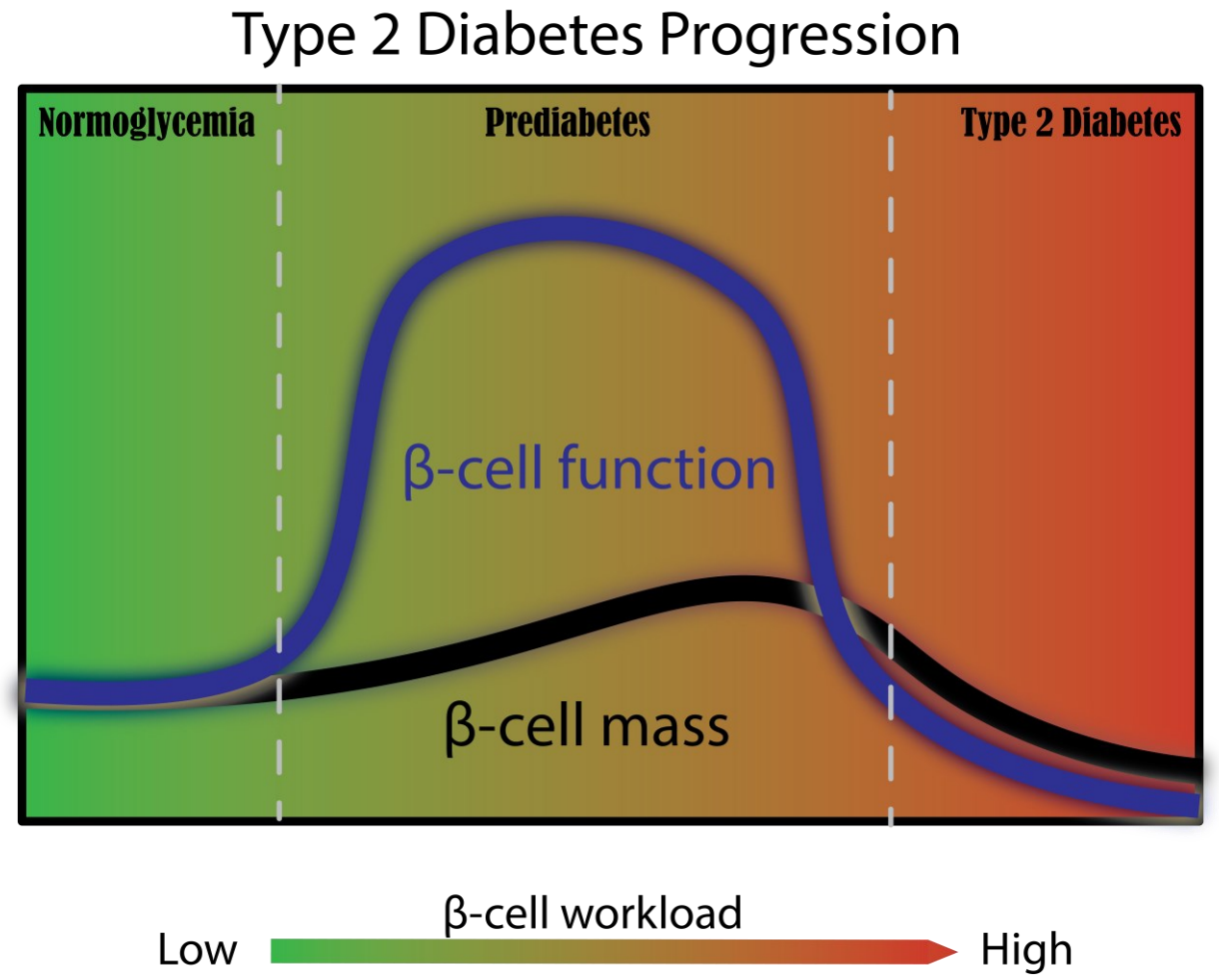
Type 2 Diabetes Progression
Normoglycemia
Prediabetes
Type 2 Diabetes
β-cell function
β-cell mass
β-cell workload
Low
High

1.3.1.A β-cell functional compensation through the triggering pathway

After overnight high glucose culture, upregulation of the triggering pathway in the β-cell can be achieved by increased glucose metabolism and reduction of K_{ATP} channel density, leading to an increase of Ca^{2+} response even at low glucose levels[129]. In line with this, islets from *ob/ob* mice had fewer K_{ATP} channels on the plasma membrane[130]. In another study, no differences in K_{ATP} channel open probability and conductance were seen, but a glucose-induced Ca^{2+} response was reported in islets from HFD obese female mice, emphasizing the importance of glucose metabolism for functional compensation[131]. Indeed, islets from *ob/ob* mice also exhibited higher glucose-induced mitochondrial activity and Ca^{2+} responses, but without changes in the KCl-induced Ca^{2+} transient[132]. Additionally, the reduced GLUT2 and unaltered glucokinase expression further indicated that glucose-induced electrical activity was primarily compensated at a step of increased mitochondrial activity instead of glycolysis[132]. Therefore, increased glucose sensitivity resulted from a left-shift of the glucose-dependent Ca^{2+} response and insulin secretion.

1.3.1.B β-cell functional compensation through amplifying pathway

The increase in the Ca^{2+} response, in fact, was mainly seen at low glucose levels and cannot entirely explain the increase in the maximal secretory response, which is largely determined by the amplification pathway independent of K_{ATP} channels (as described above in section 1.2.1)[49,127,133]. An *in vivo* longitudinal study for Ca^{2+} changes of islets transplanted into the anterior chamber of the eye hinted that HFD led to enhancement of basal Ca^{2+} and a reduction of Ca^{2+} dynamics. Whether the increased basal Ca^{2+} response is an adaptive or maladaptive process for basal hyperinsulinemia remains highly debated[134], the impaired Ca^{2+} dynamics, obviously, cannot explain the increased magnitude of GSIS. Instead, the authors reported an upregulation of the amplifying pathway and Ca^{2+} efficacy, which they suggested could involve cAMP signaling[122].

Glucose metabolism generates important metabolic coupling factors for amplifying insulin secretion[44,50]. As mentioned above, redox signals, such as NADPH from glucose metabolism, are important metabolic coupling factors for amplifying insulin secretion[50]. Interestingly, NAD(P)H signals, accompanied by increased mitochondrial oxidative metabolism, were involved in compensated exocytosis and in priming secretory granules in a mouse model of obesity[127,132]. In addition, the exocytotic machinery per se can adapt in early prediabetes to promote compound exocytosis (i.e., granule–granule fusion)[135]. Reduced expression of exocytotic granule-docking-related proteins is associated with T2D[136].

The role of FFA in β-cell function compensation is more complicated, depending on the type of FFA, concentration and, especially, exposure time[137]. While chronic exposure to free fatty acids (FFAs) causes lipotoxicity and impairs β cell function[138,139], short term challenge of FFAs can induce β-cell functional compensation, which is associated with modulation of ion channels, secretory machinery, protein synthesis, etc[139–141]. Of note, transcriptomic profiling of islets exposed to short term palmitate revealed that enhanced insulin secretion is accompanied by changes in metabolic pathways, such as accelerated glucose metabolism, fatty acid metabolism and β-oxidation[139]. Combined transcriptomic and proteomic profiling of acute palmitate treated islets also reveals increased fatty acid metabolism, inhibition of fatty acid biosynthesis and cholesterol biosynthesis[140]. Changes in intracellular lipid signaling has a broad impact on redox signaling and amplification of insulin secretion[50]. Enhanced fatty acid oxidation facilitates generation of regulatory metabolic coupling factors in mitochondria, such as NADH, an important reducing equivalent. Furthermore, fatty acid biosynthesis is a reductive process located in the cytosol requiring the presence of reducing equivalent NADPH. However, how these redox signals generated from fatty acid metabolism contribute to functional compensation remains unclear.

Amino acids play an indispensable role in amplifying insulin secretion. In obese individuals, serum insulin is positively correlated with increased branch chain amino acids (BCAA) and aromatic acids[142]. Although elevated amino acids were indicated to be biomarkers for hyperinsulinemia, insulin resistance and T2D risk[143], the beneficial effect of amino acids on T2D patients supports the idea that increased levels of amino acids level might represent an adaptive mechanism to secrete more insulin and compensate for insulin resistance[144]. However, studies to investigate how amino acid metabolism changes under compensatory conditions are very limited.

1.3.2 β-cell mass compensation

To compensate for insulin-resistance, β-cells respond by increasing their numbers or sizes. Loss of β-cell mass is reported in T2D[13]. Signals that contribute to islet expansion mainly include higher glucose, FFA and GLP-1[145–147]. Around 50-90% of islet mass expansion is observed in nondiabetic obese subjects compared to lean subjects[148–151]. However, islet proliferation and expansion in human are less pronounced than seen in mice (~9 fold)[152,153]. Moreover, the relative contribution of islet mass expansion to maintain glucose homeostasis appears to be less impactful than does functional compensation in the early stage of prediabetes[122]. Preserved islet mass compensation with abnormal β-cell function compensation cannot maintain glucose tolerance under continued HFD[154]. Instead, 60% of pancreatectomized Zucker lean rats still maintained normal glycaemia with normal insulin secretion. They developed glucose intolerance only under obesity with failed β-cell function[155]. Consistent with this, human subjects after a 50% of pancreatectomy still maintained normoglycemia with intact insulin dynamics[156]. Instead, those hemi-pancreatectomized subjects with impaired first phase insulin secretion are prone to developing T2D[45,123,157]. It is the impaired insulin dynamics, especially the impairment of first

phase insulin secretion and not the change in the islet mass, that precedes and accounts for the early progression to T2D.

1.4 SENP1 in pancreatic β-cells

1.4.1 Introduction of SUMOylation and SENPs.

The process by which small ubiquitin-related modifier (SUMO) proteins post-translationally and reversibly modify target proteins by covalent conjugation is termed SUMOylation. SUMOylation starts with the maturation of SUMO protein through sentrin-specific protease (SENP) mediated C-terminal cleavage of precursor pre-SUMO. Mature SUMO protein has C-terminal diglycine motif required for binding to an E1 enzyme (SUMO-activating enzyme). SUMO is then passed from the E1 enzyme to a conjugating enzyme E2 (Ubc9), followed by ligating protein E3-mediated attachment to a target protein at lysine residues[158]. As a member of ubiquitin protein family, although SUMO modification is not associated with proteolysis, it does shares similar features of regulating protein localization and function[159]. In human islets, SUMO members that mediate SUMOylation mainly consist of SUMO1, 2 and 3, which are widely expressed in all islet cell types[160]. SUMO1 shares only 46% sequence identity to SUMO2/3, while SUMO2 and SUMO3 are 97% identical to each other[161]. SUMO1 preferably mediates mono-SUMOylation or multiple mono-SUMOylation at different lysines. SUMO2/3 can mediate poly-SUMO chain on the same lysine (poly-SUMOylation)[162].

Other than processing the maturation of pre-SUMO precursor, SENP proteins can reverse the SUMOylation process by deconjugating SUMO from the lysine residue on target proteins, called deSUMOylation. SENP family members that carry out deSUMOylation contains SENP1, 2, 3, 5, 6, and 7, which are also expressed in human islets[125]. Even with limited isoforms, SENP can regulate a large sum of biological processes through their localization, transcriptional and post-translational control, redox-control and their differential specificity for SUMO proteins. For

example, SENP1 has a higher preference for SUMO1 deconjugation than SUMO2 and SUMO3, while SENP2 is more efficient in processing SUMO2 than SUMO1 or SUMO3[163,164]. In addition, both SENP3 and SENP5 prefers SUMO2/3 as substrates[165]. In pancreatic islets, only SENP1 and SENP2 are reported to functionally regulate biological responses[84,166].

1.4.2 Redox regulation of SUMOylation and SENP1

Among amino acids, cysteine is redox sensitive. Its redox biochemistry relies on the oxidation and reduction of the thiol group, which is involved in post-translational modification regulating an array of signaling pathways[167]. In a cellular redox reaction, H_2O_2 is the most biologically relevant and sensitive reactive oxygen species suited for cysteine modification[168]. Oxidation of thiol groups by H_2O_2 includes reversible and irreversible oxidation. In a reversible oxidation, thiol group reacts with low level of H_2O_2 to yield sulfenic acid, which can further react with a thiol group on another protein or GSH to form inter/intra molecular disulfide bond or S-glutathionylated disulfide bond. These disulfide bonds can be reversibly reduced back to free thiol groups by reducing systems, such as GSR/GSH/GRX and TrxR/Trx, which are maintained by reducing equivalent NADPH[169]. High levels of H_2O_2 induce irreversible oxidation of sulfenic acid to sulfinic acid and sulfonic acid, which cannot be reduced by biological reducing reagents. A summary of redox modification of thiols is illustrated **(Figure 4)**. While reversible oxidation is mostly implicated in transient signaling under physiological conditions, irreversible oxidation is observed in severe oxidative stress-related disease[167,170].

Figure 4. Redox modification of thiol side chain in cysteine residues.

Thiol group is reversibly oxidized by H_2O_2 to form sulfenic acid group, which can form disulfide bond or S-glutathionylated disulfide with another thiol group or GSH respectively. These disulfide bond can be reversibly reduced back to thiol groups with TrxR/Trx or GSH/GRX reducing system (green box). Alternatively, Sulfenic acid can be further irreversibly oxidized to sulfinic or sulfonic acid (red box). G: glutathione.

Figure 4.

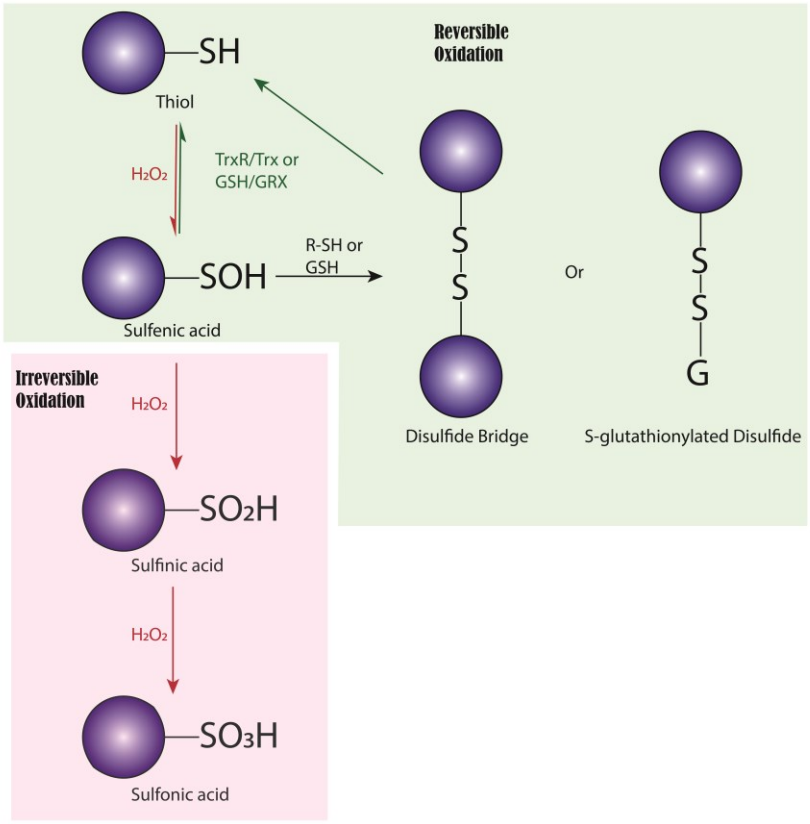
Reversible Oxidation
SH
Thiol
H2O2
TrxR/Trx or GSH/GRX
SOH
Sulfenic acid
R-SH or GSH
S
S
Disulfide Bridge
Or
S
S
G
S-glutathionylated Disulfide
Irreversible Oxidation
H2O2
SO2H
Sulfinic acid
H2O2
SO3H
Sulfonic acid

Important enzymes involved in SUMOylation and deSUMOylation harbors redox sensitive and catalytic cysteines. Upon oxidation with H_2O_2, the catalytic cysteine of SUMO E1 and E2 (Ubc9) enzymes can form a disulfide bond induced by H_2O_2 during the transfer of SUMO from E1 to E2, thus inactivating the SUMOylation process. This can be reversibly activated by reducing agents such as reduced GSH[171,172]. Similarly, SENP1 is also a redox sensitive cysteine protease under the regulation of the redox state. The catalytic C603 can form a disulfide bond with C613 upon oxidation to decrease SENP1 activity. This disulfide can be reversed by DTT (Dithiothreitol) and reduced GSH[91]. Therefore, both SUMOylation and deSUMOylation are under control of the redox state **(Figure 5)**. Interestingly, in HeLa cells, while 1 mM H_2O_2 inactivates and decreases SUMOylation by inducing disulfide bond between E1 and E2, 10 mM H_2O_2 can turn off the SENP1 activity and deSUMOylation, thus leading to a biphasic effect of H_2O_2 on whole SUMOylation level[172]. It appears that SUMOylation and deSUMOylation exhibits different sensitivity to the oxidative redox state.

Figure 5. Both the SUMOylation and deSUMOylation process are under the reversible control of redox state.

H_2O_2 induces disulfide bond formation between SUMO E1 and E2 catalytic Cysteines, while inter/intra disulfide bond is formed in SENP during exposure to H_2O_2. These processes can be reversed by reducing system. E1, E2, E3 enzymes are required for SUMOylation. S (red): SUMO, small ubiquitin-modifier.

Figure 5.

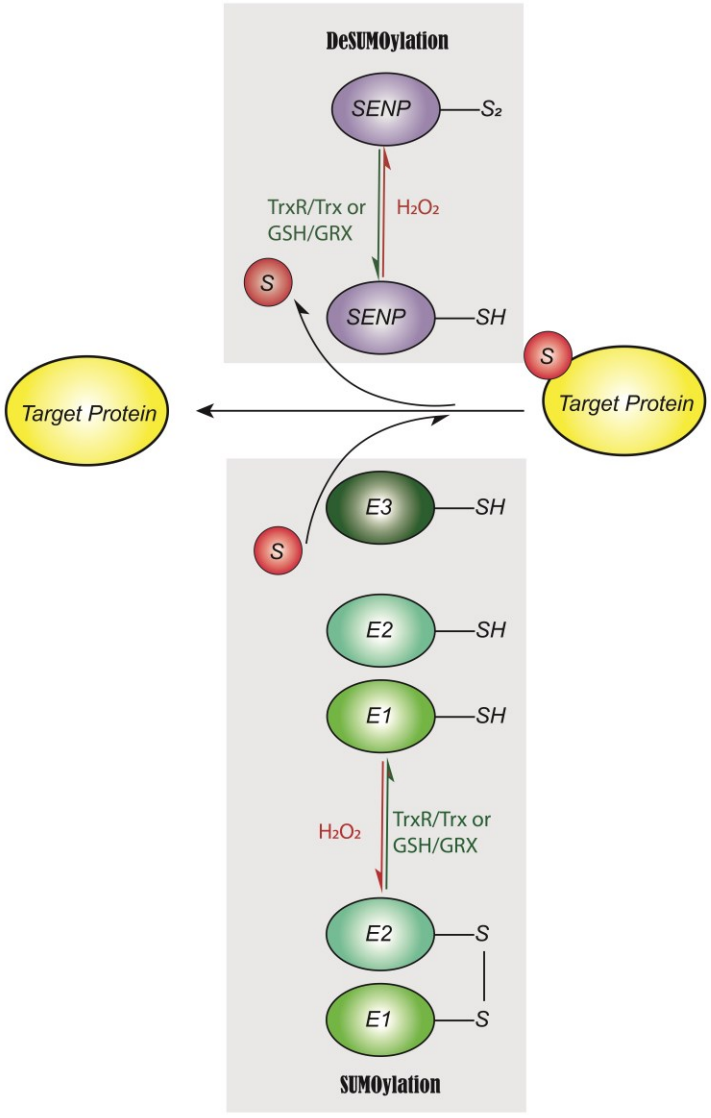
DeSUMOylation
SENP
S₂
TrxR/Trx or
GSH/GRX
H₂O₂
S
SENP
SH
S
Target Protein
Target Protein
E3
SH
S
E2
SH
E1
SH
H₂O₂
TrxR/Trx or
GSH/GRX
E2
S
E1
S
SUMOylation

1.4.3 Redox control of SENP1 in β-cell function and survival

Due to the redox chemistry of SENP1, redox dependent deSUMOylation by SENP1 is associated with different biological processes in β-cells. DeSUMOylation is a process in coupling glucose metabolism-induced redox state to insulin exocytosis. As aforementioned, SENP1 is a redox sensor and effector, coupling the redox relay (IDH-derived NADPH/GSR/GSH/GRX1) to deSUMOylated modification of exocytotic proteins, such as Tomosyn-1, Syt7, Kv2.1 channel, and Syntaxin1A[84,93,173–175]. In this case, reducing power seems to be transferred to a cytosol-localized SENP1, rather than SUMO-conjugating protein, to enhance the deSUMOylated exocytotic proteome near the plasma membrane. Treatment with H_2O_2 through cytosolic infusion abolishes the amplifying effect of SENP1[92]. In addition, chronic treatment with the saturated fatty acid palmitate or high glucose induces gluco-lipotoxicity, SUMOylation and hence impairs insulin secretion, presumably by enhancing reactive oxygen species (ROS) generation and oxidative stress[173,176,177].

While SUMOylation acts as a 'brake' on insulin exocytosis, oxidative stress seems to inactivate SENP1 and increase SUMOylation to enhance β-cell survival. For example, oxidative stress, induced by H_2O_2, can upregulate the SUMOylation of MafA, thus attenuating oxidative stress and enhancing β-cell survival[178]. Furthermore, loss of SUMOylation sensitizes β-cells to apoptosis upon exposure to cytokine IL-1β, which induced nitric oxide and apoptosis via NF-κB pathway[179,180]. Consistent with this, streptozotocin (STZ)-induced oxidative stress upregulates SUMOylation of Nrf2 for transcription of anti-oxidant genes (*Sod1*, *Sod2*, *Gpx1*), which are required for β-cell survival[181,182]. Overall, studies about the redox control of SUMOylation in β-cell support that while acute treatment of glucose induces reduction of redox state, activation of SENP1, deSUMOylation on exocytotic protein and insulin secretion, chronic treatment of high

glucose or other oxidative inducers such as palmitate and STZ lead to oxidative stress, SUMOylation and protection from apoptosis at the cost of impaired insulin exocytosis[181,183].

1.5 Incretin effect

1.5.1 Concept of incretin effect.

The incretin effect is an important regulatory signaling pathway in glucose homeostasis. It depicts a larger insulin secretory response (~60% of total insulin secretion) elicited by oral glucose compared to intravenous glucose even at identical plasma glucose levels in healthy individuals[184]. Glucose-dependent insulinotropic peptide (GIP) and Glucagon-like peptide-1 (GLP-1) were identified to be the two major incretin hormones accounting for the incretin effect[185,186]. Oral glucose enters the gut and stimulates the secretion of GIP and GLP-1, which in turn travels through blood stream and arrives at β-cells in the islets of Langerhans to increase insulin secretion. Since the secretion of GIP and GLP-1 are stimulated from the gut, intravenous glucose infusion does not activate the enteroendocrine cells to raise the plasma level of GIP and GLP-1[187]. In individuals with T2D, the incretin effect is downregulated and may contribute to the pathogenesis of T2D.

Although both GIP and GLP-1 are important for the incretin effect, the relative contribution of physiological GIP seems to be larger compared to GLP-1. The extremely low physiological level of GLP-1 argues against its direct action on β-cells as a classical incretin via an endocrine manner. Studies suggest that GLP-1 might increase insulin secretion through a gut-brain-islet axis[188]. In healthy individuals, the postprandial concentration of GIP is much higher than that of GLP-1[189]. Blockade of endogenous GIP signaling induces higher glucose excursion than blockade of endogenous GLP-1 signaling does[190,191]. In T2D individuals, GIP signaling is dramatically reduced, although oral glucose-stimulated GIP is higher compared to in non-diabetic individuals,

indicative of the impaired action of GIP[192,193]. Instead, while secretion of GLP-1 seems to be lower in T2D, the insulinotropic effectiveness of GLP-1 is still preserved to a considerable extent[194,195]. Therefore, the GLP-1 can be used therapeutically to restore the incretin effect with a pharmacological dose of GLP-1. Even so, the exact mechanism underlying the deficiency of incretin effect in T2D remains unknown[187].

1.5.2 Incretin action on pancreatic islet

The molecular signaling pathway of GLP-1 stimulated insulin secretion in pancreatic β-cells has been extensively reviewed[196,197]. Briefly, it mainly involves adenylate cyclase activation and generation of cAMP, which acts as the dominant signal via PKA/Epac to enhance glucose-dependent Ca^{2+} response and also prime insulin granules for exoytosis[198]. Importantly, the insulinotropic effect of GLP-1 is dependent on elevated glucose, and it has a critical effect on amplifying pathway via cAMP. Similar to GLP-1, GIP signaling also enhances insulin secretion mainly through cAMP. In fact, the exact difference on amplifying insulin secretion between GIP and GLP-1 receptor signaling is still not well understood. They probably share an overlapping pathway in β-cells[199].

In pancreatic α-cells, the GIP receptor is widely expressed. GIP significantly enhances glucagon secretion and, particularly when together with amino acids. This is of importance in glucagon's binding to GLP-1 receptors on neighboring β-cells to optimize insulin secretion and maintain mixed-meal tolerance[200,201]. On the contrary, GLP-1 inhibits glucagon secretion[202], even though the GLP-1 receptor is rarely expressed in α-cells[160]. Interestingly, the suppressive effect on glucagon secretion by GLP-1 is attenuated in oral glucose administration compared to intravenous glucose administration, presumably due to the glucagon-amplifying effect from GIP and GLP-

2[203–205]. The relatively higher glucagon secretion caused by oral glucose might further prime β-cell for more insulin secretion, especially to a mixed-meal. In fact, this non-classical 'incretin effect' on pancreatic α-cells might provide another layer to regulate the classical incretin effect from pancreatic β-cell[206].

1.5.3 SUMOylation and the incretin effect

Persistent activation of GLP-1 receptor signaling results in internalization of the receptor from the cell surface, which is a classical negative feedback system mediated by β-arrestins[207]. SUMOylation has been shown to be involved in the rapid loss of GLP-1 receptor signaling in response to hyperglycemia. First, chronic hyperglycemia produces elevated cAMP to activate PKA. Phosphorylation of GLP-1 receptor by PKA promotes GLP-1 receptor SUMOylation[177]. Secondly, chronic hyperglycemia could also induce an increased expression of components in the SUMOylation pathway, further strengthening the GLP-1 receptor SUMOylation, leading to GLP-1 receptor internalization and loss from the cell surface. Loss of GLP-1 receptor blunts the insulin secretion to GLP-1[208]. Therefore, SUMOylation of the GLP-1 is suggested to mediates a loss of GLP-1 receptor at the plasma membrane under hyperglycemia.

1.6 General hypothesis

The present thesis hypothesizes that SENP1 is required for β-cell functional compensation in the early stage of prediabetes, where islet mass proliferation remains unchanged. It could couple the elevated cytosolic reducing signaling to amplification of insulin secretion. In a relatively later stage of prediabetes, SENP1 activity might be downregulated by persistent oxidative stress to allow islet mass compensation at the cost of secretory function. However, this can be balanced by increased incretin signaling, a process requiring SENP1 to ensure availability of releasable insulin granules.

Collectively, this thesis hypothesizes that SENP1 activity is fine-tuned by intracellular redox change to coordinate robust insulin secretion and β-cell mass compensation to maintain normoglycemia.

1.7 SPECIFIC AIMS

1.7.1 AIM1. Investigate the mechanism underlying β-cell functional compensation and the involvement of SENP1 during early-stage prediabetes.

Functional compensation in β-cells was assessed by insulin secretion and exocytosis after short-term HFD. Intracellular changes, such as the expression of metabolic pathway genes, redox changes, and SENP1 expression, were examined to determine if they correlate with functional compensation. The necessity of SENP1 for the maintenance of functional compensation and glucose homeostasis were confirmed in gut/pancreas-specific pSENP1-KO and β-cell specific βSENP1-KO mice after short-term HFD.

1.7.2 AIM2. Investigate the molecular basis of redox-regulation of SENP1.

The molecular basis of redox-regulation of SENP1 was investigated by mutating redox-sensing cysteines in the catalytic domain of SENP1. Measuring their effects on SENP1 activity in response to redox reagents helps identify the critical cysteine required for SENP1 redox-sensing and -control of β-cell exocytosis. Zn^{2+}, which is enriched in β-cells and known to regulate cysteine protease, is examined for redox-control of SENP1 activity and SENP1-dependent exocytosis.

1.7.3 AIM3. Elucidate the role of SENP1 in β-cell compensation and glucose homeostasis during a later stage of prediabetes.

The requirement of SENP1 for glucose homeostasis was assessed in gut/pancreas specific pSENP1-KO and β-cell specific βSENP1-KO mice after a long-term HFD. Insulin secretion and exocytosis in response to glucose and other stimuli were measured to test the effect of SENP1 loss on β-cell functional compensation. Islet mass expansion were also measured in pSENP1-KO and βSENP1-KO mice.

Chapter 2.

Redox Sensing by the SUMO-Protease SENP1 Is Required for Adaptive Insulin Secretion Upon Short-Term Metabolic Stress

This chapter, and portions of Chapter 3, are part of a paper being prepared for publication.

Haopeng Lin[1, 2, 8], Kunimasa Suzuki[1, 2, 8], Nancy Smith[1, 2], Xi Li[3], Lisa Nalbach[4], Sonia Fuentes[3], Aliya F Spigelman[1, 2], Xiaoqing Dai[1, 2], Austin Bautista[1, 2], Mourad Ferdaoussi[6], Saloni Aggarwal[7], Andrew R Pepper[7], Emmanuel Ampofo[4], Leticia P Roma[5], Wen-hong Li[3], Patrick E MacDonald[1, 2]*

1. Department of Pharmacology, University of Alberta, Edmonton, AB T6G 2E1, Canada
2. Alberta Diabetes Institute, University of Alberta, Edmonton, AB, T6G 2E1, Canada
3. Departments of Cell Biology and Biochemistry, University of Texas Southwestern Medical Center, 6000 Harry Hines Blvd., Dallas, TX 75390-9039, USA
4. Institute for Clinical & Experimental Surgery, Saarland University, Homburg/Saar, Germany
5. Biophysics Department, Center for Human and Molecular Biology, Saarland University, Homburg/Saar, Germany
6. Department of Pediatrics, University of Alberta, Edmonton, AB T6G 2E1, Canada
7. Department of Surgery, University of Alberta, Edmonton, Canada
8. These authors contributed to this study equally

Contributions by co-authors to the figures are acknowledged by co-author initials.

2.1 Abstract

Pancreatic β-cells compensate for metabolic stress by upregulating insulin secretion. The underlying mechanism remains unclear. We find β-cells from young overweight humans, and mice fed high fat diet (HFD) for only 2-days, show an increased facilitation of insulin exocytosis that is unrelated to enhanced Ca^{2+} entry. RNA-seq suggests an upregulation of oxidative phosphorylation and downregulation of cholesterol biosynthesis linked to mitochondrial export of reducing equivalents after 2-day HFD. Oxygen consumption is increased and cytosolic redox is reduced in 2-day HFD islets of Cyto-roGFP2-Orp1 reporter mice. Compensatory increases in β-cell exocytosis can be blocked by direct intracellular infusion of oxidizers, and re-capitulated either by infusion of reducing agents or the SUMO-protease SENP1. Finally, while wild-type littermates maintain glucose tolerance following 2-day HFD, β-cell specific SENP1 knockout mice show rapidly worsening IP glucose tolerance and a loss of compensatory insulin exocytosis. This highlights an indispensable role for redox signaling and SENP1 in β-cell functional compensation.

2.2 Introduction

Type 2 diabetes occurs when insulin secretion from pancreatic β-cells fails to meet the peripheral insulin demand, which is increased upon the establishment of insulin resistance often coincident with obesity[12,133,209]. While obesity and insulin resistance are major risk factors for T2D, most obese individuals still maintain normoglycemia, as insulin secretion is increased adequately through β-cell functional up-regulation and mass expansion[17,210–212], although the relative contribution of each in humans remains unclear[128,151,213–215]. Functional up-regulation of β-cell insulin secretory capacity precedes increases in islet mass in mice on a high fat diet (HFD), and at early time points β-cell functional changes likely outweigh structural changes[122,216,217]. Loss of β-

cell functional adaptation may contribute to progression and deterioration to T2D even in the presence of β-cell mass enlargement[122,218,219].

Pancreatic β-cells adjust insulin secretion according to nutrient state. In a short-term fasting-refeeding study, glucose-stimulated insulin secretion (GSIS) in the fed state is enhanced along with up-regulated nutrient-sensing pathways compared to that in the fasting state[220]. In the face of short-term metabolic stress, functional up-regulation of insulin secretion compensation could be achieved at multiple points in the stimulus-secretion coupling pathway, including increased excitability, enhanced intracellular Ca^{2+} responses, or up-regulation of metabolic coupling factors and facilitation of insulin granule fusion at the plasma membrane[126,127]. The latter seem to be particularly important determinants of insulin secretory capacity during adaptation to metabolic state. In a longitudinal study linking β-cell insulin secretion and Ca^{2+} imaging, although basal Ca^{2+} was elevated (and in the face of impaired Ca^{2+} dynamics), the efficacy of Ca^{2+} induced insulin secretion was enhanced[122]. This may be due to up-regulation of the cAMP signaling and the exocytotic machinery *per se* in early prediabetes stages[122,135] (which may be subsequently followed by a reduced expression of granule-docking-related proteins in T2D[136]). Interestingly, reducing equivalents NAD(P)H signals, accompanied by increased mitochondrial oxidative metabolism, were involved in compensated exocytosis and priming of secretory granules in a mouse model of obesity[127,131,132,221]. While reducing equivalents are reported to arguably protect β-cells from oxidative stress and maintain their ability to secrete insulin during chronic HFD[98,222], the gap between reducing equivalent NADPH and improved β-cells functional performance during acute metabolic stress is still missing.

Upon glucose stimulation, NADPH can be coupled by cytosolic H_2O_2 and sentrin-specific protease-1 (SENP1), respectively to insulin exocytosis[55,84]. While NOX4-derived H_2O_2 directly inhibits K_{ATP} channels and increases Ca^{2+} influx to trigger insulin release, SENP1 is a deSUMOylating enzyme which can amplify insulin exocytosis by modifying exocytotic proteins without significant effects on Ca^{2+} entry[84,92,173,174,183,223]. The activity of SENP1 is dependent on cytosolic reducing equivalent NADPH derived from glucose metabolism[84,91]. Therefore, the subtle balance of SUMOylation may be important, both for β-cell function and viability under different pathological conditions and different stages of diabetes[183]. SUMOylation is reportedly required for the maintenance of β-cell viability in mice under excessive oxidative stress induced by STZ[181]. In contrast, deletion of SENP1 (increased SUMOylation) impaired incretin effects and oral glucose homeostasis, under the metabolic stress of a 8-week high fat diet, a functional decompensation stage characterized presumably by oxidative stress, partial inactivation of SENP1 and impaired GSIS as shown in chapter 4[223–225]. It remains unknown whether the change of redox state and SENP1 affects β-cell functional compensation and glucose homeostasis at a very early compensational stage of prediabetes.

To this aim, we assessed the change in redox signaling, including SENP1, and its effect on compensational insulin increase in response to short-term HFD. Finally, we generated islet- and β-cell- specific SENP1 knockout mice to investigate the role of SENP1 for β-cell functional compensation and glucose homeostasis under acute high fat diet.

2.3 Results

2.3.1 Secretory capacity is upregulated in β-cells of humans with elevated BMI or from mice after short-term exposure to high fat diet

Islets from young human donors (21-45 years of age) with high BMI (>25) exhibited significantly elevated insulin secretion at 10 mM and 16.7 mM glucose compared to young donors with low BMI (<25). This increased functionality was lost in T2D (BMI > 25) **(Figure 6A)**. No significant difference was seen at 1 mM **(Figure 6A)**. Intriguingly, β-cells from young donors with BMI >25 didn't show any difference in depolarization-induced exocytosis compared to BMI <25 at 5 mM or 10 mM glucose. Instead, the exocytotic response was higher at 1 mM glucose, indicative of an increase in the insulin granule priming effect occurring even at low glucose levels **(Figure 6B)**. Islets from older and overweight donors (age >45, BMI >25) showed a more modest increase in GSIS **(Figure 6C)** and no difference in β-cell exocytosis **(Figure 6D)**, although β-cells from older donors with T2D still showed lower insulin secretion and exocytosis compared to overweight non-diabetic donors **(Figure 6C, D)**.

To investigate the underlying mechanism of β-cell functional changes that occur early under metabolic stress, C57BL/6 mice were fed either a chow diet (CD) or high fat diet (HFD) for 2 days. Mice fed a 2-day HFD maintained a normal glucose response to an intraperitoneal glucose tolerance test (IPGTT) **(Figure 6E)**, along with increased plasma insulin **(Figure 6F)**. Islets isolated from 2-day HFD mice showed increased GSIS **(Figure 6G)**, without any effect on insulin content **(Figure 6H)**. By comparison, after a 4-week exposure to HFD, mice were glucose intolerant **(Figure 7A)** with increased plasma insulin **(Figure 7B)** and enhanced *in vitro* islet insulin secretion and increased insulin content **(Figure 7C, D)**.We previously showed that the

depolarization-induced exocytotic response of both mouse and human β-cells was amplified by glucose[84]. In β-cells from 2-day **(Figure 6I)** and 4-week **(Figure 7F)** HFD fed mice, exocytotic responses are increased at low glucose, to the same level as in glucose-stimulated cells. This suggests that signals to amplify insulin exocytosis are up-regulated, even at low glucose, soon after starting the HFD. This was without difference in voltage-activated Ca^{+} charge entry **(Figure 6J)** and intracellular Ca^{2+} responses **(Figure 6K**; **Figure 7G)**, consistent with previous demonstrations of 'increased Ca^{2+} efficacy' under short-term HFD[122]. Indeed, under conditions known to 'clamp' intracellular Ca^{2+} responses to assess the glucose-dependent amplification of insulin secretion[226], islets from 4-week HFD fed mice exhibited higher insulin secretion only at low glucose levels **(Figure 7E)**.

Figure 6. Islets from overweight human donors and 2-day HFD male mice exhibited higher insulin secretion and exocytosis.

(A): Insulin secretion of young (45>age>21) human islets. (N=27-47 non-diabetic donors and 4-5 diabetic donors per condition). **(B):** Exocytotic response of β-cells from young (45>age>21) human islets. (N=11-33 non-diabetic donors with 63-236 cells and 4-5 diabetic donors with 21-36 cells per condition). **(C):** Insulin secretion of older (age>45) human islets. (N=40-111 non-diabetic donors and 18-21 diabetic donors per condition). **(D):** Exocytotic response of β-cells from older (age>45) human islets. (N=30-73 non-diabetic donors with 164-473 cells and 15-18 diabetic donors with 78-112 cells per condition). **(E):** IPGTT of male C57BL/6 mice after CD and 2-day HFD (n=14 and 14 mice). **(F):** Plasma insulin level during IPGTT (n=7 and 8 mice). **(G):** Insulin secretion (n=10 and 11 mice). **(H):** Insulin contents (n=10 and 11 mice). **(I):** Representative traces (left), and average total responses, of β-cell exocytosis elicited by a series of 500 ms membrane depolarizations from -70 mV to 0 mV at 2.8- and 10-mM glucose (N=3 pairs of mice, n=21-33 cells). **(J):** Representative traces, and average voltage-dependent Ca^{2+} currents, of β-cell elicited by a single 500 ms membrane depolarization from -70 mV to 0 mV at 2.8- and 10-mM glucose (n=15-26 cells). **(K):** Single cell Ca^{2+} response (n=16, 34 cells from 5 and 4 mice). Data are mean ± SEM and were compared with student t-test, one-way or two-way ANOVA followed by Bonferroni post-test. *$P < 0.05$, **$P < 0.01$. Except in A-D, *$P < 0.05$ (BMI>25 ND vs BMI<25 ND), \$$P < 0.05$ (BMI>25 ND vs BMI>25 T2D), #$P < 0.01$ (BMI<25 ND vs BMI>25 T2D). (XD, AB, AS performed A-C. HL performed D-K except G performed by AS.)

Figure 6.

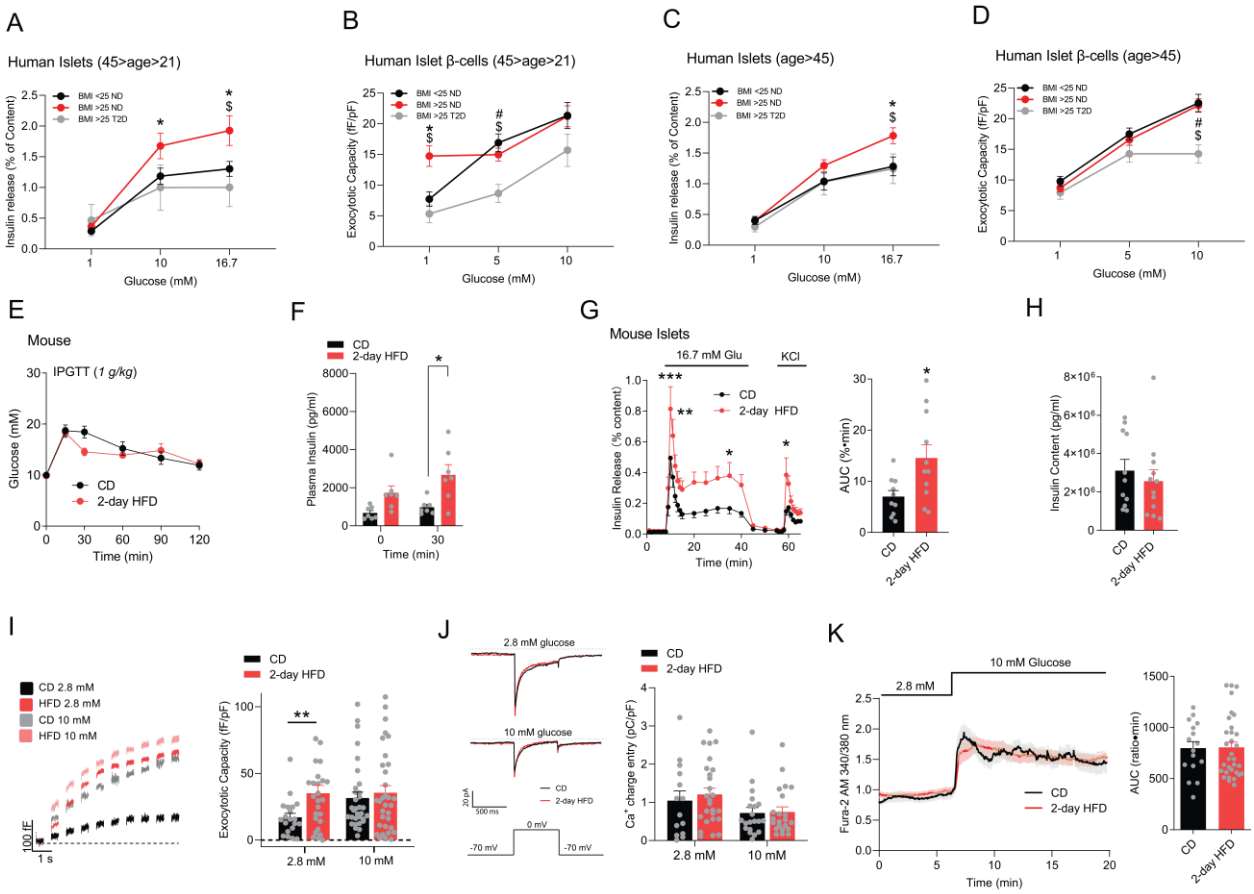
A
Human Islets (45>age>21)
Insulin release (% of Content)
Glucose (mM)
B
Human Islet β-cells (45>age>21)
Exocytotic Capacity (fF/pF)
Glucose (mM)
C
Human Islets (age>45)
Insulin release (% of Content)
Glucose (mM)
D
Human Islet β-cells (age>45)
Exocytotic Capacity (fF/pF)
Glucose (mM)
BMI <25 ND
BMI >25 ND
BMI >25 T2D
E
Mouse
IPGTT (1 g/kg)
Glucose (mM)
Time (min)
CD
2-day HFD
F
Plasma Insulin (pg/ml)
Time (min)
G
Mouse Islets
16.7 mM Glu
KCl
Insulin Release (% content)
Time (min)
AUC (%•min)
H
Insulin Content (pg/ml)
I
CD 2.8 mM
HFD 2.8 mM
CD 10 mM
HFD 10 mM
100 fF
1 s
Exocytotic Capacity (fF/pF)
2.8 mM
10 mM
J
2.8 mM glucose
10 mM glucose
20 pA
500 ms
0 mV
-70 mV
Ca2+ charge entry (pC/pF)
K
2.8 mM
10 mM Glucose
Fura-2 AM 340/380 nm
Time (min)
AUC (ratio•min)

Figure 7. Increased insulin secretion and exocytosis after 4-week HFD.

(A): IPGTT of male C57/B6 mice after CD and 4-week HFD (n=7 and 8 mice). **(B):** Plasma insulin level during IPGTT (n=3 and 3 mice) **(C):** Insulin contents (n=22 and 22 mice) **(D):** Insulin secretion (n=8 and 8 mice) **(E):** Insulin secretion in the presence of diazoxide/KCl. (n=7 and 7 mice). **(F):** Exocytotic response (n= 21, 25, 23, 25 cells from 3 pairs of mice). **(G):** Single cell Ca^{2+} response (n=40, 34 cells from 4 pairs of mice). Data are mean ± SEM and were compared with student t-test, one-way or two-way ANOVA followed by Bonferroni post-test. *$P < 0.05$, **$P < 0.01$. (All work by HL, NS, AS.)

Figure 7.

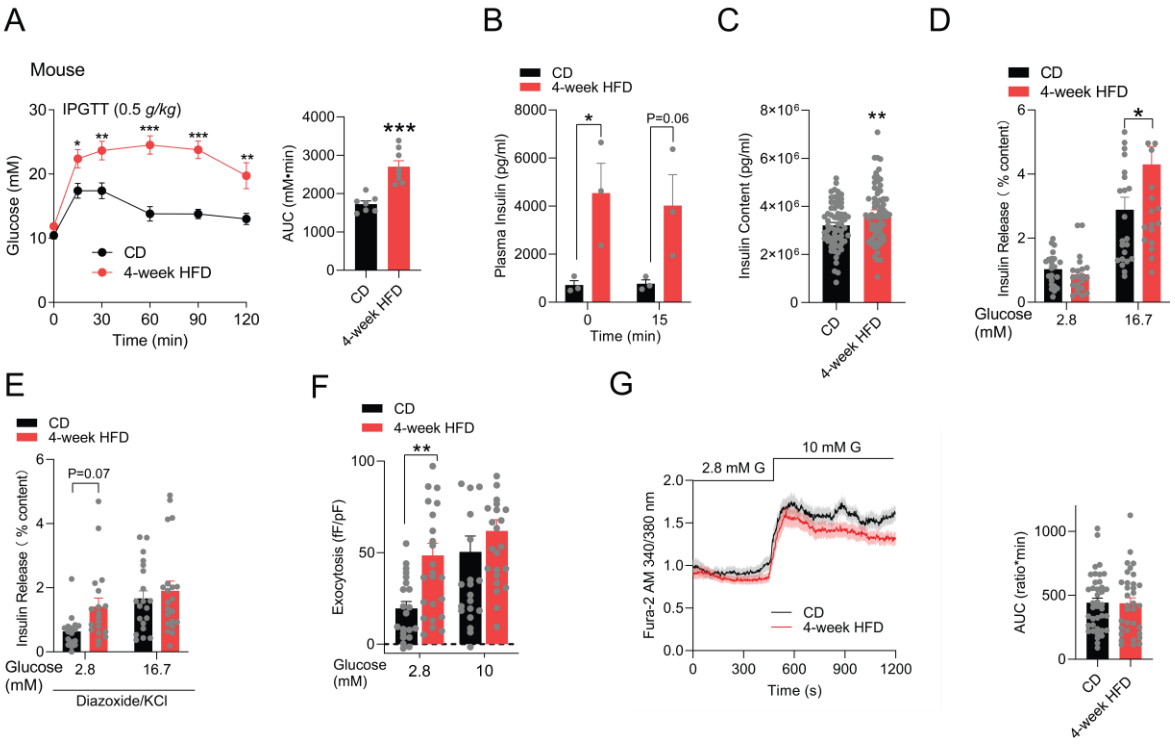
A
Mouse
IPGTT (0.5 g/kg)
Glucose (mM)
Time (min)
CD
4-week HFD
AUC (mM•min)
B
Plasma Insulin (pg/ml)
P=0.06
C
Insulin Content (pg/ml)
D
Insulin Release (% content)
Glucose (mM)
E
P=0.07
Diazoxide/KCl
F
Exocytosis (fF/pF)
G
2.8 mM G
10 mM G
Fura-2 AM 340/380 nm
AUC (ratio*min)

2.3.2 Increased glucose metabolism contributed to the reduction of cytosol

To gain insight into the mechanism that contributes to increased insulin secretory function following short-term HFD[125], we performed RNA sequencing on FACS-sorted β-cells from 2-day CD and HFD mice. We found 213 differentially expressed (DE) genes **(Figure 8A)**. Enrichment analysis of DE genes on Metascape identified pathways (PW) known to be involved in β-cell functional compensation, such as histone methylation, MAPK signaling, cholesterol biosynthesis, insulin receptor signaling, and ER-associated misfolded protein response **(Figure 8B)**[220,227–229]. As the most significantly enriched pathway in this study, histone methylation can modify the epigenomic profile and control the transcriptomic efficiency. To examine how those genes involved in histone methylation can interact or overlap with other genes from different enriched pathways, all DE genes were submitted to STRING database analysis[230] for protein-protein interaction, which were highlighted by links in the Circos plot **(Figure 8B)**. Histone methylation-related genes can interact or overlap with genes in other pathways, such as MAPK signaling, consistent with a previous study showing that methylation can adapt insulin secretion through MAPK signaling and regulation of glucose metabolism[220].

Gene set enrichment analysis (GSEA) showed that up-regulated genes were enriched for oxidative phosphorylation and glycolysis **(Figure 8C)**. DE genes over-represented in oxidative phosphorylation pathway were significantly upregulated, especially *Cdk1* (most upregulated gene) and *Ccnb2* which were shown to increase oxygen consumption rate, citrate cycling and NADPH production in islet β-cells **(Figure 8A, C)** [231], suggesting that upon 2-day HFD β-cells could favor glucose metabolism for production of NADPH in the cytosol **(Figure 8D)**.

Interestingly, the metabolic pathway associated with cholesterol biosynthesis was the second most significantly down-regulated. Those genes (*Fdft1*, *Hsd17b7*, *Msmo1*, *Fdps*, *Hmgcs1*) enriched for metabolism of cholesterol were significantly down-regulated **(Figure 8C, D)**. Cholesterol biosynthesis is a NADPH-consuming anabolic process[232]. Inhibition of cholesterol biosynthesis might enhance insulin secretion by increasing NADPH[233]. Therefore, the downregulation of cholesterol biosynthesis gene could possibly spare cytosolic NADPH for the amplification of insulin release **(Figure 8D)**[234]. Collectively, these results indicate that HFD remodels the metabolic preference from cholesterol biosynthesis to glucose metabolism and may reduce the cytosolic redox state.

Figure 8. RNA sequencing of male mice on CD and 2-day HFD.

(A): β-cells from CD and 2-day HFD were isolated through fluorescence activated cell sorting (FACS) for mRNA sequencing. 213 genes were identified differentially expressed (DE) genes after 2-day HFD (n=213 genes, N=4, 3 mice). **(B):** All DE genes were submitted to Metascape for functional enrichment analysis. Expression of DE genes on CD and HFD were normalized to z-scores by gene and colorized in circos heat map. Enrichment and cluster analysis were performed on Metascape and six most enriched pathway (PW) illustrated as circos plot. All DE genes were submitted to STRING database for protein-protein interaction. The related protein interactions for DE genes enriched in the six PW were highlighted as links in the circos plot. **(C):** Gene set enrichment analysis (GSEA) showed significant up- and down-regulated enriched pathway after HFD with false discovery rate (FDR) less than 0.05. All nominal *p*-value were less than 0.01. Normalized enrichment score (NES) reflects the degree to which a gene set is overrepresented in a ranked list of genes. **(D):** Illustration of transcriptomic changes related to metabolism after 2-day HFD. Increased glucose metabolism and downregulated cholesterol biosynthesis lead to the buildup of cytosolic NADPH, required for amplifying insulin secretion. (HL, WL and XL performed A. HL performed B-D. HL prepared all the samples.)

Figure 8.

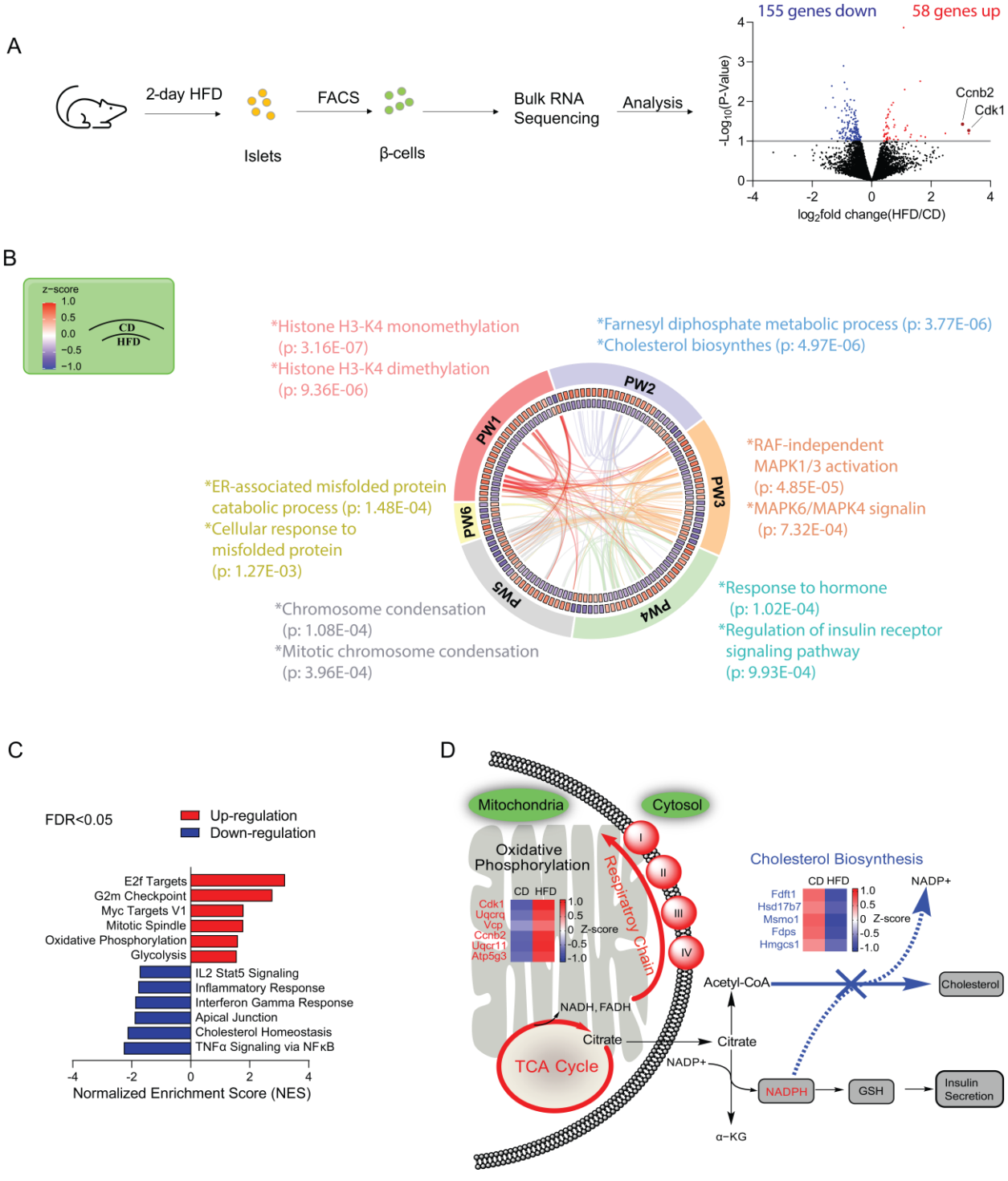
A
2-day HFD
Islets
FACS
β-cells
Bulk RNA Sequencing
Analysis
155 genes down
58 genes up
Ccnb2
Cdk1
-Log10(P-Value)
log2fold change(HFD/CD)
B
z-score
1.0
0.5
0.0
−0.5
−1.0
CD
HFD
*Histone H3-K4 monomethylation (p: 3.16E-07)
*Histone H3-K4 dimethylation (p: 9.36E-06)
*Farnesyl diphosphate metabolic process (p: 3.77E-06)
*Cholesterol biosynthes (p: 4.97E-06)
*RAF-independent MAPK1/3 activation (p: 4.85E-05)
*MAPK6/MAPK4 signalin (p: 7.32E-04)
*ER-associated misfolded protein catabolic process (p: 1.48E-04)
*Cellular response to misfolded protein (p: 1.27E-03)
*Chromosome condensation (p: 1.08E-04)
*Mitotic chromosome condensation (p: 3.96E-04)
*Response to hormone (p: 1.02E-04)
*Regulation of insulin receptor signaling pathway (p: 9.93E-04)
PW1
PW2
PW3
PW4
PW5
PW6
C
FDR<0.05
Up-regulation
Down-regulation
E2f Targets
G2m Checkpoint
Myc Targets V1
Mitotic Spindle
Oxidative Phosphorylation
Glycolysis
IL2 Stat5 Signaling
Inflammatory Response
Interferon Gamma Response
Apical Junction
Cholesterol Homeostasis
TNFα Signaling via NFκB
Normalized Enrichment Score (NES)
D
Mitochondria
Cytosol
Oxidative Phosphorylation
CD HFD
Cdk1
Uqcrq
Vcp
Ccnb2
Uqcr11
Atp5g3
Z-score
Respiratroy Chain
I
II
III
IV
NADH, FADH
Citrate
TCA Cycle
Cholesterol Biosynthesis
Fdft1
Hsd17b7
Msmo1
Fdps
Hmgcs1
NADP+
Acetyl-CoA
Cholesterol
Citrate
NADP+
NADPH
GSH
Insulin Secretion
α-KG

2.3.3 Cytosolic redox signaling via SENP1 increased β-cell function following 2-day HFD

Consistent with upregulation of transcripts involved in oxidative phosphorylation, islets from 2-day HFD consumed higher amounts of oxygen at 2.8 mM glucose **(**Error! Reference source not found.**A)**, similar to reports from a 3-month HFD model[235]. Additionally, we confirmed in islets of male mice expressing the cytosolic redox sensor Cyto-roGFP2-Orp1[236] that the cytosol in β-cells from 2-day HFD mice was more reduced compared to control mice fed CD **(**Error! Reference source not found.**B)**. A reducing signal appears responsible for enhanced β-cell exocytosis at low glucose, since this was recapitulated in CD β-cells upon direct intracellular dialysis of reduced glutathione (GSH), which could not increase exocytosis further in HFD β-cells **(**Error! Reference source not found.**C)**. Conversely, the elevated exocytosis seen in HFD β-cells was reversed by direct intracellular application of H_2O_2 **(**Error! Reference source not found.**D**). Previously we showed that the SUMO-protease SENP1 couples redox state to insulin exocytosis **(**Error! Reference source not found.**E)**[84], and here we find some evidence in our RNAseq data for a significant and selective upregulation of *Senp1* in β-cells after 2-day HFD **(**Error! Reference source not found.**F)**, which we confirmed by qPCR **(**Error! Reference source not found.**G)**. Direct intracellular infusion of active SENP1 catalytic protein increases exocytosis in CD β-cells but cannot increase exocytosis further in HFD β-cells **(**Error! Reference source not found.**H)**, similar to the effect of GSH. Zn^{2+} was shown to affect SENP1 activity as mentioned in Chapter 3, but neither cytosolic nor granular Zn^{2+} changed after 2-day HFD **(Figure 9I)**. These data suggest that short-term HFD leads to an upregulation of cytosolic reducing equivalents that augments β-cell exocytosis, possibly via SENP1.

Figure 9. Reducing redox state of cytosol contributes to exocytosis in β-cells from male mice following 2-day HFD exposure.

(A): Oxygen consumption rate at 2.8 mM glucose (N=4, 5 mice). **(B):** Representative image of pancreatic islets (white dashed circle) carrying cyto-roGFP2-Orp1 sensor (left). Scale bar = 100 μm. Redox ratio of individual islets (n= 65, 41 islets from 6 pairs of mice). **(C, D):** Exocytosis with infusion of **(C)** 10 μM GSH or **(D)** 200 μM H_2O_2 at 2.8 mM glucose after 2-day HJFD. (C - n=26-56 cells from 4, 4 mice, D - n= 39-56 cells from 7, 7 mice). **(E):** Illustration of redox-controlled insulin secretion. GSH activated GRX1 by transducing reducing power, followed by reducing power transfer from GRX1 to SENP1 and activation of SENP1, finally enhancing insulin exocytosis. **(F):** SENP isoform expression from RNA sequencing of islets from mice on chow or HFD fed mice (N=4, 3 mice)**. (G):** SENP1 gene mRNA expression after HFD (N=2-9 mice). **(H):** Exocytosis with infusion of 4 μg/mL catalytic SENP1 (cSENP1). (n=21-33cells from 4, 4 mice per group) at 2.8 mM glucose. **(I):** Normalized medium fluorescence intensity (MFI) of β-cells cytosolic Zn^{2+} (Zn-AF2) and granular Zn^{2+} (ZIGIR), n = 4 pairs of mice after 2-day HFD. MFI of CD group was arbitrarily set to 1. Data are mean ± SEM and were compared with student t-test, one-way ANOVA followed by Bonferroni post-test. *$P < 0.05$, **$P < 0.01$, * **$P < 0.001$. (LN, LPR and EA performed B-C. HL performed C-F, KS perform G. SF performed I.)

Figure 9.

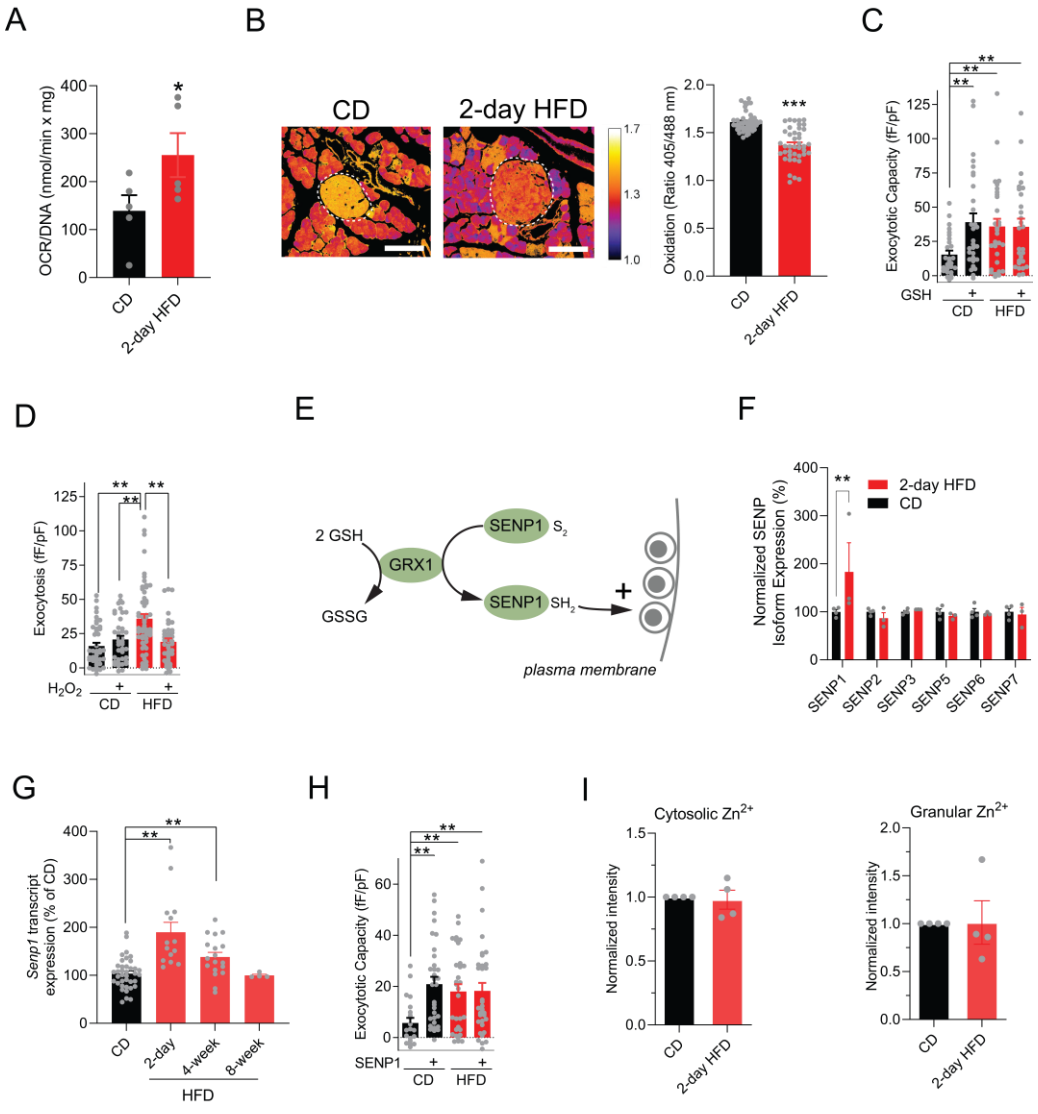
A
OCR/DNA (nmol/min x mg)
CD
2-day HFD
B
CD
2-day HFD
Oxidation (Ratio 405/488 nm)
C
Exocytotic Capacity (fF/pF)
GSH
CD
HFD
D
Exocytosis (fF/pF)
H2O2
E
2 GSH
GRX1
GSSG
SENP1 S2
SENP1 SH2
plasma membrane
F
Normalized SENP Isoform Expression (%)
2-day HFD
CD
SENP1
SENP2
SENP3
SENP5
SENP6
SENP7
G
Senp1 transcript expression (% of CD)
2-day
4-week
8-week
HFD
H
Exocytotic Capacity (fF/pF)
SENP1
I
Cytosolic Zn2+
Granular Zn2+
Normalized intensity

2.3.4 Rapid glucose intolerance during short-term HFD in βSENP-KO mice

To test if SENP1-dependent redox pathway is required for glucose homeostasis during short-term HFD, we put gut/pancreas (pSENP1-KO) and β-cell (βSENP1-KO) specific SENP1 KO mice on 2-day and 4-week HFD. After 2-day HFD, male pSENP1-KO developed impaired intraperitoneal (IP) glucose tolerance **(Figure 10A, C)**. This was similar to findings in a β-specific SENP1 knockout line **(Figure 10E, G)** with reduced IP plasma insulin **(Figure 10I)** and loss of an up-regulation of exocytosis at low glucose **(Figure 11A)** after 2-day HFD, but less obvious in female mice which are more resistant to HFD[237] **(Figure 13A-D, Figure 14A, B, D, F, G, I).** While male pSENP1-KO mice also became more intolerant of glucose when delivered orally after 2-day HFD **(Figure 10B, D)**, in general impaired IP glucose tolerance was more obvious after 2-day HFD in the βSENP1-KO **(Figure 10E-J)**. After 4-week HFD however, oral glucose intolerance became more prominent in the pSENP1-KO and βSENP1-KO males **(Figure 12)** with a loss of up-regulated exocytosis **(Figure 11B)**, although again the females were generally more insensitive to HFD-induced glucose intolerance **(Figure 13E, Figure 14C, H, E, J)**. This is consistent with our study at 8 weeks of HFD in both the pSENP1-and βSENP1-KO models shown in chapter 4[238].

Figure 10. IPGTT and OGTT of male pSENP1-KO and βSENP1-KO following CD and 2-day HFD.

(A-D): IPGTT and OGTT of male pSENP1-KO on CD and 2-day HFD (A – n=9, 8 mice, B – n=6, 6 mice, C – n=10, 11 mice, D – n= 10, 8 mice). **(E-J):** IPGTT, OGTT and plasma insulin of male βSENP1-KO on CD and 2-day HFD (E – n=6, 5, F – n=4, 4, G – n= 10, 12, H – n=12, 10, I – n= 8, 8, J – n= 4, 6). Data are mean ± SEM and were compared with student t-test, one-way or two-way ANOVA followed by Bonferroni post-test. **P* < 0.05, ***P* < 0.01. (NS and HL performed experiment and analyzed the data.)

Figure 10.

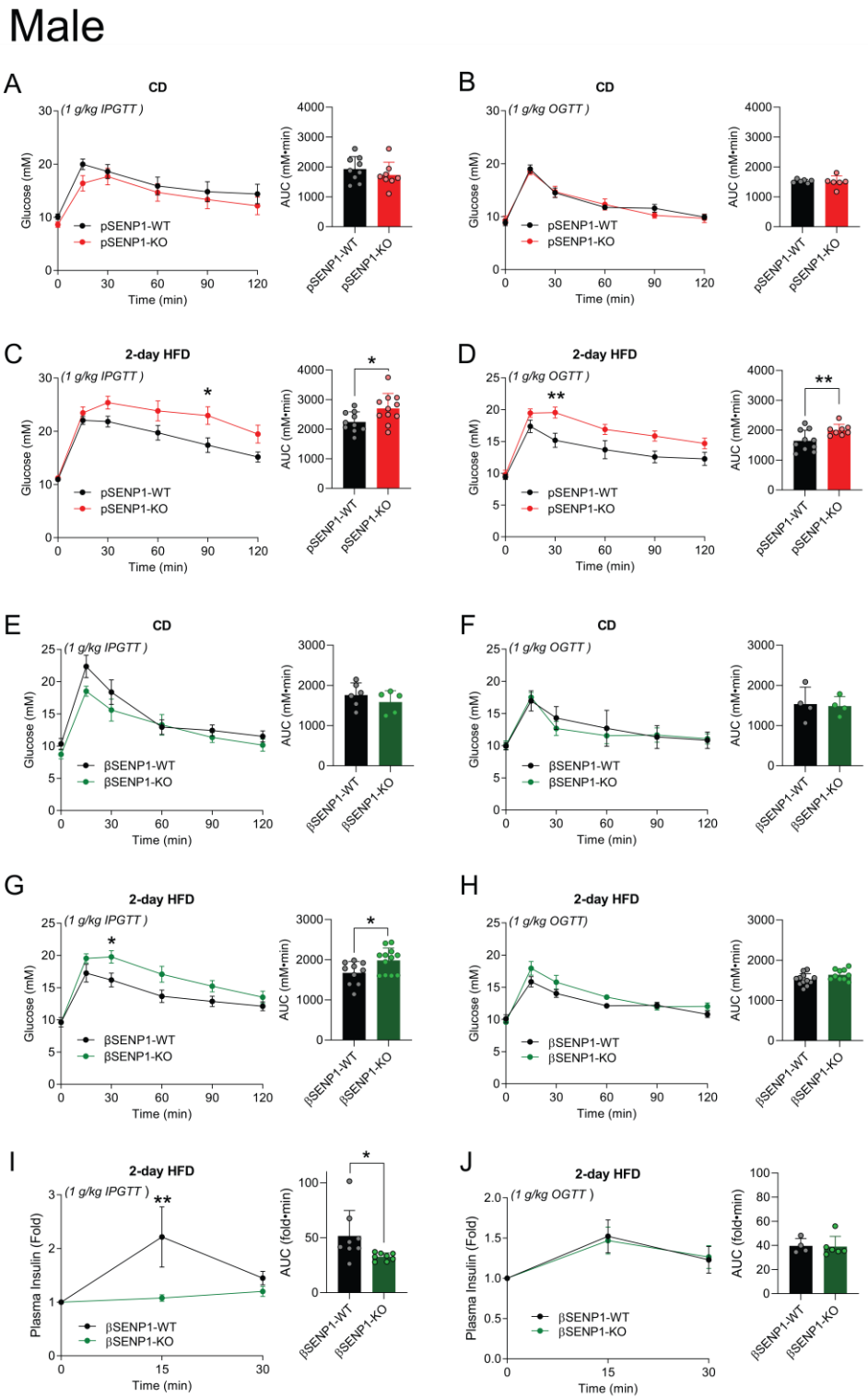
Male
A
CD
(1 g/kg IPGTT)
Glucose (mM)
Time (min)
pSENP1-WT
pSENP1-KO
AUC (mM•min)
B
CD
(1 g/kg OGTT)
C
2-day HFD
(1 g/kg IPGTT)
D
2-day HFD
(1 g/kg OGTT)
E
CD
(1 g/kg IPGTT)
βSENP1-WT
βSENP1-KO
F
CD
(1 g/kg OGTT)
G
2-day HFD
(1 g/kg IPGTT)
H
2-day HFD
(1 g/kg OGTT)
I
2-day HFD
(1 g/kg IPGTT)
Plasma Insulin (Fold)
AUC (fold•min)
J
2-day HFD
(1 g/kg OGTT)

Figure 11. ***In vitro*** **exocytosis and insulin secretion for isolated islet from male βSENP1-WT and βSENP1-KO following 2-day and 4-week HFD.**

(A): Exocytosis for isolated islet from βSENP1-WT and βSENP1-KO after 2-day HFD (n=18-56 cells). **(B):** Exocytosis for isolated islet from βSENP1-WT and βSENP1-KO after 4-week HFD (n=30-65 cells). Data are mean ± SEM and were compared using student t-test, one-way ANOVA followed by Bonferroni post-test. *$P < 0.05$, **$P < 0.01$. (All work by HL.)

Figure 11.

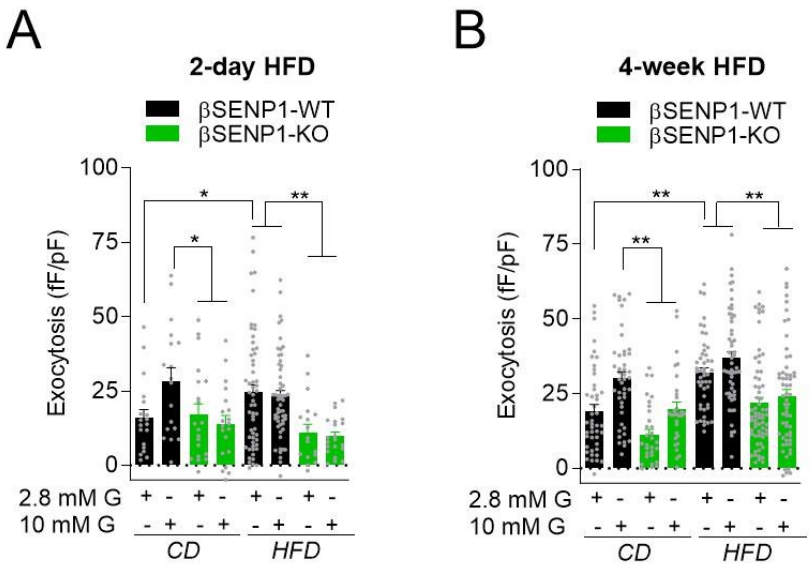
A
2-day HFD
βSENP1-WT
βSENP1-KO
Exocytosis (fF/pF)
100
75
50
25
0
*
*
**
2.8 mM G + - + - + - + -
10 mM G - + - + - + - +
CD
HFD
B
4-week HFD
βSENP1-WT
βSENP1-KO
Exocytosis (fF/pF)
100
75
50
25
0
**
**
**
2.8 mM G + - + - + - + -
10 mM G - + - + - + - +
CD
HFD

Figure 12. IPGTT and OGTT of male pSENP1-KO and βSENP1-KO following 4-week HFD.

(A): OGTT of male pSENP1-KO and -WT on 4-week HFD (n=11, 9 mice). **(B-E):** OGTT, IPGTT and plasma insulin of male βSENP1-KO and -WT on 4-week HFD (B – n=13, 11, C – n= 8, 8, D – n=8, 14, E – n=6, 11). Data are mean ± SEM and were compared using student t-test, one-way ANOVA followed by Bonferroni post-test. **P* < 0.05. (NS and HL performed experiment and analyzed the data.)

Figure 12.

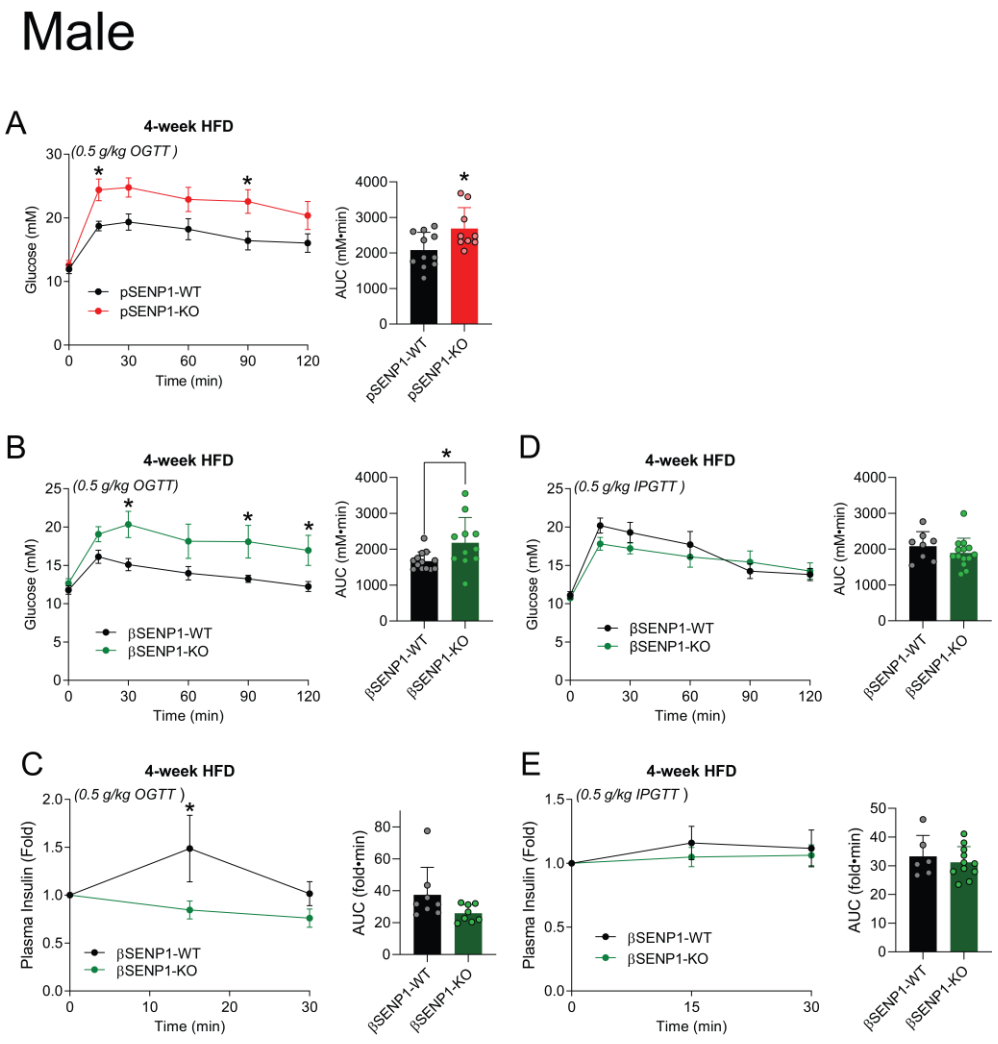
Male
A
4-week HFD
(0.5 g/kg OGTT)
Glucose (mM)
Time (min)
pSENP1-WT
pSENP1-KO
AUC (mM•min)
B
4-week HFD
(0.5 g/kg OGTT)
βSENP1-WT
βSENP1-KO
C
4-week HFD
(0.5 g/kg OGTT)
Plasma Insulin (Fold)
AUC (fold•min)
D
4-week HFD
(0.5 g/kg IPGTT)
E
4-week HFD
(0.5 g/kg IPGTT)

Figure 13. IPGTT and OGTT of female pSENP1-WT and pSENP1-KO following CD and HFD.

(A-B): IPGTT of female pSENP1-KO and -WT on CD and 2-day HFD (A - n=19, 10 mice, B - n=10, 9 mice). **(C-E):** OGTT of female pSENP1-KO and -WT on CD, 2-day, and 4-week HFD (C - n=8, 9 mice, D - n=8, 9 mice, E - n=8, 9 mice). Data are mean ± SEM and were compared with student t-test, one-way ANOVA followed by Bonferroni post-test. $*P < 0.05$. (NS and HL performed experiment and analyzed the data.)

Figure 13.

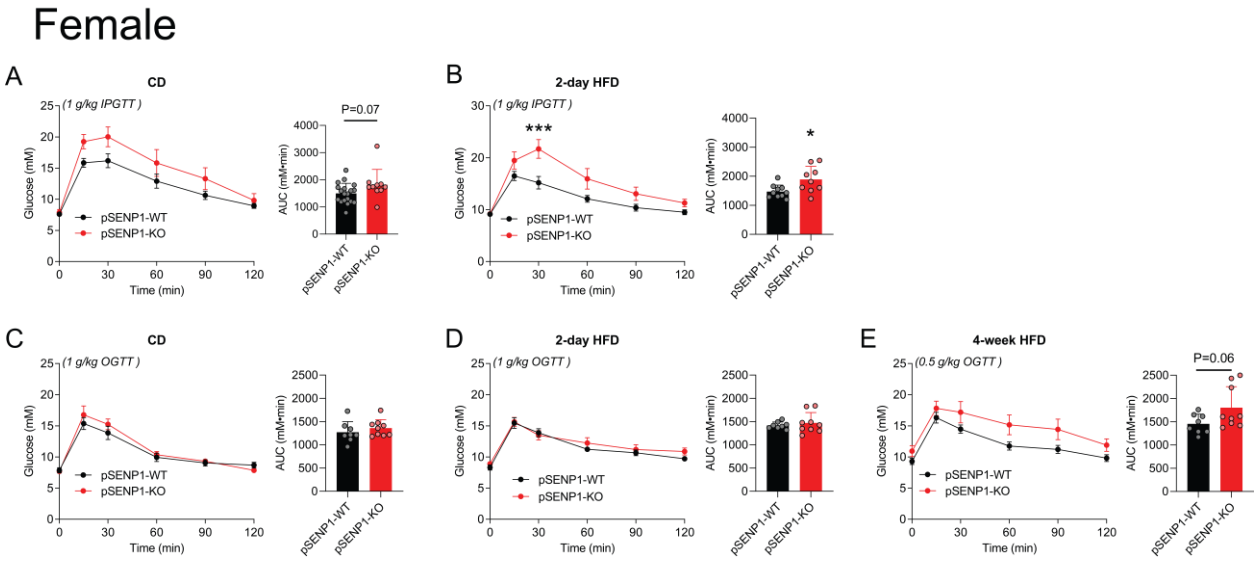
Female
A
CD
(1 g/kg IPGTT)
Glucose (mM)
Time (min)
pSENP1-WT
pSENP1-KO
P=0.07
AUC (mM•min)
B
2-day HFD
(1 g/kg IPGTT)
***
*
C
CD
(1 g/kg OGTT)
D
2-day HFD
(1 g/kg OGTT)
E
4-week HFD
(0.5 g/kg OGTT)
P=0.06

Figure 14. IPGTT and OGTT of female βSENP1-WT and βSENP1-KO during CD and short-term HFD.

(A-E): Female IPGTT on CD, 2-day and 4-week HFD (A - n=8, 7 mice, B - n=11, 14 mice, C - n=9, 10 mice), and associated insulin secretion (D - n=8, 9 mice, E - n=6, 6 mice). **(F-J):** Female OGTT on CD, 2-day, and 4-week HFD (F - n=6, 6 mice, G - n=7, 12 mice, H - n=11, 11 mice), and associated insulin secretion (I - n=7, 8 mice, J - n=7, 8 mice). Data are mean ± SEM and were compared with student t-test, one-way ANOVA followed by Bonferroni post-test. *$P < 0.05$. (NS and HL performed experiment and analyzed the data.)

Figure 14.

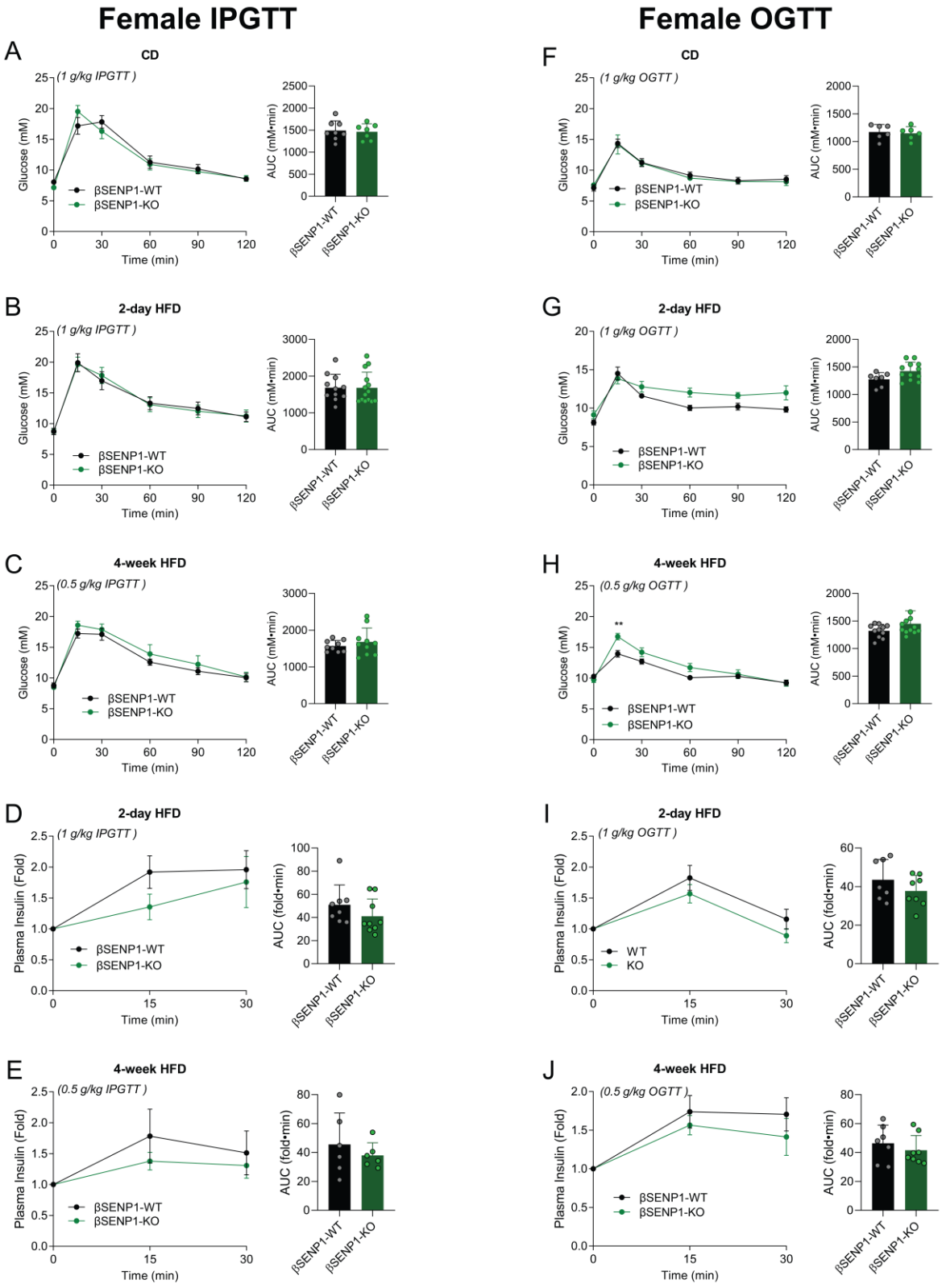
Female IPGTT
Female OGTT
A
CD
(1 g/kg IPGTT)
Glucose (mM)
Time (min)
βSENP1-WT
βSENP1-KO
AUC (mM•min)
F
(1 g/kg OGTT)
B
2-day HFD
G
C
4-week HFD
(0.5 g/kg IPGTT)
H
(0.5 g/kg OGTT)
**
D
Plasma Insulin (Fold)
AUC (fold•min)
I
WT
KO
E
J

2.4 Discussion

In the present study, we showed that following 2-day HFD exposure β-cells from male mice maintained normoglycemia by upregulating insulin secretory capacity through a pathway that requires a cytosolic redox signal via SENP1. GSIS is controlled by Ca^{2+}-dependent exocytosis, the efficacy of which can be modulated by metabolic signals[52]. Unlike previous studies of long-term HFD or prediabetic mouse models[131,132], after short-term HFD exposure, we find no evidence increased insulin secretion is related to enhanced Ca^{2+} channel activity or glucose-stimulated intracellular Ca^{2+} responses. Instead, we find enhanced β-cell exocytosis in cells with a clamped membrane potential, pointing to an upregulation of function distal to the ATP-dependent K^+ channel[122,135] and consistent with the enhanced efficacy of Ca^{2+} to stimulate insulin secretion seen with longer-term HFD exposure[122] and with the up-regulated exocytosis reported in β-cells from pre-diabetic and early diabetic *db/db* mice [135].

Redox signaling is important in insulin secretion and β-cell functional compensation[84,132]. We observed a remodeling of metabolic pathways in our RNAseq data, an increase in O_2 consumption at low glucose levels, and the reduction of cytosolic redox state after 2-day HFD as monitored by a Cyto-roGFP2-Orp1 transgenic mouse. Since the Cyto-roGFP2-Orp1 reports the steady state balance between H_2O_2 and reducing signals (NADPH, GSH…)[90,239], these findings could result from decreased H_2O_2 production or increased reducing equivalents shortly after HFD. Down-regulation of the cholesterol biosynthesis pathway, consistent with fatty acid inhibition of cholesterol biosynthesis[140], suggests a sparing of NADPH to promote exocytosis[233]. We[84] and others[59,85] have shown that NADPH augments Ca^{2+}-triggered insulin exocytosis. Cytosolic NADPH may be produced by either the mitochondrial export of reducing equivalents or, to a

smaller degree, the pentose phosphate pathway[50,80]. Interestingly, RNA sequencing data showed that the gene *Cdk1* was the most upregulated, which was previously shown to increase mitochondrial respiration and indirectly affect a target that modulated the exocytotic machinery[231]. Other genes related to electrical transport chain, such as *Uqcrq* (Ubiquinol-Cytochrome C Reductase Complex III Subunit VII), *Atp5g3* a subunit of mitochondrial ATP synthase, *Uqcr11* (Ubiquinol-Cytochrome C Reductase, Complex III Subunit XI), increased after 2-day HFD and might be involved in an acceleration of glucose metabolism. Even so, this didn't seem to affect the Ca^{2+} response to glucose, possibly because ATP may be consumed in priming more granules[240].

Knockout of SENP1 led to loss of compensatory insulin secretion and impaired IPGTT after 2-day HFD. However, OGTT was not different following 2-day HFD in most cases. This contrasts with 4-week HFD, where the SENP1-KO showed selectively impaired oral, but not IP glucose tolerance. The discrepancy could be because different adaptive responses contribute to glucose homeostasis at different stages of HFD[225]. In the long term, incretin release from the gut and β-cell incretin receptors are upregulated, compensation of incretin effect through endocrine system was important for maintenance of glucose homeostasis[201,225,233,241]. We previously identified the intracellular positive effect of SENP1 on β-cell in response to incretins and therefore this effect would be maximally revealed after 4-week in the present study as well as 8-week HFD as described in chapter 4[223,224]. Of note, insulin secretion to glucose decompensated after long term HFD-induced oxidative stress, thus leading to comparable impairment of IPGTT in SENP1-WT and SENP1-KO mice[224]. During the 2-day HFD with mild oxidative stress, functional compensation in the form of GSIS required upregulation of redox signaling via SENP1 for maintaining IPGTT. In addition, GLP-1 signaling conferred glucose competence on β-cell through local GLP-1 or glucagon[200,241–243], such that ablation of SENP1 could also impaired IPGTT via

GLP-1 signaling. However, the β-cell GLP-1 receptor was not necessary for oral glucose tolerance under normal condition[241], consistent with the dispensable role of SENP1 on OGTT after 2-day HFD under which circulating incretins remained extremely low. In addition, extra-islet glucose-lowing action from oral glucose stimulated incretins, could mask the intracellular effect of SENP1 on GSIS, such that oral glucose tolerance behaved normal in SENP1-KO compared to SENP1-WT mouse[241].

2.5 Methods

2.5.1 Animals.

9-week-old C57BL/6 mice were purchased from Charles River Laboratories. At the age of 12 weeks, C57BL/6 were put on standard chow diet (5L0D*, 12% fat, PicoLab Laboratory Rodent Diet) or 60% high fat diet (S3282, VWR) for 2 days or 4-weeks. Pdx1-Cre mice (B6.FVB-Tg (Pdx1-cre)6 Tuv/J, Jackson Lab, 014647) on a C57BL/6 background and Ins1-Cre mice on a mixed C57BL/6 and SV129 background [244] were crossed with Senp1-floxed mice on a C57BL/6 background[84] to generate gut/pancreas specific (Pdx1-Cre^{+};Senp1$^{fl/fl}$ - pSENP1-KO) and β-cell-specific knockouts (Ins1-Cre^{+};Senp1$^{fl/fl}$ - βSENP1-KO)[84,223]. Control littermates Pdx1-Cre^{+};Senp1$^{+/+}$ mice (pSENP1-WT) and Ins1-Cre^{+};Senp1$^{+/+}$ mice (βSENP1-WT) at 12 weeks of age were used for experiments. Genotypes and SENP1 expression level were confirmed as previously described[238].

2.5.2 Glucose homeostasis assessment.

Oral glucose tolerance test (OGTT), intraperitoneal tolerance test (IPGTT) and insulin tolerance test (ITT) were performed according to the procedures deposited in the protocols.io repository[245–247]. For OGTT and IPGTT on chow diet or 2-day HFD, glucose concentration was 1

g/kg dextrose, while on 4-week HFD, it was 0.5 g/kg dextrose. Tail blood was collected at indicated time for insulin (STELLUX® Chemi Rodent Insulin ELISA kit, Alpco) and glucose measurement as previously described[223]. At 12 weeks, insulin tolerance was performed with a concentration of 1 U/kg Humulin R (Eli Lilly).

2.5.3 Human and mouse islets isolation and cell culture.

Human islets were isolated at the Alberta Diabetes Institute IsletCore according to procedures deposited in the protocols.io repository and cultured in DMEM overnight (supplemented with L-glutamine, 110 mg/l sodium pyruvate, 10% FBS, and 100 U/mL penicillin/streptomycin)[248]. A total of 258 non-diabetic (ND) donors and 34 T2D donors (HbA1c>6.5) **(Table 2)** were examined in this study and specific donor information can be accessed here www.isletcore.ca. Extended donor, organ processing, and quality control information is available by searching relevant donor numbers at www.isletcore.ca. All human islet studies were approved by the Human Research Ethics Board (Pro00013094; Pro00001754) at the University of Alberta and all families of organ donors provided written informed consent. Mouse islets were isolated by collagenase digestion and purified by histopaque density gradient centrifugation before handpicking. All mouse islets or single cells were cultured in RPMI-1640 with 11.1 mM glucose, 10% FBS, 100 units/mL penicillin, and 100 mg/mL streptomycin.

Table 2. Human islet donor information and detailed characteristics of each donor is available at www.isletcore.ca.

ND	R010	R011	R012	R039	R050	R051	R052	R055	R058	R060	R061	R062
	R065	R066	R067	R072	R073	R074	R075	R076	R077	R081	R082	R084
	R085	R087	R088	R089	R090	R091	R092	R094	R096	R097	R098	R099
	R100	R101	R102	R104	R105	R106	R108	R109	R112	R113	R114	R115
	R116	R117	R118	R120	R121	R122	R123	R124	R126	R127	R128	R130
	R134	R135	R136	R138	R139	R140	R142	R144	R145	R146	R147	R148
	R149	R150	R151	R153	R156	R157	R159	R160	R161	R162	R163	R164
	R165	R167	R168	R169	R172	R174	R175	R176	R177	R178	R179	R180
	R181	R182	R183	R184	R186	R187	R188	R189	R190	R193	R194	R195
	R196	R199	R200	R202	R203	R204	R205	R207	R208	R210	R215	R216
	R217	R218	R219	R220	R221	R223	R224	R226	R227	R228	R229	R230
	R232	R233	R234	R235	R237	R238	R239	R242	R243	R245	R246	R247
	R248	R249	R250	R251	R252	R253	R254	R255	R256	R260	R264	R266
	R267	R268	R269	R270	R271	R272	R273	R274	R275	R277	R278	R279
	R280	R281	R282	R283	R284	R285	R286	R288	R290	R291	R292	R294
	R297	R299	R300	R301	R302	R303	R304	R305	R306	R308	R309	R310
	R311	R313	R314	R316	R317	R318	R319	R320	R321	R322	R323	R324
	R325	R326	R327	R328	R330	R332	R333	R334	R335	R338	R340	R341
	R342	R343	R344	R346	R348	R350	R352	R353	R354	R355	R356	R357
	R358	R360	R361	R362	R363	R364	R365	R366	R367	R368	R369	R370
	R371	R372	R373	R374	R375	R377	R379	R382	R383	R385	R387	R388
	R389	R390	R391	R392	R393							
T2D	R001	R013	R018	R023	R031	R057	R064	R070	R071	R083	R107	R110
	R125	R131	R143	R152	R154	R170	R171	R173	R191	R201	R206	R222
	R231	R236	R240	R244	R257	R263	R265	R289	R307	R312		

2.5.4 Insulin secretion.

After overnight culture for islets to recover, static insulin secretion was measured according to the detailed protocol deposited to protocols.io[249]. Glucose concentrations were 1, 10, 16.7 mM for human islets, while glucose concentration were 2.8 mM and 16.7 mM for mouse islets. Diazoxide and KCl concentration were 100 μM and 30 mM respectively. Perifused insulin secretion was measured as previously described[238]. Briefly, 25 islets were pre-perifused for 30 minutes at 2.8 mM glucose followed by 16.7 mM glucose and KCl (30 mM) at a sample collection rate of 100 ul/min every 1-5 minutes. Insulin content was extracted with acid/ethanol. The samples were stored at -20°C and assayed by using Insulin Detection Kit (STELLUX® Chemi Rodent Insulin ELISA kit, Alpco).

2.5.5 Capacitance measurements.

Human and freshly isolated mouse islets were dispersed to single cells in Ca^{2+}-free dissociation buffer and cultured in 5.5 mM glucose DMEM (11965, Thermo Fisher) and 11 mM glucose RPMI (11875, Thermo Fisher) respectively. After overnight culture, dispersed cells were used for whole-cell patch clamping. Prior to patch-clamping, dispersed cells were preincubated at 1 mM glucose (human) or 2.8 mM (mouse) for 1 hour and patched in bath solution containing 118 mM NaCl, 5.6 mM KCl, 20 mM TEA, 1.2 mM MgCl2, 2.6 mM $CaCl_2$, 5 mM HEPES at different glucose conditions (1 mM, 2.8 mM, 5mM, 10 mM) with a pH of 7.4 (adjusted by NaOH). After 10 minutes, whole-cell patch-clamp exocytosis was performed with the sine+ DC lock-in function of an EPC10 amplifier and Patchmaster software (HEKA Electronics). Exocytotic responses and inward Ca^{2+} currents were measured 1-2 minutes after obtaining the whole-cell configuration in response to ten 500 ms depolarizations to 0 mV from a holding potential of -70 mV. Changes in capacitance and integrated Ca^{2+} charge entry were normalized to cell size (fF/pF and pC/pF,

respectively). The intracellular solution contained 125 mM Cs-Glutamate, 10 mM CsCl, 10 mM NaCl, 1 mM MgCl2, 5 mM HEPES, 0.05 mM EGTA, 3 mM MgATP and 0.1 mM cAMP with pH = 7.15 (pH adjusted with CsOH).

In the infusion experiment, exocytotic responses and inward Ca^{2+} currents were measured 2-3 minutes after obtaining the whole-cell configuration. Compounds or recombinant enzymes were added to pipette solution as indicated for intracellular infusion to single cells. For mouse β cells, 200 μM H_2O_2 (Sigma), 10 μM reduced glutathione (GSH, Sigma), 4 μg/mL cSENP1-GST fusion peptide (Enzo Life Technologies) and glutathione-S-transferase (GST) peptide (Enzo Life Technologies) for SENP1 control were added at the time of experiment. Human β-cells were identified by immunostaining for insulin. Mouse β-cells were identified by size (>4 pF) and the Na^+ channel half-maximal inactivation at around -90 mV[250].

2.5.6 Ca^{2+} response imaging

Freshly isolated mouse islets cells from CD and HFD were cultured at 35 mm Glass bottom dish with 10 mm micro-well (Cellvis) overnight in 11 mM glucose RPMI media (11875, Thermo Fisher). Cells were pre-incubated with Fura-2AM (1 μM) for 15 min and perifused with KRB solution at indicated glucose level and imaged at 0.5 Hz. Fluorescence signal was excited at 340/380 nm (intensity ratio 20:8) and detected at an emission light of 510 nm using Life Acquisition software (Till Photonics) on an inverted microscope (Zeiss Axioobserver, Carl Zeiss Canada Ltd.) equipped with a rapid-switching light source (Oligochrome; Till Photonics, Grafelfing, Germany). β-cells were marked and identified by immunostaining and fluorescence ratios were calculated using ImageJ (NIH).

2.5.7 Oxygen consumption.

Isolated islets were incubated overnight after isolation and washed three times with serum-free RPMI media (11879, Thermo Fisher) at 2.8 mM glucose for 3 times. Oxygen consumption rate was measured with Fluorescence Lifetime Micro Oxygen Monitoring System (FOL/C3T500P, Instechlabs). Briefly, around 200 islets were added to the chamber for data collection for around 20 minutes. Afterwards, islets were collected for DNA content measurement. Oxygen consumption rate was normalized to DNA content using Pico Green kit (Invitrogen).

2.5.8 Methods for detecting differences in cellular Zn^{2+}.

For detecting granular or cytosolic Zn^{2+} in diet-treated mouse islet cells, islet cells from chow-diet (CD) fed mice and high-fat-diet (HFD) fed mice were labeled with ZIGIR or ZnAF2, respectively. The resulting signals from these two probes were measured using flow cytometry and analyzed by FlowJo (Version 10.7.1). Briefly, intact islets were harvested from a pair of CD or HFD mice after dissection of the pancreas, followed by digestion with collagenase solution in a 37˚C water bath for 15 minutes. Islets were handpicked into 2 mL culture medium and then labeled with 0.05 μM Ex4-Cy5 (Cy5 dye conjugate of Exendin-4) for 1 hour. The islets were then dispersed into single cells with 0.05% Trypsin solution at 37˚C for 15 minutes. The resulting cell suspensions were filtered through a 70 μm pore strainer and spun down at 500 x g for 3 minutes at 4˚C to obtain cell pellets. The cells were washed once with sorting buffer (3 mM glucose, 0.5% BSA, 0.1 mg/mL DNase I in 1× secretion assay buffer (SAB) buffer) and resuspended in 0.3 mL sorting buffer. An equivalent volume of dye labeling solution was then added to each suspension and gently mixed (dye labeling solution: 0.5 μM ZIGIR and 1 μM ZnAF-2 diacetate in 1X SAB mixed with 0.1% pluronic). The mixed cell suspensions were incubated at room temperature for 20 minutes and washed once with sorting buffer at room temperature. The cell pellets were

resuspended with 0.3 mL sorting buffer and kept on ice until they were analyzed using a BD FACSAria II SORP cell sorter. Dead cells were excluded by adding a 1:1000 dilution of DAPI to cell suspensions immediately prior to FACS analysis. ZIGIR signal was detected using 561 nm excitation laser, and ZnAF-2 signal was detected using 488 nm excitation. Islet β-cells and α-cells were identified from the 2D scatter plot (ZIGIR vs Ex4-Cy5) as described[251]. The median fluorescence intensity (MFI) of ZIGIR or ZnAF2 of β-cells and α-cells were calculated by FlowJo and normalized against the corresponding cell type of the CD group.

2.5.9 Fluorescence activated cell sorting (FACS) of β-cells and sequencing.

As mentioned previously, islet α- and β-cells from 4 mice on CD and 3 mice on HFD were identified by ZIGIR vs Ex4-Cy5 through FACS analysis[251]. Total RNA was isolated from sorted islet α- and β-cells using TRIzol reagent (Thermo Fisher) according to the manufacturer's protocol and cDNA libraries were prepared using Illumina's TruSeq Stranded mRNA Library Prep kit with slight modifications of the manufacturer's protocol to improve yield. The cDNA libraries were validated by TapeStation DNA 1000 High Sensitivity assay (Agilent) and quantified by Qubit dsDNA High Sensitivity assay (ThermoFisher). High quality libraries were submitted to the UT Southwestern Next Generation Sequencing Core facility and RNA sequencing was performed using Illumina's NextSeq 500 High Output instrument. Raw reads were processed to transcripts per million (TPM) and differentially expressed (DE) genes were initially determined by using the edgeR package.

2.5.10 mRNA-seq data analysis.

Genes with P-value<0.1, coefficient of variation (CV) of less than 1, same change of direction (either positive or negative) and specific gene counts range (i.e., mean gene counts in at

least one experimental group should be higher than 5 RPKM) were considered differentially expressed between CD and HFD.

2.5.11 Function and pathway enrichment analysis.

Differentially expressed gene function and enriched pathways were identified with Metascape (http://metascape.org/). KEGG Pathway, GO Biological Processes, Reactome Gene Sets, CORUM, TRRUST and PaGenBase were included in pathway enrichment analysis with a p-value <0.01. Terms with an enrichment factor > 1.5 and a similarity of >0.3 are grouped into a cluster represented by the most significant term[252]. To examine protein-protein interaction (PPI), STRING database (https://string-db.org/) was used and only PPIs with interaction score higher than 0.70 were retrieved and linked in the circos plot by using R-studio (circlize package) [230,253].

To run an unbiased gene set enrichment analysis (GSEA)[254], all Genes with CV of less than 1, same change of direction and specific gene counts range (at least one experimental group should be higher than 5 RPKM) were submitted. H.all.v7.4.symbols.gmt[Hallmarks] gene dataset was used as reference data set. Enriched gene sets were considered significant with gene size over 50, false discovery rate less than 0.05, nominal *p*-value less than 0.01.

2.5.12 Redox measurement.

Measurements of the intracellular H_2O_2 levels were made using a redox histology approach with transgenic mice carrying redox sensor Cyto-roGFP2-Orp1 gene, as previously described[236,255,256]. Briefly, batches of 30 islets were collected and immersed in 50-mM N-ethyl-maleimide (NEM) dissolved in PBS for 20 min for sensor chemical fixation. The NEM was then removed, and islets fixed in 4% paraformaldehyde for 30 min. After paraformaldehyde removal, the islets were incubated in 100-µL HepatoQuick (Roth, Karlsruhe, Germany) mixed with human

citrate plasma (1:2 v/v) and 1% $CaCl_2$ for 1 h at 37 ˚C. Clots were then incubated in 95% ethanol at 4°C overnight and subsequently dehydrated in ethanol prior to paraffin embedding. The paraffin embedded clots were cut in 3-µm thick sections with a semi-automated rotary microtome (Leica Biosystems, Wetzlar, Germany) and placed on salinized glass slides. Images of all the islets in each slide were obtained by the Axio Observer 7 fluorescence microscope (Zeiss, Oberkochen, Germany) with a 20x objective using excitation 405 nm and 488 nm, emission 500-530nm. The images were analyzed with ImageJ Fiji Software using Huang's threshold plugín[236], and the normalized ratio (405/488 nm) was used to compare different groups.

2.5.13 Statistics.

Data analysis was performed using Fit Master (HEKA Electronik) and GraphPad Prism (v7.0c). All data are shown as the mean ± SEM. Statistical outliers were identified and removed by an unbiased ROUT (robust regression followed by outlier identification) test. Normally distributed data were analyzed by the 2-tailed Student's t test (for two groups), or ANOVA and Bonferroni post-test (for multiple groups). Data that failed normality tests were analyzed by the non-parametric Mann-Whitney test (for two groups), or the Kruskal–Wallis one-way analysis of variance followed by Mann-Whitney post-test (for multiple groups). A *p*-value less than 0.05 was considered significant.

Chapter 3.

Redox and Zn^{2+} co-regulate SENP1 activity for insulin exocytosis

This chapter, and portions of Chapter 2, are part of a paper being prepared for publication.

Haopeng Lin[1, 2, 8], Kunimasa Suzuki[1, 2, 8], Nancy Smith[1, 2], Xi Li[3], Lisa Nalbach[4], Sonia Fuentes[3], Aliya F Spigelman[1, 2], Xiaoqing Dai[1, 2], Austin Bautista[1, 2], Mourad Ferdaoussi[6], Saloni Aggarwal[7], Andrew R Pepper[7], Emmanuel Ampofo[4], Leticia P Roma[5], Wen-hong Li[3], Patrick E MacDonald[1, 2]*

1. Department of Pharmacology, University of Alberta, Edmonton, AB T6G 2E1, Canada
2. Alberta Diabetes Institute, University of Alberta, Edmonton, AB, T6G 2E1, Canada
3. Departments of Cell Biology and Biochemistry, University of Texas Southwestern Medical Center, 6000 Harry Hines Blvd., Dallas, TX 75390-9039, USA
4. Institute for Clinical & Experimental Surgery, Saarland University, Homburg/Saar, Germany
5. Biophysics Department, Center for Human and Molecular Biology, Saarland University, Homburg/Saar, Germany
6. Department of Pediatrics, University of Alberta, Edmonton, AB T6G 2E1, Canada
7. Department of Surgery, University of Alberta, Edmonton, Canada
8. These authors contributed to this study equally

Contributions by co-authors to the figures are acknowledged by co-author initials.

3.1 Abstract

SENP1 has emerged as an important redox sensor and effector transducing glucose-dependent redox signals to insulin granule exocytosis. To further investigate the molecular basis for redox-sensing regulation of SENP1, we generated several cysteine-specific mutants of the SENP1 core catalytic domain. We found that a C535S mutant is resistant to oxidation-induced inhibition, indicating Cys535 (C535) is a negative regulator to restrict SENP1 activity. Loss of the C535 thiol leads to hyperactive SENP1 and abolishes redox-regulation of human β-cell exocytosis. In addition, binding of Zn^{2+}, instead of other metals such as Ca^{2+} or Co^{2+}, with C535 inhibits SENP1 and tunes SENP1 sensitivity to redox state, allowing robust activation by glutathione and glutaredoxin1 (GRX1). In mouse β-cells, intracellular dialysis of Zn^{2+} significantly restrained insulin exocytosis, and this required SENP1. Thus, redox and Zn^{2+} fine-tune SENP1 activity. This may contribute to the sensing of glucose-stimulated redox changes via C535, and control of downstream insulin exocytosis.

3.2 Introduction

SUMOylation is a posttranslational modification (PTM), conjugating small ubiquitin-like modifier (SUMO) peptides to target proteins to regulate protein localization and function. This process is mediated by SUMO-specific E1, E2, and E3 enzymes and reversed by deSUMOylating proteins, i.e., sentrin-specific proteases (SENPs)[165]. SENP1 is a redox-sensing cysteine protease transducing cellular redox signals, and mediating amplification of insulin secretion in pancreatic β-cells[84,175]. Under physiological conditions, activation of SENP1 is depends on the reducing power derived from glucose metabolism to generate an active thiol group at the catalytic cysteine 603 (C603)[84]. Through pyruvate-isocitrate shuttling, glucose metabolism generates cytosolic

NADPH, which transduces reducing power to SENP1 via a GSR/GSH/GRX1 redox relay[84]. Activated SENP1 deSUMOylates the exocytotic proteome and enhances insulin release[173–175]. On the other hand, thiol groups can be oxidized to reversible disulfide bridges or further oxidized to irreversible sulfinic and sulfonic acid upon increased oxidative stress, leading to inactivation of SENP1[91,257].

A previous study identified C613 as a positive regulator required for reversible intermolecular disulfide bond formation with C603, protecting SENP1 against irreversible oxidation[91]. This reversible cysteine C603/613 modification might allow β-cells to switch on/off the insulin granule exocytosis in response to a glucose-induced reduction of cytosolic redox [84,91]. However, an *in vitro* study showed that only highly oxidizing conditions can restrain SENP1 activity[172], indicating that SENP1 activity might remain constantly high even at low glucose levels and barely increase upon glucose stimulation under physiological conditions. It appears that SENP1 activity is subject to an unknown regulation, besides redox, that permits a significant change of deconjugating activity in response to glucose.

The catalytic triad (H533, D550, and C603) in SENP1 is an integral part of SENP1 activity[258]. DeSUMOylation by SENP1 requires the deprotonation of the C603 thiol group via a proton transfer pathway. Specifically, the proton transfers from the thiol group of C603 to the carboxyl group of D550 via H533, resulting in an active thiolate in SENP1[259]. It is worth noting that other than redox modification, the thiolate in cysteine protease is also subject to Zn^{2+} binding and modification, leading to protein inhibition[116]. Most cysteine enzymes can be inhibited by low nanomolar or even picomolar concentrations of Zn^{2+}[260–264]. In addition, Zn^{2+} binding/release can be also regulated by redox changes[119]. Zn^{2+} is significantly enriched within insulin secretory

granules and when co-released with insulin can re-enter β-cells to inhibit insulin secretion via K_{ATP} channel activation[111].

In the present study, we identify that C535 is a negative regulator of SENP1 activity. C535 increases SENP1 sensitivity to inhibition by H_2O_2. Mutation of C535 causes hyperactivity of SENP1, loss of redox regulation, and unrestrained increase in insulin exocytosis in the presence of H_2O_2. We also predict that C535 is the allosteric Zn^{2+}-binding residue and confirm that $ZnCl_2$ inhibits SENP1 activity through C535, allowing robust re-activation by reduced glutathione and glutaredoxin1 (GRX1). Zn^{2+} inhibits insulin exocytosis without changing Ca^{2+} entry. This is lost in β-cells lacking SENP1, indicating that SENP1 is the target for Zn^{2+}-mediated inhibition of insulin exocytosis.

3.3 Results

3.3.1 Cys535 is a negative regulator for SENP1 redox regulation.

SENP1 activity is subject to redox regulation via a thiol group on catalytic C603 forming a disulfide bond with C613[91]. The catalytic cysteine C603, required for deSUMOylation, was the most conserved cysteine across isoforms and species **(Figure 15A)**. SENP1 was reported to have a distinctive redox regulation by formation of an intermolecular disulfide bond with C613, compared to SENP2 and SENP1 (yeast)[91]. Interestingly, C535 was the least conserved cysteine compared to other human SENP isoforms **(Figure 15A)** and is closer to the C603 catalytic site, which constitutes a catalytic triad with D550 and H533 **(Figure 15B)**. However, the distance between C535 and C603 was up to 7.1 Å, which was far greater than 3.0 Å required to form an intramolecular disulfide bond[265]. Similarly, the distance between C603 and C613 was 17 Å, and was the only intermolecular disulfide bond reported in SENP1 dimer[91]**(Figure 15B)**.

Figure 15. Potential redox-sensing cysteines in SENP1.

(A): A schematic representation of two reported redox-sensing cysteines (C603 and C613) and three potential redox-sensing cysteines (C535, C560, C608) from catalytic domain (residues 419-644, green) in human SENP1. Human SENP1 was aligned with other isoforms and across species to identify potential cysteines and their conservativeness. **(B):** Structure representation of SENP1-SUMO complex (ID: 2IYD, SENP1: green. SUMO: red) extracted from PDB database. Potential redox-sensing cysteines (C535, C560, C603, C608, C613, yellow), another two catalytic triad (D550, H533, orange), and catalytic "floor" (W534, purple blue) and "lid" (W465, purple blue) were labeled. On the right panel, the catalytic region along with potential cysteines were outlined and zoomed in. Dashed lines indicated the measured distance (Å) between thiol group from catalytic (C603, yellow) to the ones from other potential cysteines (C535, C560, C603, C608, C613, yellow). (All panels by HL and significant conceptual contribution by KS)

Figure 15.

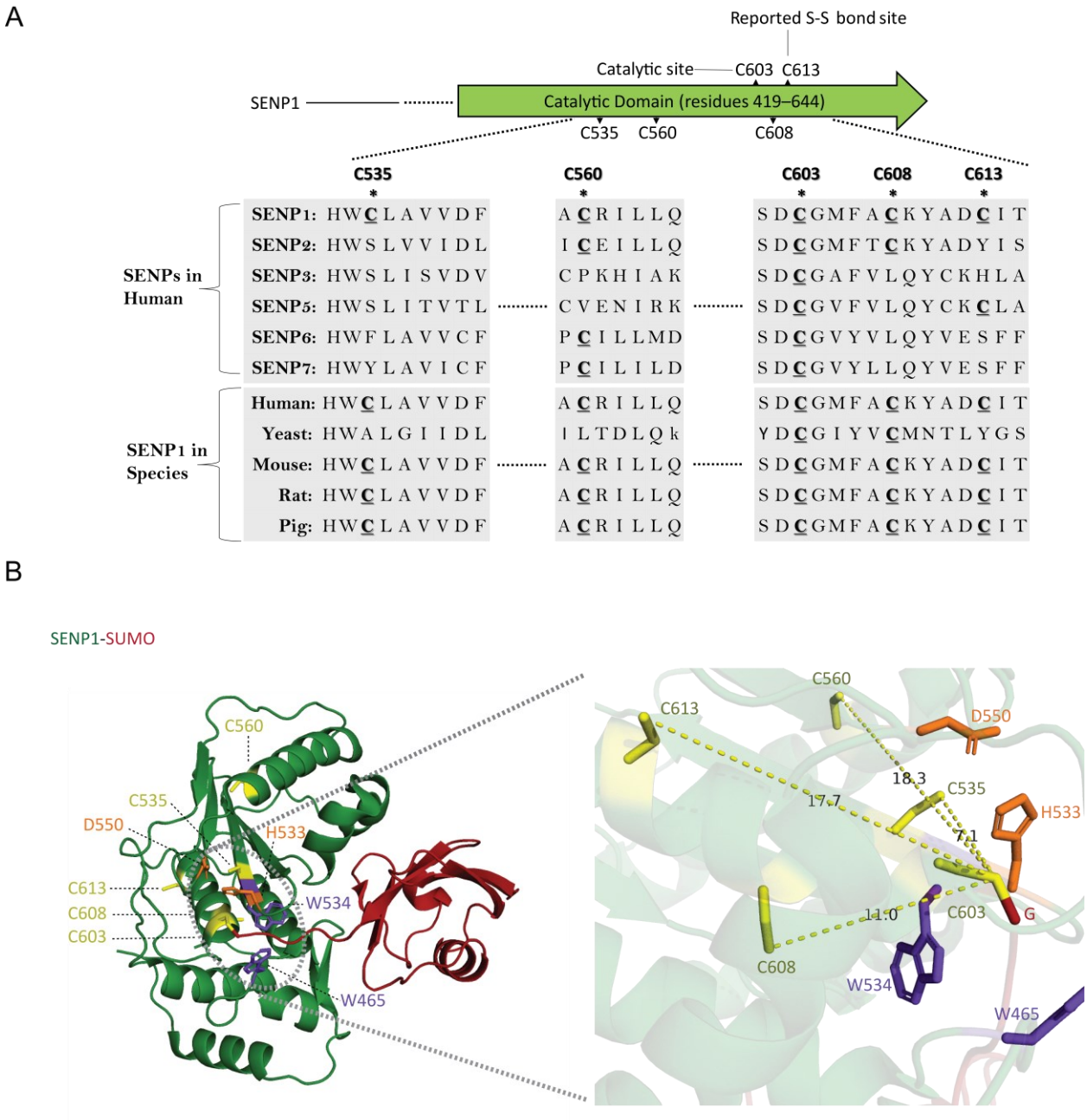
A
Reported S-S bond site
Catalytic site
C603 C613
SENP1
Catalytic Domain (residues 419–644)
C535 C560 C608
C535 C560 C603 C608 C613
SENPs in Human
SENP1: HWCLAVVDF ACRILLQ SDCGMFACKYADCIT
SENP2: HWSLVVIDL ICEILLQ SDCGMFTCKYADYIS
SENP3: HWSLISVDV CPKHIAK SDCGAFVLQYCKHLA
SENP5: HWSLITVTL CVENIRK SDCGVFVLQYCKCLA
SENP6: HWFLAVVCF PCILLMD SDCGVYVLQYVESFF
SENP7: HWYLAVICF PCILILD SDCGVYLLQYVESFF
SENP1 in Species
Human: HWCLAVVDF ACRILLQ SDCGMFACKYADCIT
Yeast: HWALGIIDL ILTDLQk YDCGIYVCMNTLYGS
Mouse: HWCLAVVDF ACRILLQ SDCGMFACKYADCIT
Rat: HWCLAVVDF ACRILLQ SDCGMFACKYADCIT
Pig: HWCLAVVDF ACRILLQ SDCGMFACKYADCIT
B
SENP1-SUMO
C560
C535
D550
H533
C613
C608
C603
W534
W465
C560
C613
D550
18.3
C535
17.7
H533
7.1
11.0
C603
G
C608
W534
W465

To further examine SENP1 redox regulation, we generated SENP1 catalytic domain peptides with cysteine-to-serine substitutions (C535S, C560S, C603S, C613S, and C608S) and measured SUMO-protease activity *in vitro* using recombinant His×6-SUMO1-mCherry **(Figure 16A)**. As expected, the C603S mutant completely lost SENP1 activity **(Figure 16B)**. Intriguingly, C535S mutant exhibited constitutively higher SENP1 activity **(Figure 16B)** and was modestly less sensitive to inactivation by H_2O_2 (IC_{50}=2.5 mM) compared to SENP1 WT (IC_{50}= 1 mM) **(Figure 16C)**. Intracellular dialysis of either SENP1 WT or C535S into human β-cells was able to increase exocytotic capacity **(Figure 16D)**. However, while co-dialysis of H_2O_2 blocked the action of SENP1 WT, the C535S mutant was still able to maintain its functional activity **(Figure 16D)**, suggesting that C535 is required for the redox regulation of SENP1 actions on β-cell exocytosis.

Figure 16. Loss of C535 leads to a hyperactive SENP1 and abolished redox-regulation of insulin exocytosis in human β-cells.

(A): A schematic representation of measuring SENP1 activity. His×6-SUMO-mcherry protein acts as a SENP1 substrate for SENP1. Active SENP1 can identify specific regions on SUMO protein to cut SUMO protein at the C-terminal Gly-Gly motif, releasing fluorescent mCherry protein. Undigested substrates are captured by Nickel NTA agarose bead and removed by centrifugation. Fluorescent intensity of free mCherry protein in the supernatant corresponds to the SENP1 activity. **(B):** SENP1 activity after cysteine-to-serine substitution (n=3). **(C):** Dose-response curve of SENP1 activity under H_2O_2 after being fully activated by 10 mM reducing reagent DTT (n=3). **(D):** 4 μg/mL glutathione-S-transferase (GST) peptide (control), SENP1 WT, C535S and C603 were infused into human β-cells with/without 200 μM H_2O_2 to assess their effects on exocytosis at 5 mM glucose (n=28-46 cells per group from 7 human donors). Data are mean ± SEM and were compared with student t-test, one-way ANOVA or two-way ANOVA followed by Bonferroni post-test. *$P < 0.05$, **$P < 0.01$, ***$P < 0.001$. In panel C, * indicated comparison between SENP1 WT and C535S. (KS developed the deSUMOylation assay and performed A-C. HL performed D.)

Figure 16.

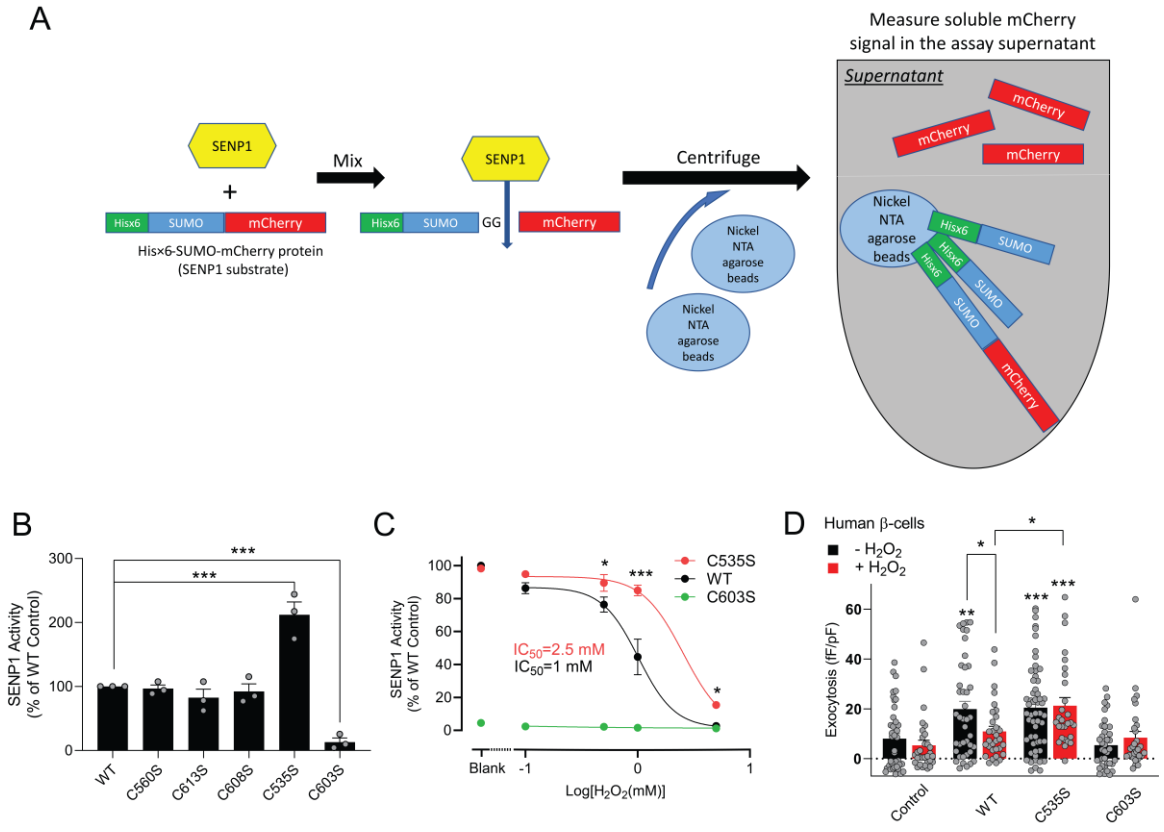
A
Measure soluble mCherry signal in the assay supernatant
Supernatant
SENP1
+
Hisx6-SUMO-mCherry protein (SENP1 substrate)
Mix
SENP1
GG
Centrifuge
Nickel NTA agarose beads
Nickel NTA agarose beads
Hisx6
SUMO
mCherry
B
SENP1 Activity (% of WT Control)
WT
C560S
C613S
C608S
C535S
C603S
C
SENP1 Activity (% of WT Control)
C535S
WT
C603S
IC50=2.5 mM
IC50=1 mM
Blank
Log[H2O2(mM)]
D
Human β-cells
- H2O2
+ H2O2
Exocytosis (fF/pF)
Control
WT
C535S
C603S

3.3.2 Proposed molecular mechanism for C535 restraint of SENP1.

The SENP1 gains catalytic activity via a proton transfer pathway. Briefly, the C603 thiol group donates a proton to the adjacent H533, which transfers another proton to D550. This proton transfer pathway increases the electronegativity for the C603 thiol to attack the carbonyl carbon of a glycine residue and form a covalent link with the SUMO protein to initiate the catalytic cycle[259]. To understand how C535 affects SENP1 activity structurally, I morphed the free SENP1 into SUMO-bound SENP1 structurally in Pymol and observed the key residues change from their native states to intermediate states and to the final SENP1-SUMO complex state. In the native SENP1, the C603 thiol was 3.6 Å away from the ND1 of H533 **(Figure 17A)**. In the intermediate state of SENP1-SUMO binding, the SUMO protein induced a conformational change in SENP1, leading to the shorter distance of 2.6 Å between the C603 thiol and ND1 of H533 **(Figure 17A)**. The proton transfer pathway could occur with a proton being transferred from C603 to D550. In the final state of SENP1-SUMO binding, H553 underwent a 90-degree flip-over. The deprotonated thiol from C603 moved closer to the carbonyl carbon of the glycine residue of SUMO to initiate the hydrolytic reaction. During the whole binding process, the thiol group of C535 was located close to H533 and D550, and rarely underwent significant movement. C535 may donate a proton to either H533 or D550, like C603 does, and competitively restrain the proton transfer from C603 to H533, leading to the inhibition of SENP1 **(Figure 17B)**. Loss of C535 could therefore abolish this competitive inhibition and strengthen the proton transfer from C603, thus resulting in higher SENP1 activity.

Figure 17. Proposed redox-dependent mechanism for C535 to restrain SENP activity.

(A): Native SENP1 (2IYC) was morphed into SENP1-SUMO (2IYD) in Pymol to observe the dynamic changes of SENP1. Dashed lines indicated the distance between the indicated residues. **(B):** C535 might competitively donate proton to the adjacent catalytic site (D550 and H533), preventing the proton transfer pathway from C603 to H533 and D550. (All panels by HL and significant conceptual contribution by KS.)

Figure 17.

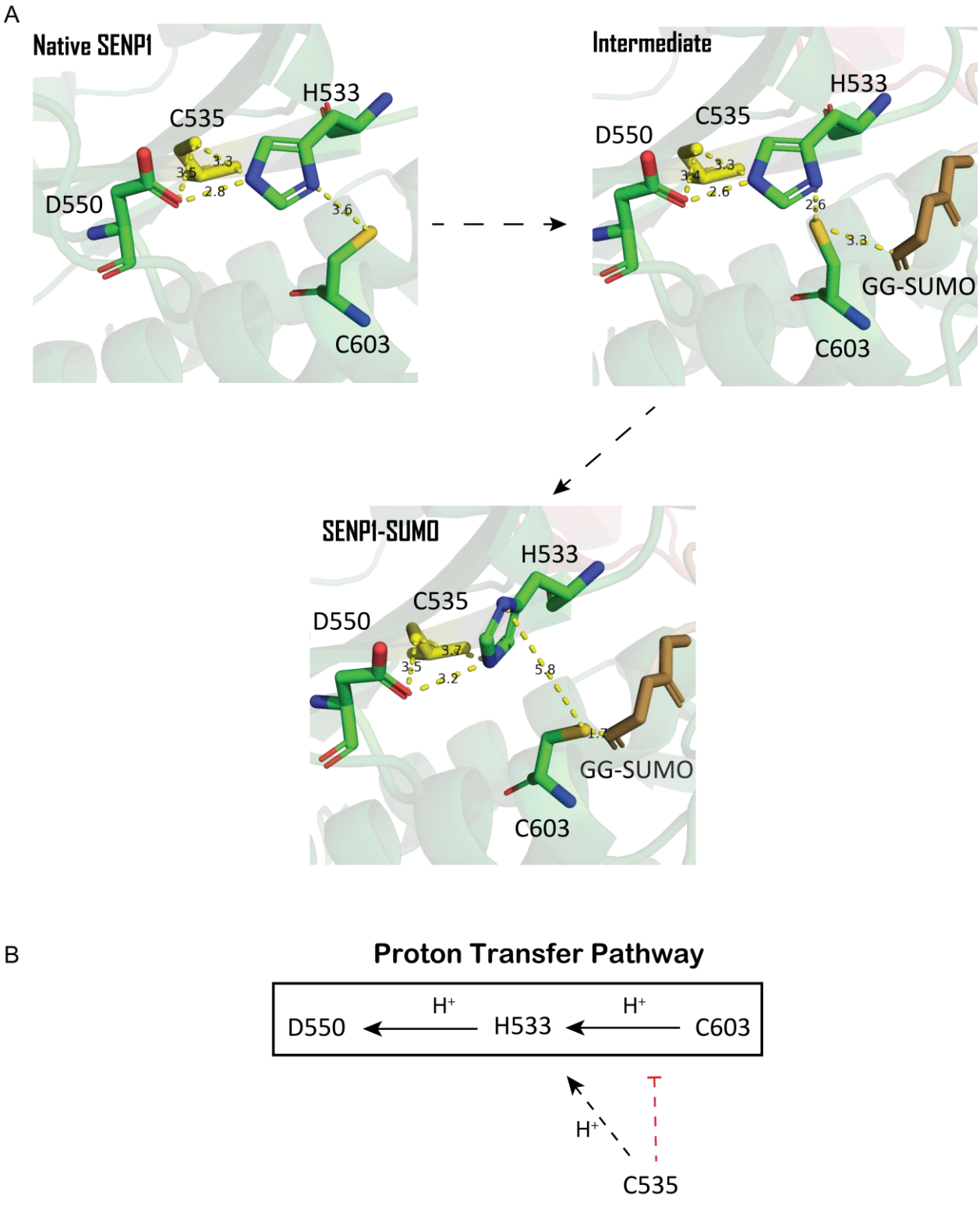
A
Native SENP1
H533
C535
D550
C603
Intermediate
H533
C535
D550
GG-SUMO
C603
SENP1-SUMO
H533
C535
D550
GG-SUMO
C603
B
Proton Transfer Pathway
H+
H+
D550
H533
C603
H+
C535

3.3.3 C535 is the allosteric binding site for Zn^{2+} to inhibit SENP1 activity.

The IC_{50} for H_2O_2 to inhibit SENP1 is 1 mM, which is super-physiological for redox-regulation of insulin exocytosis *in vivo*. Since deSUMOylation was glucose-dependent in β-cells under physiological conditions[175], there might exist another regulatory mechanism to tune SENP1 activity within a more physiologic dynamic range . We noticed initially that removal of nickel after protein refolding was required for strong activity of SENP1 (not shown). However nickel content is relatively low within cells[266], while Zn^{2+} can affect cysteine protease activity by forming Zn^{2+}-thiolate on cysteines[116]. Prediction of Zn^{2+}-binding sites showed that C603, C535 and H533 is one of the most favorable Zn^{2+}-binding site in SENP1**(Figure 18A)**, and which is lost in the C535S mutant[267] **(Figure 18B)**. Indeed, Zn^{2+} and nickel inhibition of SENP1 is lost in the C535S mutant, while other divalent metals such as Ca^{2+} and Co^{2+} had no effect **(Figure 18C)**. The IC_{50} for SENP1 inhibition by Zn^{2+} is right-shifted by nearly-30-fold from 1.1 μM in the WT to 28 μM in the C535S mutant **(Figure 18D)**. Re-folding of SENP1 with Zn^{2+} present increases the sensitivity of SENP1 activity to H_2O_2 by about 3-fold **(Figure 18E)**. Importantly, the presence of Zn^{2+} allows reactivation of SENP1 by GSH and glutaredoxin-1 (GRX1), a dynamic regulation that is lost in the C535S mutant **(Figure 18F)**. C535 is important for C535, H533 and C603 Zn^{2+} binding site. Zn^{2+} might prevent the efficient deprotonation of C603, dampening the SENP1 activity **(Figure 18G)**.

Figure 18. C535 regulates SENP1 with Zn^{2+} and redox.

(A): Prediction of Zn^{2+}-binding site in SENP1 WT (ID: 2IYC) and **(B):** C535S mutant derived from SENP1 WT (ID: 2IYC) using Pymol mutagenesis. **(C):** Effect of different metal ions on SENP1 activity. Data are normalized to C535S, as C535S mutant activity were more stable and resistant to oxidation (n=3). **(D):** Dose-response curve of SENP1 activity under different concentration of $ZnCl_2$ (n=3). **€:** Dose-response curve of SENP1 mutants prepared with or without $ZnCl_2$ under inhibition of H_2O_2 (n=3-6). **(F):** Wild-type SENP1 and mutants were reduced with 0.1 mM reduced glutathione and 10 μg/mL glutaredoxin1 (GSH+GRX1) after inhibition of 1 μM $ZnCl_2$ (n=4). **(G):** Illustration of Zn^{2+} binding to C535, H533 and C603. Data are mean ± SEM and were compared with student t-test, one-way ANOVA or two-way ANOVA followed by Bonferroni post-test. *$P < 0.05$, **$P < 0.01$, ***$P < 0.001$. In panel C, * indicated comparison between SENP1 WT and C535S. (KS performed A-F. HL performed G.)

Figure 18.

A

SENP1 WT

Predicted Zinc-bind Site	Probability
Cys603, Cys535, His533	1
Asp550, His533	1
Asp468, His529	1
Asp517, His491	1
Asp529, His533, His539	1
Glu430, His640	0.96

B

SENP1 C535S mutant

Predicted Zinc-bind Site	Probability
Asp550, His533	1
Asp468, His529	1
Asp517, His491	1
Glu430, His640	0.96

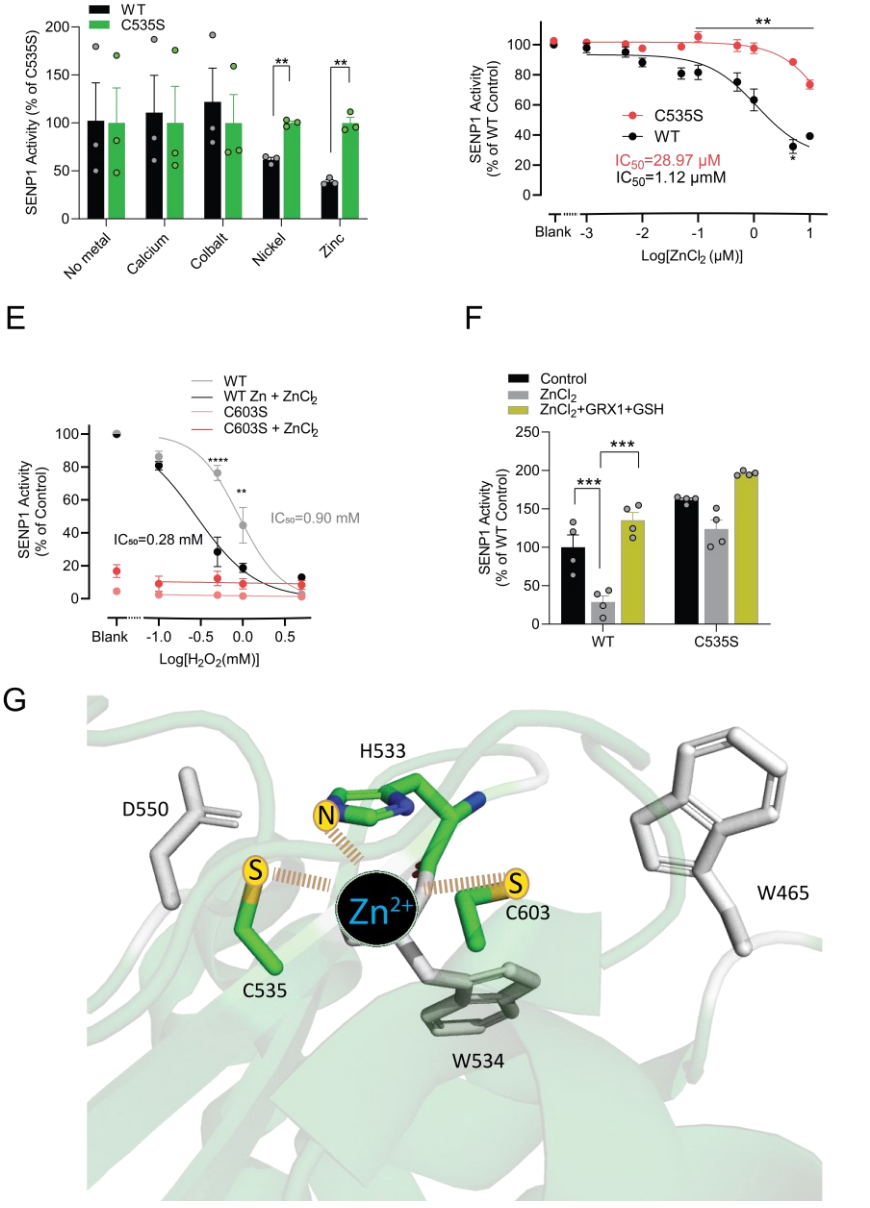

3.3.4 Zn^{2+} inhibits insulin exocytosis through SENP1

Finally, Zn^{2+} is an important regulator of insulin secretion[111,114]. We find that while intracellular application of 1 mM $ZnCl_2$ reduces β-cell exocytosis by blocking Ca^{+} channels, a lower concentration (100 μM) reduces exocytosis independent of Ca^{+} channel inactivation **(Figure 19A, B)**. In β-cells lacking SENP1 (βSENP1-KO), exocytosis is reduced[84], and 100 μM $ZnCl_2$ impaired exocytosis of βSENP-WT mouse β-cells without further decreasing exocytosis of βSENP-KO mouse β-cells **(Figure 19C, D)**[84]. This suggests that SENP1 is the target for Zn^{2+} to inhibit the insulin secretory response.

Figure 19. Zn^{2+} inhibits insulin exocytosis through SENP1.

(A): Effect of Zn^{2+} on Ca^{2+} charge entry and **(B):** exocytosis elicited by a single or a series of 500 ms membrane depolarizations from -70 mV to 0 mV at 5 mM glucose from C57 mice (n= 21-34 cells from 3 pairs of mice per group). **(C):** Effect of Zn^{2+} on Ca^{2+} charge entry and **(D):** exocytosis elicited by a single or a series of 500 ms membrane depolarizations from -70 mV to 0 mV at 5 mM glucose from βSENP1-KO and -WT mouse β-cells (n= 15-46 cells from 6 pairs of mice per group). Data are mean ± SEM and were compared with one-way ANOVA or two-way ANOVA followed by Bonferroni post-test. $*P < 0.05$, $**P < 0.01$, $***P < 0.001$. (All work by HL.)

Figure 19.

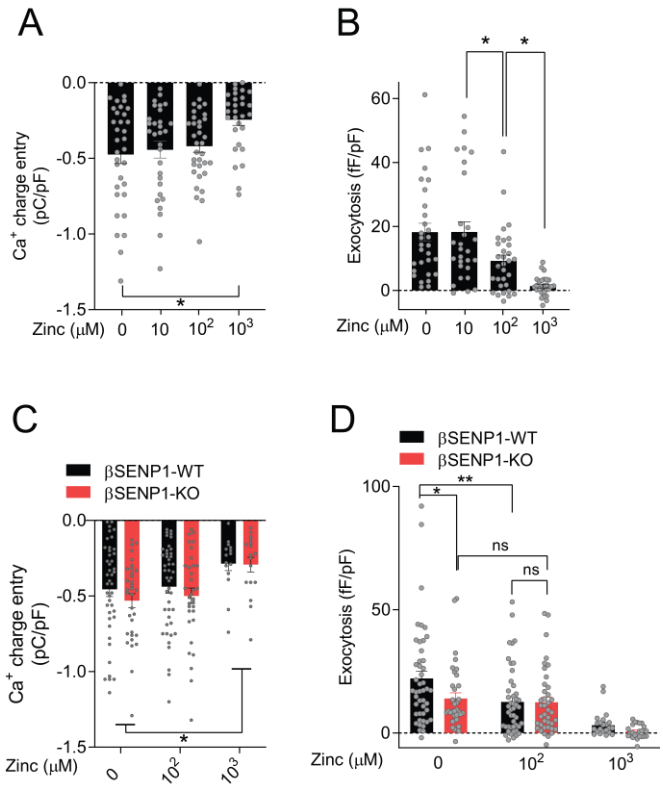
A
B
C
D
Ca+ charge entry (pC/pF)
Exocytosis (fF/pF)
Zinc (μM)
0
10
10^2
10^3
βSENP1-WT
βSENP1-KO
ns
*
**

In addition to autocrine Zn^{2+}, cytosolic free Zn^{2+} release/binding, presumably from cysteine-rich metallothionein (MT), is subject to an oxidation/reduction reaction[119]. Besides, glucose was reported to increase NADPH and decrease H_2O_2 in the cytosol, resulting in a reduced redox state[81,90]. Therefore, I investigated if redox change and glucose stimulation can induce Zn^{2+} dynamics in β-cells. Instead of localizing in Zn^{2+}-containing insulin granules indicated by ZIGIR[251], low levels of ZnAF2 were uniformly distributed in cytosol[268], allowing the detection of cytosolic Zn^{2+} changes **(Figure 20A)**. Upon treatment of H_2O_2, free Zn^{2+} significantly increased in the cytosol of mouse β-cells, indicating oxidation-induced Zn^{2+} release **(Figure 20B)**. NEM, alkylating thiol on cysteine, significantly enhanced the Zn^{2+} release, suggesting that the free Zn^{2+} release came from cysteine thiol groups, possibly from MT **(Figure 20C)**. Diazoxide was used to prevent the release of Zn^{2+}-containing insulin granules and allow the detection of cytosolic Zn^{2+}. However, glucose was not able to induce an observable change of intracellular Zn^{2+} **(Figure 20D)**. This suggested that although Zn^{2+} can be released under high oxidative stress, glucose cannot affect the cytosolic free Zn^{2+} release/binding under physiological condition.

Figure 20. Redox, not glucose, regulated cytosolic free Zn^{2+} fluctuation.

(A): Staining of mouse β-cell with ZnAF2 and ZIGIR (n=3). Free Zn^{2+} release in response to extracellular application of **(B):** 200 μM H_2O_2 (n= 6 cells), **(C):** 50 μM N-ethylmaleimide (NEM) (n= 6 cells) and **(D):** different concentration of glucose. 2.8 and 16.7 indicated 2.8 mM and 16.7 mM glucose (n=6 cells). 50 μM TPEN: N,N,N′,N′,-tetrakis-(2-pyridylmethyl) ethylenediamine. 100 μM DTT: Dithiothreitol. 100 μM Diazoxide. (All work by HL.)

Figure 20.

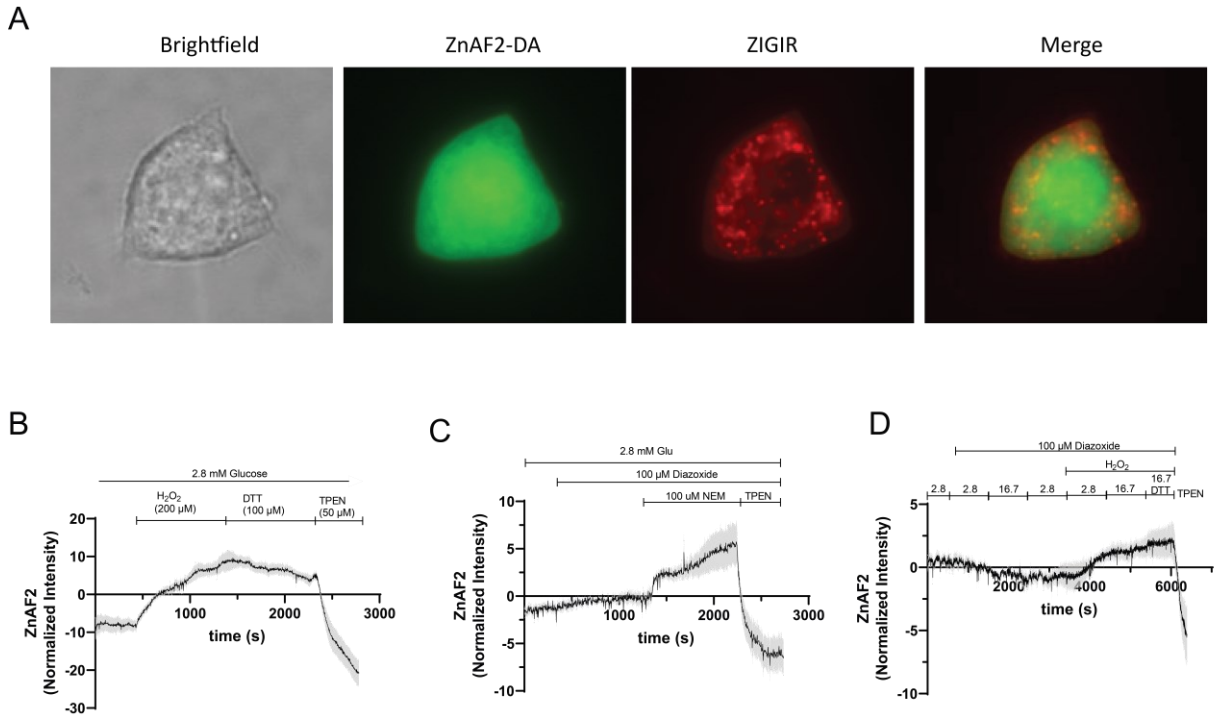
A
Brightfield
ZnAF2-DA
ZIGIR
Merge
B
2.8 mM Glucose
H2O2 (200 µM)
DTT (100 µM)
TPEN (50 µM)
ZnAF2 (Normalized Intensity)
time (s)
C
2.8 mM Glu
100 µM Diazoxide
100 uM NEM
TPEN
ZnAF2 (Normalized Intensity)
time (s)
D
100 µM Diazoxide
H2O2
2.8
2.8
16.7
2.8
2.8
16.7
16.7
DTT
TPEN
ZnAF2 (Normalized Intensity)
time (s)

3.4 Discussion

The redox-regulation of SENP1 was first revealed with the realization that SUMOylation level was subject to redox state and this redox-regulation was linked to glucose-stimulated insulin secreton[84,91]. However, the exact redox biochemical mechanism of SENP1 is not fully understood. In the present study, we found that C535 is an important negative regulator to restrain SENP1 activity and loss of C535 abolishes SENP1 redox-regulation of insulin exocytosis. Importantly, C535 is also an important allosteric Zn^{2+}-binding site to mediating the Zn^{2+} inhibitory effect on SENP1 and insulin exocytosis. Co-regulation by Zn^{2+} and redox through C535 are likely important to tune SENP1 dynamic activity for the control of insulin secretion.

The molecular basis of SENP1 redox regulation was reported that C603 formed a disulfide bond with C613 to make a dimerized SENP1, which can be reversibly reduced. C613 decreased the sensitivity to oxidation and acted as a positive regulator to protect from irreversible oxidation[91]. In our study, loss of C613 seemed to result in lower SENP1 activity but the decrease was only around 17%. Instead, loss of C535 caused a significant 2-fold increase in SENP1 activity, indicating that C535 is an important negative regulator. Initially, we hypothesized that C535 might form a similar intermolecular disulfide bond with C603 as C613. However, loss of C535 should prevent formation of the disulfide and make the mutant more prone to inactivation by oxidation as reported in the loss of C613. Instead, C535 showed much higher SENP1 activity in response to H_2O_2. In addition, the atomic distance between C535 and C603 is 7.1 Å, exceeding the cutoff value of 3 Å to form an intramolecular disulfide bond (truthfully, the same can be said about C613 which is even further from C603). Furthermore, existing SENP1 structures do not show any intramolecular disulfide bonds (data not shown). Therefore, the current data doesn't support C535

as a potential cysteine to form a disulfide bond with C603. One possibility for C535 to affect SENP1 redox regulation is through transferring a proton from C603 to H533. C535 is positioned nearby the His533 and might competitively inhibit the donation of proton from C603 to H533, thus restricting the deprotonation of C603 and SENP1 activity.

Zn^{2+} could allosterically inhibit SENP1 by binding to C535. Thus, loss of C535 increased the Zn^{2+} IC_{50} for SENP1 by 30-fold, suggesting that C535 not only mediates the redox regulation, but also plays a significant role in Zn^{2+}-mediated inhibition. The predicted Zn^{2+}-binding site contained C603, His533 and C535. The Cys-His-Cys motif is one of the most ubiquitous Zn^{2+} binding motifs[269]. This binding motif is specific to Zn^{2+} and not affected by other endogenous divalent metals, such as Ca^{2+} and Co^{2+}. Although nickel has similar effect on SENP1, it rarely exists in pancreatic islets. As a strong negative regulator of SENP1, C535 prevents the hyperactivity of SENP1, which might otherwise abolish the redox regulation of SENP1 and cause dysregulated β-cell function or survival[183].

DeSUMOylation was reportedly inhibited by high levels of H_2O_2 (10 mM)[172]. Consistent with this, IC_{50} for SENP1 WT is 1 mM and 2.5 mM for SENP1 C535S mutant. The biological relevance of SENP1 in β-cell is to couple reducing power from NADPH derived from TCA cycle to the GSIS[58,84,174,175]. However, the IC_{50} for H_2O_2 to depress SENP1 activity is too high to match the normal physiological redox state in the β-cell, thus making it unlikely to conclude that SENP1 is regulated only by glucose-stimulated redox change under physiological condition. Instead, this high level of H_2O_2 is more likely to match pathological oxidative stress which would inactivate SENP1, resulting in β-cell functional deficiency. Compared to H_2O_2, Zn^{2+} inhibits SENP1 activity more efficiently, with a IC_{50} of only 1 μM, which more closely resembles the Zn^{2+} level observed

in the β-cell[270]. In the presence of Zn^{2+}, H_2O_2 reduces SENP1 activity more efficiently, and it can be reactivated by GSH+GRX1 via C535. The binding of Zn^{2+} to SENP1, probably occurring during protein folding in ER, might be highly relevant for redox regulation of SENP1 in β-cell function. This is because less H_2O_2 is required to inactivate SENP1 in the presence of Zn^{2+}, conferring a responsive sensitivity to glucose-stimulated redox change under normal conditions.

Other than its role in protein folding, Zn^{2+} is important in insulin biosynthesis and plays as an autocrine inhibitory signal to prevent insulin hypersecretion[111,114,270]. We showed that SENP1 was the target for Zn^{2+} to inhibited exocytosis. The identification of SENP1 as a Zn^{2+} target indicates that autocrine Zn^{2+} released from the insulin granule could possibly re-enter the cytosol and prevent overstimulation of insulin release. Consistent with this, our previous data showed that the deSUMOylation profile of Syt7 peaked at 15 minutes after glucose stimulation and decreased afterwards[175]. This could be associated with increase of glucose-stimulated reducing equivalent in the cytosol, followed by the inhibition of autocrine Zn^{2+}[111]. Other than the autocrine pathway, cytosolic Zn^{2+} release is subject to the redox regulation of metallothionein protein, which shows high binding affinity for Zn^{2+}, with a dissociation constant K_d of 3.2×10^{-13} M[115]. Since cytosolic free Zn^{2+} in the β-cell is around 4×10^{-10} M[270], this means 99.9 % of MT protein is in theory bound to Zn^{2+}. In contrast, SENP1 has a lower affinity for Zn^{2+}, with a K_i of 10^{-6} M. Therefore, the direct effect of Zn^{2+} on SENP1 could be dependent on the control of Zn^{2+} from MT. However, the level of free-Zn^{2+} level seems to be rarely perturbed in response to glucose[271]. Even so, other mechanisms might still mediate the glucose-induced transfer of Zn^{2+} from MT to SENP1 or the other way around. Indeed, Zn^{2+} is always transferred in a complex with other agents, instead of as a free Zn^{2+} ion[115]. Some specific agents, such as GSH and citrate, have been reported to be involved in Zn^{2+} transfer[115]. In β-cells, metallothionein was proposed to a negative regulator of insulin

secretion[121]. In the future, it is tempting to investigate if Zn^{2+}-bound MT could affect SENP1 activity via Zn^{2+} transfer.

3.5 Methods

3.5.1 The DNA cloning of SENP1 expression vectors.

Plasmid, pT7JLH[76], was used to express SENP1 and its mutant in *Escherichia coli* (*E.coli*). The pT7JLH plasmid drives protein expression with T7 promoter, and His×6 tag is added at N-terminal of SENP1 protein. First, the cDNA of human SENP1 catalytic domain (residues 419-644) was cloned downstream of His×6 tag between Xba-I and BamH-I sites. Site directed mutagenesis by primer extension was used to make the expression of plasmids SENP1 mutants, C535S, C560S, C603S, C608S, C613S, C535S/C608S and C603S/C613S. In brief, two sets of overwrapping mutagenesis primers were used to amplify SENP1 catalytic domain using Phusion DNA polymerase. The SENP1 cDNA was cloned between Xba-I and BamH-I sites using Gibson assembly.

3.5.2 Recombinant SENP1 expression in *E.coli*.

Rosetta strain of *E.coli* (Novagen) was transformed with each SENP1 expression vector. The transformed *E.coli* was grown in 50 mL LB broth containing 100 μg/mL Ampicillin at 37 ºC with shaking at 200 rpm until A600 reached between 0.6 and 0.8. Each SENP1 protein was over expressed by addition of 1 mM IPTG into the culture. After 2 hours induction, the *E.coli* pellet was harvested by centrifugation at 10,000 ×g for 10 minutes.

3.5.3 Purification of SENP1 proteins.

Inclusion bodies of SENP1 proteins were prepared from *E.coli* pellet[272]. Each SENP1 protein was solubilized in 6 M guanidine HCl, 20 mM Tris, 0.1% Tween20, 1 mM 2-mercaptoethanol, pH 8, and then captured with a HisPur Nickel-NTA resin column (1.5 × 3cm). The column was washed with 4 M Guanidine HCl, 20 mM Tris, 0.1 % Tween20, 1 mM 2-mercaptoethanol, pH 8 and then SENP1 protein was eluted with 4 M guanidine HCl, 50 mM Sodium acetate, 0.05 % Tween20, pH 4. The absorbance at 280 nm of each SENP1 protein was measured to estimate the concentration. SENP1 proteins were stored at -80 ^{o}C until *in vitro* refolding.

3.5.4 Removal of nickel in the purified SENP1 proteins.

The purified SENP1 proteins contain nickel that was leached out from nickel-NTA resin. For the most of experiments, nickel in SENP1 proteins were removed by precipitation in the presence of 20 mM Tris, 5 mM EDTA, pH 8. In brief, the concentration of each SENP1 protein was adjusted to 4 mg/mL with 4 M guanidine HCl, 20 mM Tris, 0.1% Tween20, 1 mM 2-mercaptoethanol, 50 mM EDTA and 0.2 M Tris, pH 8. Ten volume of water was added to dilute the concentration of 4 M guanidine HCl to 0.4 M. The rapid decrease of guanidine HCl concentration causes the precipitation of SENP1 protein. The precipitated SENP1 protein without nickel was recovered by centrifugation at 8000 ×g for 20 minutes.

3.5.5 *In vitro* refolding of SENP1.

The refolding of SENP1 protein was carried out *in vitro* by gradual decrease of guanidine HCl concentration with dialysis[273]. The concentration of SENP1 protein was adjusted to 1 mg/ml with 6 M guanidine HCl, 20 mM Tris, 0.1 % Tween20, 0.2 M Arginine, pH 7.2, and for each

refolding 4-5 mg of SENP1 was used. The cysteines of SENP1 proteins were reduced to thiol with 10 mM DTT for 1 hour at room temperature. The SENP1 proteins were dialyzed against 10 volumes of 0.5 M guanidine HCl, 0.2 M Arginine, 0.1 M Tris, 2 mM Cysteine, 0.2 mM Cystine, 0.05 % Tween20, pH 7.2 for 24 hours, and then against 20 volumes of same solution without guanidine HCl for 24 hours. SENP1 proteins were finally dialyzed against 50 volumes of SENP1 assay buffer, 20 mM Tris, 0.1 M sodium chloride, 0.05 % Tween20, pH 7.2 for 24 hours with changing to fresh buffer twice. The precipitated SENP1 proteins were removed by centrifugation at 8000 ×g for 10 minutes. Absorbance at 280 nm of the supernatant were measured to estimate the concentration of SENP1 proteins. For the experiments to study the effect of divalent transient metals on SENP1 activity, 0.1 mM of calcium chloride, cobalt chloride, nickel chloride and Zn^{2+} chloride was added in the refolding solution.

3.5.6 SENP1 assay using recombinant His×6-SUMO1-mCherry.

The recombinant SENP1 protein (0.1 μM) was mixed with 0.25 μM of His×6-SUMO1-mCherry, and then was incubated at 37 ºC for 2 hours. The mCherry was separated from His×6 tag-SUMO1 upon the cleavage with SENP1. The undigested substrate was captured and removed by the addition of 25 μl of HisPur Nickel-NTA resin suspension (1:1, v/v). After vortexing for 10 seconds, HisPur Nickel-NTA resin was precipitated by centrifugation at 10,000 ×g for 30 seconds at 4 ºC. Each supernatant was transferred into a 96-well clear bottom black plate and then fluorescent intensity, Ex544 nm/Em615 nm, was measured **(Figure 16A)**.

3.5.7 Preparation of recombinant His×6-SUMO1-mCherry.

Recombinant His×6-SUMO1-mCherry was used as substrate to measure SENP1 activity for the most of experiments. The cDNA of full size human SUMO1, including the cleavage site,

and mCherry were amplified with PCR using Phusion DNA polymerase and the PCR fragments were cloned into a pT7JLH plasmid at Xba-I site using Gibson assembly to make pT7JLH-SUMO1-mCherry plasmid. Rosetta strain of *E.coli* was transfected with the plasmid. The transformed *E.coli* was grown in 50 mL LB broth containing 100 µg/mL Ampicillin at 37 ºC with shaking at 200 rpm until A600 reached between 0.6 and 0.8. His×6-SUMO1-mCherry protein was expressed by slow induction with 0.1 mM IPTG at 20 ºC overnight. Next day, the *E.coli* pellet was harvested by centrifugation at 10,000 ×g for 10 minutes. Pink color of *E.coli* pellet indicated the proper folding of His×6-SUMO1-mCherry protein. The *E.coli* pellet was incubated with 500 µg/mL lysozyme, 1 mM PMSF, 50 mM Tris, 0.2 M sodium chloride, pH8 for 3 hour at 4 ºC, and then sonicated five times in short burst of 30 seconds on ice. Soluble His×6-SUMO1-mCherry protein was harvested by centrifugation at 10,000 ×g for 10 minutes at 4 ºC. The His×6-SUMO1-mCherry in the supernatant was purified with a HisPur Nickel-NTA resin column (1 × 5 cm). The purified His×6-SUMO1-mCherry was dialyzed against 10 volume of 50 mM EDTA, pH 8 for 6 hours and then 50 volumes of SENP1 assay buffer, 20 mM Tris, 0.1 M Sodium Chloride, 0.05 % Tween20, pH 7.2 for 24 hours. The final dialysis buffer was changed to fresh buffer twice. The concentration of the purified His×6-SUMO1-mCherry protein was estimated by the absorbance at 280 nm.

3.5.8 Preparation of recombinant GRX1.

The cDNA of human GRX1 was cloned into expression vector, pT7JLH. Recombinant GRX1 was produced in *E.coli*, purified and carried out *in vitro* refolding as same methods as described for SENP1 preparation.

3.5.9 SENP1 mutant activity.

To compare SENP1 mutant activity, WT, C535S, C560S, C603S, C608S, C613S, C535S/C608S and C603A/C613S were purified and refolded in the presence of 1 mM $ZnCl_2$. $ZnCl_2$ was removed by dialysis without being fully activated, 0.5 μM SENP1 and 1 μM His×6-SUMO1-mCherry were incubated at 37 ºC for 2 hours to measure SENP1 mutant activity.

3.5.10 Preparation of fully activated SENP1 WT and C535S.

Because SENP1 activity constantly changes during the storage due to inactivation with oxidation, wild type SENP1 and C535S were fully activated with 10 mM DTT before subjecting to the activation or inactivation studies of SENP1 and C535S. SENP1 wild type and mutants were fully activated by incubation with 10 mM DTT at 4 ºC overnight. Amicon Ultra-4 10,000NMWL was used to remove DTT and then replaced the buffer to SENP1 assay buffer, 20 mM Tris, 0.1 M Sodium Chloride, 0.05 % Tween20, pH 7.2. Final concentration of SENP1 and mutants were estimated by the absorbance at 280nm. To preserve the activity of SENP1 25 % glycerol (w/w) was added and store under nitrogen gas at -20 ºC.

3.5.11 IC_{50} of inhibition of SENP1 WT and C535S by H_2O_2.

SENP1 proteins were prepared without $ZnCl_2$ in the refolding process. The fully activated wild type SENP1 and C535S (0.1 μM) were incubated with various concentration of hydrogen peroxide (0.1, 0.5, 1 or 5 mM) for 1 hour at 20ºC. Catalase (20 μg) was added into each tube and then incubated for 30 minutes at 20ºC to remove hydrogen peroxide. The activity of the oxidized SENP1 and mutants were measured by SENP1 assay with recombinant His×6-SUMO1-mCherry (2.5 μM).

3.5.12 IC_{50} of inhibition of SENP1 WT and C535S by Zn^{2+}.

SENP1 proteins were prepared without $ZnCl_2$ in the refolding process. The fully activated wild type SENP1 and C535S (0.1 μM) were incubated with of 0.001, 0.005, 0.01, 0.05, 0.1, 0.5, 1, 5 or 10 μM $ZnCl_2$ overnight at 4 ºC. The activities of SENP1 and mutants with Zn^{2+} were measured by SENP1 assay with recombinant His×6-SUMO1-mCherry. *K*i value was calculated at a webserver https://bioinfo-abcc.ncifcrf.gov/IC50_Ki_Converter/index.php[274]. Free Zn^{2+} level was calculated at a webserver https://somapp.ucdmc.ucdavis.edu/pharmacology/bers/maxchelator/.

3.5.13 IC_{50} of inhibition of SENP1 WT by H_2O_2 with Zn^{2+} in the refolding process .

SENP1 and mutants were refolded with/without 0.1mM $ZnCl_2$, and then $ZnCl_2$ was removed by dialysis. Fully activated SENP1 and mutant were incubated with various concentration of H_2O_2 for 30 minutes at room temperature. Catalase (100ug) was added into each tube to remove H_2O_2 and then SENP1 activity was measured. Inactive mutant C603S was used as negative control.

3.5.14 Activation of SENP1 with reducing agents .

SENP1 and mutants were prepared without $ZnCl_2$ in the refolding buffer. SENP1 and mutants were incubated with 1μM $ZnCl_2$ for 1 hour to suppress SENP1 activities and reactivated by 0.1mM GSH+10ug/ml GRX1.

3.5.15 Patch-clamp analysis.

Human islets from a total of 13 non-diabetic (ND) donors and freshly isolated mouse islets were dispersed to single cells in calcium-free dissociation buffer and cultured in 5.5 mM glucose DMEM (11965, Thermo Fisher) and 11 mM glucose RPMI (11875, Thermo Fisher) respectively. After overnight culture, dispersed cells were used for whole-cell patch clamping. Prior to patch-

clamping, dispersed cells were preincubated at 1 mM glucose (human) or 2.8 mM (mouse) for 1 hour and patched in bath solution containing 118 mM NaCl, 5.6 mM KCl, 20 mM TEA, 1.2 mM $MgCl_2$, 2.6 mM $CaCl_2$, 5 mM HEPES at different glucose conditions (1 mM, 2.8 mM, 5mM, 10 mM) with a pH of 7.4 (adjusted by NaOH). After 10 minutes, whole-cell patch-clamp exocytosis was performed with the sine+ DC lock-in function of an EPC10 amplifier and Patchmaster software (HEKA Electronics). Exocytotic responses and inward Ca^{2+} currents were measured 1-2 minutes after obtaining the whole-cell configuration in response to ten 500 ms depolarizations to 0 mV from a holding potential of -70 mV. Changes in capacitance and integrated Ca^{2+} charge entry were normalized to cell size (fF/pF and pC/pF, respectively). The intracellular solution contained 125 mM Cs-Glutamate, 10 mM CsCl, 10 mM NaCl, 1 mM $MgCl_2$, 5 mM HEPES, 0.05 mM EGTA, 3 mM MgATP and 0.1 mM cAMP with pH = 7.15 (pH adjusted with CsOH). In the infusion experiment, exocytotic responses and inward Ca^{2+} currents were measured 2-3 minutes after obtaining the whole-cell configuration. Compounds or recombinant enzymes were added to pipette solution as indicated for intracellular infusion to single cells. For human β cells infusion experiments, the control vector, 4 μg/mL wild type SENP1, C535S and C603 mutants were pretreated with or without 200 μM H_2O_2 for 10 minutes. For Zn^{2+} infusion experiments, $ZnCl_2$ were included and free Zn^{2+} level was approximated at https://somapp.ucdmc.ucdavis.edu/pharmacology/bers/maxchelator/webmaxc/webmaxcS.htm. Human β cells were identified by immunostaining for insulin. Mouse β cells were identified by size (>4 pF) and the Na+ channel half-maximal inactivation at around -90 mV[250]. Human islets isolation by the Human Research Ethics Board (Pro00013094; Pro00001754) were approved at the Alberta Diabetes Institute IsletCore according to methods deposited in the protocols.io

repository [248]. Full details of donor information, organ processing, and quality control information can be assessed with donor number at www.isletcore.ca.

3.5.16 Bioinformatics analysis.

Sequence comparison was performed by multiple sequence blast function in Pubmed. Pymol2 was used to analyze the structure of native SENP1 protein (2IYC) and SENP1-SUMO protein (2IYD) from PDB database. ZincBind https://zincbind.net/ was used to predict the Zn^{2+}-binding site in SENP1 (2IYC)[267].

3.5.17 Zn^{2+} staining and imaging.

Freshly isolated islets were dispersed into single cells and seeded in glass bottom dishes overnight. Mouse islets cells were loaded with 8 μM ZnAF-2 (abcam, ab145422) in mouse islet culture media (11 mM glucose, 11875) at 37 ºC and 5% CO_2 for 1 hour, then with ZIGIR (0.5 μM) for 15 minutes. Islets cells were washed with KRB solution (2.8 mM Glu, 140 mM NaCl, 3.6 mM KCl, 0.5 mM MgSO4($7H_2O$), 1.5 mM CaCl2($6H_2O$), 10 mM Hepes, 5mM $NaHCO_3$, 0.5 mM NaH_2PO_4. PH 7.4.) three times and perifused at 2.8 mM glucose for at least 15 minutes prior to Zn^{2+} dynamic imaging at an inverted microscope (Zeiss Axioobserver, Carl Zeiss Canada Ltd.) with a rapid-switching light source (Oligochrome; Till Photonics, Grafelfing, Germany). Imaging was performed at around 37 ºC at an excitation wavelength of 480 nm and a frequency of 0.5 Hz[275]. For the Zn^{2+} staining experiment, a Cell-TIRF motorized system (IX83P2ZF, Olympus Canada) with a 100×/1.49 NA TIRFM objective, a Photometrics Evolve 512 camera (Photometrics), and Metamorph Imaging software (Molecular Devices) was used[93]. Stimulation at 491 nm (LAS-491-50) was used for ZnAF2 and stimulation at 561 nm (LAS-561-50, Olympus, Germany) was used

for ZIGIR staining with a quad filter passing through a major dichroic and band pass filter (405/488/561/640, Chroma Technology, Bellows Falls, VT).

Chapter 4.

β-Cell Knockout of SENP1 Reduces Responses to Incretins and Worsens Oral Glucose Tolerance in High Fat Diet-Fed Mice

The following chapter is adapted from work published in ***Diabetes***. It is reprinted with the permission of the American Diabetes Association:

Haopeng Lin, Nancy Smith, Aliya F Spigelman, Kunimasa Suzuki, Mourad Ferdaoussi, Tamadher A. Alghamdi, Sophie L Lewandowski, Yaxing Jin, Austin Bautista, Ying Wayne Wang, Jocelyn E. Manning Fox, Matthew J Merrins, Jean Buteau, Patrick E MacDonald. Diabetes 70.11 (2021): 2626-2638.

β-Cell Knockout of SENP1 Reduces Responses to Incretins and Worsens Oral Glucose Tolerance in High-Fat Diet–Fed Mice.

Contributions by co-authors to the figures are acknowledged by co-author initials.

4.1 Abstract

SUMOylation reduces oxidative stress and preserves islet mass at the expense of robust insulin secretion. To investigate a role for the deSUMOylating enzyme sentrin-specific protease 1 (SENP1) following metabolic stress, we put pancreas/gut-specific SENP1 knockout mice (pSENP1-KO) on a high-fat diet (HFD). Male pSENP1-KO mice were more glucose intolerant following HFD than littermate controls but only in response to oral glucose. A similar phenotype was observed in females. Plasma glucose-dependent insulinotropic polypeptide (GIP) and glucagon-like-peptide 1 (GLP-1) responses were identical in pSENP1-KO and -WT littermates, including the HFD-induced upregulation of GIP responses. Islet mass was not different, but insulin secretion and β-cell exocytotic responses to the GLP-1 receptor agonist Exendin-4 (Ex4) and GIP were impaired in islets lacking SENP1. Glucagon secretion from pSENP1-KO islets was also reduced, so we generated β-cell-specific SENP1 KO mice. These phenocopied the pSENP1-KO mice with selective impairment in oral glucose tolerance following HFD, preserved islet mass expansion, and impaired β-cell exocytosis and insulin secretion to Ex4 and GIP without changes in cAMP or Ca^{2+} levels. Thus, β-cell SENP1 limits oral glucose intolerance following HFD by ensuring robust insulin secretion at a point downstream of incretin signaling.

4.2 Introduction

Glucose metabolism is the primary driver for insulin secretion, stimulating electrical activity and Ca^{2+} entry to trigger the exocytosis of insulin granules. Multiple additional factors serve either to maintain or augment the pool of secretory granules available to respond to the Ca^{2+} increase[276]. These pathways could be required for robust insulin secretory responses to receptor-mediated secretagogues such as the incretin hormones glucose-dependent insulinotropic

polypeptide (GIP) and glucagon-like peptide-1 (GLP-1)[65]. The action of the incretins to facilitate insulin secretion is impaired in type 2 diabetes (T2D), although the underlying mechanism appears complex[277] and could involve altered receptor signaling[278]. Incretin-induced insulin secretion from human islets correlates with the ability of glucose to augment depolarization-induced insulin exocytosis in single β-cells[223]. In mice with impaired metabolism-insulin granule coupling, achieved by β-cell specific deletion of the sentrin-specific protease-1 (SENP1), we showed that the β-cell response to the GLP-1 receptor agonist Exendin-4 (Ex4) was impaired and the ability of DPP4 inhibition to improve oral glucose tolerance was greatly reduced[223].

Glucose metabolism drives the export of mitochondrial reducing equivalents, and the resulting redox signal relay increases the small ubiquitin-like modifier (SUMO) protease activity of SENP[84]. A resulting deSUMOylation of exocytotic proteins, such as Syt7, facilitates Ca^{2+}-dependent insulin granule exocytosis[84,92,173–175]. This redox-dependent pathway appears to be impaired in T2D, likely a result of upstream mitochondrial dysfunction, and loss of islet SENP1 results in moderate oral glucose intolerance with impaired insulin secretion[84]. Somewhat contradicting this, overexpression of SENP1 induces apoptosis in β-cells[179], and mice lacking the SUMO-conjugating enzyme Ubc9 develop diabetes as a result of β-cell death[181]. Effectively, SUMOylation appears required for β-cell viability at the cost of β-cell function[183]. It remains unknown whether the deSUMOylating enzyme SENP1 is required for the facilitation of insulin secretory responses and glucose tolerance under metabolic stress, such as high fat diet (HFD), or conversely, whether loss of SENP1 would protect against glucose intolerance by preserving β-cell mass and insulin secretion.

Here we investigated two interrelated questions in both gut/pancreas-specific SENP1 knockout (pSENP1-KO) and β-cell-specific (βSENP1-KO) SENP1 knockout mice. We asked

whether the loss of β-cell SENP1 sensitizes mice to HFD-induced glucose-intolerance and whether altered incretin responsiveness contributes to this. We find that following HFD, both pSENP1-KO mice and βSENP1-KO mice show a worsening of oral glucose intolerance. This is accompanied by a decreased insulin secretory response to glucose and incretin receptor activation, without any difference in β-cell mass and little or no effect on cAMP or Ca^{2+} responses to incretin receptor activation. Our findings support a model whereby SENP1 is required to ensure the availability of releasable insulin granules. This is important for limiting oral glucose intolerance following HFD where incretins, notably plasma GIP, are increased and require a robust pool of release-competent insulin granules on which to act.

4.3 Results

4.3.1 Mice lacking islet SENP1 develop worsened oral glucose intolerance after HFD

We previously showed that SENP1 is required for insulin exocytosis, and that male pSENP1-KO mice are mildly intolerant of oral glucose[84]. Because of loss of Cre-expression in the previous colony, we made the pSENP1-KO mice by crossing Pdx1-Cre^{+} mice from Jackson Labs [B6.FVB-Tg (Pdx1-cre)6 Tuv/J] and Pdx1-Cre^{-} $Senp1^{fl/fl}$ and confirmed loss of SENP1 **(Figure 21Ai)** and increased SUMOylation **(Figure 21Aii, arrows)** in islets. β-cells from pSENP1-KO mice have impaired glucose-dependent facilitation of exocytosis **(Figure 21B)** and unaffected voltage-dependent Ca^{2+} currents **(Figure 21C**). The pSENP1-KO mice have modest fasting hyperinsulinemia compared with littermates **(Figure 22A)**. We performed OGTT, IPGTT, and ITT on male and female mice at 10-12 weeks of age **(Figure 21D)**. Male pSENP1-KO mice were not obviously intolerant to oral or IP glucose **(Figure 21E and F and Figure 22A-D**), despite

reduced glucose-stimulated plasma insulin **(Figure 21G)**. Female mice exhibited a similar phenotype, with some indication of IP glucose intolerance **(Figure 21H-J and Figure 22E-H**).

Figure 21. Normal glucose tolerance, but impaired insulin responses, of pSENP1-KO mice on CD.

(A): (i) Western blot of SENP1 expression in tissues from pSENP1-WT and -KO mice. **(ii)** SUMOylation profiles of islet lysates from pSENP1-WT and -KO mice showing numerous SUMOylated proteins. IB: immunoblotting. **(B):** Representative traces (left) and average total responses of β-cell exocytosis elicited by a series of 500-ms membrane depolarizations from -70 to 0 mV at 2.8 and 10 mmol/L glucose (n=28, 22, 22, 20 cells, n values correspond to graph bars from left to right, respectively). 0.1 mmol/L cAMP was included in pipette solution. **(C):** Representative traces, and average β-cell voltage-dependent Ca^{2+} currents, elicited by a single 500 ms membrane depolarization from -70 to 0 mV at 2.8- and 10-mM glucose (n=26, 18, 25, 16 cells). 0.1 mmol/L cAMP was included in pipette solution. **(D):** Schematic diagram of experiments on CD-fed mice. **(E)** OGTT in male pSENP1-WT, -HET, and -KO mice (n=6, 6, 6 mice). **(F and G):** IPGTT in male pSENP1-WT, -HET, and -KO mice (F - n=8, 13, 10 mice) and associated plasma insulin responses (G - n=8, 9, 8 mice). **(H):** OGTT in female pSENP1-WT, -HET, and -KO mice (n=8, 9, 9 mice). **(I, J):** IPGTT in female pSENP1-WT, -HET, and -KO mice (I - n=9, 7, 7), and associated plasma insulin responses (J - n=8, 6, 5 mice). AUC - area under the curve. Data are mean ± SEM and were compared with one-way or two-way ANOVA followed by Bonferroni post-test. Unless stated otherwise, **P*<0.05, ***P*<0.01, ****P*<0.001 indicated comparison between pSENP1-WT and -KO, while #*P*<0.05 indicates comparison between pSENP1-HET and pSENP1-WT. $*P*<0.05, $$*P*< 0.01 indicates comparison between pSENP1-HET and pSENP1-KO. (HL performed B-C, KS and TA performed A and HL prepared all the samples for test. NS performed E-J.)

Figure 21.

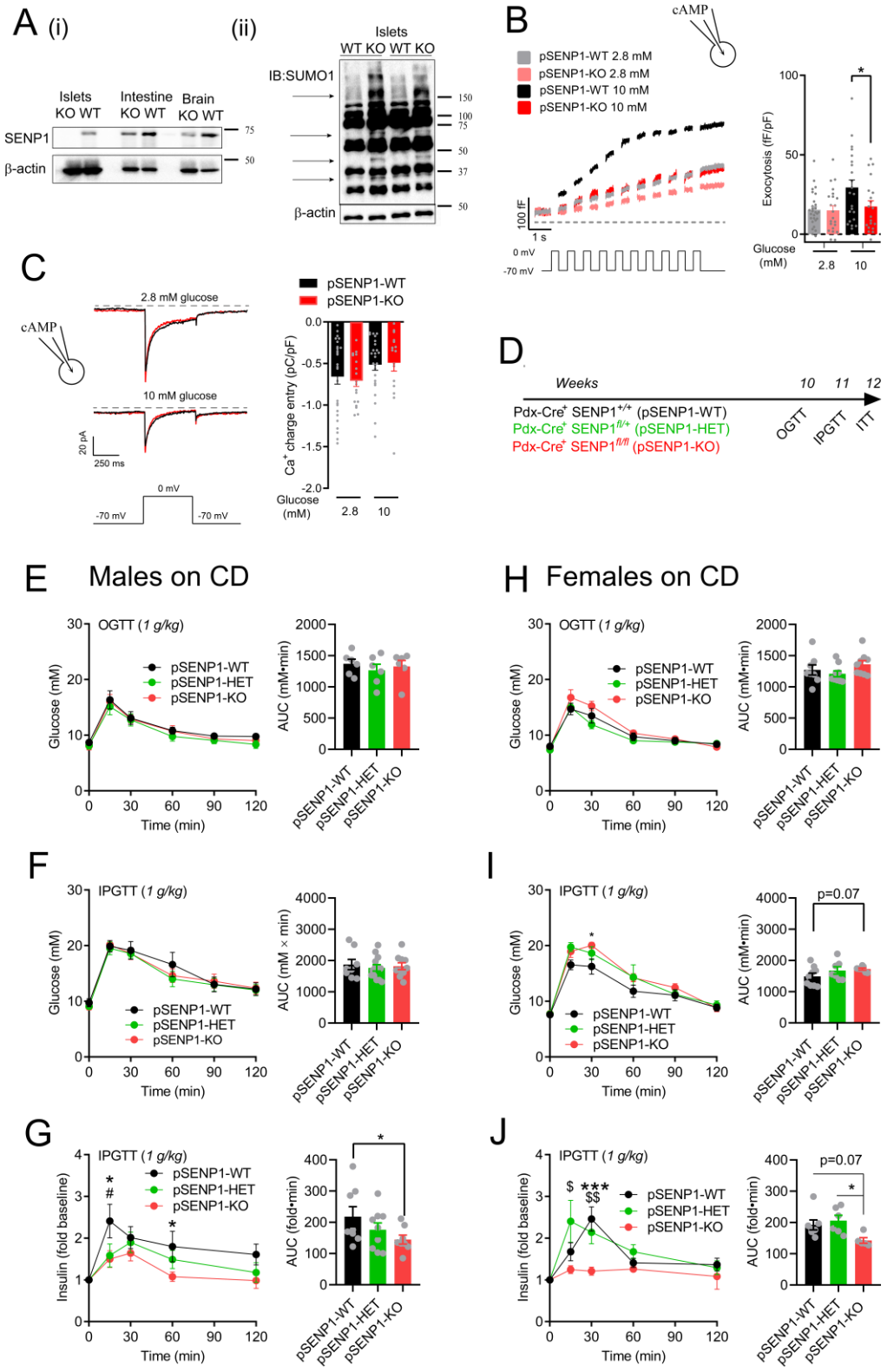
A (i)
Islets KO WT
Intestine KO WT
Brain KO WT
SENP1
β-actin
(ii)
Islets
WT KO WT KO
IB:SUMO1
β-actin
B
cAMP
pSENP1-WT 2.8 mM
pSENP1-KO 2.8 mM
pSENP1-WT 10 mM
pSENP1-KO 10 mM
100 fF
1 s
0 mV
-70 mV
Exocytosis (fF/pF)
Glucose (mM)
2.8
10
C
cAMP
2.8 mM glucose
10 mM glucose
20 pA
250 ms
0 mV
-70 mV
-70 mV
pSENP1-WT
pSENP1-KO
Ca+ charge entry (pC/pF)
Glucose (mM)
2.8
10
D
Weeks
10
11
12
Pdx-Cre+ SENP1+/+ (pSENP1-WT)
Pdx-Cre+ SENP1fl/+ (pSENP1-HET)
Pdx-Cre+ SENP1fl/fl (pSENP1-KO)
OGTT
IPGTT
ITT
E Males on CD
OGTT (1 g/kg)
pSENP1-WT
pSENP1-HET
pSENP1-KO
Glucose (mM)
Time (min)
AUC (mM•min)
H Females on CD
F
IPGTT (1 g/kg)
AUC (mM × min)
I
p=0.07
G
Insulin (fold baseline)
AUC (fold•min)
J
$
$$
***

Figure 22. Additional *in vivo* glucose homeostasis assessment of male and female pSENP1-KO mice on CD.

(A): Fasting insulin; **(B):** fasting glucose, **(C):** body weight, and **(D):** IP insulin tolerance of pSENP1-WT, -HET and -KO male mice on CD (n=6-22 mice). **(E):** Fasting insulin, **(F):** fasting glucose, **(G):** body weight, and **(H):** IP insulin tolerance of pSENP1-WT, -HET and -KO female mice on CD (n=7-17 mice). AUC - area under the curve. Data are mean ± SEM and were compared with student t test, one-way or two-way ANOVA followed by Bonferroni post-test. Unless stated otherwise, **P*<0.05, indicated comparison between pSENP1-WT and -KO. (NS performed A-H and HL analyzed the data.)

Figure 22.

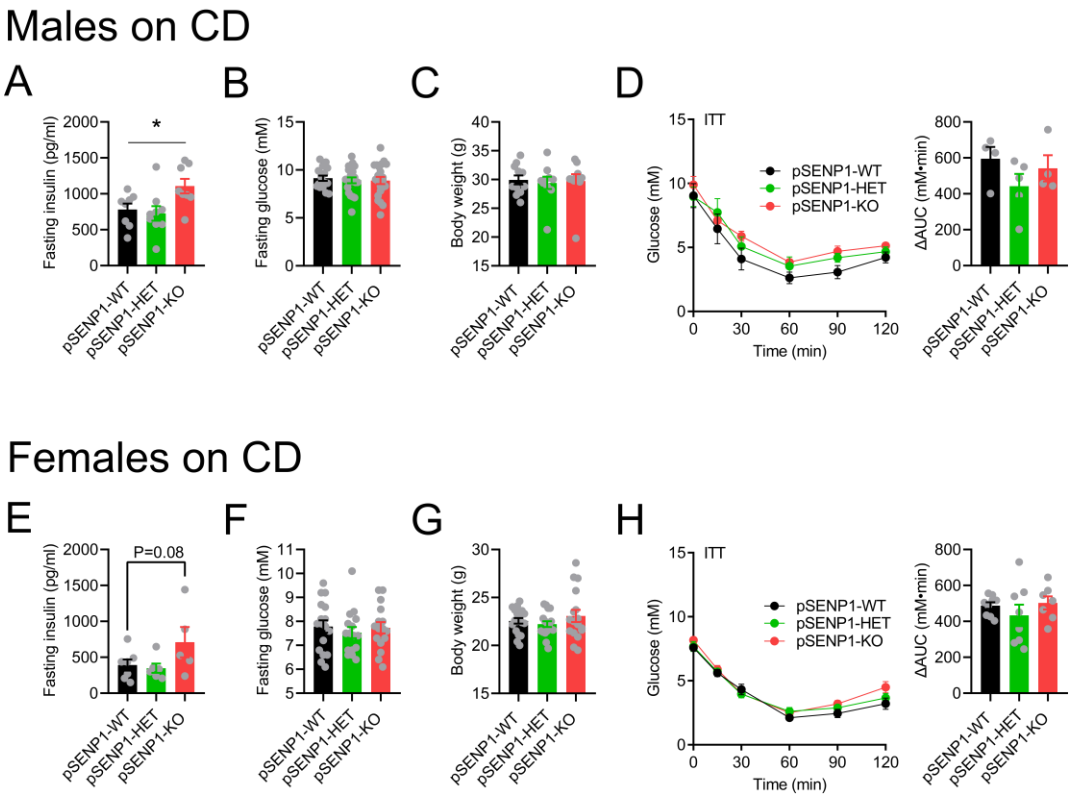
Males on CD
A
B
C
D
Fasting insulin (pg/ml)
2000
1500
1000
500
0
*
pSENP1-WT
pSENP1-HET
pSENP1-KO
Fasting glucose (mM)
15
10
5
0
Body weight (g)
40
35
30
25
20
15
ITT
Glucose (mM)
Time (min)
0
30
60
90
120
pSENP1-WT
pSENP1-HET
pSENP1-KO
ΔAUC (mM•min)
800
600
400
200
0
Females on CD
E
F
G
H
P=0.08
11
10
9
8
7
6
5

After HFD **(Figure 23A)**, there was no difference in insulin tolerance or fasting insulin **(Figure 23B and C)**, but male pSENP1-KO mice exhibited elevated fasting glucose and body weight **(Figure 23D and E**). IP glucose intolerance was only modestly worsened in the pSENP1-KO mice **(Figure 23F**), but these mice were clearly more intolerant of an oral glucose challenge with decreased plasma insulin compared to littermate controls **(Figure 23G and H)**. With a higher dose of glucose, there was still no worsened IP glucose intolerance in the pSENP1-KO mice **(Figure 23I)**, but a larger oral glucose challenge resulted in severely impaired glucose tolerance and plasma insulin **(Figure 23J and K)**. Similar to other reports[237], female mice were relatively resistant to HFD, and we did not observe any worsening of oral glucose intolerance in the female pSENP1-KO mice **(0A-F)**.

Figure 23. Selective worsening of oral glucose tolerance in pSENP1-KO mice after high fat feeding.

(A): Schematic diagram of experiments on HFD. IHC, immunohistochemistry. **(B-E):** Insulin tolerance test (ITT) fasting insulin, fasting glucose and body weight of male pSENP1-WT, -HET, -KO mice on HFD (B - n=15, 22, 17 mice; C - n=10, 17, 12 mice; D - n=13, 21, 14 mice; E - =14, 23, 14 mice). **(F)** IPGTT with 0.5 g/kg of dextrose in male pSENP1-WT, -HET, and -KO mice after HFD (n= 6, 9, 10 mice). **(G and H):** OGTT (0.5 g/kg dextrose) of male pSENP1-WT, -HET, and -KO mice after HFD (G - n=10, 12, 9 mice), and associated plasma insulin responses (H - n=6, 6, 5 mice). **(I):** IPGTT with 1 g/kg of dextrose in male pSENP1-WT, -HET, and -KO mice after HFD (n=8, 10, 4 mice). **(J and K):** OGTT (1 g/kg dextrose) of male pSENP1-WT, -HET, and -KO mice after HFD (J - n=5, 11, 6 mice), and associated plasma insulin responses (K - n=5, 11, 6 mice). AUC - area under the curve. Data are mean ± SEM and were compared with student t test, one-way or two-way ANOVA followed by Bonferroni post-test. Unless stated otherwise, **P*<0.05, ***P*<0.01, ****P*<0.001 indicated comparison between pSENP1-WT and -KO, while ##*P*<0.01, ###*P*<0.001 indicated comparison between pSENP1-HET and pSENP1-WT. (NS, MF, HL and AS performed A-H, and HL analyzed the data.)

Figure 23.

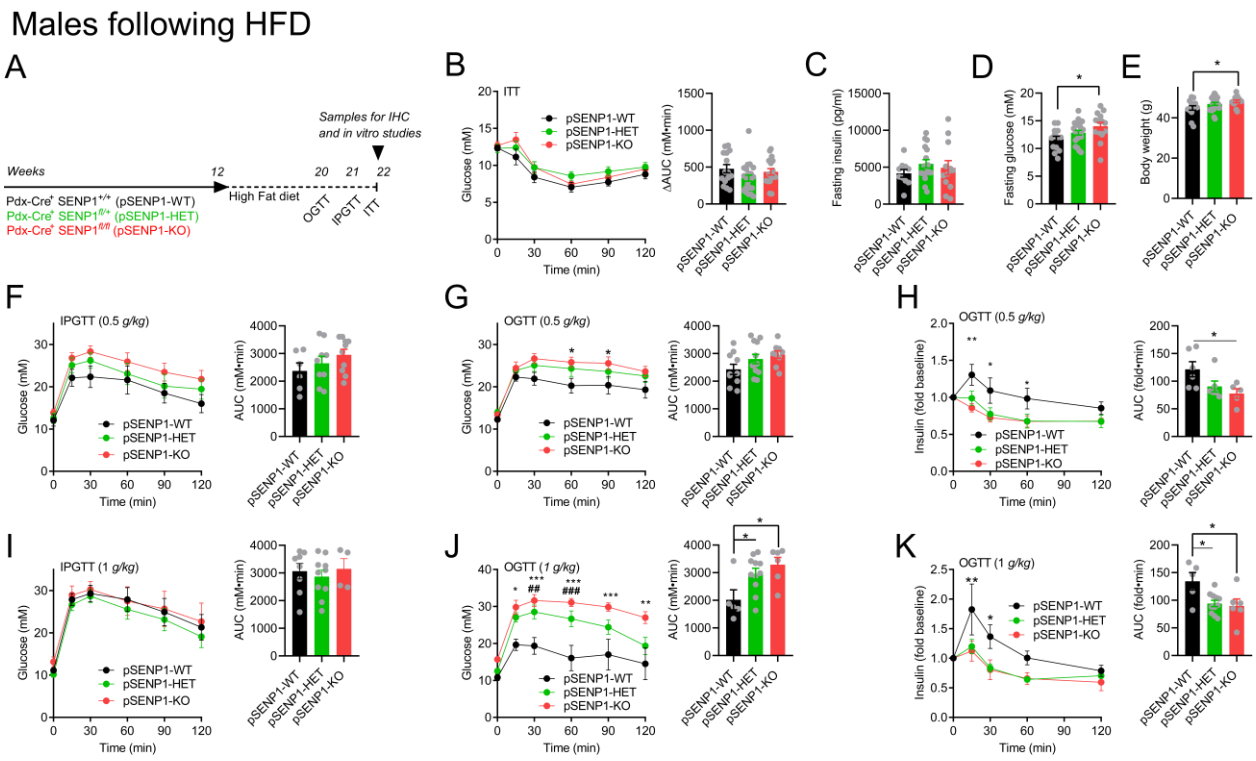
Males following HFD
A
Samples for IHC and in vitro studies
Weeks
12
20
21
22
High Fat diet
OGTT
IPGTT
ITT
Pdx-Cre+ SENP1+/+ (pSENP1-WT)
Pdx-Cre+ SENP1fl/+ (pSENP1-HET)
Pdx-Cre+ SENP1fl/fl (pSENP1-KO)
B
ITT
Glucose (mM)
Time (min)
ΔAUC (mM•min)
C
Fasting insulin (pg/ml)
D
Fasting glucose (mM)
E
Body weight (g)
F
IPGTT (0.5 g/kg)
AUC (mM•min)
G
OGTT (0.5 g/kg)
H
OGTT (0.5 g/kg)
Insulin (fold baseline)
AUC (fold•min)
I
IPGTT (1 g/kg)
J
OGTT (1 g/kg)
K
OGTT (1 g/kg)
pSENP1-WT
pSENP1-HET
pSENP1-KO

Figure 24. *In vivo* glucose homeostasis assessment of female pSENP1-KO mice following HFD.

(A) OGTT (0.5 g/kg dextrose) and **(B)** associated plasma insulin responses, **(C)** IP insulin tolerance, **(D)** body weight, **(E)** fasting glucose, and **(F)** fasting insulin of pSENP1-WT, -HET and -KO female mice following HFD (n=9-14 mice). (NS, MF, HL and AS performed A-H, and HL analyzed the data.)

Figure 24.

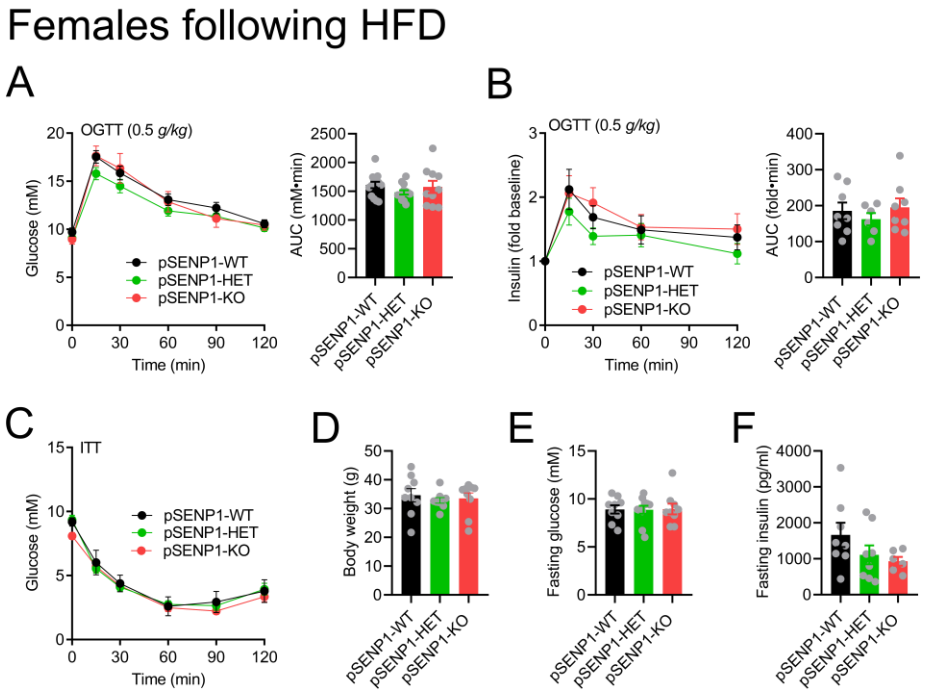
Females following HFD
A
OGTT (0.5 g/kg)
Glucose (mM)
Time (min)
pSENP1-WT
pSENP1-HET
pSENP1-KO
AUC (mM•min)
B
OGTT (0.5 g/kg)
Insulin (fold baseline)
AUC (fold•min)
C
ITT
Glucose (mM)
D
Body weight (g)
E
Fasting glucose (mM)
F
Fasting insulin (pg/ml)

A previous study showed that increasing SUMOylation protects from oxidative stress and preserves islet mass[181]. Following HFD we found no differences in β-cell mass, islet number, and islet size either in male **(Figure 25A)** or female **(Figure 26)** pSENP1-KO mice compared with controls. Since only OGTT, but not IPGTT, showed impairment in pSENP1-KO mice after HFD, this prompted us to examine the response of islets from these mice to incretin signaling. Single β-cells from pSENP1-KO mice fed HFD showed lower exocytotic responses, and this was more obvious in the presence of the GLP-1 receptor agonist Exendin-4 (Ex4, 10 nmol/L) or GIP (100 nmol/L) **(Figure 25B)**. Furthermore, voltage-dependent Ca^{2+} currents were similar between pSENP1-WT and -KO β-cells **(Figure 25C)**. Although incretin receptor activation still increased insulin secretion from pSENP1-KO islets, the secretory response to glucose, Ex4 and GIP remained much lower in islets from HFD-fed pSENP1-KO mice compared with islets from pSENP1-WT littermates **(Figure 25D-F)**.

Figure 25. Impaired insulin secretion and exocytosis to glucose and incretins from male pSENP1-KO mice following HFD.

(A): Representative immunostaining and quantification of β-cell mass, islet number, and islet size distribution in male pSENP1-WT (n=5 mice, 15 sections and 220 islets) and pSENP1-KO (n=3 mice, 9 sections and 116 islets) pancreas following HFD. Insulin (green), glucagon (red), and nuclei (blue). Scale bar=100 μm. **(B):** β-cell exocytosis, following HFD, elicited by a series of 500-ms membrane depolarization from -70 mV to 0 mV in the presence of 5 mmol/L glucose alone, and together with Exendin-4 (Ex4, 10 nmol/L) or GIP (100 nmol/L) (n = 24-42 cells from 3-5 pairs of male mice). cAMP was omitted from the pipette solution. **(C):** Average integrated Ca^{2+} currents elicited by a single 500 ms membrane depolarization from -70 mV to 0 mV at 5 mmol/L glucose or with Ex4 or GIP (n = 21-48 cells). cAMP was omitted in pipette solution. **(D and E):** Insulin secretion from male pSENP1-WT and -KO islets following HFD in response to glucose alone (D and E - n=8, 6), or together with Ex4 (10 nmol/L) (D - n=7, 6) or GIP (100 nmol/L) (E - n=6, 6). **(F):** Area under the curve (AUC) during the glucose stimulation from (D and E). Data are mean ± SEM and were compared using Student t test or one-way or two-way ANOVA followed by Bonferroni posttest. *$P < 0.05$, **$P < 0.01$, ***$P < 0.001$ compared with the control condition. In panels D and E, we show significance comparing the pSENP1-WT and -KO in the presence of Ex4 or GIP only. (HL performed A-C. AS performed D-F. HL prepared all the samples and analyzed the data.)

Figure 25.

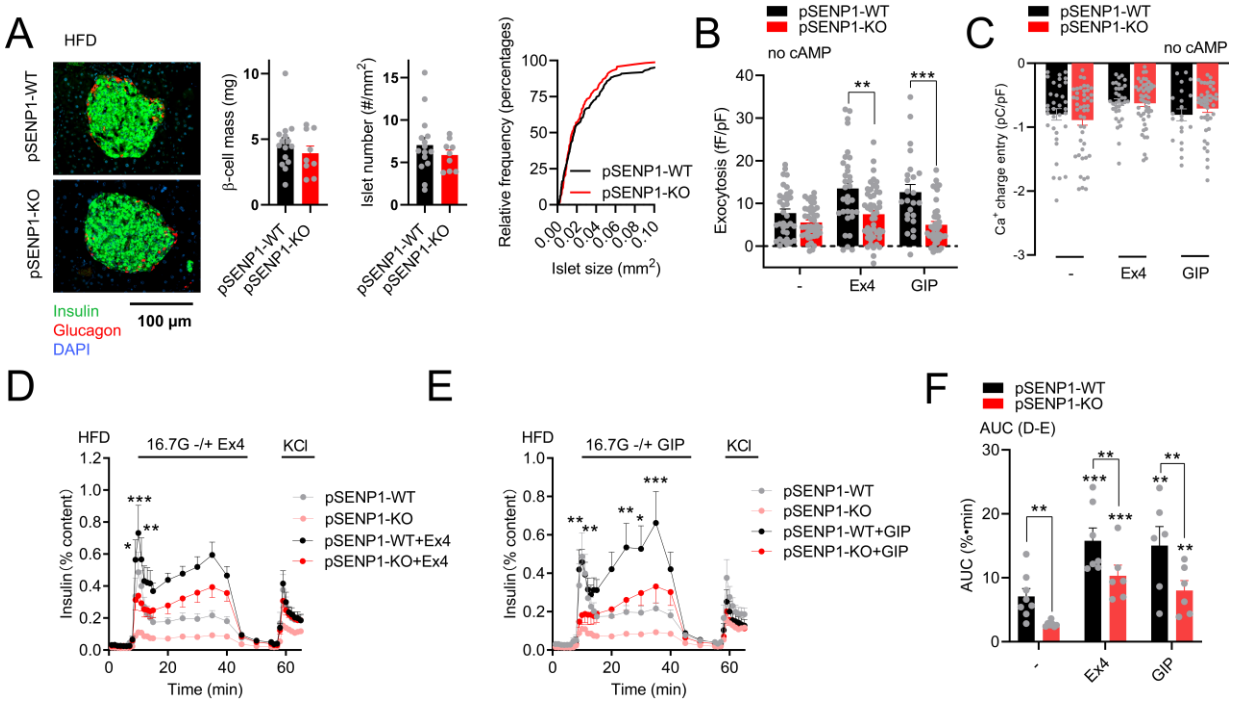
A
HFD
pSENP1-WT
pSENP1-KO
Insulin
Glucagon
DAPI
100 µm
β-cell mass (mg)
Islet number (#/mm²)
pSENP1-WT
pSENP1-KO
Relative frequency (percentages)
Islet size (mm²)
B
no cAMP
Exocytosis (fF/pF)
Ex4
GIP
C
Ca⁺ charge entry (pC/pF)
D
HFD
16.7G -/+ Ex4
KCl
Insulin (% content)
Time (min)
pSENP1-WT+Ex4
pSENP1-KO+Ex4
E
16.7G -/+ GIP
pSENP1-WT+GIP
pSENP1-KO+GIP
F
AUC (D-E)
AUC (%•min)

Figure 26. Islet morphometry analysis of female pSENP1-KO mice after HFD.

(A): Representative immunostaining, β-cell mass, islet number, and islet size distribution of female pSENP1-WT (n = 5 mice, 15 sections and 189 islets) and pSENP1-KO (n = 6 mice, 18 sections and 197 islets) following HFD. Insulin (green), glucagon (red), and nuclei (blue). Scale bar=100 μm. Data are presented as mean ± SEM. (HL, MF, YJ and YWW performed the experiment and analyzed the data.)

Figure 26.

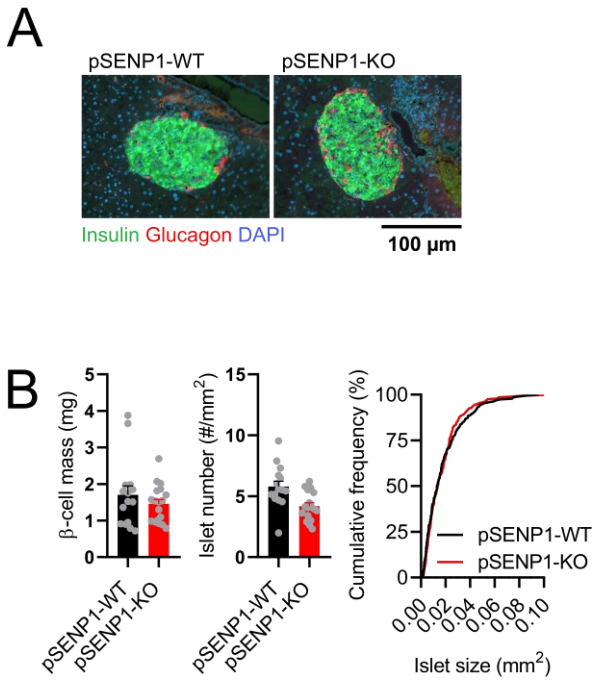
A
pSENP1-WT
pSENP1-KO
Insulin Glucagon DAPI
100 µm
B
β-cell mass (mg)
Islet number (#/mm2)
Cumulative frequency (%)
pSENP1-WT
pSENP1-KO
Islet size (mm2)

4.3.2 Loss of islet SENP1 impairs glucagon secretion

With the Pdx1 promoter as the driver of Cre expression, loss of SENP1 will not be restricted to β-cells **(Figure 27A)**[279]. Indeed, *Senp1* was around 80% lost in the proximal intestine and absent from islets of pSENP1-KO mice **(Figure 27B)**, suggesting that oral glucose tolerance might be impacted by deletion of SENP1 from incretin-producing intestinal cells or glucagon-producing α-cells. However, total plasma GLP-1 and GIP levels during an oral glucose challenge were similar between pSENP1-WT and -KO mice either on CD or HFD **(Figure 27C and D)**. Fasting plasma glucagon appears decreased in the pSENP1-KO, and this is significant after HFD **(Figure 27E)**. *In vitro* glucagon secretion from pSENP1-KO islets is reduced compared with control littermates **(Figure 27F and G)**, including at low glucose and in response to GIP alone[280] or with alanine which we used together to potently activate α-cells[281]. Similar results were observed from islets of pSENP1-KO mice following HFD (not shown). Although GIP-dependent α-to-β-cell communication primarily impacts the incretin response to a mixed meal, rather than oral glucose[201], an overall reduction in intra-islet glucagon could reduce insulin secretion by lowering β-cell cAMP tone [200]. We wanted to focus on the role for β-cell SENP1 and so generated β-cell specific knockout mice (βSENP1-KO) **(Figure 27A)**. Approximately 80% *Senp1* was lost in islets from βSENP1-KO but was unaffected in other tissues **(Figure 27H)**, fasting plasma glucagon is not decreased in βSENP-KO mice on CD or HFD **(Figure 27I)**, and *in vitro* glucagon secretion from βSENP-KO islets was not different from littermate controls **(Figure 27J and K)**.

Figure 27. Generation of a βSENP1-KO.

(A): Expected tissue selectivity of SENP1 KO in the pSENP1-KO and βSENP1-KO mice. **(B)**: qPCR of *Senp1* expression in tissues from pSENP1-WT and -KO mice (n = 3 and 3). **(C)**: Oral glucose–stimulated total plasma GLP-1 in CD (n = 10 and 9) and HFD (n = 10 and 9) mice. **(D)**: Oral glucose–stimulated plasma GIP in CD and HFD mice (n = 5–9 mice). **(E)**: Fasting plasma glucagon from pSENP1-WT and -KO mice fed CD or HFD (n = 16, 14, 19, and 9). **(F and G)**: Glucagon secretion at indicated glucose levels in the presence of GIP (n = 3 and 3) (F) or GIP + alanine from islets of pSENP1-WT and -KO mice on CD (n = 4 and 4) (G). **(H)**: qPCR of Senp1 expression in tissues from βSENP1-WT and -KO mice (n = 3 and 3). **(I)**: Fasting plasma glucagon from βSENP1-WT and -KO mice fed CD or HFD (n = 4, 5, 5, and 4). **(J and K)**: Glucagon secretion at indicated glucose level in the presence of GIP (n = 4 and 4) (J) or GIP+ alanine from islets of βSENP1-WT and -KO mice on CD (n = 5 and 4) (K). Data from male and female islets were combined and are mean ± SEM and were compared using Student t test or one-way or two-way ANOVA followed by Bonferroni posttest. *$P < 0.05$, **$P < 0.01$, ***$P < 0.001$ between pSENP1-WT and pSENP1-KO or between βSENP1-WT and βSENP1-KO. Glu, glucose. (HL and AS performed the experiment, except panel H performed by KS. HL prepared all the samples and analyzed the data.)

Figure 27.

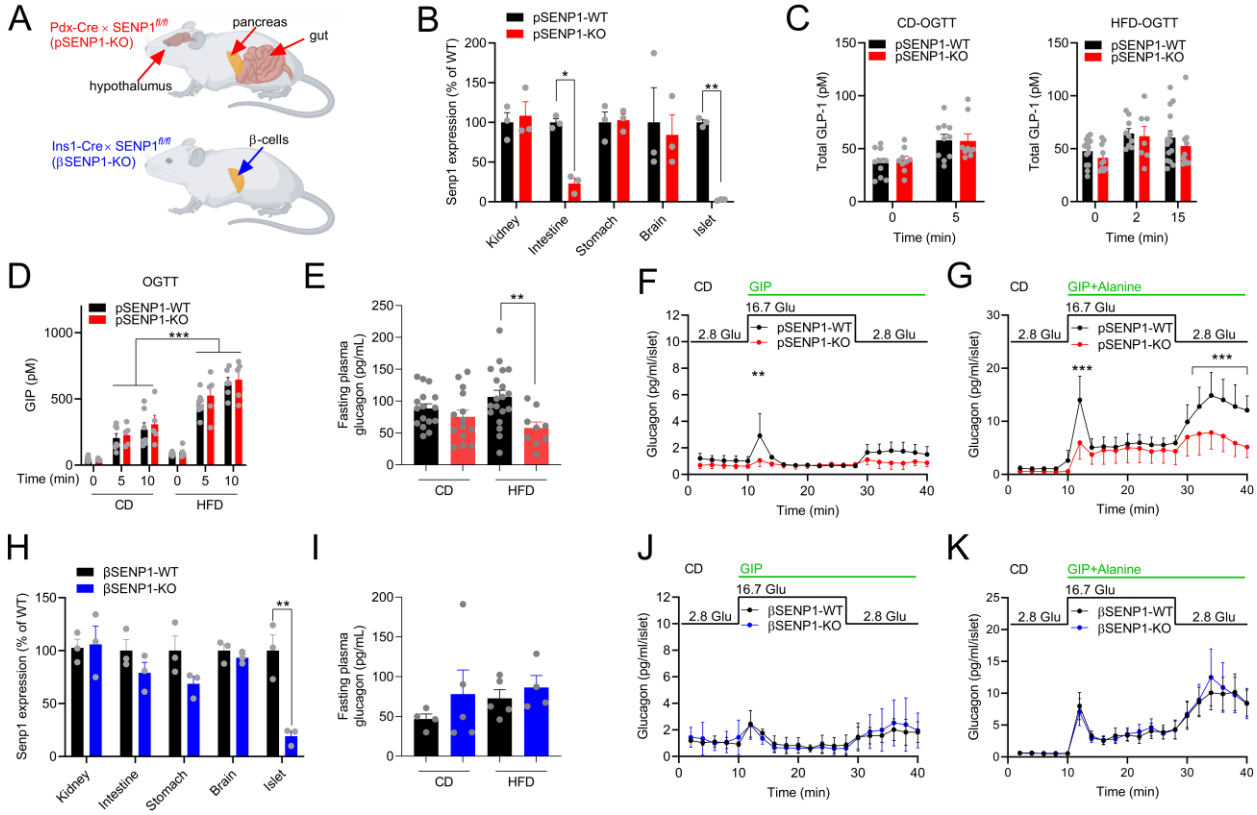
A
Pdx-Cre × SENP1fl/fl
(pSENP1-KO)
pancreas
gut
hypothalamus
Ins1-Cre× SENP1fl/fl
(βSENP1-KO)
β-cells
B
pSENP1-WT
pSENP1-KO
Senp1 expression (% of WT)
Kidney
Intestine
Stomach
Brain
Islet
C
CD-OGTT
HFD-OGTT
Total GLP-1 (pM)
Time (min)
D
OGTT
GIP (pM)
CD
HFD
E
Fasting plasma glucagon (pg/mL)
F
CD
GIP
16.7 Glu
2.8 Glu
Glucagon (pg/ml/islet)
G
GIP+Alanine
H
βSENP1-WT
βSENP1-KO
I
J
K

4.3.3 β-Cell specific deletion of SENP1 leads to worsened oral glucose tolerance after HFD

We observed no differences in insulin tolerance, fasting insulin, fasting glucose, and body weight in these mice on CD or HFD **(Figure 28A, B; Figure 29; Figure 30)**. Both oral and glucose tolerance were similar in βSENP1-KO and wild-type littermates on CD in both males **(Figure 28C, D)** and females **(Figure 30D, E)**. After HFD male βSENP1-KO mice were more glucose intolerant than βSENP1-WT littermates to oral **(Figure 28E)** but not IP glucose **(Figure 28G)**. Plasma insulin responses to oral glucose were impaired **(Figure 28F)**, but not in response to IP glucose **(Figure 28H).** Similar, but less striking, differences were observed in females **(Figure 28G-K)**. We found no difference in β-cell mass, islet number, or islet size in βSENP1-KO mice compared with littermate controls **(Figure 31A-D)** and confirmed impaired single-β-cell exocytosis **(Figure 32A)** with no significant difference in Ca^{2+} currents **(Figure 32B)**. GSIS from islets of chow-fed βSENP1-KO mice is reduced **(Figure 32C)**. After HFD insulin secretion from islets of βSENP1-KO mice and littermate controls was impaired to the same degree **(Figure 32D)**. However, insulin secretion from HFD βSENP1-WT islets was potentiated to a greater degree by Ex4 and GIP than from βSENP1-KO islets **(Figure 32D-F)**. Consistently, Ex4 and GIP were unable to increase exocytosis to the same extent from β-cells of HFD βSENP1-KO mice compared with littermate controls **(Figure 32G)**, independent of any changes in Ca^{2+} currents **(**Error! Reference source not found.**A)**.

Although SUMOylation may inhibit GLP-1 receptor activity[177,208], we find no difference in the cAMP response to Ex4 or GIP between βSENP1-WT and -KO islets expressing the β-cell-specific cAMP sensor **(Figure 32H, I; Figure 34)**. Even though our experiments include cAMP in the patch-pipette, exocytosis from β-cells of βSENP1-KO mice following HFD was still much

lower than in littermate controls **(Figure 32J-K)**. While the cycling period of Ca^{2+} oscillations was higher in βSENP1-KO β-cells, the time in the active phase remained the same **(Figure 32L, M)**, suggesting that SENP1 acts downstream of the Ca^{2+} response and the increased cycling period may be secondary to the reduced workload (ATP hydrolysis) in the βSENP1-KO β-cells due to loss of exocytosis[53]. Ex4 and GIP maintained their effect on Ca^{2+} responses **(Figure 32L, M;** Error! Reference source not found.**D, E)**, and βSENP1-KO islets exhibited impaired oleate-stimulated and glutamine/leucine-stimulated insulin secretion **(**Error! Reference source not found.**B, C)**. This all points to a mechanism downstream of cAMP and Ca^{2+} responses[73,174,175].

Figure 28. Male βSENP1-KO worsens oral, but not IP, glucose tolerance following HFD.

(A): Schematic diagram of experiments on CD and HFD. **(B)**: ITT of male βSENP1-WT, -HET, and -KO mice on CD (n = 6, 6, and 6 mice). **(C)**: OGTT of male βSENP1-WT, -HET, and -KO mice on CD (n = 9, 8, and 9 mice). **(D)**: IPGTT of male βSENP1-WT, -HET, and -KO mice on CD (n = 3, 5, and 5 mice). **(E and F)**: OGTT of male βSENP1- WT, -HET, and -KO mice following HFD (n = 13, 9, and 9 mice) (E) and associated plasma insulin responses (F - n = 6, 7, and 7 mice). **(G and H)**: IPGTT (0.5 g/kg) of male βSENP1-WT, -HET, and -KO mice after HFD (G - n = 6, 9, and 9 mice) and associated plasma insulin responses (H - n = 4, 9, and 7 mice). Data are mean ± SEM and were compared using one-way or two-way ANOVA followed by Bonferroni posttest. **P* < 0.05 between βSENP1-WT and βSENP1-KO; ##*P* < 0.01, ###*P* < 0.001 between βSENP1-HET and βSENP1-WT, unless otherwise indicated. AUC, area under the curve; IHC, immunohistochemistry. (NS and HL performed the experiment and analyzed the data.)

Figure 28.

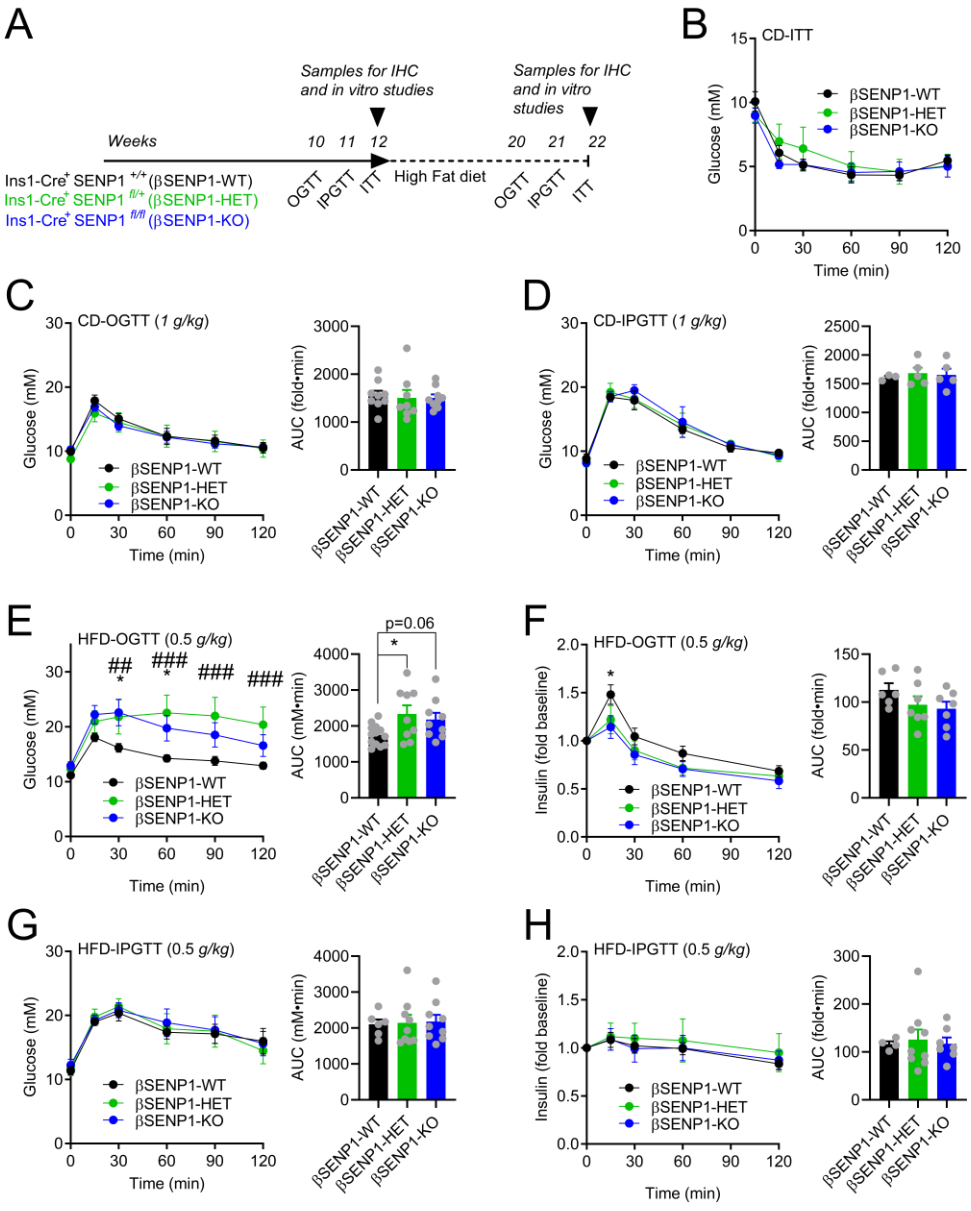
A
Samples for IHC and in vitro studies
Samples for IHC and in vitro studies
Weeks
10 11 12
20 21 22
Ins1-Cre+ SENP1 +/+ (βSENP1-WT)
Ins1-Cre+ SENP1 fl/+ (βSENP1-HET)
Ins1-Cre+ SENP1 fl/fl (βSENP1-KO)
OGTT IPGTT ITT
High Fat diet
OGTT IPGTT ITT
B
CD-ITT
Glucose (mM)
Time (min)
βSENP1-WT
βSENP1-HET
βSENP1-KO
C
CD-OGTT (1 g/kg)
AUC (fold•min)
D
CD-IPGTT (1 g/kg)
E
HFD-OGTT (0.5 g/kg)
p=0.06
AUC (mM•min)
F
HFD-OGTT (0.5 g/kg)
Insulin (fold baseline)
G
HFD-IPGTT (0.5 g/kg)
H
HFD-IPGTT (0.5 g/kg)

Figure 29. Additional *in vivo* glucose homeostasis assessment of βSENP1-KO male mice.

(A): IP insulin tolerance of male βSENP1-WT, -HET, and -KO mice following HFD (n=15, 8, 8 mice). **(B):** Delta area under the curve (ΔAUC) of IP insulin tolerance tests of male βSENP1-WT, -HET, and -KO mice on CD and following HFD (n=6, 6, 6, 15, 8, 8 mice). **(C):** Fasting insulin of male βSENP1-WT, -HET, and -KO mice on CD and following HFD (n=6, 4, 5, 13, 17, 14). **(D):** fasting glucose (n=15-22 mice) levels and **(E):** Body weight (n=18-23 mice) in male βSENP1-WT and -KO mice on CD and following HFD. Data are presented as mean ± SEM. AUC - area under the curve. Data are mean ± SEM and were compared with student t test, one-way or two-way ANOVA followed by Bonferroni post-test. Unless stated otherwise, $*P<0.05$, indicated comparison between βSENP1-WT and -KO. (NS and HL performed the experiment and analyzed the data.)

Figure 29.

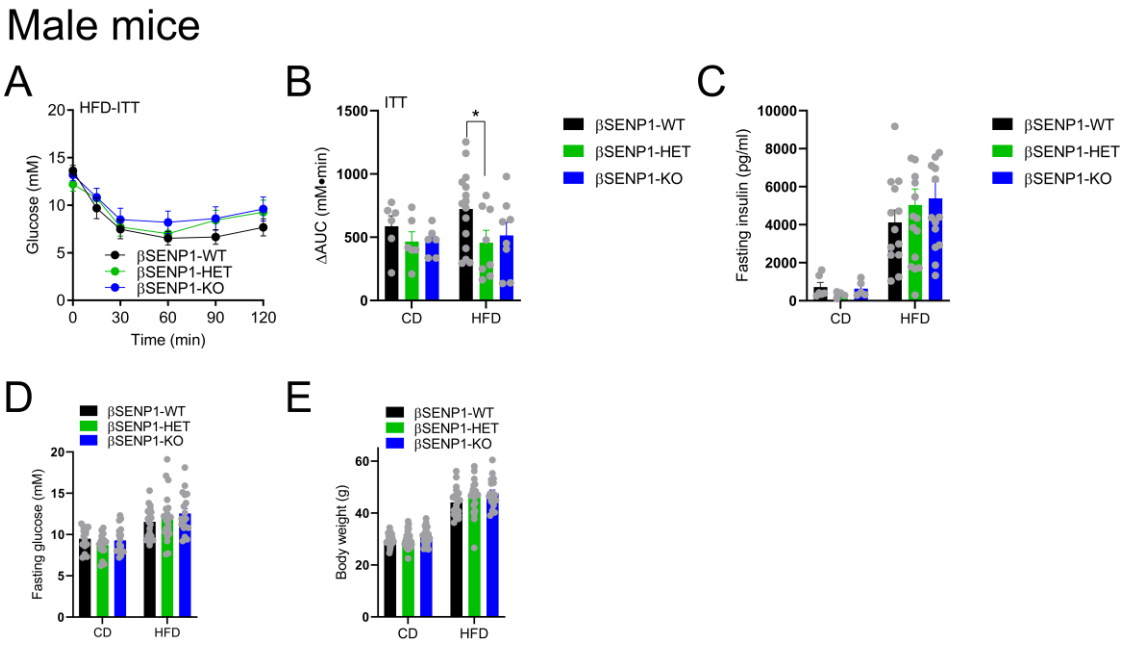
Male mice
A
HFD-ITT
Glucose (mM)
Time (min)
βSENP1-WT
βSENP1-HET
βSENP1-KO
B
ITT
ΔAUC (mM•min)
CD
HFD
C
Fasting insulin (pg/ml)
D
Fasting glucose (mM)
E
Body weight (g)

Figure 30. ***In vivo*** **glucose homeostasis assessment of βSENP1-KO female mice.**

(A): Fasting insulin (n=6, 8, 4, 13, 16, 14 mice), **(B):** fasting glucose (n=21, 22, 20, 21, 21, 22), and **(C):** body weights (n=30, 23, 25, 20, 22, 22) of female βSENP1-WT, -HET, and -KO mice on CD and following HFD. **(D):** OGTT (n=11, 12, 12 mice), **(E):** IPGTT (n=10, 11, 9 mice), and **(F):** IP insulin tolerance (n=6, 9, 8) of female βSENP1-WT, -HET and -KO mice on CD. **(G)** OGTT (n=11, 13, 11 mice) and **(H):** associated plasma insulin response (n=7, 7, 8 mice) of female βSENP1-WT, -HET, and -KO mice following HFD. **(I):** IPGTT (n=8, 9, 10 mice), and **(J):** associated plasma insulin response (n=6, 9, 6 mice) of female βSENP1-WT, -HET, and -KO mice following HFD. **(K):** IP insulin tolerance (n=11, 11, 12 mice) of female βSENP1-WT, -HET and -KO female mice following HFD and associated ΔAUC for CD and HFD. Data are presented as mean ± SEM. AUC - area under the curve. Data are mean ± SEM and were compared with student t test, one-way or two-way ANOVA followed by Bonferroni post-test. Unless stated otherwise, $*P<0.05$, $**P<0.01$, indicated comparison between βSENP1-WT and -KO. (NS and HL performed the experiment and analyzed the data.)

Figure 30.

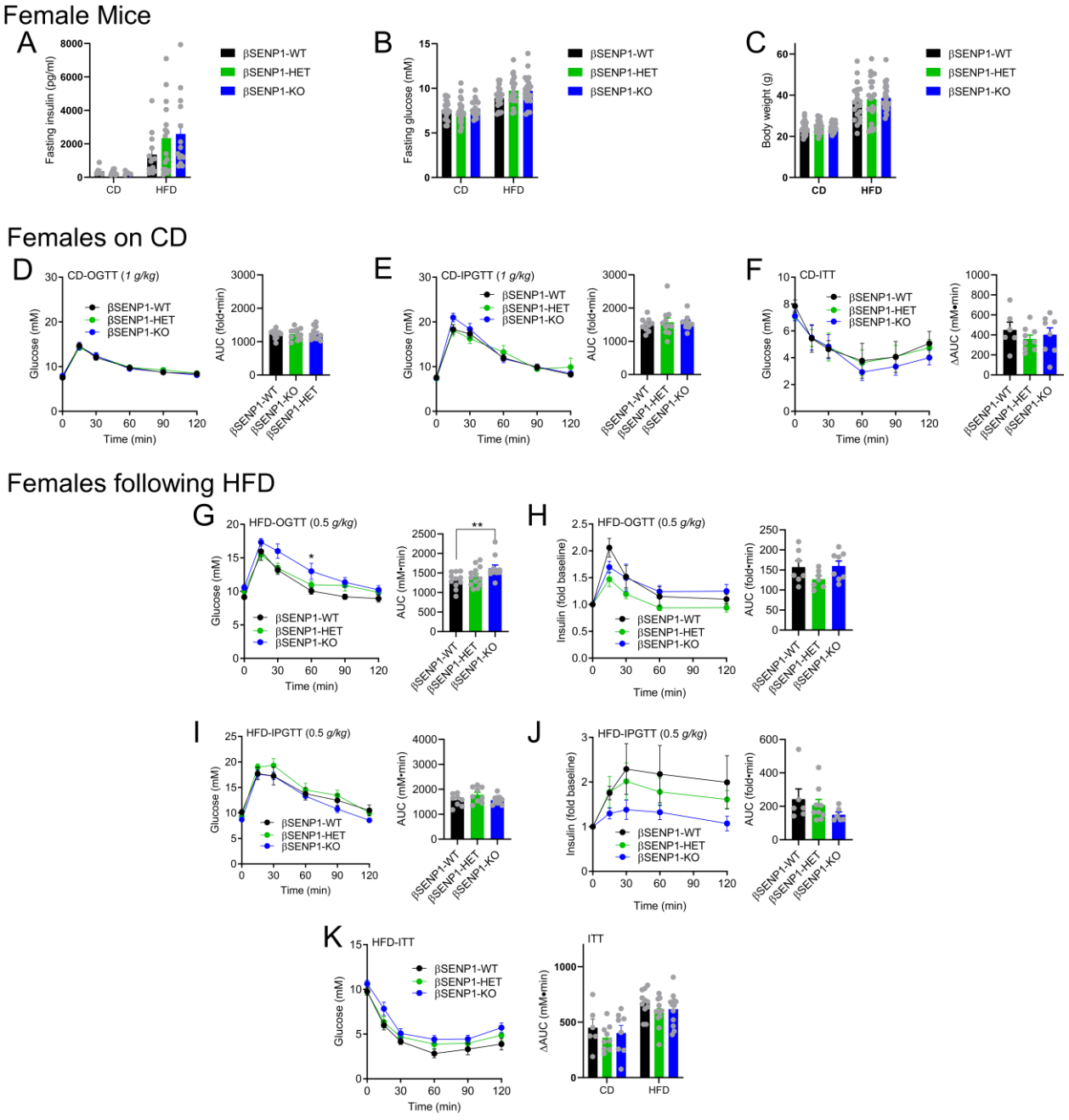
Female Mice
A
Fasting insulin (pg/ml)
CD
HFD
βSENP1-WT
βSENP1-HET
βSENP1-KO
B
Fasting glucose (mM)
C
Body weight (g)
Females on CD
D
CD-OGTT (1 g/kg)
Glucose (mM)
Time (min)
AUC (fold•min)
E
CD-IPGTT (1 g/kg)
F
CD-ITT
ΔAUC (mM•min)
Females following HFD
G
HFD-OGTT (0.5 g/kg)
AUC (mM•min)
H
Insulin (fold baseline)
AUC (fold•min)
I
HFD-IPGTT (0.5 g/kg)
J
K
HFD-ITT
ITT

Figure 31. Islet mass analysis of male and female βSENP1-KO mice after CD and HFD feeding.

(A): Representative immunostaining images, and **(B):** β-cell mass, islet number, and islet size distribution of male βSENP1-WT mice on CD (n = 3 mice, 9 sections and 162 islets), male βSENP1-KO mice on CD (n = 4 mice, 13 sections and 139 islets), male βSENP1-WT mice following HFD (n = 6 mice,18 sections and 340 islets) and βSENP1-KO mice following HFD (n = 3 mice, 9 sections and 200 islets). **(C):** Representative immunostaining image, **(D):** islet mass, islet number, islet size accumulative frequency of female βSENP1-WT mice on CD (n = 5 mice, 14 sections and 146 islets), βSENP1-KO mice on CD (n = 4 mice, 12 sections and 101 islets), βSENP1-WT mice following HFD (n = 5 mice,15 sections and 155 islets) and βSENP1-KO mice following HFD (n = 4 mice, 11 sections and 141 islets). Insulin (green), glucagon (red), and nuclei (blue). Scale bar=100 μm. Data are mean ± SEM and were compared with one-way or two-way ANOVA followed by Bonferroni post-test. **P*<0.05, ***P*<0.01, ****P*<0.001 indicated comparison between HFD and CD. (HL and YJ performed the experiment and analyzed the data.)

Figure 31.

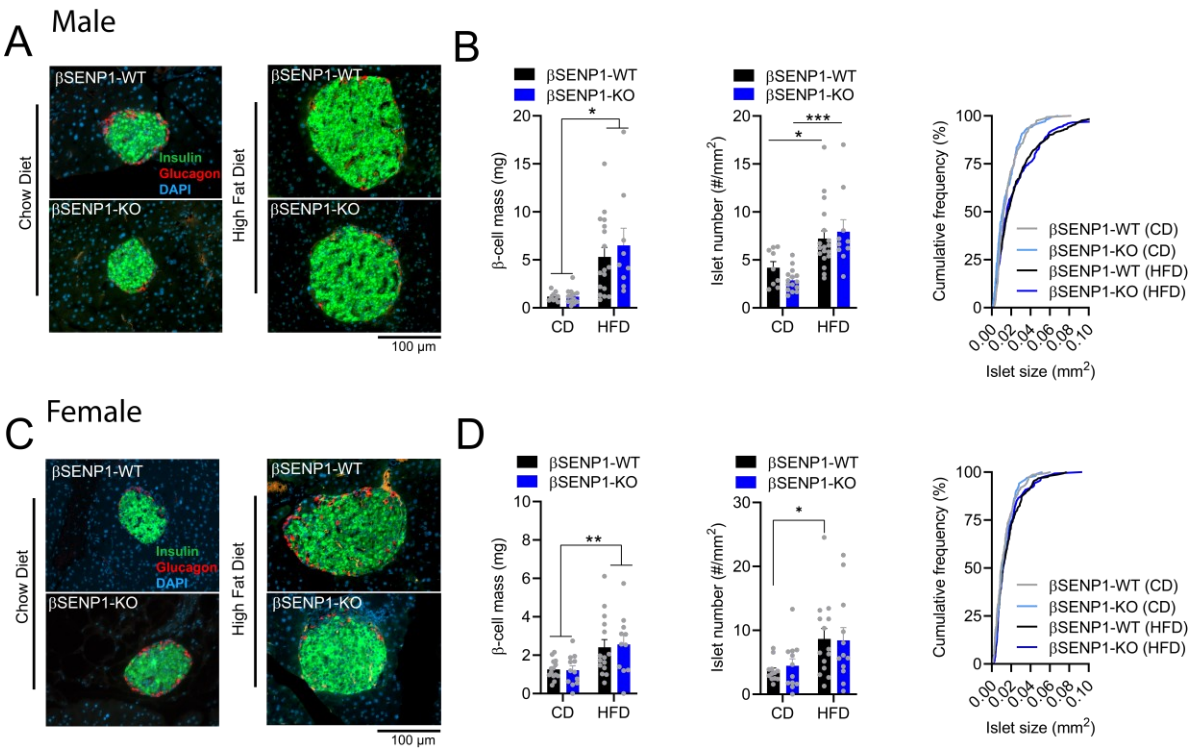
A
Male
βSENP1-WT
βSENP1-KO
Insulin
Glucagon
DAPI
Chow Diet
High Fat Diet
100 μm
B
βSENP1-WT
βSENP1-KO
β-cell mass (mg)
Islet number (#/mm²)
CD
HFD
Cumulative frequency (%)
βSENP1-WT (CD)
βSENP1-KO (CD)
βSENP1-WT (HFD)
βSENP1-KO (HFD)
Islet size (mm²)
C
Female
D

Figure 32. Impaired insulin secretion and exocytosis to glucose and incretins from male βSENP1-KO islets following HFD.

(A): Representative traces (left) and averaged exocytosis elicited by a series of 500-ms membrane depolarizations from 70 to 0 mV in β-cells from male βSENP1-WT and -KO mice on CD at 10 mmol/L glucose (n = 55 and 61 cells from 5 and 7 mice). The pipette solution included 0.1 mmol/L cAMP. **(B)**: Representative Ca^{2+} current traces and average integrated Ca^{2+} entry of β-cell elicited by a single 500-ms membrane depolarization from 70 to 0 mV at 10 mmol/L glucose (n = 51 and 57 cells). The pipette solution included 0.1 mmol/L cAMP. **(C)**: Insulin secretion from male βSENP1-WT and -KO islets from mice on CD in response to glucose (n = 8 and 7). **(D and F)**: Side-by-side insulin secretion from βSENP1-WT and -KO islets from male mice following HFD in response to glucose alone (D -F - n = 9 and 12) or together with Ex4 (10 nmol/L) (D - n = 8 and 9) or GIP (100 nmol/L) (E - n = 7 and 7) and (F) respective area under the curve (AUC) during the glucose stimulation. **(G)**: Exocytosis in β-cells of male βSENP1-WT and -KO mice, following HFD, elicited by a series of 500-ms membrane depolarization from 70 to 0 mV at 5 mmol/L glucose alone or with Ex4 (10 nmol/ L) or GIP (100 nmol/L) (n = 44, 46, 47, 38, 40, and 41 cells from 5 mice per group). cAMP 0.1 mmol/L was omitted from pipette solution. **(H and I)**: The cAMP response at 10 mmol/L glucose to Ex4 (10 nmol/L) (H - n = 4 pairs of mice, 68 and 74 islets) or GIP (100 nmol/L) (I - n = 4 pairs of mice, 73 and 88 islets). **(J)**: Exocytosis in β-cells of male βSENP1-WT and -KO mice following HFD at 2.8 and 10 mmol/L glucose, with 0.1 mmol/L cAMP included in the pipette solution (n = 26, 35, 29, and 38 cells from 3, 4, 3, and 4 mice). **(K)**: Average integrated Ca^{2+} charge entry during voltage-dependent Ca^{2+} currents elicited from β-cells by a single 500-ms membrane depolarization from 70 to 0 mV at 2.8 and 10 mmol/L glucose (n = 26, 30, 30, and 38 cells from 3, 4, 3, and 4 mice). The pipette solution included 0.1 mmol/L cAMP.

(L and M): Representative Ca^{2+} responses (left), oscillation period, and Ca^{2+} plateau fraction at 10 mmol/L glucose to Ex4 (L - n = 4 pairs of mice, 73 and 88 cells) and to GIP (M - n = 4 pairs of mice, 68 and 74 cells). Data are mean ± SEM and were compared using Student t test or one-way or two-way ANOVA followed by Bonferroni posttest. *$P < 0.05$, **$P < 0.01$, ***$P < 0.001$ between βSENP1-WT and -KO under the same condition. (HL performed A, B, C, J, K. AS performed D, E. SLL H, I, L, M. HL prepared all the samples.)

Figure 32.

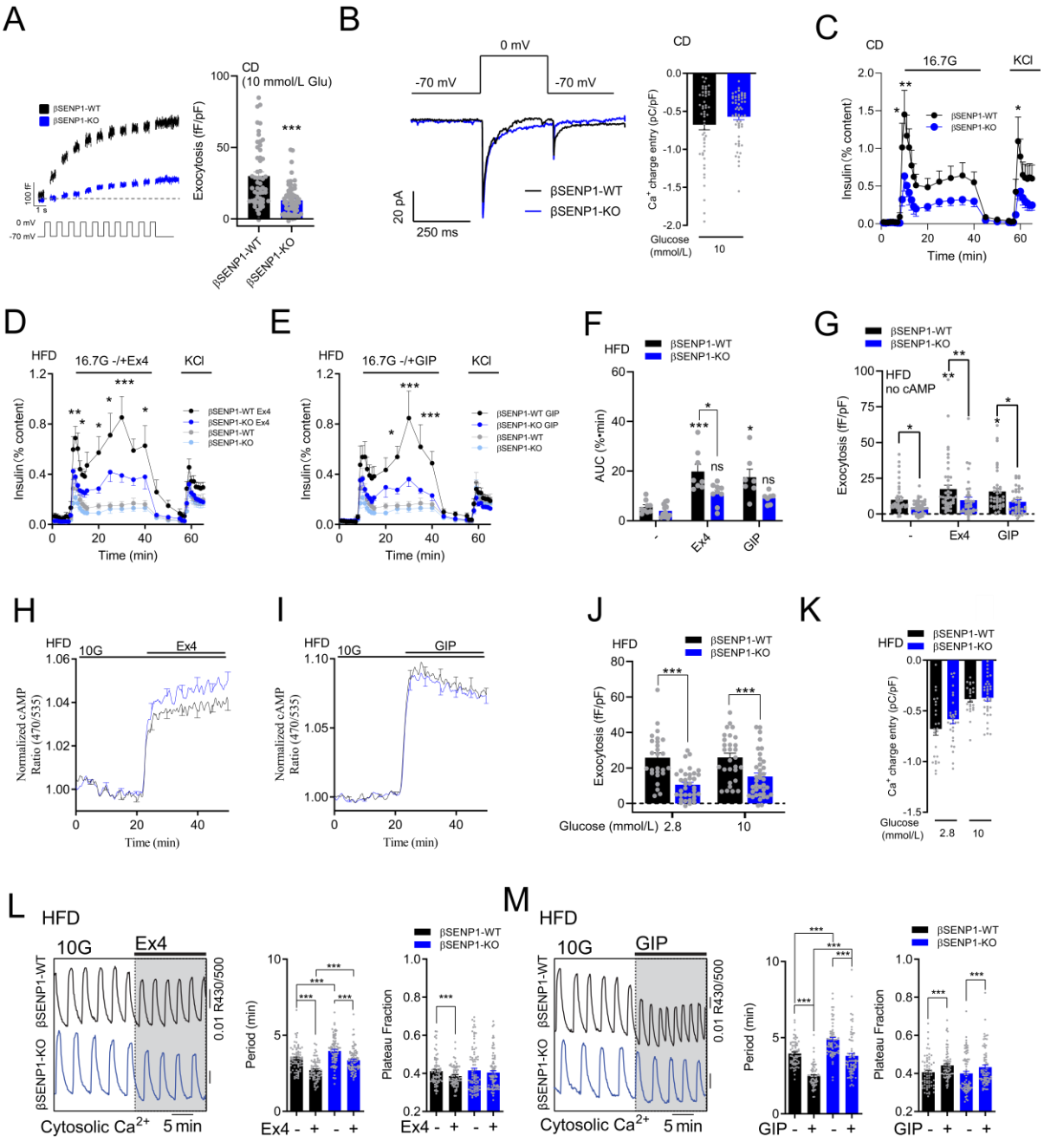
A
βSENP1-WT
βSENP1-KO
100 fF
1 s
0 mV
-70 mV
CD
(10 mmol/L Glu)
Exocytosis (fF/pF)
***
βSENP1-WT
βSENP1-KO
B
0 mV
-70 mV
-70 mV
20 pA
250 ms
βSENP1-WT
βSENP1-KO
CD
Ca2+ charge entry (pC/pF)
Glucose (mmol/L)
10
C
CD
16.7G
KCl
Insulin (% content)
βSENP1-WT
βSENP1-KO
Time (min)
D
HFD
16.7G -/+Ex4
KCl
Insulin (% content)
βSENP1-WT Ex4
βSENP1-KO Ex4
βSENP1-WT
βSENP1-KO
Time (min)
E
HFD
16.7G -/+GIP
KCl
Insulin (% content)
βSENP1-WT GIP
βSENP1-KO GIP
βSENP1-WT
βSENP1-KO
Time (min)
F
HFD
βSENP1-WT
βSENP1-KO
AUC (%•min)
ns
ns
Ex4
GIP
G
βSENP1-WT
βSENP1-KO
HFD
no cAMP
Exocytosis (fF/pF)
Ex4
GIP
H
HFD
10G
Ex4
Normalized cAMP Ratio (470/535)
Time (min)
I
HFD
10G
GIP
Normalized cAMP Ratio (470/535)
Time (min)
J
HFD
βSENP1-WT
βSENP1-KO
Exocytosis (fF/pF)
Glucose (mmol/L) 2.8
10
K
HFD
βSENP1-WT
βSENP1-KO
Ca2+ charge entry (pC/pF)
Glucose (mmol/L)
2.8
10
L
HFD
10G
Ex4
βSENP1-WT
βSENP1-KO
0.01 R430/500
Cytosolic Ca2+
5 min
Period (min)
Plateau Fraction
βSENP1-WT
βSENP1-KO
Ex4 - + - +
Ex4 - + - +
M
HFD
10G
GIP
βSENP1-WT
βSENP1-KO
0.01 R430/500
Cytosolic Ca2+
5 min
Period (min)
Plateau Fraction
βSENP1-WT
βSENP1-KO
GIP - + - +
GIP - + - +

Figure 33. Ca^{2+} response and nutrient-stimulated insulin secretion βSENP1-KO mice after HFD feeding.

(A): Average voltage-dependent Ca^{2+} currents of β-cell elicited by a single 500 ms membrane depolarization from -70 mV to 0 mV at 5mM glucose or with Ex4 or GIP (n=50, 55, 56, 47, 51, 46 cells from 5 mice per group). cAMP was omitted in pipette solution. **(B):** Insulin secretion to glucose and oleate (n=3 pairs of mice after HFD). **(C):** Insulin secretion to glucose and amino acids (n=5 pairs of mice after CD). **(D-E):** Ca^{2+} response, baseline, and amplitude in response to glucose with Ex4 (D - n=4 pairs of mice, 73 and 88 cells) or GIP (E – n= 4 pairs of mice, 68 and 74 cells). AUC - area under the curve. Data are mean ± SEM and were compared with student t test, one-way or two-way ANOVA followed by Bonferroni post-test. Unless stated otherwise, $^{**}P<0.01$, $^{***}P<0.001$ indicated comparison between βSENP1-WT and -KO. (HL performed A. AS performed B, C. SLL performed D, E. HL prepared all the samples.)

Figure 33.

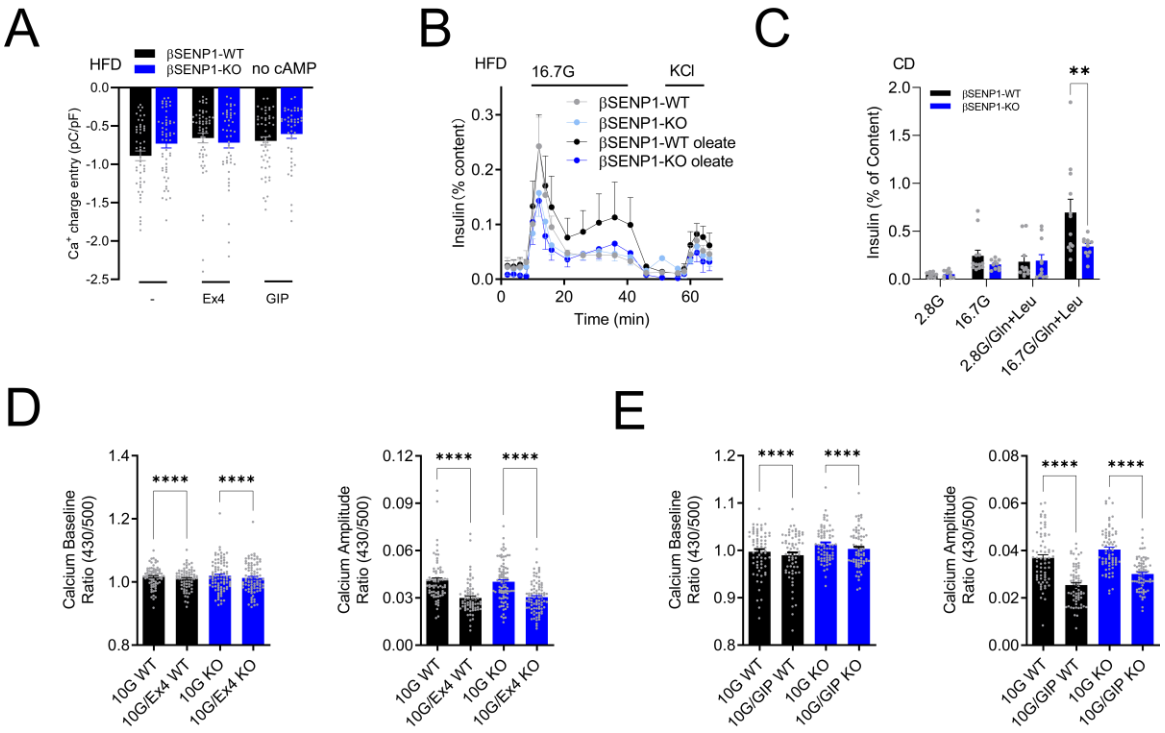
A
HFD
βSENP1-WT
βSENP1-KO
no cAMP
Ca+ charge entry (pC/pF)
0.0
-0.5
-1.0
-1.5
-2.0
-2.5
-
Ex4
GIP
B
HFD
16.7G
KCl
βSENP1-WT
βSENP1-KO
βSENP1-WT oleate
βSENP1-KO oleate
Insulin (% content)
0.3
0.2
0.1
0.0
0
20
40
60
Time (min)
C
CD
**
βSENP1-WT
βSENP1-KO
Insulin (% of Content)
2.0
1.5
1.0
0.5
0.0
2.8G
16.7G
2.8G/Gln+Leu
16.7G/Gln+Leu
D
Calcium Baseline Ratio (430/500)
1.4
1.2
1.0
0.8
****
****
10G WT
10G/Ex4 WT
10G KO
10G/Ex4 KO
Calcium Amplitude Ratio (430/500)
0.12
0.09
0.06
0.03
0.00
****
****
10G WT
10G/Ex4 WT
10G KO
10G/Ex4 KO
E
Calcium Baseline Ratio (430/500)
1.2
1.1
1.0
0.9
0.8
****
****
10G WT
10G/GIP WT
10G KO
10G/GIP KO
Calcium Amplitude Ratio (430/500)
0.08
0.06
0.04
0.02
0.00
****
****
10G WT
10G/GIP WT
10G KO
10G/GIP KO

Figure 34. FRET-based imaging of cAMP in whole islets.

Islets were infected with adenovirus expressing the cAMP biosensor (Epac-SH187, *Kd* = 4 μmol/L) under control of the rat insulin promoter. **(A)**: Representative images of 1,1-dioctadecyl-3,3,3,3-tetramethylindotricarbocyanine iodide (DiR) loaded islets, and R470/535 emission ratios at time=0 and time=25 minutes. **(B)**: Normalized single wavelength emission of the probe at 470 and 535 nm is shown, with expected increases (470 nm) and decreases (535 nm) of emission in response to Ex4 (10 nmol/L; n=4 pairs of mice, 68 and 74 islets) or GIP (100 nmol/L; n=4 pairs of mice, 73 and 88 islets). (SLL performed this figure and HL prepared samples.)

Figure 34.

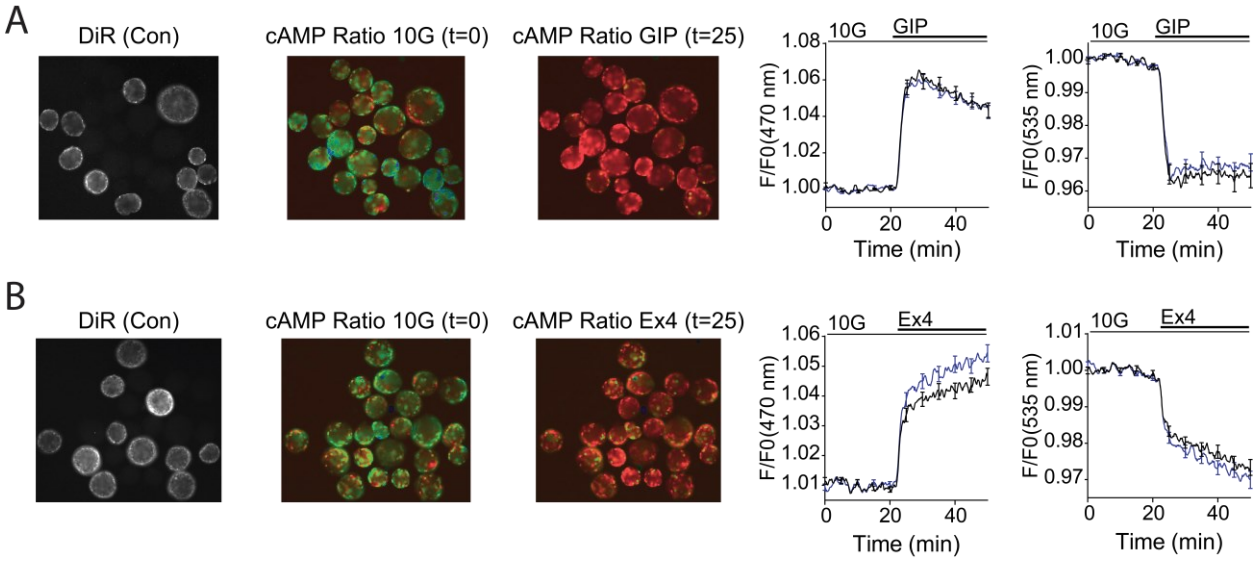
A
DiR (Con)
cAMP Ratio 10G (t=0)
cAMP Ratio GIP (t=25)
10G
GIP
F/F0(470 nm)
Time (min)
F/F0(535 nm)
B
DiR (Con)
cAMP Ratio 10G (t=0)
cAMP Ratio Ex4 (t=25)
10G
Ex4
F/F0(470 nm)
Time (min)
F/F0(535 nm)

4.4 Discussion

We aimed to investigate the role of the deSUMOylating enzyme SENP1 within the β-cell following HFD-induced metabolic stress. In two models we confirmed that loss of β-cell SENP1 results in impaired exocytosis and reduced insulin secretion, consistent with the SUMOylation-dependent inhibition of insulin secretion in insulinoma cells, human, and mouse β-cells[84,174,175]. DeSUMOylation, likely of multiple targets[133], is an important mechanism facilitating insulin secretion. *In vivo*, over-expression of the SUMO-conjugating enzyme Ubc9 within β-cells leads to an obvious IP glucose intolerance[181]. While we see impaired insulin secretion, we do not find robust glucose intolerance in young chow-fed mice following islet or β-cell SENP1 knockout. Thus, insulin secretion may not be sufficiently limited *in vivo* to consistently impact glucose homeostasis in the absence of a stressor. At present we also cannot rule out potential compensatory mechanisms *in vivo*, such as increased insulin sensitivity that might be difficult to detect in our insulin tolerance tests. Nonetheless, high fat feeding revealed the importance SENP1-dependent insulin secretion in the maintenance of glucose homeostasis.

A worsening of HFD-induced glucose intolerance in both the pSENP1-KO and βSENP1-KO mice was observed selectively in response to oral, but not IP, glucose. This suggests an important interaction with the incretin response, which is upregulated in HFD [225,282,283] consistent with the enhanced GIP response we observed. Recent work suggests an important interaction between incretin responses, glucagon secretion, and insulin release[284]. GIP-induced glucagon secretion supports insulin secretion following a mixed meal[200,242,285,286], but does not likely contribute in the response to oral glucose alone[201]. Thus, the reduced glucagon response to

GIP+alanine in the pSENP1-KO islets used here as a strong stimulus of α-cell function likely doesn't contribute to worsened oral glucose intolerance. It is possible however that reduced glucagon 'tone' in the pSENP1-KO islets could impact insulin secretion by lowering baseline β-cell cAMP[200], and contribute to the lower insulin response in the pSENP1-KO compared with the βSENP1-KO. Regardless, the observation that HFD-induced oral glucose intolerance persists in the βSENP-KO model suggests that loss of SENP1 in the β-cell, rather than in α-cells or in the intestine, is primarily responsible for the impaired oral glucose tolerance following HFD.

But why is IP glucose tolerance after HFD not worsened in these models, particularly given the role for SENP1 in GSIS? In the βSENP1-KO this is easier to explain since GSIS is similarly impaired after HFD in both the KO and WT islets. In the pSENP1-KO a lower GSIS *in vitro* after HFD has only a small impact, if any, to worsen IP glucose intolerance. The reasons for this are likely two-fold: Firstly, after the 8-week HFD insulin secretion from the pSENP1-WT islets is already impaired (a peak of ~0.4% of content, in **Figure 25D,E**) compared with chow-fed WT mice in our hands (peak of ~1.5% as in **Figure 32C** or elsewhere[84]). The additional reduction of glucose-stimulated secretion may be insufficient to worsen an already impaired IP glucose tolerance. Secondly, plasma glucose clearance following IP administration is more greatly impacted by insulin-independent mechanisms than glucose via the oral route[287]. Glucose effectiveness, the ability of glucose to promote its own insulin-independent clearance, contributes 2/3 of clearance following IP glucose in mice[34], and this proportion increases substantially following high fat feeding[40,288]. This, coupled with upregulation of incretin responses upon high fat feeding, may explain why we see a stronger effect of islet SENP1 knockout on oral glucose tolerance in our HFD mice.

Although SUMOylation is suggested to reduce GLP-1 receptor activity[177,208], cAMP and Ca^{2+} responses to Ex4 and GIP were similar between βSENP1-WT and -KO islets. Therefore SENP1 does not appear to control incretin receptor activity directly, although it is possible that other SUMO proteases[289] may be key determinants of upstream incretin signaling. Also, β-cells lacking SENP1 show decreased exocytosis even though most patch-clamp experiments included high cAMP in the pipette solution which should bypass the need for incretin receptor activation. This suggests the impaired response upon loss of SENP1 resides downstream of receptor signaling and cAMP, although it could be possible that effectors such as PKA or EPAC are directly impacted by loss of SENP1. The observation that insulin secretion from βSENP1-KO islets was also impaired upon to fatty acid or amino acid stimulation suggests that SENP1 acts far downstream in the regulation of insulin granule fusion. Although we see reduced Ca^{2+} oscillation frequency in the βSENP1-KO, this is likely secondary to the reduced workload resulting from a loss of exocytosis[53]. It therefore seems that SENP1 is required to ensure the availability of insulin granules on which cAMP-dependent signals act, or that these converge on common exocytotic protein targets, such as Syt7, shared by other metabolic pathways[73,175].

As such, we do not believe that SENP1 activity 'mediates' incretin signaling, but rather serves an important role in maintaining, or augmenting, the pool of release-ready insulin granules on which incretins ultimately act. Interestingly, the activity of SENP1 is linked to metabolism and the mitochondrial export of reducing equivalents[84,133] to mediate an amplification of insulin secretion. This occurs very far downstream in the secretory pathway, as increased SUMOylation blocks granule fusion while producing a 'traffic jam' of insulin granules at the plasma membrane[175]. This suggests that SENP1 acts to maintain, or perhaps amplify, the availability of secretory granules for subsequent release, whether in response to glucose, incretins, or other

stimuli. This suggests that a glucose-dependent effect to enhance the secretory granule pool will augment the secretory response to incretins. Indeed, the ability of glucose to facilitate β-cell exocytosis by SENP1 is correlated with Exendin4-dependent insulin secretion from human islets[223].

The SENP1 pathway itself may be impaired by HFD, possibly due to inactivation of SENP1 by oxidative stress[91] and similar to what occurs in islets from human donors with T2D[84]. The export of mitochondrial reducing equivalents activates SENP1 by reducing a thiol group via a redox-relay involving NADPH and reduction of glutathione[84,91]. On the other hand H_2O_2, which can oxidize and inactivate SENP1[92], is also produced from NADPH through NOX4 and this is also required for GSIS[55,105]. It remains unclear how SENP1 may evade H_2O_2-induced inactivation and compete with NOX4 for NADPH. One possibility may involve compartmentalization, either spatially or temporally. SENP1 potentiates insulin secretion by modulating exocytotic proteins[133,173–175] while NOX4-induced H_2O_2 primarily acts via K_{ATP} channel inhibition[55]. Here, excessive oxidative stress induced by HFD could lead to basal hyperinsulinemia and defective GSIS [45] as occurs in islets from donors with impaired glucose tolerance or T2D[290]. Indeed, NOX4-induced islet H_2O_2 may drive β-cell dysfunction and glucose intolerance after HFD[291], and it is interesting to speculate that overproduction of H_2O_2 could spill-over and limit SENP1 activity and increase SUMOylation. While inhibition or loss of SENP1 may protect against β-cell apoptosis[181], it comes at the cost of robust incretin-induced insulin secretion in the face of metabolic stressors.

4.5 Methods

4.5.1 Animals, diets, and *in vivo* studies.

Transgenic mice were generated as described in section 2.5.1. Loss of SENP1 expression was confirmed by nested PCR and Western blot. At 12 weeks of age, mice were fed with HFD (60 % fat; Bio-Serv, CA89067-471) for 8-10 weeks.

Mice were fasted 4-5 hours prior to oral glucose tolerance test (OGTT)[245] or intraperitoneal glucose tolerance tests (IPGTT)[246], or insulin tolerance test (ITT)[247]. OGTT and IPGTT was with dextrose at doses indicated in the Figures, and ITT was with IP injection of 1 U/kg Humulin R (Eli Lilly). The timeline of glucose and insulin tolerance tests are shown in the Figures. Tail blood was collected for glucose and insulin measurement[84]. To measure total plasma GLP-1, GIP, and glucagon, prior to or after oral glucose gavage (2 g/kg dextrose), tail blood was collected at the indicated times and plasma was frozen until assay (Multi Species GLP-1 Total ELISA kit, Millipore; Mouse GIP ELISA Kit, Crystal Chem; U-Plex mouse glucagon ELISA kit, Mesoscale Discovery).

4.5.2 Western blotting.

SENP1 antibody-C12 (1:500, Santa Cruz sc-271360), SUMO1 antibody (1:1000, abcam ab133352) and β-actin antibody (1:2000, Santa Cruz sc-47778) were used as primary antibodies. Anti-mouse (1:5000, GE healthcare NA934V) or anti-rabbit (1:5000, GE healthcare NA931V) were used as secondary antibodies. Mouse islets, gut, and brain were homogenized with 7M Guanidine HCl. The protein was precipitated by addition of methanol, chloroform and water in 4:1:3 ration (v/v) and the pellet were recovered (10,000 rpm for 10mins) and dissolved in 1% SDS, 0.2 mol/L Tris, 10 mmol/L DTT, pH 6.5. Protein concentration was estimated by the absorbance

at 280 nm. Fifty, 10 and 10 μg protein from islets, intestine, and brain, respectively, were separated by SDS-PAGE (7.5% gel), transferred to PVDF membrane, and probed with primary antibody in the presence of 5% skim milk. For SUMOylation[249], islets were incubated in KRBH with 2.8 mmol/L glucose for 2 hours, followed by 16.7 mmol/L glucose for 15 min. Islets were washed with cold PBS and put in lysis buffer with 10 mmol/L N-ethylmaleimide (NEM, Millipore Sigma 128-53-0), 100 μL PhosStop (1 tablet in 1 mL lysis buffer, Millipore Sigma) and 10 μL protease inhibitor (Millipore Sigma P8340). Ten micrograms of protein were loaded for SDS-PAGE (10% gel).

4.5.3 Nested qPCR of SENP1.

To evaluate knockout efficiency, the cDNA encoding Exon14 and 15 was quantified by nested qPCR. Total RNA was extracted from kidney, brain, stomach, intestine and islets using TRIzol reagent (Thermo Fisher Scientific, 15596018). cDNA was prepared from total RNA (50-100 ng) with ABM 5x All-In-One RT Master Mix (G486, Applied Biological Materials Inc.). The cDNAs of *Senp1* and *Ppia* were amplified using preamplification primers and Platinum Taq DNA polymerase (10966-018, Thermo Fisher Scientific) with cycling parameter: 15 cycles of 94ºC for 30s, 60ºC for 10s, 55ºC for 10s and 72ºC for 25s. To remove Taq DNA polymerase and the primers, the PCR fragment was incubated with 4 mol/L Guanidine HCl for 10 min at room temperature and precipitated with 80% ethanol in the presence of glycogen (50 mg/mL). The nested qPCR was carried out with the qPCR primers, Fast SYBRGreen Master mix (438512, Applied Biosystems), 7900HT Fast real-time PCR system (Applied Biosystems) and the pre-amplified cDNAs as the templates with cycling parameter: 40 cycles of 95ºC for 5 s, 60ºC for 20s. All primers are listed in **Table 3**.

Table 3. PCR primers used for nested qPCR.

Primer Name	Accession	5'-3' primer sequence	Amplicon length (bp)
SENP1 Preamplification	NM_144851.5	FW-CTACATGAACATGCTAATGGAACG RV-AAGAGGATCCTGCAGGCC	284
SENP1 Nested qPCR	NM_144851.5	FW-AAGAGAAGGGGTTTCCAAGTG RV-CCTCGTTGTTTATTCCACCCATAG	228
Cyclophilin A Preamplification	NM_008907.2	FW-TGCAGACAAAGTTCCAAAGACAGCAG RV-TGGTGATCTTCTTGCTGGTCTTGC	398
Cyclophilin A Nested qPCR	NM_008907.2	FW-TGGCTATAAGGGTTCCTCCTTTCACAG RV-GCCAGGACCTGTATGCTTTAGGATG	151

4.5.4 Pancreatic islet isolation, insulin and glucagon secretion.

Islets were isolated by collagenase digestion of the pancreas[292] and cultured overnight. Insulin secretion was measured by perifusion [84]. Briefly, 25 (insulin) or 75-85 (glucagon) islets were pre-perifused for 30 minutes at 2.8 mmol/L glucose before sample collection and treatments with 16.7 mmol/L glucose, Exendin-4 (Ex4, 10 nmol/L, Millipore Sigma), GIP (100 nmol/L, Anaspec), alanine (10 mmol/L Millipore Sigma), oleate[293,294] (0.5 mmol/L, Millipore Sigma) or KCl (30 mmol/L). Samples were collected every 1-5 min at a flow rate of 100 μL/min, and then islets were lysed in acid/ethanol. All samples were stored at -20ºC until assayed for insulin (STELLUX® Chemi Rodent Insulin ELISA kit, Alpco) glucagon (Rodent glucagon ELISA kit or U-Plex mouse glucagon ELISA kit, Mesoscale Discovery). For the glutamine- and leucine-stimulated insulin secretion (10 mmol/L each, Millipore Sigma), it was performed with static insulin secretion [249].

4.5.5 Patch-clamp analysis.

Islets were hand-picked and incubated with Ca^{2+}-free buffer at 37°C for 10 minutes before being shaken and dispersed into single cells[175]. Cells were incubated in 35 mm dishes (430165, Thermo Fisher Scientific) in RPMI-1640 (11875, Thermo Fisher Scientific) with 11.1 mmol/L glucose, 10% FBS and 100 units/mL penicillin/streptomycin for up to two days. In the experiments examining low (2.8 mmol/L) or high (10 mmol/L) glucose **(Figure 21B-C, Figure 31A-B and Figure 31J-K)** cells were preincubated in DMEM (11966025, Gibco) with 10% FBS, 100 U/mL penicillin/streptomycin and 2.8 mmol/L glucose for 1 hour prior to switching to bath solution. For remaining experiments (5 mmol/L glucose) cells were switched to the bath without preincubation. Bath solution contained (in mmol/L): 118 NaCl, 5.6 KCl, 20 TEA, 1.2 $MgCl_2$•$6H_2O$, 2.6 $CaCl_2$, 5

HEPES, with glucose, Ex4 (10 nmol/L; Millipore Sigma) and/or GIP (100 mmol/L; Anaspec) as indicated (pH 7.4 adjusted with NaOH) at 32-35°C. Pipette solution contained (in mmol/L): 125 Cs-glutamate, 10 NaCl, 10 CsCl, 1 $MgCl_2$•$6H_2O$, 0.05 EGTA, 5 HEPES, and 3 MgATP (solution pH=7.15 adjusted with CsOH) with or without 0.1 mmol/L cAMP as indicated in figure legends. Patch-clamp was performed in the standard whole-cell configuration with sine+DC lockin function of EPC10 amplifier (HEKA Electronik) 5-30 min after switching cells to the bath solution. As such, cells were pre-exposed to bath glucose, Ex4, or GIP prior to establishment of the whole-cell configuration. Exocytotic responses and inward Ca^{2+} currents were measured 1-2 minutes after obtaining the whole-cell configuration in response to 10 500-ms depolarizations to 0 mV from a holding potential of -70 mV. Changes in capacitance and integrated Ca^{2+} charge entry were normalized to cell size (fF/pF and pC/pF, respectively). Mouse β-cells were identified by cell size (>4 pF) and half-maximal inactivation of Na^+ currents near -90 mV [250].

4.5.6 β-cell cAMP and intracellular Ca^{2+} imaging.

The cAMP biosensor (Epac-S^{H187}, K_d = 4 μM)[295] under control of the rat insulin promoter (RIP) was expressed by adenoviral expression [200]. Islets were infected immediately post-isolation with 1.5 μL of high-titer adenovirus for 2 hours at 37°C, then moved to fresh media overnight. Islets from βSENP1-WT and -KO mice were imaged simultaneously; one group was pre-labeled with 1μg/mL DiR (1,1-dioctadecyl-3,3,3,3-tetramethylindotricarbocyanine iodide) (Molecular Probes, Eugene, OR) for 10 min. DiR labeling had no effect on islet metabolic or Ca^{2+} oscillations (data not shown). For measurements of cytosolic Ca^{2+}, islets were pre-incubated in 2.5 μmol/L FuraRed (Molecular Probes F3020) at 37°C for 45 min before they were placed in a glass-bottomed imaging chamber (Warner Instruments) and mounted on a Nikon Ti-Eclipse inverted microscope with a 10X/0.50 numerical aperture SuperFluor objective (Nikon Instruments). The chamber was

perfused with external solution containing (in mmol/L): 135 NaCl, 4.8 KCl, 2.5 $CaCl_2$, 1.2 $MgCl_2$, 20 HEPES (pH 7.35). The flow rate and temperature were maintained at 0.25 mL/min and 33°C using feedback control (Fluigent MCFS-EZ). Excitation was by a SOLA SEII 365 (Lumencor) at 10% output. Single DiR images utilized a Chroma Cy7 cube (710/75x, T760lpxr, 810/90m). For FuraRed, excitation (430/24x and 500/20x, ET type, Chroma Technology Corporation) and emission (650/60m) filters (BrightLine type, Semrock) were used in with an FF444/521/608-Di01 dichroic (Semrock) and reported as an excitation ratio (R430/500). The same dichroic mirror was used for cAMP biosensor FRET imaging, with CFP excitation provided by an ET430/24x filter and emission filters for CFP and Venus emission (ET470/24m and ET535/30m, Chroma) reported as an emission ratio (R470/535). Fluorescence emission was collected with a Hamamatsu ORCA-Flash4.0 V2 Digital CMOS camera every 6 seconds. A single region of interest was used to quantify the average response of each islet using Nikon Elements and custom MATLAB software (MathWorks).

4.5.7 Histological analysis.

Pancreata were weighed prior to being fixed in Z-fix (VWR Canada) and embedded in paraffin. Blocks were sectioned at 5-µm thickness with a total of three to five slides (each separated by 500 µm) for immunostaining and imaging [84]. Paraffin sections were rehydrated, permeabilized, blocked and incubated with guinea pig polyclonal insulin antibody (1:60, Dako, A0564) and mouse polyclonal glucagon antibody (1:1000, Millipore Sigma) overnight. Sections were washed and incubated with Alexa Fluor 488 goat anti-guinea Pig IgG (1:500, A-11073-Thermo Fisher Scientific) and Alexa Fluor 594 goat anti-mouse IgG (1:500 A11037-Thermo Fisher Scientific) for 1 hour, washed, and mounted in ProLong gold antifade reagent with DAPI (Life Technologies). To determine islet area, insulin-positive cells were identified with tools from ImageJ (NIH) and

normalized to total pancreas area. The islet mass was calculated as pancreas weight × relative islet area (as a proportion of pancreas section area). Islet size was determined by manual outlining in a blinded fashion using ZEN Pro (Zeiss) and ImageJ (NIH).

4.5.8 Statistical analysis.

Graphpad Prism 8 for Mac OS X was used for one-way or two-way ANOVA analysis followed by Bonferroni post-test to compare means between groups. Unbiased ROUT (robust regression followed by outlier identification) analysis was used for outlier identification and removal.

Chapter 5.

Summary, Discussion and Future Directions

5.1 Summary

β-cells can adapt to metabolic stress by increasing both their secretory function and their mass. In the early stage of prediabetes, functional compensation, especially pathways that enhance insulin secretion, has been reported to outweigh the mass expansion to increase insulin output. In later stages of prediabetes, mass expansion is of significance to complement the increased function to cope with deteriorating hyperglycemia. SENP1 is a major contributor coupling the generation of reducing equivalents to β-cell secretory capacity, accounting for perhaps 50% of insulin secretion. Given its role in insulin output, SENP1 is likely involved in the early β-cell functional compensation. However, SENP1 over-expression was shown to have a distinctive effect on β-cell survival, specifically, sensitizing β-cells to cytokine- or oxidative stress-induced apoptosis. In addition, metabolic stress-induced redox changes are implicated in functional compensation and mass expansion. In light of a complicated compensation and pleiotropic effects of SENP1 on β-cell function and survival, my work attempts to investigate the role of SENP1 on β-cell function and mass during acute and chronic metabolic stress, while exploring the intracellular signaling events and molecular mechanism of SENP1 redox sensing. The principal findings in this thesis are summarized below:

- β-cells from young organ donors without diabetes with BMI>25 exhibit greater insulin secretion and exocytosis than β-cells from donors with a lower BMI.
- Following a short-term HFD exposure, mice maintain IP glucose tolerance with a compensatory increase of *in vivo* plasma insulin secretion and enhanced β-cell secretory function, which is dependent on upregulation of cytosolic reducing signaling and SENP1

expression. SENP1 is required for transducing these intracellular changes to enhance β-cell secretory function and maintain IP glucose tolerance.

- Redox regulation of SENP1 is dependent on an interaction between Zn^{2+} and C603 and C535. Loss of C535 abolishes the redox regulation of SENP1 and the Zn^{2+}-mediated inhibition on SENP1. The molecular basis of these effects by C535 is probably through affecting proton transfer pathway.
- Following a long-term HFD exposure, mice are characterized by hyperinsulinemia, impaired glucose tolerance, islet mass compensation, compensatory increase of GIP but reduced *in vitro* GSIS. SENP1 in β-cells limited oral glucose intolerance by ensuring robust incretin-stimulated insulin secretion at a point downstream of incretin receptor signaling without changing the intracellular Ca^{2+} response or voltage-activated currents.
- Following a long-term HFD, SENP1 in α-cells is required for GIP-stimulated glucagon secretion and might participate in limiting oral glucose intolerance by enhancing GIP-dependent insulin secretion.
- Upon HFD exposure, SENP1 either in whole islets or β-cells does not contribute to islet mass compensation.

5.2 General Discussion

5.2.1 The physiological role of SENP1 in functional compensation and glucose homeostasis during high fat feeding.

5.2.1.A Evidence that SENP1 in β-cells does not contribute to glucose homeostasis in the absence of metabolic stress.

SENP1 is a SUMO-deconjugating enzyme regulating deSUMOylation. Transgenic mice with loss or overexpression of SUMO-conjugating and -deconjugating enzymes are valuable tools to examine the requirement of SUMOylation for glucose homeostasis *in vivo*. A SENP1 KO mouse model (pSENP1-KO) generated by crossing Pdx1-Cre and $Senp1^{fl/fl}$ was reported to have impaired oral glucose tolerance[84]. Similarly, induced deletion of β-cell SENP1 in adulthood (iβSENP1-KO), achieved by crossing Pdx1-CreER with $Senp1^{fl/fl}$, resulted in impaired oral glucose tolerance[84]. Consistent with this, β-cell-inducible overexpression of the SUMO-conjugating enzyme UBC9 ($Ubc9^{TG}$) under the control of Rip-CreER also manifested glucose intolerance and insulin deficiency[181]. However, those impairments, if any, were mild. Indeed, pSENP1-KO glucose intolerance on a normal chow diet was not evident in my studies **(Figure 21)**. Another concern from the previous studies is the possible off-target effects in non-β cells. For example, Rip-CreER using Ins2 as promoter can drive recombination in the brain[296]. Pdx1-Cre or Pdx-CreER can induce recombination in whole islets, hypothalamus and gut as shown here and elsewhere[296,297]. All these off-target deletions cannot deconvolve the relative contribution of β-cell specific SENP1 to glucose homeostasis. Therefore, I used β-cell specific SENP1 knockout mice (βSENP1-KO) controlled by the Ins1 promoter[244]. These βSENP1-KO mice did not manifest any abnormal glucose tolerance under normal conditions **(Figure 28)**. Although we cannot exclude the possibility that a non-inducible SENP1 knockout might induce chronic compensation for the

glucose intolerance, a 50% reduction of insulin secretion in βSENP1-KO mice might not be able to induce significant glucose intolerance, as reported in mice with 60% pancreatectomy or 50% deletion of insulin genes[155,298]. Overall, although I clearly show the impact of SENP1 loss on insulin secretory function *in vitro*, the role of β-cell SENP1 in glucose regulation under chow fed conditions in young mice is minimal.

5.2.1.B Evidence that intracellular redox signaling via β-cell SENP1 is required for functional compensation and maintaining glucose homeostasis on a short-term HFD.

β-cell functional compensation is of importance in glucose homeostasis during metabolic stress. While mice showed upregulated insulin secretion following 2-day and 4-week HFD exposure, IPGTT only remained intact in 2-day HFD-exposed mice **(Figure 6, Figure 7)**. This indicates a successful functional compensation of insulin secretion early in the HFD exposure, justifying the examination of β-cell adaptation after 2-day HFD treatment. The includes SENP1 adaptation, as shown by a rise of SENP1 expression levels **(Figure 9F, G)** and a reduction of cytosolic oxidation **(Figure 9B),** along with increased oxidative phosphorylation **(Figure 9A)**. Deletion of SENP1 caused loss of 2-day HFD-induced insulin exocytosis compensation **(Figure 11)**, which is required to maintain IP glucose tolerance in both the pSENP1-KO and βSENP1-KO mice **(Figure 10)**. Interestingly, oral glucose tolerance was impaired in pSENP1-KO but not βSENP1-KO mice. This could be because deletion of SENP1 in α-cells in pSENP1-KO mice impaired glucagon secretion in the OGTT, and thus further depresses insulin secretion by lowering cAMP tone through reduced paracrine signaling to β-cells[200] **(Figure 27)**. Compared to pSENP1-KO, β-cell specific SENP1-KO mice (βSENP1-KO) had intact α-cell function and relatively less impairment of the incretin effect, which might still maintain oral glucose tolerance at 2-day HFD.

After the 4-week HFD exposure, both the SENP1 expression **(Figure 9G)** and redox state **(Figure 35)** returned to normal levels. Although functional compensation still occurred, it seemed β-cells were no longer able to catch up with the demand for insulin to maintain IP glucose tolerance **(Figure 7)**. Indeed, IP glucose tolerance were equally impaired in βSENP1-KO and -WT mice exposed to 4-week HFD **(Figure 12)**. However, SENP1-KO mice showed worsened oral glucose tolerance, indicating that SENP1 was required to preserve the incretin effect after 4-week HFD, which was also later confirmed in 8-week HFD-exposed mice in chapter 4. Thus, while the adaptive reducing signaling and SENP1 successfully compensated for a 2-day HFD metabolic stress to maintain IP glucose tolerance, they suffered a mild maladaptation, i.e., gradually decreased following the early compensation, accompanied by impaired IP glucose tolerance during progression into 4-week HFD exposure. The transition from reduced signaling and SENP1 adaptation to maladaptation might underlie the impairment of IP glucose tolerance, an early manifestation of T2D.

Figure 35. Cytosolic redox measurement on CD, 2-day HFD and 4-week HFD.

(A): Cytosolic redox state after 2-day HFD. This data is the same data as Figure 9B but normalized to make a comparison with 4-week HFD (N=6, 6 mice, n=65, 41 islets). **(B):** Cytosolic redox state after 4-week HFD. The ratio indicated the oxidation state. The higher the ratio was, the more oxidized the cytosolic state was (N=4, 3 mice, n=79, 59 islets). (Work by LN, LPR and EA.)

Figure 35.

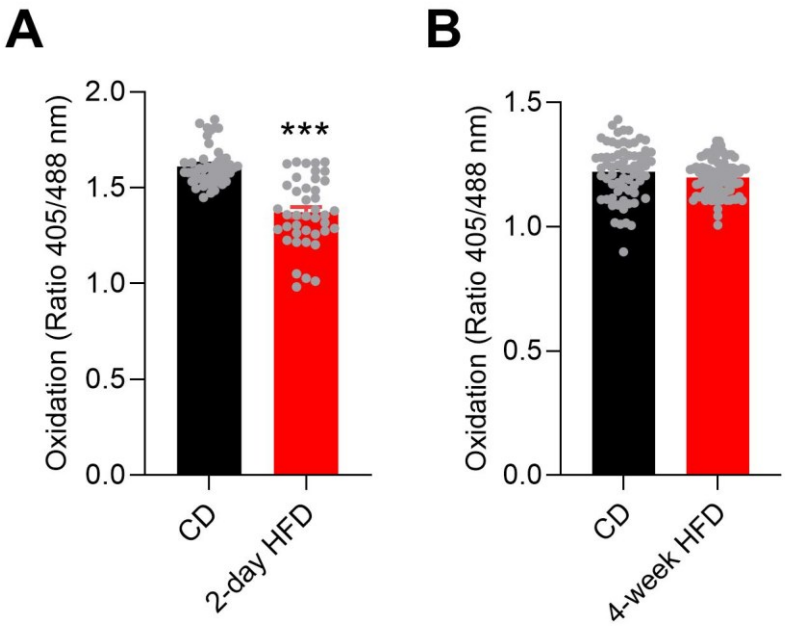
A
B
Oxidation (Ratio 405/488 nm)
2.0
1.5
1.0
0.5
0.0
***
CD
2-day HFD
Oxidation (Ratio 405/488 nm)
1.5
1.0
0.5
0.0
CD
4-week HFD

5.2.1.C Evidence that β-cell SENP1 is required for preserving an adaptive incretin effect and glucose homeostasis following long-term HFD.

Over the course of T2D, β-cells compensate by amplifying secretory responses, but excessive workload leads eventually to β-cell exhaustion and decompensation. Unlike 2-day and 4-week HFD, 8-week HFD mouse islets exhibits oxidative stress[299], severely impaired GSIS **(Figure 32C-E)** but apparent mass expansion **(Figure 31)**, enabling us to study the effect of SENP1 on functional and mass compensation under long-term metabolic stress[299]. DeSUMOylation was reported to be deleterious to β-cell survival and induce spontaneous diabetes by sensitizing oxidative-stress induced apoptosis[179,181]. I expected that ablation of SENP1 would protect and even facilitate islet mass expansion after 8-week HFD. However, islet mass expansion remained unchanged in pSENP1-KO and βSENP-KO mice **(Figure 25, Figure 26, Figure 31)**. One possibility might be that the oxidative stress induced by HFD was still too mild to induce β-cell apoptosis. Another possibility could be that redox-dependent SENP1 activity in wild type mice was downregulated by oxidative stress to a level only modestly higher than in the SENP1-KO mice. Indeed, GSIS from βSENP-WT was significantly impaired by 8-week HFD to a level that was barely higher than that of βSENP-KO islets **(Figure 32C-F)**. Therefore, a mild oxidative stress or a smaller SENP1 activity difference after HFD might underlie the unaffected islet mass expansion in SENP-KO mice. Of note, if we extend the duration of HFD to greater than 8 weeks, islet mass from SENP1-KO might be protected from continued apoptosis and preserved, but at a cost of impaired insulin secretion[181].

The pSENP1-KO and βSENP-KO mice were more intolerant of oral, rather than intraperitoneal, glucose, and that higher glucose challenge can further deteriorate glucose intolerance with diminished insulin secretion, which was not explained by change of islet mass

(Figure 23, Figure 28). Instead, it was the deletion of SENP1 and impaired β-cell response to incretin that accounted for this oral glucose intolerance **(Figure 32)**. As previously reported[283], the 8-week HFD impaired GSIS, indicating that this stage might not represent a so-called 'β-cell functional compensation stage'. One of the possible reasons could be, as discussed above, the predominant oxidative stress after 8-week HFD inactivated SENP1 activity and blunted insulin secretion. Although I didn't directly measure cytosolic redox stress in the β-cells, our longitudinal measurement of cytosolic state at different HFD durations (0, 2-day, 4 week) showed that the cytosolic state became reduced on 2-day HFD and return to a normal redox state after 4-week exposure **(Figure 35)**, but might shift towards oxidized after 8-week HFD according to previous report[299]. Additionally, SENP1 expression from 8-week HFD also came back to similar level as that on CD **(Figure 9G)**. Therefore, mice on 8-week HFD might be at an 'intrinsic decompensation stage'. However, functional compensation is not limited to β-cell changes only. Rather, signaling via endocrine hormones, such as incretins, was augmented, which made a substantial contribution to glucose homeostasis after prolonged HFD treatment[225,282,283]. In agreement with this, I observed adaptive upregulation of GIP in the plasma after HFD in both βSENP1-WT and -KO mice **(Figure 27D)**, suggested of an 'extrinsic functional compensation'. However, the reduced incretin signaling in SENP1-KO β-cells failed to transduce the compensatory increase of GIP into a robust insulin secretion, leading to an impaired oral glucose after HFD.

β-cells are highly plastic and might undergo complex changes in function and mass during HFD. That means the severely impaired incretin signaling in SENP1-KO β-cells after HFD exposure could possibly be a consequence, instead of a cause, of a long-term hyperglycemia, which was mainly caused by impaired GSIS. However, the impaired incretin signaling had already existed in βSENP1-KO β-cell on CD **(Figure 36A)** and proved to underlie a failure in a

pharmacological intervention via DPP4 inhibitor, which should increase incretin levels and improves glucose tolerance **(Figure 36B)**. Altogether, this indicates that the SENP1 effect on glucose homeostasis via incretin signaling is redundant on CD but unmasked in a pharmacological context or by a long-term HFD, where the incretin response is upregulated. A summary of the role of SENP1 during different duration of HFD is illustrated in **Figure 37**.

Figure 36. βSENP1-KO showed reduced exocytosis to Ex4 and failed glucose tolerance improvement upon treatment of DPP4 inhibitor.

(A): Cumulative exocytosis trace (left) and bar graph (right) from β-cells (confirmed by insulin immunostaining) subjected to a series of 10 depolarizing pulses. Exocytosis is facilitated by 100 nM Exendin-4 (Ex4) in cells from βSENP1$^{+/+}$ mice, but not βSENP1$^{-/-}$ mice. Data are from 24–37 cells and 4 pairs of mice for each group, from four βSENP1$^{+/+}$ and four βSENP1$^{-/-}$ mice. ***-P < .001 compared with WT vehicle control; in grey is the p-value comparing Exendin-4 in the knockout with its vehicle control (red) **(B):** Oral glucose tolerance in male littermate βSENP1$^{+/+}$ (n = 4, 4 mice) and βSENP1−/− (n = 8, 7 mice) mice at 1 h following gavage of the DPPIV inhibitor MK-0626 (3 mg/Kg). Loss of β-cell SENP1 blunts the ability of DPP4 inhibition to improve glucose tolerance. *-P < .05, **-P < .01, and ***-P < .001 comparing vehicle control versus DPP4 inhibitor. (HL performed panel A. NS and MF performed the panel B. Adapted with permission from Ferdaoussi et al, 2020)

Figure 36.

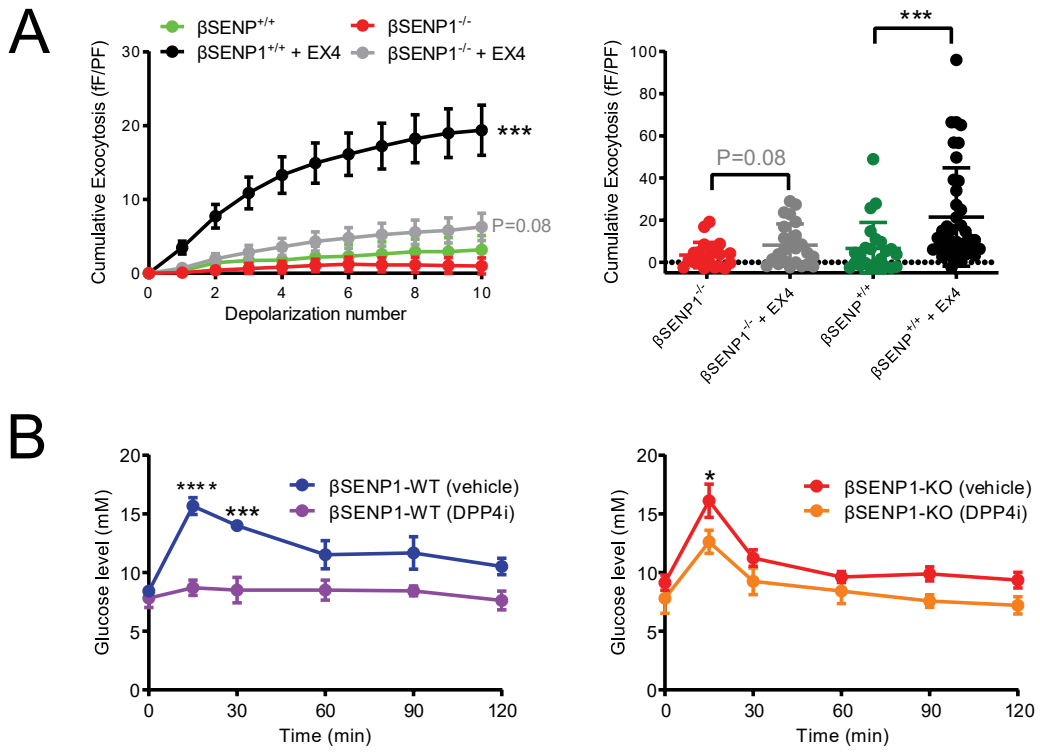
A
βSENP+/+
βSENP1-/-
βSENP1+/+ + EX4
βSENP1-/- + EX4
Cumulative Exocytosis (fF/PF)
Depolarization number
***
P=0.08
P=0.08
***
βSENP1-/-
βSENP1-/- + EX4
βSENP+/+
βSENP+/+ + Ex4
B
βSENP1-WT (vehicle)
βSENP1-WT (DPP4i)
Glucose level (mM)
Time (min)
****
***
βSENP1-KO (vehicle)
βSENP1-KO (DPP4i)
*

Figure 37. Proposed role of SENP1 signaling for functional compensation along the time course of a HFD.

On 2-day HFD, increased SENP1 expression and reduced oxidation state adaptively contributed to the functional compensation and glucose tolerance, especially the IP glucose tolerance. Both pSENP1-KO and βSENP1-KO after 2-day HFD showed impaired IP glucose tolerance. On 4-week HFD, mice showed functional compensation. However, further adaption from SENP1 expression and oxidation state halted, failing to keep up with the metabolic stress and thus impairing IP glucose tolerance. Therefore, IP glucose tolerance were equally impaired in both SENP-KO and SENP1-WT mice after 4-week HFD compared to chow fed condition. At this stage, incretin compensation, requiring the presence of SENP1, kicked in and increased insulin secretion along with islet mass compensation. Deletion of SENP1 lost this incretin compensation and deteriorated oral glucose tolerance. During the progression to 8-week HFD, persistent hyperglycemia and workload stressed β-cell and further increased oxidative stress, worsening the maladaptation of SENP1 activity and decompensation of GSIS. Incretin output continued to upregulate insulin secretion but failed to maintain glucose tolerance. Deletion of SENP further worsened oral intolerance. Note that over the course of HFD, the change of SENP1 expression and redox state followed an anti-phase pattern, which correlated with the β-cell functional compensation. Pause of SENP1 pathway compensation on 4-week HFD caused impaired IP glucose tolerance, and maladaptation of SENP1 on 8-week further worsened IP glucose tolerance. But residue level of SENP1 could still limit deterioration of incretin effect and oral glucose intolerance. (Work by HL.)

Figure 37.

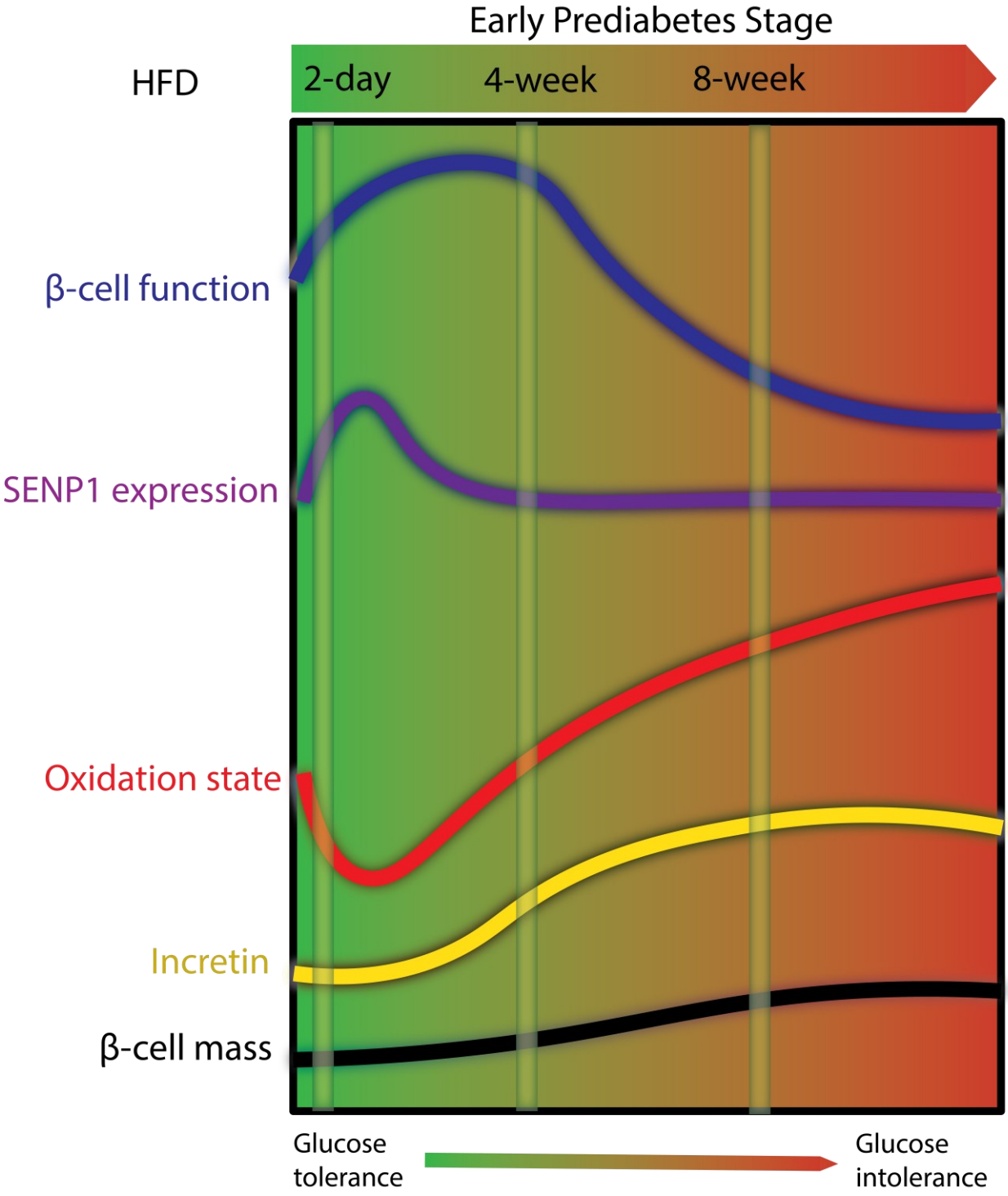
Early Prediabetes Stage
HFD
2-day
4-week
8-week
β-cell function
SENP1 expression
Oxidation state
Incretin
β-cell mass
Glucose tolerance
Glucose intolerance

5.2.2 A mechanism for SENP1 regulation and action.

5.2.2.A Potential mechanism for redox-regulation of SENP1 during short-term HFD.

Regulation of SENP is dependent on NADPH, an important metabolic coupling factor, generated in the cytosol from (iso)citrate via IDH1 upon glucose metabolism. The reducing power is relayed to GSH/GRX1, which activates SENP1[84]. The work in this thesis suggested that, after 2-day HFD, upregulation of the redox relay is largely responsible for the enhanced β-cell function. First and foremost, SENP1 expression was increased, and its activity was switched on by a reduced cytosolic state, which was possibly due to the upregulation of cytosolic NADPH **(Figure 9)**. Genes that directly regulated signals in this pathway, such as GSR, GSH, GRX1, remained unchanged (data not shown). I initially attributed the increase of NADPH to a rise in glucose metabolism, which could accelerate the export of isocitrate for NADPH generation **(Figure 9)**. However, RNA sequencing data showed that *Idh1*, which used isocitrate as substrate for producing NADPH in the cytosol, was significantly downregulated following 2-day HFD **(Figure 38A)**. Even though the increase of exported isocitrate from glucose metabolism might cancel out the effect of reduced IDH1, the current data cannot establish a causal link between glucose metabolism and NADPH production after 2-day HFD. Alternatively, NADPH might be increased by downregulated cholesterol biosynthesis. RNA sequencing data showed that the NADPH-consuming cholesterol biosynthesis was downregulated **(Figure 8)**. One caveat from the measurement of cytosolic redox state is that the redox sensor Cyto-roGFP2-Orp1 reflects the balance between oxidation and reduction, involving NADPH, GSH and H_2O_2. Therefore, the reduction of the cytosolic redox state was not only limited to NADPH. A recent study describes the *de novo* GSH biosynthesis through increased glucose metabolism via pyruvate carboxylase, which can enhance GSH independent of NADPH generation when increased glucose metabolism was still adaptive and protective. This

means that the reduced cytosolic state from a 2-day HFD exposure might be also explained by *de novo* GSH biosynthesis in addition to NADPH generation[300]. Alternatively, H_2O_2 levels may decrease transiently upon HFD exposure. *Gpx1*, which tended to be higher after 2-day HFD, might scavenge the H_2O_2 and promote the activation of SENP1, thus leading to amplification of insulin secretion **(Figure 38B)**[102].

The molecular basis of SENP1 redox regulation is dependent on the interaction between Zn^{2+} and cysteines 603 and 535 as shown in chapter 3. Zn^{2+} might bind to SENP1 during refolding and formation in the ER. This could lower SENP1 activity and prevent the hyperactivation of SENP1 through C535, setting a responsive range of SENP1 to sense the redox change induced by glucose. On 2-day HFD, cytosolic Zn^{2+} remained unchanged, indicating that Zn^{2+} was not involved in modulating SENP1 activity. A previous study showed that the Zn^{2+}-binding protein MT1 is a negative regulator for insulin secretion[121]. It is adaptively reduced for β-cell functional compensation. Indeed, *Mt1* gene expression was downregulated after 2-day HFD **(Figure 38C)**. Our preliminary data showed that MT1 can inhibit SENP1 activity, probably via the Zn^{2+} transfer to SENP1 **(Figure 38D)**. Therefore, the reduction of MT1 could possibly relieve the inhibition of SENP1, which would await further investigation. A summary proposed for regulation of SENP1 signaling on 2-day HFD is illustrated **(Figure 38E)**.

Figure 38. Proposed changes contribute to SENP1 upregulation on 2-day HFD.

(A): *Idh1* expression after 2-day HFD (n=4, 3). **(B):** *Gpx1* expression after 2-day HFD (n=4, 3). **(C):** *Mt1* expression after 2-day HFD (n=4, 3). **(D):** SENP1 and SENP1 substrate were added to assess the effect of MT1 on SENP1. MT1 protein were prepared by forming complexes with Zn^{2+}. SENP1 cannot digest the substrate due to the inhibition by higher level of MT1 (100 μg/mL), which can be abrogated by depletion of Zn^{2+} from MT1 using EDTA. Under low level of MT1 (10 μg/mL), SENP1 can successfully digest the substrate. **(E):** SENP1 activity can be upregulated at multiple steps. First, SENP1 expression was upregulated as seen in (Figure 9). Second, it can be activated by increased reduced GSH, which were explained either by a yet-to-be-identified de novo GSH biosynthesis or a rise in NADPH. Increased NADPH might be due to the elevated glucose metabolism and diminished cholesterol biosynthesis. Thirdly, increase of Gpx1 might detoxify H_2O_2 and prevent the inactivation of SENP1. Finally, SENP1 activity can be upregulated in the limited expression of MT1, which can negatively regulate SENP1 activity and insulin secretion. Data are mean ± SEM and were compared with student t test. **P*<0.05. RPKM: Reads Per Kilobase of transcript per Million mapped reads. (WL, XL, HL performed the A-C. KS performed D. HL performed E.)

Figure 38.

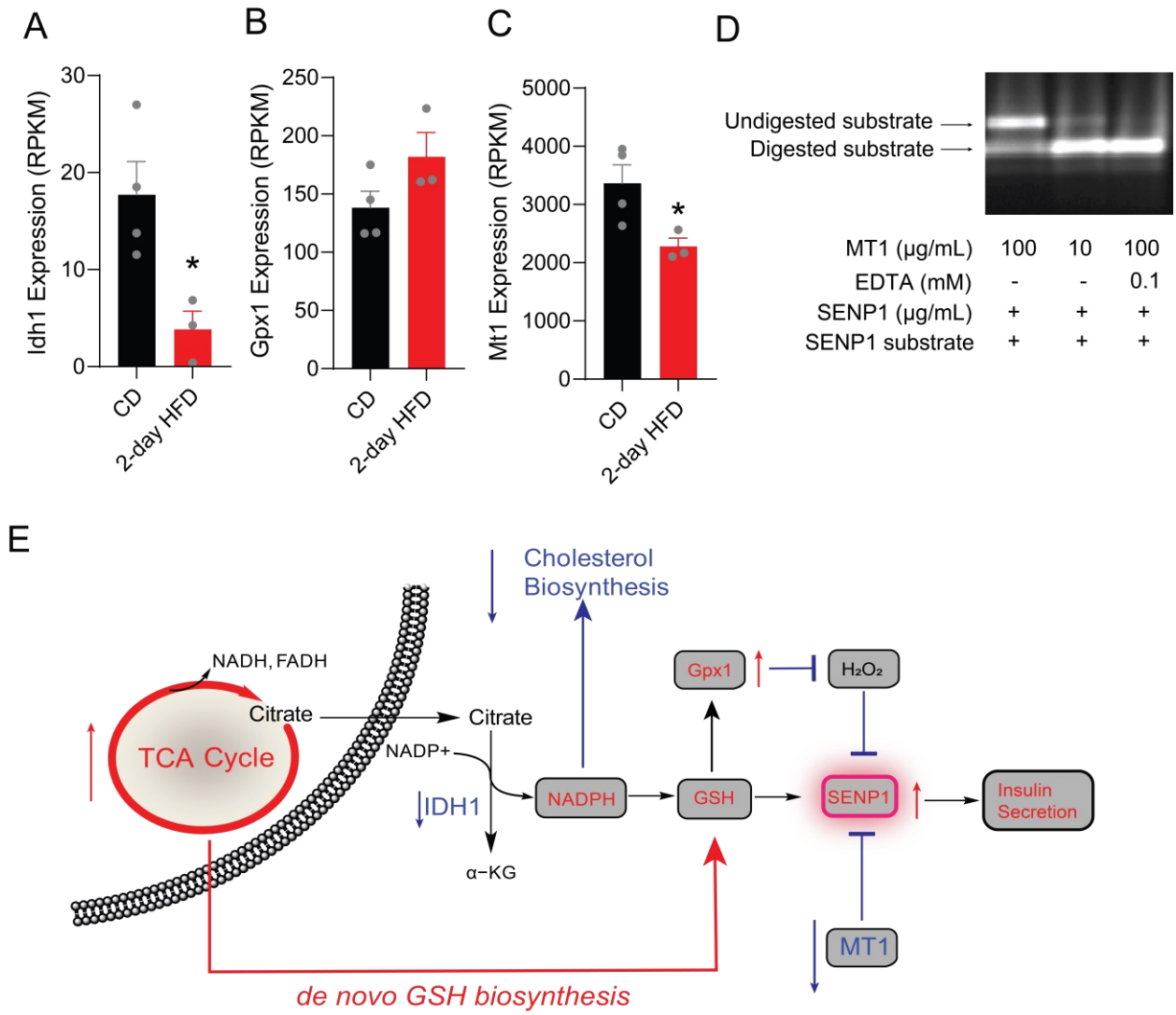
A
Idh1 Expression (RPKM)
30
20
10
0
*
CD
2-day HFD
B
Gpx1 Expression (RPKM)
250
200
150
100
50
0
CD
2-day HFD
C
Mt1 Expression (RPKM)
5000
4000
3000
2000
1000
0
*
CD
2-day HFD
D
Undigested substrate
Digested substrate
MT1 (μg/mL) 100 10 100
EDTA (mM) - - 0.1
SENP1 (μg/mL) + + +
SENP1 substrate + + +
E
Cholesterol Biosynthesis
NADH, FADH
Citrate
TCA Cycle
Citrate
NADP+
IDH1
α-KG
NADPH
GSH
Gpx1
H₂O₂
SENP1
Insulin Secretion
MT1
de novo GSH biosynthesis

5.2.2.B Mechanism underlying SENP1 action during short-term HFD.

Insulin secretion is a biphasic process, of which the first phase insulin secretion is mainly attributed to a near-membrane readily releasable pool (RRP), containing granules that are functionally primed for release after a series of reactions (i.e., granule priming). Before entering RRP, unprimed granules from an intermediate pool are docked close to the membrane and the RRP, awaiting priming signals. Sustained insulin secretion during the second phase is largely dependent on recruitment of granules from the reserve pool to dock and prime at the plasma membrane[301]. Most SENP1 targets required for modulating insulin exocytosis are reported to be exocytotic machinery, such as Tomosyn-1, Syt7, and Syntaxin1A and the Kv2.1 channel. DeSUMOylation of these proteins facilitates the priming of docked insulin granules from an intermediate pool into the RRP, which is required for insulin granule fusion and exocytosis[93,173–175].

After 2-day HFD, β-cells had higher exocytosis and insulin secretion without a change in intracellular Ca^{2+} response or voltage-dependent Ca^{2+} current, indicating an enhanced secretory response at a step distal to Ca^{2+} influx. High glucose levels can increase insulin secretion by causing essential metabolic coupling factors required for docking and priming insulin granules to be generated[51,302]. In the present study, the enhanced exocytosis at low glucose mainly indicated upregulated metabolic coupling factors and priming effect soon after 2-day HFD, since this can be recapitulated by high glucose or intracellular dialysis of SENP1, which mainly exert a priming effect on insulin granules **(Figure 6I, Figure 9H)**[175]. This enhanced priming impact was further manifested by increased insulin secretion upon high glucose stimulation in a dynamic insulin perifusion experiment **(Figure 6I)**. Consistent with this, SENP1 amplified insulin secretion **(Figure 9H)** without affecting glucose-stimulated or depolarization-induced Ca^{2+} influx **(Figure 32B, L, M)**. Previous study suggested that deSUMOylation of Syt7 and Tomosyn are the targets

for SENP1 to mediate priming effect, but more studies are needed to confirm if this is also true in the context of β-cell functional compensation. The present work suggests an up-regulated activity of the amplifying pathway at low glucose levels, requiring SENP1 actions on priming more granules for the RRP[175], thus contributing to the increased insulin secretion upon subsequent high glucose stimulation **(Figure 6)**.

5.2.2.C Underlying mechanism for SENP1 action and incretin signaling.

Previous studies found that GLP-1 receptor SUMOylation downregulated cAMP levels and insulin secretion by inducing a loss of the receptor from the plasma membrane[177,208]. In contrast, I found that this is not consistent with the following evidence from this my studies. First, ablation of SENP1 did not affect cAMP responses **(Figure 32H, I)**. Second, bypassing the receptor activation and clamping the cAMP level still enabled me to see impaired insulin exocytosis in SENP1-KO islets **(Figure 32G)**. Third, SENP1 deletion not only impaired GLP-1 receptor-, but also GIP receptor-stimulated insulin secretion. These data suggested that SENP1 acted at a level downstream of the incretin receptors. One possible discrepancy might be that other isoforms of SENP could affect the attachment of SUMO-1 to GLP-1 receptor as shown in Rajan et al's study[208] which was not focused specifically on SENP1.

How does SENP1 affect the secretory response to incretin? Our previous work demonstrated that the ability of Ex4 to amplify insulin secretion was linked to the glucose-regulated insulin secretory capacity, indicating that glucose-metabolism and incretin-signaling pathways share converging signals that ultimately enhance insulin secretion. Those signals probably act via exocytotic machinery proteins subject to SENP1 deSUMOylation[133]. Indeed, the present work showed that deletion of SENP1 not only impaired glucose- and incretin-stimulated

insulin secretion, but also fatty acid- and amino-acid stimulated insulin secretion (Error! Reference source not found.**B, C**). Most importantly, SENP1-KO reduced insulin secretion by a similar proportion (~50%) in response to glucose, incretin, amino acid (leucine + glutamate) and fatty acid (oleate), suggesting that all these fuel or non-fuel stimuli might converge on common signals, i.e., the exocytotic machinery. In contrast, if SENP1-KO affected those pathways independently, insulin secretion stimulated by these would be differentially impacted. For example, the exocytotic Ca^{2+}-sensor Syt7 is a top common target on which glucose metabolism and incretin signaling might converge. Syt7 is not only deSUMOylated during glucose stimulation[175], but also phosphorylated by GLP-1 activation[73]. For amino acid signaling, leucine and glutamate might activate GDH and reductive TCA cycles, coincident with isocitrate to SENP1 signaling[58,84]. For fatty acid signaling, another exocytotic protein Munc-13 receives an amplifying signal (1-MAG) from fatty acid metabolism and interacts with syntaxin, which is released upon Tomosyn deSUMOylation[174,303,304]. This promotes insulin granule priming and coordinates an exocytotic repertoire for a robust insulin exocytosis. Altogether, modulation of the exocytotic machinery by SENP1 underlies the ability of fuel and non-fuel (incretins) to facilitate insulin secretion.

5.2.3 Molecular basis of SENP1 redox regulation and its biological relevance

A previous study identified a C613 interaction with C603 to form a disulfide bond and protect SENP1 from irreversible oxidation[91]. This would essentially be a positive regulation of SENP1 activity, however my found that mutation of C613 had only minor effect on the SENP1. Instead, we found that C535 is a significant negative regulator of SENP1 activity in response to redox changes. Knowledge about the molecular mechanism underlying the effect of C535 is still relatively limited. Our study supported the idea that C535 might intervene in SENP1 redox regulation through the proton transfer pathway, instead of forming inter- or intra-molecular

disulfide bonds, as suggested by Xu et al's work[91] and the long distance between C535 and C603 **(Figure 17A)**.

Redox regulation has significant implications for transducing a biological response. Previous work found that the redox regulation of SENP1 couples reducing signaling to insulin secretion[84]. Here, we showed that C535 was engaged in this redox regulation. Interestingly, Zn^{2+} could also inhibit SENP1 activity through C535. Autocrine Zn^{2+} was reported to inhibit the amplification of glucose through an unidentified target[111]. SENP1 could be that target. However, this was contrasted by an unperturbed low level of glucose-stimulated cytosolic free Zn^{2+} (~400 pM), which was way below IC_{50} (~1 μM) required to acutely inhibit SENP1 activity. Even so, it is still possible that cytosolic Zn^{2+} could be tightly controlled by MT1 (enriched Zn^{2+}-binding protein) as discussed in section 5.2.2B, and the autocrine Zn^{2+} could indirectly inhibit SENP1 activity by binding to MT1.

Is Zn^{2+} itself biologically relevant for SENP1 redox regulation? Given that the acute inhibition of Zn^{2+} on SENP1 via C535 is dependent on a level much higher than the cytosolic Zn^{2+}, Zn^{2+} might exert its effect by slowly incorporating to SENP1 in cytosol or at early stages of protein folding in ER. Consistent with this, SENP1 refolding with Zn^{2+} **(Figure 16B)** could still inhibit SENP activity. This is important in preventing overstimulation of SENP1 under low glucose and allowing robust activation by glucose-stimulated reducing equivalents. Therefore, Zn^{2+} might set a responsive range of SENP1 to sense the redox change induced by glucose and play a permissive role in redox regulation of SENP1 activity through C535 in the β-cell.

5.2.4 Therapeutic potential of reducing signaling and SENP1 as drug target.

Since reducing signaling is important for functional compensation, one might conclude that it can be a potential drug target to recover functional compensation. Nowadays, some existing anti-oxidant therapies on clinical trial are suggested as T2D treatments. For example, ALT-2704 (ebselen analogue), a GPX1 mimetic which can activate GPX1, is in a phase II clinical trial to treat diabetes[305]. Previous either gain- or loss- of function studies confirmed that GPX1 was required to promote insulin secretion[102,104]. Treatment with the GPX1 mimetic ebselen can directly increase insulin secretion and rescue the insulin deficiency of GPX1-KO islets by scavenging H_2O_2[306]. Therefore, targeting the reducing signaling could offer therapeutic advantages in T2D. However, some antioxidant treatments, such as supplementation of antioxidant vitamins, failed to reach ideal therapeutic performance[307]. However, such therapies have their own limitations, especially inducing aberrant redox signaling and other unwanted outcomes[305]. Redox signaling is highly complex and tightly controlled, both spatially and temporally[75], and more studies are needed. In addition, global overexpression or deletion of SUMOylation has also proved to be detrimental to β-cell[173,181,183]. Therefore, a delicate balance of redox signaling and SUMOylation that control insulin secretion may be challenging to target for pharmacological intervention at present.

5.3 Future Directions

Although my thesis provides information about the regulation of SENP1 and how SENP1 compensates and fails to compensate during HFD, some further questions are worth pursuing:

- How does glucose metabolism drive the reduction of cytosolic state during 2-day HFD? How does it become maladaptive and promotes oxidative stress after 4- or 8-week HFD?
- Beside GRX1, are there any redox proteins, such as GPX or PRDX proteins, that directly regulate SENP1 activity?
- Besides redox regulation, are there any other processes that change the SENP1 activity? What about Zn^{2+} and MT1? Is the binding/release of Zn^{2+} from MT1 also subject to redox control?
- What is the temporal and spatial control of SENP1 versus H_2O_2 signaling in response to glucose and other pathological conditions?
- Is there a difference in redox regulation between the SUMO conjugating and deconjugating systems in β-cell?
- Is tweaking the cytosolic reducing signaling and SENP1 enough to evade off-target harmful effect and exert positive effect on insulin secretion?
- What is the exact molecular basis for C535 to regulate SENP1 redox regulation?
- Do human islets from overweight donors have increased reducing signaling and SENP1 but lose this in the evolution towards T2D?

5.4 Conclusion

β-cell function compensation is important to maintain glucose homeostasis, especially at the early stage of prediabetes. My thesis has demonstrated that reducing signaling and SENP1 are adaptive in mouse β-cells shortly after HFD exposure. SENP1 couples the upregulation of reducing signaling to increased insulin secretion via an interaction between Zn^{2+} and cysteines 535 and 603. This is important to maintain glucose tolerance, especially when it bypasses the gut. SENP1 is required for the insulin secretory response to incretin and its effect on glucose tolerance is more obviously manifested on pharmacological intervention or a long-term HFD. As the duration of HFD extends to 4 weeks, the adaptation of reducing signaling and SENP1 diminishes and by 8 weeks, oxidative stress contributes to decompensation and impairs glucose tolerance. At this stage, the incretin effect compensates for insulin resistance by upregulating the GIP output in the plasma and here loss of SENP1 worsens oral glucose tolerance. All in all, reducing signaling and SENP1 are important for prevention of glucose intolerance through β-cell functional compensation, and might be exploited for therapeutic usage in the future.

Reference List

1. Ahmed AM. History of diabetes mellitus. *Saudi Med J*. 2002;23(4):373-378.

2. Zhou B, Lu Y, Hajifathalian K, et al. Worldwide trends in diabetes since 1980: a pooled analysis of 751 population-based studies with 4·4 million participants. *The Lancet*. 2016;387(10027):1513-1530. doi:10.1016/S0140-6736(16)00618-8

3. Apicella M, Campopiano MC, Mantuano M, Mazoni L, Coppelli A, Prato SD. COVID-19 in people with diabetes: understanding the reasons for worse outcomes. *Lancet Diabetes Endocrinol*. 2020;8(9):782-792. doi:10.1016/S2213-8587(20)30238-2

4. Langerhans P, Morrison H. Contributions to the microscopic anatomy of the pancreas. *Bull Inst Hist Med*. 1937;5(3):259-297.

5. Mering J, Minkowski O. Diabetes mellitus nach Pankreasexstirpation. *Arch Für Exp Pathol Pharmakol*. 1890;26(5-6):371-387. doi:10.1007/BF01831214

6. Laguesse ME. Sur la formation des ilots de Langerhans dans le pancreas. *Comptes Rendus Seances Soc Biol*. 1893;47:699-701.

7. MacCallum W. On the relation of the islands of Langerhans to glycosuria. 1909;20:265-268.

8. Banting, Frederick Grant. The effect produced on diabetes by extracts of pancreas. Published 1922. Accessed May 14, 2020. https://insulin.library.utoronto.ca/islandora/object/insulin%3AT10010

9. Himsworth HP. Diabetes mellitus. Its differentiation into insolin-sensitive and insulin-insensitive types. *Lancet*. 1936;230:127-130.

10. Tripathi BK, Srivastava AK. Diabetes mellitus: Complications and therapeutics. *Med Sci Monit*.:18.

11. Johnson JD. On the causal relationships between hyperinsulinaemia, insulin resistance, obesity and dysglycaemia in type 2 diabetes. *Diabetologia*. 2021;64(10):2138-2146. doi:10.1007/s00125-021-05505-4

12. Esser N, Utzschneider KM, Kahn SE. Early beta cell dysfunction vs insulin hypersecretion as the primary event in the pathogenesis of dysglycaemia. *Diabetologia*. 2020;63(10):2007-2021. doi:10.1007/s00125-020-05245-x

13. Prentki M, Nolan CJ. Islet β cell failure in type 2 diabetes. *J Clin Invest*. 2006;116(7):1802-1812. doi:10.1172/JCI29103

14. Kahn SE, Hull RL, Utzschneider KM. Mechanisms linking obesity to insulin resistance and type 2 diabetes. *Nature*. 2006;444(7121):840-846. doi:10.1038/nature05482

15. Weir GC, Bonner-Weir S. Five stages of evolving beta-cell dysfunction during progression to diabetes. *Diabetes*. 2004;53(suppl 3):S16-S21. doi:10.2337/diabetes.53.suppl_3.S16

16. Aubert R, Suquet JP, Lemonnier D. Long-term morphological and metabolic effects of early under- and over-nutrition in mice. *J Nutr*. 1980;110(4):649-661. doi:10.1093/jn/110.4.649

17. Polonsky KS, Given BD, Van Cauter E. Twenty-four-hour profiles and pulsatile patterns of insulin secretion in normal and obese subjects. *J Clin Invest*. 1988;81(2):442-448.

18. Reaven GM. Role of Insulin Resistance in Human Disease. *Diabetes*. 1988;37(12):1595-1607. doi:10.2337/diab.37.12.1595

19. Kahn SE, Prigeon RL, McCulloch DK, et al. Quantification of the relationship between insulin sensitivity and beta-cell function in human subjects: evidence for a hyperbolic function. *Diabetes*. 1993;42(11):1663-1672. doi:10.2337/diab.42.11.1663

20. Bergman RN, Phillips LS, Cobelli C. Physiologic evaluation of factors controlling glucose tolerance in man: measurement of insulin sensitivity and beta-cell glucose sensitivity from the response to intravenous glucose. *J Clin Invest*. 1981;68(6):1456-1467. doi:10.1172/JCI110398

21. Bergman RN, Ader M, Huecking K, Citters GV. Accurate assessment of β-cell function: the hyperbolic correction. *Diabetes*. 2002;51(suppl 1):S212-S220. doi:10.2337/diabetes.51.2007.S212

22. Weyer C, Bogardus C, Mott DM, Pratley RE. The natural history of insulin secretory dysfunction and insulin resistance in the pathogenesis of type 2 diabetes mellitus. *J Clin Invest*. 1999;104(6):787-794.

23. Punthakee Z, Goldenberg R, Katz P. Definition, classification and diagnosis of diabetes, prediabetes and metabolic syndrome. *Can J Diabetes*. 2018;42:S10-S15. doi:10.1016/j.jcjd.2017.10.003

24. Duckworth WC, Bennett RG, Hamel FG. Insulin degradation: progress and potential. *Endocr Rev*. 1998;19(5):608-624. doi:10.1210/edrv.19.5.0349

25. Najjar SM, Perdomo G. Hepatic insulin clearance: mechanism and physiology. *Physiology*. 2019;34(3):198-215. doi:10.1152/physiol.00048.2018

26. Mittelman SD, Citters GWV, Kim SP, et al. Longitudinal compensation for fat-induced insulin resistance includes reduced insulin clearance and enhanced beta-cell response. *Diabetes*. 2000;49(12):2116-2125. doi:10.2337/diabetes.49.12.2116

27. Marini MA, Frontoni S, Succurro E, et al. Differences in insulin clearance between metabolically healthy and unhealthy obese subjects. *Acta Diabetol*. 2014;2(51):257-261. doi:10.1007/s00592-013-0511-9

28. Lee CC, Haffner SM, Wagenknecht LE, et al. Insulin clearance and the incidence of type 2 diabetes in Hispanics and African Americans: the IRAS family study. *Diabetes Care*. 2013;36(4):901-907. doi:10.2337/dc12-1316

29. Mittendorfer B, Patterson BW, Smith GI, Yoshino M, Klein S. Beta-cell function and plasma insulin clearance in people with obesity and different glycemic status. *J Clin Invest*. Published online December 14, 2021:e154068. doi:10.1172/JCI154068

30. Aronoff SL, Berkowitz K, Shreiner B, Want L. Glucose Metabolism and Regulation: Beyond Insulin and Glucagon. *Diabetes Spectr*. 2004;17(3):183-190. doi:10.2337/diaspect.17.3.183

31. Petersen MC, Shulman GI. Mechanisms of Insulin Action and Insulin Resistance. *Physiol Rev*. 2018;98(4):2133-2223. doi:10.1152/physrev.00063.2017

32. Dube S, Errazuriz-Cruzat I, Basu A, Basu R. The forgotten role of glucose effectiveness in the regulation of glucose tolerance. *Curr Diab Rep*. 2015;15(6):31. doi:10.1007/s11892-015-0605-6

33. Kahn SE, Prigeon RL, McCulloch DK, et al. The contribution of insulin-dependent and insulin-independent glucose uptake to intravenous glucose tolerance in healthy human subjects. *Diabetes*. 1994;43(4):587-592. doi:10.2337/diab.43.4.587

34. Pacini G, Thomaseth K, Ahrén B. Contribution to glucose tolerance of insulin-independent vs. insulin-dependent mechanisms in mice. *Am J Physiol Endocrinol Metab*. 2001;281(4):E693-703. doi:10.1152/ajpendo.2001.281.4.E693

35. Sacca L, Hendler R, Sherwin RS. Hyperglycemia inhibits glucose production in man independent of changes in glucoregulatory hormones. *J Clin Endocrinol Metab*. 1978;47(5):1160-1163. doi:10.1210/jcem-47-5-1160

36. Petersen KF, Laurent D, Rothman DL, Cline GW, Shulman GI. Mechanism by which glucose and insulin inhibit net hepatic glycogenolysis in humans. *J Clin Invest*. 1998;101(6):1203-1209. doi:10.1172/JCI579

37. Best JD, Kahn SE, Ader M, Watanabe RM, Ni TC, Bergman RN. Role of glucose effectiveness in the determination of glucose tolerance. *Diabetes Care*. 1996;19(9):1018-1030. doi:10.2337/diacare.19.9.1018

38. Galante P, Mosthaf L, Kellerer M, et al. Acute hyperglycemia provides an insulin-independent inducer for glut4 translocation in c2c12 myotubes and rat skeletal muscle. Diabetes. *Diabetes*. 1995;44(6):646-651. doi:10.2337/diab.44.6.646

39. Basu A, Caumo A, Bettini F, et al. Impaired basal glucose effectiveness in NIDDM: contribution of defects in glucose disappearance and production, measured using an optimized minimal model independent protocol. *Diabetes*. 1997;46(3):421-432. doi:10.2337/diab.46.3.421

40. Ahrén B, Pacini G. Insufficient islet compensation to insulin resistance vs. reduced glucose effectiveness in glucose-intolerant mice. *Am J Physiol Endocrinol Metab*. 2002;283(4):E738-744. doi:10.1152/ajpendo.00199.2002

41. Mehran AE, Templeman NM, Brigidi GS, et al. Hyperinsulinemia drives diet-induced obesity independently of brain insulin production. *Cell Metab*. 2012;16(6):723-737. doi:10.1016/j.cmet.2012.10.019

42. Mitrakou A, Kelley D, Mokan M, et al. Role of reduced suppression of glucose production and diminished early insulin release in impaired glucose tolerance. *N Engl J Med*. 1992;326(1):22-29. doi:10.1056/NEJM199201023260104

43. Dankner R, Chetrit A, Shanik MH, Raz I, Roth J. Basal-state hyperinsulinemia in healthy normoglycemic adults is predictive of type 2 diabetes over a 24-year follow-up: a preliminary report. *Diabetes Care*. 2009;32(8):1464-1466. doi:10.2337/dc09-0153

44. Prentki M, Peyot ML, Masiello P, Madiraju SRM. Nutrient-induced metabolic stress, adaptation, detoxification, and toxicity in the pancreatic β-cell. *Diabetes*. 2020;69(3):279-290. doi:10.2337/dbi19-0014

45. Cohrs CM, Panzer JK, Drotar DM, et al. Dysfunction of persisting β cells is a key feature of early type 2 diabetes pathogenesis. *Cell Rep*. 2020;31(1). doi:10.1016/j.celrep.2020.03.033

46. Henquin JC. Triggering and amplifying pathways of regulation of insulin secretion by glucose. *Diabetes*. 2000;49(11):1751-1760. doi:10.2337/diabetes.49.11.1751

47. Gaisano HY. Recent new insights into the role of SNARE and associated proteins in insulin granule exocytosis. *Diabetes Obes Metab*. 2017;19(S1):115-123. doi:10.1111/dom.13001

48. Rorsman P, Ashcroft FM. Pancreatic β-cell electrical activity and insulin secretion: of mice and men. *Physiol Rev*. 2018;98(1):117-214. doi:10.1152/physrev.00008.2017

49. Gembal M, Gilon P, Henquin JC. Evidence that glucose can control insulin release independently from its action on ATP-sensitive K+ channels in mouse β cells. *J Clin Invest*. 1992;89(4):1288-1295. doi:10.1172/JCI115714

50. Prentki M, Matschinsky FM, Madiraju SRM. Metabolic signaling in fuel-induced insulin secretion. *Cell Metab*. 2013;18(2):162-185. doi:10.1016/j.cmet.2013.05.018

51. Mourad NI, Nenquin M, Henquin JC. Metabolic amplifying pathway increases both phases of insulin secretion independently of β-cell actin microfilaments. *Am J Physiol-Cell Physiol*. 2010;299(2):C389-C398. doi:10.1152/ajpcell.00138.2010

52. Henquin JC. Regulation of insulin secretion: a matter of phase control and amplitude modulation. *Diabetologia*. 2009;52(5):739-751. doi:10.1007/s00125-009-1314-y

53. Lewandowski SL, Cardone RL, Foster HR, et al. Pyruvate Kinase Controls Signal Strength in the Insulin Secretory Pathway. *Cell Metab*. 2020;32(5):736-750.e5. doi:10.1016/j.cmet.2020.10.007

54. Jesinkey SR, Madiraju AK, Alves TC, et al. Mitochondrial GTP links nutrient sensing to β cell health, mitochondrial morphology, and insulin secretion independent of OxPhos. *Cell Rep*. 2019;28(3):759-772.e10. doi:10.1016/j.celrep.2019.06.058

55. Plecitá-Hlavatá L, Jabůrek M, Holendová B, et al. Glucose-stimulated insulin secretion fundamentally requires H2O2 signaling by NADPH Oxidase 4. *Diabetes*. 2020;69(7):1341-1354. doi:10.2337/db19-1130

56. Shyng SL, Nichols CG. Membrane phospholipid control of nucleotide sensitivity of KATP channels. *Science*. 1998;282(5391):1138-1141. doi:10.1126/science.282.5391.1138

57. Campbell JE, Newgard CB. Mechanisms controlling pancreatic islet cell function in insulin secretion. *Nat Rev Mol Cell Biol*. Published online January 4, 2021:1-17. doi:10.1038/s41580-020-00317-7

58. Zhang GF, Jensen MV, Gray SM, et al. Reductive TCA cycle metabolism fuels glutamine- and glucose-stimulated insulin secretion. *Cell Metab*. Published online December 8, 2020. doi:10.1016/j.cmet.2020.11.020

59. Ivarsson R, Quintens R, Dejonghe S, et al. Redox control of exocytosis: regulatory role of NADPH, thioredoxin, and glutaredoxin. *Diabetes*. 2005;54(7):2132-2142. doi:10.2337/diabetes.54.7.2132

60. Gooding JR, Jensen MV, Dai X, et al. Adenylosuccinate is an insulin secretagogue derived from glucose-induced purine metabolism. *Cell Rep*. 2015;13(1):157-167. doi:10.1016/j.celrep.2015.08.072

61. Maechler P, Wollheim CB. Mitochondrial glutamate acts as a messenger in glucose-induced insulin exocytosis. *Nature*. 1999;402(6762):685-689. doi:10.1038/45280

62. Vetterli L, Carobbio S, Pournourmohammadi S, et al. Delineation of glutamate pathways and secretory responses in pancreatic islets with β-cell-specific abrogation of the glutamate dehydrogenase. *Mol Biol Cell*. 2012;23(19):3851-3862. doi:10.1091/mbc.E11-08-0676

63. Michaelidis TM, Tzimagiorgis G, Moschonas NK, Papamatheakis J. The human glutamate dehydrogenase gene family: gene organization and structural characterization. *Genomics*. 1993;16(1):150-160. doi:10.1006/geno.1993.1152

64. Tomita T, Kuzuyama T, Nishiyama M. Structural basis for leucine-induced allosteric activation of glutamate dehydrogenase. *J Biol Chem*. 2011;286(43):37406-37413. doi:10.1074/jbc.M111.260265

65. Gheni G, Ogura M, Iwasaki M, et al. Glutamate acts as a key signal linking glucose metabolism to incretin/camp action to amplify insulin secretion. *Cell Rep*. 2014;9(2):661-673. doi:10.1016/j.celrep.2014.09.030

66. Prentki M, Corkey BE, Madiraju SRM. Lipid-associated metabolic signalling networks in pancreatic beta cell function. *Diabetologia*. 2020;63(1):10-20. doi:10.1007/s00125-019-04976-w

67. Zhao S, Mugabo Y, Iglesias J, et al. A/β-hydrolase domain-6-accessible monoacylglycerol controls glucose-stimulated insulin secretion. *Cell Metab*. 2014;19(6):993-1007. doi:10.1016/j.cmet.2014.04.003

68. Tunaru S, Bonnavion R, Brandenburger I, et al. 20-HETE promotes glucose-stimulated insulin secretion in an autocrine manner through FFAR1. *Nat Commun*. 2018;9(1):177. doi:10.1038/s41467-017-02539-4

69. Hodson DJ, Mitchell RK, Marselli L, et al. ADCY5 couples glucose to insulin secretion in human islets. *Diabetes*. 2014;63(9):3009-3021. doi:10.2337/db13-1607

70. Tian G, Sandler S, Gylfe E, Tengholm A. Glucose- and hormone-induced cAMP oscillations in α- and β-Cells within intact pancreatic islets. *Diabetes*. 2011;60(5):1535-1543. doi:10.2337/db10-1087

71. Shuai H, Xu Y, Ahooghalandari P, Tengholm A. Glucose-induced cAMP elevation in β-cells involves amplification of constitutive and glucagon-activated GLP-1 receptor signalling. *Acta Physiol Oxf Engl*. 2021;231(4):e13611. doi:10.1111/apha.13611

72. Rutter GA, Pullen TJ, Hodson DJ, Martinez-Sanchez A. Pancreatic β-cell identity, glucose sensing and the control of insulin secretion. *Biochem J*. 2015;466(2):203-218. doi:10.1042/BJ20141384

73. Wu B, Wei S, Petersen N, et al. Synaptotagmin-7 phosphorylation mediates GLP-1–dependent potentiation of insulin secretion from β-cells. *Proc Natl Acad Sci*. 2015;112(32):9996-10001. doi:10.1073/pnas.1513004112

74. Renström E, Eliasson L, Rorsman P. Protein kinase A-dependent and -independent stimulation of exocytosis by cAMP in mouse pancreatic B-cells. *J Physiol*. 1997;502(Pt 1):105-118.

75. Roma LP, Jonas JC. Nutrient metabolism, subcellular redox state, and oxidative stress in pancreatic islets and β-cells. *J Mol Biol*. 2020;432(5):1461-1493. doi:10.1016/j.jmb.2019.10.012

76. Brand MD. Mitochondrial generation of superoxide and hydrogen peroxide as the source of mitochondrial redox signaling. *Free Radic Biol Med*. 2016;100:14-31. doi:10.1016/j.freeradbiomed.2016.04.001

77. Schuit F, Vos AD, Farfari S, et al. Metabolic fate of glucose in purified islet cells: glucose-regulated anaplerosis in β cells. *J Biol Chem*. 1997;272(30):18572-18579. doi:10.1074/jbc.272.30.18572

78. Toye AA, Lippiat JD, Proks P, et al. A genetic and physiological study of impaired glucose homeostasis control in C57BL/6J mice. *Diabetologia*. 2005;48(4):675-686. doi:10.1007/s00125-005-1680-z

79. Santos LRB, Muller C, de Souza AH, et al. NNT reverse mode of operation mediates glucose control of mitochondrial NADPH and glutathione redox state in mouse pancreatic β-cells. *Mol Metab*. 2017;6(6):535-547. doi:10.1016/j.molmet.2017.04.004

80. Plecitá-Hlavatá L, Engstová H, Holendová B, et al. Mitochondrial superoxide production decreases on glucose-stimulated insulin secretion in pancreatic β Cells due to decreasing mitochondrial matrix NADH/NAD+ ratio. *Antioxid Redox Signal*. 2020;33(12):789-815. doi:10.1089/ars.2019.7800

81. Cameron WD, Bui CV, Hutchinson A, Loppnau P, Gräslund S, Rocheleau JV. Apollo-NADP + : a spectrally tunable family of genetically encoded sensors for NADP +. *Nat Methods*. 2016;13(4):352-358. doi:10.1038/nmeth.3764

82. Takahashi HK, Santos LRB, Roma LP, et al. Acute nutrient regulation of the mitochondrial glutathione redox state in pancreatic β-cells. *Biochem J*. 2014;460(3):411-423. doi:10.1042/BJ20131361

83. Liu X, Han S, Yang Y, Kang J, Wu J. Glucose-induced glutathione reduction in mitochondria is involved in the first phase of pancreatic β-cell insulin secretion. *Biochem Biophys Res Commun*. 2015;464(3):730-736. doi:10.1016/j.bbrc.2015.07.016

84. Ferdaoussi M, Dai X, Jensen MV, et al. Isocitrate-to-SENP1 signaling amplifies insulin secretion and rescues dysfunctional β cells. *J Clin Invest*. 2015;125(10):3847-3860. doi:10.1172/JCI82498

85. Reinbothe TM, Ivarsson R, Li DQ, et al. Glutaredoxin-1 mediates NADPH-dependent stimulation of calcium-dependent insulin secretion. *Mol Endocrinol*. 2009;23(6):893-900. doi:10.1210/me.2008-0306

86. Bauchle CJ, Rohli KE, Boyer CK, et al. Mitochondrial efflux of citrate and isocitrate is fully dispensable for glucose-stimulated insulin secretion and pancreatic islet β-cell function. *Diabetes*. 2021;70(8):1717-1728. doi:10.2337/db21-0037

87. Ge T, Yang J, Zhou S, Wang Y, Li Y, Tong X. The role of the pentose phosphate pathway in diabetes and cancer. *Front Endocrinol*. 2020;11:365. doi:10.3389/fendo.2020.00365

88. Spégel P, Sharoyko VV, Goehring I, et al. Time-resolved metabolomics analysis of β-cells implicates the pentose phosphate pathway in the control of insulin release. *Biochem J*. 2013;450(3):595-605. doi:10.1042/BJ20121349

89. Pi J, Bai Y, Zhang Q, et al. Reactive oxygen species as a signal in glucose-stimulated insulin secretion. *Diabetes*. 2007;56(7):1783-1791. doi:10.2337/db06-1601

90. Deglasse JP, Roma LP, Pastor-Flores D, Gilon P, Dick TP, Jonas JC. Glucose acutely reduces cytosolic and mitochondrial H2O2 in rat pancreatic beta cells. *Antioxid Redox Signal*. 2019;30(3):297-313. doi:10.1089/ars.2017.7287

91. Xu Z, Lam LSM, Lam LH, Chau SF, Ng TB, Au SWN. Molecular basis of the redox regulation of SUMO proteases: a protective mechanism of intermolecular disulfide linkage against irreversible sulfhydryl oxidation. *FASEB J Off Publ Fed Am Soc Exp Biol*. 2008;22(1):127-137. doi:10.1096/fj.06-7871com

92. Vergari E, Plummer G, Dai X, MacDonald PE. DeSUMOylation controls insulin exocytosis in response to metabolic Signals. *Biomolecules*. 2012;2(2):269-281. doi:10.3390/biom2020269

93. Fu J, Githaka JM, Dai X, et al. A glucose-dependent spatial patterning of exocytosis in human β cells is disrupted in type 2 diabetes. *JCI Insight*. 4(12). doi:10.1172/jci.insight.127896

94. Dai XQ, Kolic J, Marchi P, Sipione S, MacDonald PE. SUMOylation regulates Kv2.1 and modulates pancreatic β-cell excitability. *J Cell Sci*. 2009;122(6):775-779. doi:10.1242/jcs.036632

95. Lacraz G, Figeac F, Movassat J, et al. Diabetic β-cells can achieve self-protection against oxidative stress through an adaptive up-regulation of their antioxidant defenses. *Plos One*. 2009;4(8):e6500. doi:10.1371/journal.pone.0006500

96. Stancill JS, Broniowska KA, Oleson BJ, Naatz A, Corbett JA. Pancreatic β-cells detoxify H2O2 through the peroxiredoxin/thioredoxin antioxidant system. *J Biol Chem*. 2019;294(13):4843-4853. doi:10.1074/jbc.RA118.006219

97. Stancill JS, Happ JT, Broniowska KA, Hogg N, Corbett JA. Peroxiredoxin 1 plays a primary role in protecting pancreatic β-cells from hydrogen peroxide and peroxynitrite. *Am J Physiol-Regul Integr Comp Physiol*. 2020;318(5):R1004-R1013. doi:10.1152/ajpregu.00011.2020

98. Tanaka Y, Tran POT, Harmon J, Robertson RP. A role for glutathione peroxidase in protecting pancreatic beta cells against oxidative stress in a model of glucose toxicity. *Proc Natl Acad Sci U S A*. 2002;99(19):12363-12368. doi:10.1073/pnas.192445199

99. Chen H, Li X, Epstein PN. MnSOD and catalase transgenes demonstrate that protection of islets from oxidative stress does not alter cytokine toxicity. *Diabetes*. 2005;54(5):1437-1446. doi:10.2337/diabetes.54.5.1437

100. Robertson RP, Harmon JS. Pancreatic islet β-cell and oxidative stress: the importance of glutathione peroxidase. *FEBS Lett*. 2007;581(19):3743-3748. doi:10.1016/j.febslet.2007.03.087

101. Lortz S, Gurgul-Convey E, Naujok O, Lenzen S. Overexpression of the antioxidant enzyme catalase does not interfere with the glucose responsiveness of insulin-secreting INS-1E cells and rat islets. *Diabetologia*. 2013;56(4):774-782. doi:10.1007/s00125-012-2823-7

102. Wang XD, Vatamaniuk MZ, Wang SK, Roneker CA, Simmons RA, Lei XG. Molecular mechanisms for hyperinsulinaemia induced by overproduction of selenium-dependent glutathione peroxidase-1 in mice. *Diabetologia*. 2008;51(8):1515-1524. doi:10.1007/s00125-008-1055-3

103. McClung JP, Roneker CA, Mu W, et al. Development of insulin resistance and obesity in mice overexpressing cellular glutathione peroxidase. *Proc Natl Acad Sci U S A*. 2004;101(24):8852-8857. doi:10.1073/pnas.0308096101

104. Wang X, Vatamaniuk MZ, Roneker CA, et al. Knockouts of SOD1 and GPX1 exert different impacts on murine islet function and pancreatic integrity. *Antioxid Redox Signal*. 2011;14(3):391-401. doi:10.1089/ars.2010.3302

105. Leloup C, Tourrel-Cuzin C, Magnan C, et al. Mitochondrial reactive oxygen species are obligatory signals for glucose-induced insulin secretion. *Diabetes*. 2009;58(3):673-681. doi:10.2337/db07-1056

106. Zhang IX, Raghavan M, Satin LS. The endoplasmic reticulum and calcium homeostasis in pancreatic beta cells. *Endocrinology*. 2020;161(bqz028). doi:10.1210/endocr/bqz028

107. Llanos P, Contreras-Ferrat A, Barrientos G, Valencia M, Mears D, Hidalgo C. Glucose-dependent insulin secretion in pancreatic β-cell islets from male rats requires Ca2+ release via ROS-stimulated ryanodine receptors. *PLOS ONE*. 2015;10(6):e0129238. doi:10.1371/journal.pone.0129238

108. Hasnain SZ, Prins JB, McGuckin MA. Oxidative and endoplasmic reticulum stress in β-cell dysfunction in diabetes. *J Mol Endocrinol*. 2016;56(2):R33-R54. doi:10.1530/JME-15-0232

109. Tiedge M, Lortz S, Drinkgern J, Lenzen S. Relation between antioxidant enzyme gene expression and antioxidative defense status of insulin-producing cells. *Diabetes*. 1997;46(11):1733-1742. doi:10.2337/diab.46.11.1733

110. Lenzen S. Oxidative stress: the vulnerable beta-cell. *Biochem Soc Trans*. 2008;36(Pt 3):343-347. doi:10.1042/BST0360343

111. Slepchenko KG, Daniels NA, Guo A, Li YV. Autocrine effect of Zn2+ on the glucose-stimulated insulin secretion. *Endocrine*. 2015;50(1):110-122. doi:10.1007/s12020-015-0568-z

112. Slepchenko KG, James CBL, Li YV. Inhibitory effect of zinc on glucose-stimulated zinc/insulin secretion in an insulin-secreting β-cell line. *Exp Physiol*. 2013;98(8):1301-1311. doi:10.1113/expphysiol.2013.072348

113. Bloc A, Cens T, Cruz H, Dunant Y. Zinc-induced changes in ionic currents of clonal rat pancreatic β-cells: activation of ATP-sensitive K+ channels. *J Physiol*. 2000;529(Pt 3):723-734. doi:10.1111/j.1469-7793.2000.00723.x

114. Ghafghazi T, McDANIEL ML, Lacy PE. Zinc-induced inhibition of insulin secretion from isolated rat islets of Langerhans. 1981;30:5.

115. Jacob C, Maret W, Vallee BL. Control of zinc transfer between thionein, metallothionein, and zinc proteins. *Proc Natl Acad Sci*. 1998;95(7):3489-3494. doi:10.1073/pnas.95.7.3489

116. Krężel A, Hao Q, Maret W. The zinc/thiolate redox biochemistry of metallothionein and the control of zinc ion fluctuations in cell signaling. *Arch Biochem Biophys*. 2007;463(2):188-200. doi:10.1016/j.abb.2007.02.017

117. Maret W. Zinc and sulfur: a critical biological partnership. *Biochemistry*. 2004;43(12):3301-3309. doi:10.1021/bi036340p

118. Maret W. Zinc coordination environments in proteins as redox sensors and signal transducers. *Antioxid Redox Signal*. 2006;8(9-10):1419-1441. doi:10.1089/ars.2006.8.1419

119. Maret W, Vallee BL. Thiolate ligands in metallothionein confer redox activity on zinc clusters. *Proc Natl Acad Sci U S A*. 1998;95(7):3478-3482. doi:10.1073/pnas.95.7.3478

120. Jiang LJ, Maret W, Vallee BL. The glutathione redox couple modulates zinc transfer from metallothionein to zinc-depleted sorbitol dehydrogenase. *Proc Natl Acad Sci*. 1998;95(7):3483-3488. doi:10.1073/pnas.95.7.3483

121. Bensellam M, Shi YC, Chan JY, et al. Metallothionein 1 negatively regulates glucose-stimulated insulin secretion and is differentially expressed in conditions of beta cell compensation and failure in mice and humans. *Diabetologia*. 2019;62(12):2273-2286. doi:10.1007/s00125-019-05008-3

122. Chen C, Chmelova H, Cohrs CM, et al. Alterations in β-cell calcium dynamics and efficacy outweigh islet mass adaptation in compensation of insulin resistance and prediabetes onset. *Diabetes*. 2016;65(9):2676-2685. doi:10.2337/db15-1718

123. Mezza T, Ferraro PM, Giuseppe GD, et al. Pancreaticoduodenectomy model demonstrates a fundamental role of dysfunctional β cells in predicting diabetes. *J Clin Invest*. 2021;131(12). doi:10.1172/JCI146788

124. Weir GC, Bonner-Weir S. Reduced glucose-induced first-phase insulin release is a danger signal that predicts diabetes. *J Clin Invest*. 2021;131(12). doi:10.1172/JCI150022

125. Piñeros AR, Gao H, Wu W, Liu Y, Tersey SA, Mirmira RG. Single-cell transcriptional profiling of mouse islets following short-term obesogenic dietary intervention. *Metabolites*. 2020;10(12):513. doi:10.3390/metabo10120513

126. Stožer A, Hojs R, Dolenšek J. Beta cell functional adaptation and dysfunction in insulin resistance and the role of chronic kidney disease. *Nephron*. 2019;143(1):33-37. doi:10.1159/000495665

127. Khaldi MZ, Guiot Y, Gilon P, Henquin JC, Jonas JC. Increased glucose sensitivity of both triggering and amplifying pathways of insulin secretion in rat islets cultured for 1 wk in high glucose. *Am J Physiol-Endocrinol Metab*. 2004;287(2):E207-E217. doi:10.1152/ajpendo.00426.2003

128. Chen C, Cohrs CM, Stertmann J, Bozsak R, Speier S. Human beta cell mass and function in diabetes: Recent advances in knowledge and technologies to understand disease pathogenesis. *Mol Metab*. 2017;6(9):943-957. doi:10.1016/j.molmet.2017.06.019

129. Glynn E, Thompson B, Vadrevu S, et al. Chronic glucose exposure systematically shifts the oscillatory threshold of mouse islets: experimental evidence for an early intrinsic mechanism of compensation for hyperglycemia. *Endocrinology*. 2016;157(2):611-623. doi:10.1210/en.2015-1563

130. Park SH, Ryu SY, Yu WJ, et al. Leptin promotes KATP channel trafficking by AMPK signaling in pancreatic β-cells. *Proc Natl Acad Sci*. 2013;110(31):12673-12678. doi:10.1073/pnas.1216351110

131. Gonzalez A, Merino B, Marroquí L, et al. Insulin hypersecretion in islets from diet-induced hyperinsulinemic obese female mice is associated with several functional adaptations in individual β-cells. *Endocrinology*. 2013;154(10):3515-3524. doi:10.1210/en.2013-1424

132. Irles E, Ñeco P, Lluesma M, et al. Enhanced glucose-induced intracellular signaling promotes insulin hypersecretion: pancreatic beta-cell functional adaptations in a model of genetic obesity and prediabetes. *Mol Cell Endocrinol*. 2015;404:46-55. doi:10.1016/j.mce.2015.01.033

133. Ferdaoussi M, MacDonald PE. Toward connecting metabolism to the exocytotic site. *Trends Cell Biol*. 2017;27(3):163-171. doi:10.1016/j.tcb.2016.10.003

134. Jahan I, Corbin KL, Bogart AM, et al. Reducing glucokinase activity restores endogenous pulsatility and enhances insulin secretion in islets from db/db mice. *Endocrinology*. 2018;159(11):3747-3760. doi:10.1210/en.2018-00589

135. Do OH, Gunton JE, Gaisano HY, Thorn P. Changes in beta cell function occur in prediabetes and early disease in the Lepr db mouse model of diabetes. *Diabetologia*. 2016;59(6):1222-1230. doi:10.1007/s00125-016-3942-3

136. Gandasi NR, Yin P, Omar-Hmeadi M, Ottosson Laakso E, Vikman P, Barg S. Glucose-dependent granule docking limits insulin secretion and is decreased in human type 2 diabetes. *Cell Metab*. 2018;27(2):470-478.e4. doi:10.1016/j.cmet.2017.12.017

137. Bermudez B, Ortega-Gomez A, Varela LM, et al. Clustering effects on postprandial insulin secretion and sensitivity in response to meals with different fatty acid compositions. *Food Funct*. 2014;5(7):1374-1380. doi:10.1039/c4fo00067f

138. Malmgren S, Spégel P, Danielsson APH, et al. Coordinate changes in histone modifications, mrna levels, and metabolite profiles in clonal INS-1 832/13 β-cells accompany functional adaptations to lipotoxicity. *J Biol Chem*. 2013;288(17):11973-11987. doi:10.1074/jbc.M112.422527

139. Sargsyan E, Cen J, Roomp K, Schneider R, Bergsten P. Identification of early biological changes in palmitate-treated isolated human islets. *BMC Genomics*. 2018;19(1):629. doi:10.1186/s12864-018-5008-z

140. Lytrivi M, Ghaddar K, Lopes M, et al. Combined transcriptome and proteome profiling of the pancreatic β-cell response to palmitate unveils key pathways of β-cell lipotoxicity. *BMC Genomics*. 2020;21(1):590. doi:10.1186/s12864-020-07003-0

141. Busch AK, Cordery D, Denyer GS, Biden TJ. Expression profiling of palmitate- and oleate-regulated genes provides novel insights into the effects of chronic lipid exposure on pancreatic β-cell function. *Diabetes*. 2002;51(4):977-987. doi:10.2337/diabetes.51.4.977

142. Felig P, Marliss E, Cahill GF. Plasma amino acid levels and insulin secretion in obesity. *N Engl J Med*. 1969;281(15):811-816. doi:10.1056/NEJM196910092811503

143. Wang TJ, Larson MG, Vasan RS, et al. Metabolite profiles and the risk of developing diabetes. *Nat Med*. 2011;17(4):448-453. doi:10.1038/nm.2307

144. Tricò D, Frascerra S, Baldi S, et al. The insulinotropic effect of a high-protein nutrient preload is mediated by the increase of plasma amino acids in type 2 diabetes. *Eur J Nutr*. 2019;58(6):2253-2261. doi:10.1007/s00394-018-1778-y

145. Van Citters GW, Kabir M, Kim SP, et al. Elevated glucagon-like peptide-1-(7–36)-amide, but not glucose, associated with hyperinsulinemic compensation for fat feeding. *J Clin Endocrinol Metab*. 2002;87(11):5191-5198. doi:10.1210/jc.2002-020002

146. Srinivasan S, Bernal-Mizrachi E, Ohsugi M, Permutt MA. Glucose promotes pancreatic islet β-cell survival through a PI 3-kinase/Akt-signaling pathway. *Am J Physiol-Endocrinol Metab*. 2002;283(4):E784-E793. doi:10.1152/ajpendo.00177.2002

147. Steil GM, Trivedi N, Jonas JC, et al. Adaptation of β-cell mass to substrate oversupply: enhanced function with normal gene expression. *Am J Physiol-Endocrinol Metab*. 2001;280(5):E788-E796. doi:10.1152/ajpendo.2001.280.5.E788

148. Ogilvie RF. The islands of Langerhans in 19 cases of obesity. *J Pathol Bacteriol*. 1933;37(3):473-481. doi:10.1002/path.1700370314

149. Matsumoto I, Sawada T, Nakano M, et al. Improvement in islet yield from obese donors for human islet transplants. *Transplantation*. 2004;78(6):880-885. doi:10.1097/01.TP.0000134396.03440.1E

150. Butler AE, Janson J, Bonner-Weir S, Ritzel R, Rizza RA, Butler PC. β-cell deficit and increased β-cell apoptosis in humans with type 2 diabetes. *Diabetes*. 2003;52(1):102-110. doi:10.2337/diabetes.52.1.102

151. Rahier J, Guiot Y, Goebbels RM, Sempoux C, Henquin JC. Pancreatic β-cell mass in European subjects with type 2 diabetes. *Diabetes Obes Metab*. 2008;10(s4):32-42. doi:10.1111/j.1463-1326.2008.00969.x

152. Linnemann AK, Baan M, Davis DB. Pancreatic β-cell proliferation in obesity. *Adv Nutr*. 2014;5(3):278-288. doi:10.3945/an.113.005488

153. Butler AE, Janson J, Soeller WC, Butler PC. Increased beta-cell apoptosis prevents adaptive increase in beta-cell mass in mouse model of type 2 diabetes: evidence for role of islet amyloid formation rather than direct action of amyloid. *Diabetes*. 2003;52(9):2304-2314. doi:10.2337/diabetes.52.9.2304

154. Peyot ML, Pepin E, Lamontagne J, et al. Beta-cell failure in diet-induced obese mice stratified according to body weight gain: secretory dysfunction and altered islet lipid metabolism without steatosis or reduced beta-cell mass. *Diabetes*. 2010;59(9):2178-2187. doi:10.2337/db09-1452

155. Delghingaro-Augusto V, Nolan CJ, Gupta D, et al. Islet beta cell failure in the 60% pancreatectomised obese hyperlipidaemic Zucker fatty rat: severe dysfunction with altered glycerolipid metabolism without steatosis or a falling beta cell mass. *Diabetologia*. 2009;52(6):1122. doi:10.1007/s00125-009-1317-8

156. Kendall DM, Sutherland DER, Najarian JS, Goetz FC, Robertson RP. Effects of hemipancreatectomy on insulin secretion and glucose tolerance in healthy humans. *N Engl J Med*. 1990;322(13):898-903. doi:10.1056/NEJM199003293221305

157. Brunzell JD, Robertson RP, Lerner RL, et al. Relationships between fasting plasma glucose levels and insulin secretion during intravenous glucose tolerance tests. *J Clin Endocrinol Metab*. 1976;42(2):222-229. doi:10.1210/jcem-42-2-222

158. Kunz K, Piller T, Müller S. SUMO-specific proteases and isopeptidases of the SENP family at a glance. *J Cell Sci*. 2018;131(6). doi:10.1242/jcs.211904

159. Gill G. SUMO and ubiquitin in the nucleus: different functions, similar mechanisms? *Genes Dev*. 2004;18(17):2046-2059. doi:10.1101/gad.1214604

160. Segerstolpe Å, Palasantza A, Eliasson P, et al. Single-cell transcriptome profiling of human pancreatic islets in health and type 2 diabetes. *Cell Metab*. 2016;24(4):593-607. doi:10.1016/j.cmet.2016.08.020

161. Kamitani T, Kito K, Nguyen HP, Fukuda-Kamitani T, Yeh ETH. Characterization of a second member of the sentrin family of ubiquitin-like proteins. *J Biol Chem*. 1998;273(18):11349-11353. doi:10.1074/jbc.273.18.11349

162. Ulrich HD. The fast-growing business of SUMO chains. *Mol Cell*. 2008;32(3):301-305. doi:10.1016/j.molcel.2008.10.010

163. Sharma P, Yamada S, Lualdi M, Dasso M, Kuehn MR. Senp1 is essential for desumoylating Sumo1-modified proteins but dispensable for Sumo2 and Sumo3 deconjugation in the mouse embryo. *Cell Rep*. 2013;3(5):1640-1650. doi:10.1016/j.celrep.2013.04.016

164. Mikolajczyk J, Drag M, Békés M, Cao JT, Ronai Z, Salvesen GS. Small ubiquitin-related modifier (SUMO)-specific proteases: profiling the specificities and activities of human SENPs. *J Biol Chem*. 2007;282(36):26217-26224. doi:10.1074/jbc.M702444200

165. Yeh ETH. SUMOylation and De-SUMOylation: wrestling with life's processes. *J Biol Chem*. 2009;284(13):8223-8227. doi:10.1074/jbc.R800050200

166. Jung HS, Kang YM, Park HS, et al. Senp2 expression was induced by chronic glucose stimulation in INS1 cells, and it was required for the associated induction of Ccnd1 and Mafa. *Islets*. 2016;8(6):207-216. doi:10.1080/19382014.2016.1235677

167. Paulsen CE, Carroll KS. Cysteine-mediated redox signaling: chemistry, biology, and tools for discovery. *Chem Rev*. 2013;113(7):4633-4679. doi:10.1021/cr300163e

168. Winterbourn CC, Hampton MB. Thiol chemistry and specificity in redox signaling. *Free Radic Biol Med*. 2008;45(5):549-561. doi:10.1016/j.freeradbiomed.2008.05.004

169. Berndt C, Lillig CH, Holmgren A. Thiol-based mechanisms of the thioredoxin and glutaredoxin systems: implications for diseases in the cardiovascular system. *Am J Physiol-Heart Circ Physiol*. 2007;292(3):H1227-H1236. doi:10.1152/ajpheart.01162.2006

170. D'Autréaux B, Toledano MB. ROS as signalling molecules: mechanisms that generate specificity in ROS homeostasis. *Nat Rev Mol Cell Biol*. 2007;8(10):813-824. doi:10.1038/nrm2256

171. Redox regulation of SUMO enzymes is required for ATM activity and survival in oxidative stress. *EMBO J*. 2016;35(12):1312-1329. doi:10.15252/embj.201593404

172. Bossis G, Melchior F. Regulation of sumoylation by reversible oxidation of SUMO conjugating enzymes. *Mol Cell*. 2006;21(3):349-357. doi:10.1016/j.molcel.2005.12.019

173. Davey JS, Carmichael RE, Craig TJ. Protein SUMOylation regulates insulin secretion at multiple stages. *Sci Rep*. 2019;9(1):2895. doi:10.1038/s41598-019-39681-6

174. Ferdaoussi M, Fu J, Dai X, et al. SUMOylation and calcium control syntaxin-1A and secretagogin sequestration by tomosyn to regulate insulin exocytosis in human ß cells. *Sci Rep*. 2017;7(1):248. doi:10.1038/s41598-017-00344-z

175. Dai XQ, Plummer G, Casimir M, et al. SUMOylation regulates insulin exocytosis downstream of secretory granule docking in rodents and humans. *Diabetes*. 2011;60(3):838-847. doi:10.2337/db10-0440

176. Nemecz M, Constantin A, Dumitrescu M, et al. The distinct effects of palmitic and oleic acid on pancreatic beta cell function: the elucidation of associated mechanisms and effector molecules. *Front Pharmacol*. 2019;9:1554. doi:10.3389/fphar.2018.01554

177. Rajan S, Dickson LM, Mathew E, et al. Chronic hyperglycemia downregulates GLP-1 receptor signaling in pancreatic β-cells via protein kinase A. *Mol Metab*. 2015;4(4):265-276. doi:10.1016/j.molmet.2015.01.010

178. Shao C, Cobb MH. Sumoylation regulates the transcriptional activity of MafA in pancreatic β Cells. *J Biol Chem*. 2009;284(5):3117-3124. doi:10.1074/jbc.M806286200

179. Hajmrle C, Ferdaoussi M, Plummer G, et al. SUMOylation protects against IL-1β-induced apoptosis in INS-1 832/13 cells and human islets. *Am J Physiol Endocrinol Metab*. 2014;307(8):E664-673. doi:10.1152/ajpendo.00168.2014

180. Giannoukakis N, Rudert WA, Trucco M, Robbins PD. Protection of Human Islets from the Effects of Interleukin-1β by Adenoviral Gene Transfer of an IκB Repressor *. *J Biol Chem*. 2000;275(47):36509-36513. doi:10.1074/jbc.M005943200

181. He X, Lai Q, Chen C, et al. Both conditional ablation and overexpression of E2 SUMO-conjugating enzyme (UBC9) in mouse pancreatic beta cells result in impaired beta cell function. *Diabetologia*. 2018;61(4):881-895. doi:10.1007/s00125-017-4523-9

182. Li N, Zhang S, Xiong F, Eizirik DL, Wang CY. SUMOylation, a multifaceted regulatory mechanism in the pancreatic beta cells. *Semin Cell Dev Biol*. 2020;103:51-58. doi:10.1016/j.semcdb.2020.03.008

183. MacDonald PE. A post-translational balancing act: the good and the bad of SUMOylation in pancreatic islets. *Diabetologia*. 2018;61(4):775-779. doi:10.1007/s00125-017-4543-5

184. Elrick H, Stimmler L, Hlad CJ JR, Arai Y. Plasma insulin response to oral and intravenous glucose administration. *J Clin Endocrinol Metab*. 1964;24(10):1076-1082. doi:10.1210/jcem-24-10-1076

185. Kreymann B, Williams G, Ghatei MA, Bloom SR. Glucagon-like peptide-1 7-36: a physiological incretin in man. *Lancet Lond Engl*. 1987;2(8571):1300-1304. doi:10.1016/s0140-6736(87)91194-9

186. Dupre J, Ross SA, Watson D, Brown JC. Stimulation of insulin secretion by gastric inhibitory polypeptide in man. *J Clin Endocrinol Metab*. 1973;37(5):826-828. doi:10.1210/jcem-37-5-826

187. Nauck MA, Quast DR, Wefers J, Pfeiffer AFH. The evolving story of incretins (GIP and GLP-1) in metabolic and cardiovascular disease: A pathophysiological update. *Diabetes Obes Metab*. 2021;23(S3):5-29. doi:10.1111/dom.14496

188. Cabou C, Burcelin R. GLP-1, the gut-brain, and brain-periphery axes. *Rev Diabet Stud*. 2011;8(3). doi:10.1900/RDS.2011.8.418

189. Nauck MA, Bartels E, Orskov C, Ebert R, Creutzfeldt W. Additive insulinotropic effects of exogenous synthetic human gastric inhibitory polypeptide and glucagon-like peptide-1-(7-36)

amide infused at near-physiological insulinotropic hormone and glucose concentrations. *J Clin Endocrinol Metab*. 1993;76(4):912-917. doi:10.1210/jcem.76.4.8473405

190. Gasbjerg LS, Helsted MM, Hartmann B, et al. Separate and combined glucometabolic effects of endogenous glucose-dependent insulinotropic polypeptide and glucagon-like peptide 1 in healthy individuals. *Diabetes*. 2019;68(5):906-917. doi:10.2337/db18-1123

191. Gasbjerg LS, Helsted MM, Hartmann B, et al. GIP and GLP-1 receptor antagonism during a meal in healthy individuals. *J Clin Endocrinol Metab*. 2020;105(3):e725-e738. doi:10.1210/clinem/dgz175

192. Jones IR, Owens DR, Luzio S, Williams S, Hayes TM. The glucose dependent insulinotropic polypeptide response to oral glucose and mixed meals is increased in patients with Type 2 (non-insulin-dependent) diabetes mellitus. *Diabetologia*. 1989;32(9):668-677. doi:10.1007/BF00274255

193. Nauck M, Stöckmann F, Ebert R, Creutzfeldt W. Reduced incretin effect in Type 2 (non-insulin-dependent) diabetes. *Diabetologia*. 1986;29(1):46-52. doi:10.1007/BF02427280

194. Nauck MA, Heimesaat MM, Orskov C, Holst JJ, Ebert R, Creutzfeldt W. Preserved incretin activity of glucagon-like peptide 1 [7-36 amide] but not of synthetic human gastric inhibitory polypeptide in patients with type-2 diabetes mellitus. *J Clin Invest*. 1993;91(1):301-307. doi:10.1172/JCI116186

195. Færch K, Torekov SS, Vistisen D, et al. GLP-1 response to oral glucose is reduced in prediabetes, screen-detected type 2 diabetes, and obesity and influenced by sex: the ADDITION-PRO study. *Diabetes*. 2015;64(7):2513-2525. doi:10.2337/db14-1751

196. MacDonald PE, El-kholy W, Riedel MJ, Salapatek AMF, Light PE, Wheeler MB. The multiple actions of GLP-1 on the process of glucose-stimulated insulin secretion. *Diabetes*. 2002;51(suppl 3):S434-S442. doi:10.2337/diabetes.51.2007.S434

197. Tomas A, Jones B, Leech C. New insights into Beta-cell GLP-1 receptor and cAMP signaling. *J Mol Biol*. 2020;432(5):1347-1366. doi:10.1016/j.jmb.2019.08.009

198. Seino S, Takahashi H, Fujimoto W, Shibasaki T. Roles of cAMP signalling in insulin granule exocytosis. *Diabetes Obes Metab*. 2009;11(s4):180-188. doi:10.1111/j.1463-1326.2009.01108.x

199. Yabe D, Seino Y. Two incretin hormones GLP-1 and GIP: Comparison of their actions in insulin secretion and β cell preservation. *Prog Biophys Mol Biol*. 2011;107(2):248-256. doi:10.1016/j.pbiomolbio.2011.07.010

200. Capozzi ME, Svendsen B, Encisco SE, et al. β Cell tone is defined by proglucagon peptides through cAMP signaling. *JCI Insight*. 2019;4(5). doi:10.1172/jci.insight.126742

201. El K, Gray SM, Capozzi ME, et al. GIP mediates the incretin effect and glucose tolerance by dual actions on α cells and β cells. *Sci Adv*. 2021;7(11):eabf1948. doi:10.1126/sciadv.abf1948

202. Zhang Y, Parajuli KR, Fava GE, et al. GLP-1 receptor in pancreatic α-Cells regulates glucagon secretion in a glucose-dependent bidirectional manner. *Diabetes*. 2018;68(1):34-44. doi:10.2337/db18-0317

203. Meier JJ, Deacon CF, Schmidt WE, Holst JJ, Nauck MA. Suppression of glucagon secretion is lower after oral glucose administration than during intravenous glucose administration in human subjects. *Diabetologia*. 2007;50(4):806-813. doi:10.1007/s00125-007-0598-z

204. Meier JJ, Gallwitz B, Siepmann N, et al. Gastric inhibitory polypeptide (GIP) dose-dependently stimulates glucagon secretion in healthy human subjects at euglycaemia. *Diabetologia*. 2003;46(6):798-801. doi:10.1007/s00125-003-1103-y

205. Meier JJ, Nauck MA, Pott A, et al. Glucagon-like peptide 2 stimulates glucagon secretion, enhances lipid absorption, and inhibits gastric acid secretion in humans. *Gastroenterology*. 2006;130(1):44-54. doi:10.1053/j.gastro.2005.10.004

206. Nauck MA, Meier JJ. The incretin effect in healthy individuals and those with type 2 diabetes: physiology, pathophysiology, and response to therapeutic interventions. *Lancet Diabetes Endocrinol*. 2016;4(6):525-536. doi:10.1016/S2213-8587(15)00482-9

207. Hanyaloglu AC, von Zastrow M. Regulation of GPCRs by endocytic membrane trafficking and its potential implications. *Annu Rev Pharmacol Toxicol*. 2008;48:537-568. doi:10.1146/annurev.pharmtox.48.113006.094830

208. Rajan S, Torres J, Thompson MS, Philipson LH. SUMO downregulates GLP-1-stimulated cAMP generation and insulin secretion. *Am J Physiol - Endocrinol Metab*. 2012;302(6):E714-E723. doi:10.1152/ajpendo.00486.2011

209. Ashcroft FM, Rorsman P. Diabetes mellitus and the β cell: the last ten years. *Cell*. 2012;148(6):1160-1171. doi:10.1016/j.cell.2012.02.010

210. Perley MJ, Kipnis DM. Plasma insulin responses to oral and intravenous glucose: studies in normal and diabetic subjects. *J Clin Invest*. 1967;46(12):1954-1962. doi:10.1172/JCI105685

211. Perley M, Kipnis DM. Plasma insulin responses to glucose and tolbutamide of normal weight and obese diabetic and nondiabetic subjects. *Diabetes*. 1966;15(12):867-874. doi:10.2337/diab.15.12.867

212. Camastra S, Manco M, Mari A, et al. β-cell function in morbidly obese subjects during free living: long-term effects of weight loss. *Diabetes*. 2005;54(8):2382-2389. doi:10.2337/diabetes.54.8.2382

213. Olehnik SK, Fowler JL, Avramovich G, Hara M. Quantitative analysis of intra- and inter-individual variability of human beta-cell mass. *Sci Rep*. 2017;7(1):16398. doi:10.1038/s41598-017-16300-w

214. Saisho Y, Butler AE, Manesso E, Elashoff D, Rizza RA, Butler PC. β-cell mass and turnover in humans: effects of obesity and aging. *Diabetes Care*. 2013;36(1):111-117. doi:10.2337/dc12-0421

215. Kou K, Saisho Y, Satoh S, Yamada T, Itoh H. Change in β-cell mass in japanese nondiabetic obese individuals. *J Clin Endocrinol Metab*. 2013;98(9):3724-3730. doi:10.1210/jc.2013-1373

216. Ha J, Satin LS, Sherman AS. A mathematical model of the pathogenesis, prevention, and reversal of type 2 diabetes. *Endocrinology*. 2016;157(2):624-635. doi:10.1210/en.2015-1564

217. Hull RL, Kodama K, Utzschneider KM, Carr DB, Prigeon RL, Kahn SE. Dietary-fat-induced obesity in mice results in beta cell hyperplasia but not increased insulin release: evidence for specificity of impaired beta cell adaptation. *Diabetologia*. 2005;48(7):1350-1358. doi:10.1007/s00125-005-1772-9

218. Elbein SC, Wegner K, Kahn SE. Reduced beta-cell compensation to the insulin resistance associated with obesity in members of Caucasian familial type 2 diabetic kindreds. *Diabetes Care*. 2000;23(2):221-227. doi:10.2337/diacare.23.2.221

219. Kahn SE, Prigeon RL, McCulloch DK, et al. Quantification of the Relationship Between Insulin Sensitivity and β-Cell Function in Human Subjects: Evidence for a Hyperbolic Function. *Diabetes*. 1993;42(11):1663-1672. doi:10.2337/diab.42.11.1663

220. Wortham M, Liu F, Fleischman JY, et al. Nutrient Regulation of the Islet Epigenome Controls Adaptive Insulin Secretion. *bioRxiv preprint*. Published online August 21, 2019. doi:10.1101/742403

221. Valle MMR, Graciano MFR, Lopes de Oliveira ER, et al. Alterations of NADPH oxidase activity in rat pancreatic islets induced by a high-fat diet. *Pancreas*. 2011;40(3):390-395. doi:10.1097/MPA.0b013e31820569d0

222. Koulajian K, Desai T, Liu GC, et al. NADPH oxidase inhibition prevents beta cell dysfunction induced by prolonged elevation of oleate in rodents. *Diabetologia*. 2013;56(5):1078-1087. doi:10.1007/s00125-013-2858-4

223. Ferdaoussi M, Smith N, Lin H, et al. Improved glucose tolerance with DPPIV inhibition requires β-cell SENP1 amplification of glucose-stimulated insulin secretion. *Physiol Rep*. 2020;8(8). doi:10.14814/phy2.14420

224. Lin H, Smith N, Spigelman AF, et al. β-cell SENP1 facilitates responsiveness to incretins and limits oral glucose intolerance in high fat fed mice. *bioRxiv*. Published online December 2, 2020:2020.11.30.402644. doi:10.1101/2020.11.30.402644

225. Gupta D, Jetton TL, LaRock K, et al. Temporal characterization of β cell-adaptive and -maladaptive mechanisms during chronic high-fat feeding in C57BL/6NTac mice. *J Biol Chem*. 2017;292(30):12449-12459. doi:10.1074/jbc.M117.781047

226. Gembal M, Detimary P, Gilon P, Gao ZY, Henquin JC. Mechanisms by which glucose can control insulin release independently from its action on adenosine triphosphate-sensitive K+ channels in mouse β cells. *J Clin Invest*. 1993;91(3):871-880. doi:10.1172/JCI116308

227. Bowe JE, Chander A, Liu B, Persaud SJ, Jones PM. The permissive effects of glucose on receptor-operated potentiation of insulin secretion from mouse islets: a role for ERK1/2 activation and cytoskeletal remodelling. *Diabetologia*. 2013;56(4):783-791. doi:10.1007/s00125-012-2828-2

228. Hennige AM, Burks DJ, Ozcan U, et al. Upregulation of insulin receptor substrate-2 in pancreatic beta cells prevents diabetes. *J Clin Invest*. 2003;112(10):1521-1532. doi:10.1172/JCI18581

229. Kang T, Boland BB, Jensen P, et al. Characterization of signaling pathways associated with pancreatic β-cell adaptive flexibility in compensation of obesity-linked diabetes in db/db mice. *Mol Cell Proteomics*. Published online January 1, 2020. doi:10.1074/mcp.RA119.001882

230. Szklarczyk D, Gable AL, Lyon D, et al. STRING v11: protein–protein association networks with increased coverage, supporting functional discovery in genome-wide experimental datasets. *Nucleic Acids Res*. 2019;47(D1):D607-D613. doi:10.1093/nar/gky1131

231. Gregg T, Sdao SM, Dhillon RS, et al. Obesity-dependent CDK1 signaling stimulates mitochondrial respiration at complex I in pancreatic β-cells. *J Biol Chem*. 2019;294(12):4656-4666. doi:10.1074/jbc.RA118.006085

232. Cerqueira NMFSA, Oliveira EF, Gesto DS, et al. Cholesterol biosynthesis: a mechanistic overview. *Biochemistry*. 2016;55(39):5483-5506. doi:10.1021/acs.biochem.6b00342

233. Hao M, Head WS, Gunawardana SC, Hasty AH, Piston DW. Direct effect of cholesterol on insulin secretion: a novel mechanism for pancreatic beta-cell dysfunction. *Diabetes*. 2007;56(9):2328-2338. doi:10.2337/db07-0056

234. Nakamura M, Bhatnagar A, Sadoshima J. Overview to pyridine nucleotides review series. *Circ Res*. 2012;111(5):604-610. doi:10.1161/CIRCRESAHA.111.247924

235. Roat R, Rao V, Doliba NM, et al. Alterations of pancreatic islet structure, metabolism and gene expression in diet-Induced obese C57BL/6J mice. *PLOS ONE*. 2014;9(2):e86815. doi:10.1371/journal.pone.0086815

236. Fujikawa Y, Roma LP, Sobotta MC, et al. Mouse redox histology using genetically encoded probes. *Sci Signal*. 2016;9(419):rs1. doi:10.1126/scisignal.aad3895

237. Pettersson US, Waldén TB, Carlsson PO, Jansson L, Phillipson M. Female mice are protected against high-fat diet induced metabolic syndrome and increase the regulatory T cell population in adipose tissue. *PloS One*. 2012;7(9):e46057. doi:10.1371/journal.pone.0046057

238. Lin H, Smith N, Spigelman AF, et al. β-cell knockout of senp1 reduces responses to incretins and worsens oral glucose tolerance in high fat diet-fed mice. *Diabetes*. Published online August 27, 2021. doi:10.2337/db20-1235

239. Gutscher M, Sobotta MC, Wabnitz GH, et al. Proximity-based protein thiol oxidation by H2O2-scavenging peroxidases. *J Biol Chem*. 2009;284(46):31532-31540. doi:10.1074/jbc.M109.059246

240. Takahashi N, Kadowaki T, Yazaki Y, Ellis-Davies GCR, Miyashita Y, Kasai H. Post-priming actions of ATP on Ca2+-dependent exocytosis in pancreatic beta cells. *Proc Natl Acad Sci*. 1999;96(2):760-765. doi:10.1073/pnas.96.2.760

241. Smith EP, An Z, Wagner C, et al. The role of β cell glucagon-like peptide-1 signaling in glucose regulation and response to diabetes drugs. *Cell Metab*. 2014;19(6):1050-1057. doi:10.1016/j.cmet.2014.04.005

242. Capozzi ME, Wait JB, Koech J, et al. Glucagon lowers glycemia when β cells are active. *JCI Insight*. 4(16). doi:10.1172/jci.insight.129954

243. Holz GG, Kühtreiber WM, Habener JF. Pancreatic beta-cells are rendered glucose-competent by the insulinotropic hormone glucagon-like peptide-1(7-37). *Nature*. 1993;361(6410):362-365. doi:10.1038/361362a0

244. Thorens B, Tarussio D, Maestro MA, Rovira M, Heikkilä E, Ferrer J. Ins1(Cre) knock-in mice for beta cell-specific gene recombination. *Diabetologia*. 2015;58(3):558-565. doi:10.1007/s00125-014-3468-5

245. Smith N. Oral glucose tolerance test in mouse. Published online April 14, 2020. doi:10.17504/protocols.io.ujjeukn

246. Smith N. IP glucose tolerance test in mouse. Published online April 14, 2020. doi:10.17504/protocols.io.wxhffj6

247. Smith N. Insulin tolerance test in mouse. Published online April 14, 2020. doi:10.17504/protocols.io.wxjffkn

248. Lyon J, Spigelman AF, Bautista A, et al. Isolation of human pancreatic islets of langerhans for research. protocols.io. Published April 30, 2021. Accessed October 20, 2021. https://www.protocols.io/view/isolation-of-human-pancreatic-islets-of-langerhans-bt55nq86

249. Spigelman AF. Static glucose-stimulated insulin secretion (GSIS) protocol: mouse islets. Published online May 5, 2021. doi:10.17504/protocols.io.sp7edrn

250. Zhang Q, Chibalina MV, Bengtsson M, et al. Na+ current properties in islet α- and β-cells reflect cell-specific Scn3a and Scn9a expression. *J Physiol*. 2014;592(21):4677-4696. doi:10.1113/jphysiol.2014.274209

251. Ghazvini Zadeh EH, Huang Z, Xia J, Li D, Davidson HW, Li W hong. ZIGIR, a granule-specific Zn2+ indicator, reveals human islet α cell heterogeneity. *Cell Rep*. 2020;32(2):107904. doi:10.1016/j.celrep.2020.107904

252. Zhou Y, Zhou B, Pache L, et al. Metascape provides a biologist-oriented resource for the analysis of systems-level datasets. *Nat Commun*. 2019;10(1):1523. doi:10.1038/s41467-019-09234-6

253. Gu Z. *Circular Visualization in R*. Accessed December 31, 2020. https://bookdown.org/jokergoo/circlize-book/book

254. Subramanian A, Tamayo P, Mootha VK, et al. Gene set enrichment analysis: A knowledge-based approach for interpreting genome-wide expression profiles. *Proc Natl Acad Sci*. 2005;102(43):15545-15550. doi:10.1073/pnas.0506580102

255. Vilas-Boas EA, Nalbach L, Ampofo E, et al. Transient NADPH oxidase 2-dependent H2O2 production drives early palmitate-induced lipotoxicity in pancreatic islets. *Free Radic Biol Med*. 2021;162:1-13. doi:10.1016/j.freeradbiomed.2020.11.023

256. Nalbach L, Roma LP, Schmitt BM, et al. Improvement of islet transplantation by the fusion of islet cells with functional blood vessels. *EMBO Mol Med*. 2021;13(1):e12616. doi:10.15252/emmm.202012616

257. Barford D. The role of cysteine residues as redox-sensitive regulatory switches. *Curr Opin Struct Biol*. 2004;14(6):679-686. doi:10.1016/j.sbi.2004.09.012

258. Shen LN, Dong C, Liu H, Naismith JH, Hay RT. The structure of SENP1–SUMO-2 complex suggests a structural basis for discrimination between SUMO paralogues during processing. *Biochem J*. 2006;397(Pt 2):279-288. doi:10.1042/BJ20052030

259. Shi T, Han Y, Li W, et al. Exploring the desumoylation process of SENP1: a study combined MD simulations with QM/MM calculations on SENP1-SUMO1-RanGAP1. *J Chem Inf Model*. 2013;53(9):2360-2368. doi:10.1021/ci4002487

260. Eron SJ, MacPherson DJ, Dagbay KB, Hardy JA. Multiple mechanisms of zinc-mediated inhibition for the apoptotic caspases -3, -6, -7, & -8. *ACS Chem Biol*. 2018;13(5):1279-1290. doi:10.1021/acschembio.8b00064

261. Hogstrand C, Verbost PM, Wendelaar Bonga SE. Inhibition of human erythrocyte Ca2+-ATPase by Zn2+. *Toxicology*. 1999;133(2):139-145. doi:10.1016/S0300-483X(99)00020-7

262. Maret W, Yetman CA, Jiang LJ. Enzyme regulation by reversible zinc inhibition: glycerol phosphate dehydrogenase as an example. *Chem Biol Interact*. 2001;130-132:891-901. doi:10.1016/S0009-2797(00)00243-X

263. Bellomo E, Massarotti A, Hogstrand C, Maret W. Zinc ions modulate protein tyrosine phosphatase 1B activity†. *Metallomics*. 2014;6(7):1229-1239. doi:10.1039/c4mt00086b

264. Laity JH, Andrews GK. Understanding the mechanisms of zinc-sensing by metal-response element binding transcription factor-1 (MTF-1). *Arch Biochem Biophys*. 2007;463(2):201-210. doi:10.1016/j.abb.2007.03.019

265. Sun M an, Wang Y, Zhang Q, Xia Y, Ge W, Guo D. Prediction of reversible disulfide based on features from local structural signatures. *BMC Genomics*. 2017;18:279. doi:10.1186/s12864-017-3668-8

266. Wong WP, Allen NB, Meyers MS, et al. Exploring the association between demographics, SLC30A8 genotype, and human islet content of zinc, cadmium, copper,iron, manganese and nickel. *Sci Rep*. 2017;7(1):473. doi:10.1038/s41598-017-00394-3

267. Ireland SM, Martin ACR. ZincBind—the database of zinc binding sites. *Database*. 2019;2019(baz006). doi:10.1093/database/baz006

268. Hirano T, Kikuchi K, Urano Y, Nagano T. Improvement and Biological Applications of Fluorescent Probes for Zinc, ZnAFs. *J Am Chem Soc*. 2002;124(23):6555-6562. doi:10.1021/ja025567p

269. Ebert JC, Altman RB. Robust recognition of zinc binding sites in proteins. *Protein Sci Publ Protein Soc*. 2008;17(1):54-65. doi:10.1110/ps.073138508

270. Rutter GA, Chabosseau P, Bellomo EA, et al. Intracellular zinc in insulin secretion and action: a determinant of diabetes risk? *Proc Nutr Soc*. 2016;75(1):61-72. doi:10.1017/S0029665115003237

271. Vinkenborg JL, Nicolson TJ, Bellomo EA, Koay MS, Rutter GA, Merkx M. Imaging of intracellular free Zn2+ in real time using genetically-encoded FRET sensors. *Nat Methods*. 2009;6(10):737-740. doi:10.1038/nmeth.1368

272. Haneskog L. Preparation of Denatured Protein Samples from Inclusion Bodies. *Cold Spring Harb Protoc*. 2006;2006(1):pdb.prot4265. doi:10.1101/pdb.prot4265

273. Umetsu M, Tsumoto K, Hara M, et al. How additives influence the refolding of immunoglobulin-folded proteins in a stepwise dialysis system. Spectroscopic evidence for highly efficient refolding of a single-chain Fv fragment. *J Biol Chem*. 2003;278(11):8979-8987. doi:10.1074/jbc.M212247200

274. Cer RZ, Mudunuri U, Stephens R, Lebeda FJ. IC50-to-Ki: a web-based tool for converting IC50 to Ki values for inhibitors of enzyme activity and ligand binding. *Nucleic Acids Res*. 2009;37(Web Server issue):W441-W445. doi:10.1093/nar/gkp253

275. Khan S, Yan-Do R, Duong E, et al. Autocrine activation of P2Y1 receptors couples Ca2+ influx to Ca2+ release in human pancreatic beta cells. *Diabetologia*. 2014;57(12):2535-2545. doi:10.1007/s00125-014-3368-8

276. Kalwat MA, Cobb MH. Mechanisms of the amplifying pathway of insulin secretion in the β cell. *Pharmacol Ther*. 2017;179:17-30. doi:10.1016/j.pharmthera.2017.05.003

277. Campbell JE, Drucker DJ. Pharmacology, physiology, and mechanisms of incretin hormone action. *Cell Metab*. 2013;17(6):819-837. doi:10.1016/j.cmet.2013.04.008

278. Oduori OS, Murao N, Shimomura K, et al. Gs/Gq signaling switch in β cells defines incretin effectiveness in diabetes. *J Clin Invest*. Published online November 16, 2020. doi:10.1172/JCI140046

279. Magnuson MA, Osipovich AB. Pancreas-specific Cre driver lines and considerations for their prudent use. *Cell Metab*. 2013;18(1):9-20. doi:10.1016/j.cmet.2013.06.011

280. El K, Campbell JE. The role of GIP in α-cells and glucagon secretion. *Peptides*. 2020;125:170213. doi:10.1016/j.peptides.2019.170213

281. Galsgaard KD, Jepsen SL, Kjeldsen SAS, Pedersen J, Wewer Albrechtsen NJ, Holst JJ. Alanine, arginine, cysteine, and proline, but not glutamine, are substrates for, and acute mediators of, the liver-α-cell axis in female mice. *Am J Physiol Endocrinol Metab*. 2020;318(6):E920-E929. doi:10.1152/ajpendo.00459.2019

282. Yamane S, Harada N, Inagaki N. Mechanisms of fat-induced gastric inhibitory polypeptide/glucose-dependent insulinotropic polypeptide secretion from K cells. *J Diabetes Investig*. 2016;7(S1):20-26. doi:https://doi.org/10.1111/jdi.12467

283. Ahrén B, Winzell MS, Pacini G. The augmenting effect on insulin secretion by oral versus intravenous glucose is exaggerated by high-fat diet in mice. *J Endocrinol*. 2008;197(1):181-187. doi:10.1677/JOE-07-0460

284. El K, Capozzi ME, Campbell JE. Repositioning the alpha cell in postprandial metabolism. *Endocrinology*. doi:10.1210/endocr/bqaa169

285. Zhu L, Dattaroy D, Pham J, et al. Intraislet glucagon signaling is critical for maintaining glucose homeostasis. *JCI Insight*. 4(10). doi:10.1172/jci.insight.127994

286. Svendsen B, Larsen O, Gabe MBN, et al. Insulin secretion depends on intra-islet glucagon signaling. *Cell Rep*. 2018;25(5):1127-1134.e2. doi:10.1016/j.celrep.2018.10.018

287. Virtue S, Vidal-Puig A. GTTs and ITTs in mice: simple tests, complex answers. *Nat Metab*. Published online June 11, 2021. doi:10.1038/s42255-021-00414-7

288. Ahrén B, Pacini G. Glucose effectiveness: Lessons from studies on insulin-independent glucose clearance in mice. *J Diabetes Investig*. 2021;12(5):675-685. doi:10.1111/jdi.13446

289. Nayak A, Müller S. SUMO-specific proteases/isopeptidases: SENPs and beyond. *Genome Biol*. 2014;15(7):422. doi:10.1186/s13059-014-0422-2

290. Sakuraba H, Mizukami H, Yagihashi N, Wada R, Hanyu C, Yagihashi S. Reduced beta-cell mass and expression of oxidative stress-related DNA damage in the islet of Japanese Type II diabetic patients. *Diabetologia*. 2002;45(1):85-96. doi:10.1007/s125-002-8248-z

291. Anvari E, Wikström P, Walum E, Welsh N. The novel NADPH oxidase 4 inhibitor GLX351322 counteracts glucose intolerance in high-fat diet-treated C57BL/6 mice. *Free Radic Res*. 2015;49(11):1308-1318. doi:10.3109/10715762.2015.1067697

292. Smith N. Mouse pancreatic islet isolation. Published online April 14, 2020. doi:10.17504/protocols.io.sqaedse

293. Ferdaoussi M, Bergeron V, Zarrouki B, et al. G protein-coupled receptor (GPR)40-dependent potentiation of insulin secretion in mouse islets is mediated by protein kinase D1. *Diabetologia*. 2012;55(10):2682-2692. doi:10.1007/s00125-012-2650-x

294. Spigelman AF. Complexing Sodium Oleate for use in insulin secretion. Published online May 5, 2021. doi:10.17504/protocols.io.buamnsc6

295. Klarenbeek J, Goedhart J, Batenburg A van, Groenewald D, Jalink K. Fourth-generation Epac-based FRET sensors for cAMP feature exceptional brightness, photostability and dynamic range: characterization of dedicated sensors for FLIM, for ratiometry and with high affinity. *PLOS ONE*. 2015;10(4):e0122513. doi:10.1371/journal.pone.0122513

296. Wicksteed B, Brissova M, Yan W, et al. Conditional gene targeting in mouse pancreatic β-cells: analysis of ectopic Cre transgene expression in the brain. *Diabetes*. 2010;59(12):3090-3098. doi:10.2337/db10-0624

297. Sabatini PV, Speckmann T, Nian C, et al. Neuronal PAS domain protein 4 suppression of oxygen sensing optimizes metabolism during excitation of neuroendocrine cells. *Cell Rep*. 2018;22(1):163-174. doi:10.1016/j.celrep.2017.12.033

298. Mehran AE, Templeman NM, Brigidi GS, et al. Hyperinsulinemia drives diet-induced obesity independently of brain insulin production. *Cell Metab*. 2012;16(6):723-737. doi:10.1016/j.cmet.2012.10.019

299. Auberval N, Dal S, Bietiger W, et al. Metabolic and oxidative stress markers in Wistar rats after 2 months on a high-fat diet. *Diabetol Metab Syndr*. 2014;6(1):130. doi:10.1186/1758-5996-6-130

300. Fu A, Rooyen L van, Evans L, et al. Glucose metabolism and pyruvate carboxylase enhance glutathione synthesis and restrict oxidative stress in pancreatic islets. *Cell Rep*. 2021;37(8). doi:10.1016/j.celrep.2021.110037

301. Omar-Hmeadi M, Idevall-Hagren O. Insulin granule biogenesis and exocytosis. *Cell Mol Life Sci*. 2021;78(5):1957-1970. doi:10.1007/s00018-020-03688-4

302. Pedersen MG, Tagliavini A, Henquin JC. Calcium signaling and secretory granule pool dynamics underlie biphasic insulin secretion and its amplification by glucose: experiments and modeling. *Am J Physiol-Endocrinol Metab*. 2019;316(3):E475-E486. doi:10.1152/ajpendo.00380.2018

303. Zhao S, Poursharifi P, Mugabo Y, et al. α/β-Hydrolase domain-6 and saturated long chain monoacylglycerol regulate insulin secretion promoted by both fuel and non-fuel stimuli. *Mol Metab*. 2015;4(12):940-950. doi:10.1016/j.molmet.2015.09.012

304. Ma C, Li W, Xu Y, Rizo J. Munc13 mediates the transition from the closed syntaxin–Munc18 complex to the SNARE complex. *Nat Struct Mol Biol*. 2011;18(5):542-549. doi:10.1038/nsmb.2047

305. Forman HJ, Zhang H. Targeting oxidative stress in disease: promise and limitations of antioxidant therapy. *Nat Rev Drug Discov*. 2021;20(9):689-709. doi:10.1038/s41573-021-00233-1

306. Wang X, Yun JW, Lei XG. Glutathione peroxidase mimic ebselen improves glucose-stimulated insulin secretion in murine islets. *Antioxid Redox Signal*. 2013;20(2):191-203. doi:10.1089/ars.2013.5361

307. Vincent AM, Russell JW, Low P, Feldman EL. Oxidative stress in the pathogenesis of diabetic neuropathy. *Endocr Rev*. 2004;25(4):612-628. doi:10.1210/er.2003-0019